Development of a full flexion 3D musculoskeletal model of the knee considering intersegmental contact and deep muscle activity during high knee flexion

by

David Cornelius Kingston

A thesis
presented to the University of Waterloo
in partial fulfillment of the
thesis requirements for the degree of
Doctor of Philosophy
in
Kinesiology

Waterloo, Ontario, Canada, 2019

Examining Committee Membership

The following served on the Examining Committee for this thesis. The decision of the Examining Committee is by majority vote.

External examiner	Dr. Janie Wilson Professor
Supervisors	Dr. Stacey Acker Assistant Professor
	Dr. Jack Callaghan Professor
Internal members	Dr. Andrew Laing Associate Professor
	Dr. Clark Dickerson Professor
Internal-external member	Dr. Arash Arami Assistant Professor

Author's Declaration

This thesis consists of material all of which I authored or co-authored. This is a true copy of the thesis, including any required final revisions, as accepted by my examiners. I understand that my thesis may be made electronically available to the public.

David Cornelius Kingston

Abstract

Habitual kneeling in high knee flexion postures is a risk factor for knee joint dysfunction yet critical parameters for modeling this range of motion remain unknown or untested in three dimensions. High flexion is defined as postures exceeding 120° at the knee joint to a maximum of approximately 165°. Specific occupational and ethnic populations that regularly use high knee flexion postures have increased prevalence of degenerative knee diseases. This could suggest a causal relationship between habitual kneeling and disease prevalence resulting from repeated exposures. Therefore, this thesis was designed to explore two critical components for high knee flexion biomechanical modeling: intersegmental (thigh-calf and heel-gluteal) contact forces and lower limb muscular activation patterns across the full range of knee flexion. The global objective of this work was to develop a 3D musculoskeletal (MSK) model of the knee to estimate tibial contact forces in high knee flexion postures for determining the effect of intersegmental contact on these calculations. Two experimental studies, verification against a 'gold-standard' dataset, and an application study supported this global objective.

Study 1: The purposes of this study were: 1) to measure total intersegmental contact force magnitude and centre of force (CoF) location during six high knee flexion movements and 2) to define regression models, based on anthropometrics, for the estimation of intersegmental contact parameters. Fifty eight participants completed six high knee flexion movements while motion capture and pressure data from the right lower limb were recorded. High knee flexion movements had average peak total intersegmental contact force magnitudes ranging from ~50-200N or ~8-30 %BW. Intersegmental CoF locations were segregated between thigh-calf and

heel-gluteal regions with CoF, at peak total force, being ~6.2 cm and ~32.7 cm distal from the functional knee joint center about the long axis of the femur respectively.

Five parameters of intersegmental contact (onset, maximum knee flexion angle, total contact force, thigh-calf CoF, and thigh-calf contact area) were then assessed for anthropometric based regression model fit. Strong correlations and linear regression models were found for maximum knee flexion angle and thigh-calf CoF, but only moderate to weak results were found for all other intersegmental contact parameters. The overall poor fit and variance explained by the linear regression models for onset, total force, and contact area suggest further work is needed to provide estimations of these parameters for use in future modeling efforts.

Study 2: The purposes of this study were: 1) to measure surface and fine-wire EMG activation profiles in six high knee flexion movements and 2) to establish if surface EMG sites can be used as a proxy for fine-wire activation profiles. Sixteen participants completed the same high knee flexion movements, and level walking, as study 1 while activation waveforms from three deep muscles—vastus intermedius (VI), adductor magnus (AM), and semimembranosus (SM)—were recorded using fine-wire electrodes for comparison to easily accessible surface sites. Average peaks of VI, AM, and SM fine-wire activations during high knee flexion movements were approximately 30, 85, and 35 %MVC respectively. None of the surface sites recorded satisfied our criteria to successfully model fine-wire recordings. This was largely due to the considerable variability of surface-indwelling comparisons between participants. Our findings would suggest that the use of fine-wire EMG to obtain representative activation waveforms from VI, AM, or SM may be required if isolated muscle/motor unit activity is needed.

MSK model: A full range of knee motion MSK model was developed for the estimation of tibial contact forces. Verification of the MSK model was completed by calculating the error between tibial compressive force estimates and measurements from an instrumented knee implant (gold standard). Vertex based object files of participant bones and CAD files of implant components were obtained from a public repository for gold standard data with muscle geometry scaled from our MSK model. Tibial compression estimates strongly fit implant data shape during walking (R^2 0.83), squatting (R^2 0.93), and ‘bouncy’ walking (R^2 0.74) with an RMSD of 0.47, 0.16 and 0.58 BW respectively. Qualitative assessments of recorded EMG and muscle force estimations showed poor agreement between time-series data. Therefore, the strong fit of MSK tibial compression estimates to gold standard data would suggest this model is phenomenological in nature and does not accurately represent neuromuscular control.

Application: The purpose of this study was to quantify the effect of including intersegmental contact on external knee joint moments and tibial contact force estimations. This study used participant data collected from study 2. There was an average RMSD of 3.56, 0.16, and 0.06 %BW*HT in flexion/extension, ab/adduction, and int/external external moments respectively when considering intersegmental contact parameters. Reductions in external moments caused changes to mean RMSD tibial contact force estimates: 0.14 BW lower compression, 0.2 BW lower posterior shear, and 0.03 BW higher lateral shear. Muscle force estimates generally followed EMG waveforms in shape for vastii, gluteus medius, and AM with

SM having an improved agreement using its indwelling signal compared to surface measurements.

General conclusions: Intersegmental contact forces must be considered when reporting tibial contact forces during high knee flexion movements as significant reductions to tibial posterior shear and increases in lateral shear were observed. Further work is required to refine MSK models in these ranges of knee motion as pressure sensor technology and soft tissue artifact are considerable limitations. Measurement of populations who habitually perform these activities needs to be completed to assess the translation of these findings to appropriate individuals.

Acknowledgements

I would like to thank all of those whole supported me completing this scope of work; most importantly Murielle and my family. I will fondly remember my years at the University of Waterloo and cannot express enough gratitude for the technical training, experiences, and companionship of the faculty, graduate student body, and administrative complement. Although I cannot repay the countless debts of time accrued to many of you, I am fortunate to have been your colleague.

Table of Contents

List of Figures

List of Tables

List of Abbreviations

ADLs	Activities of Daily Living
AP	Anterior/Posterior
ASIS	Anterior Superior Illiac Spine
BW	Body Weight
CI	Confidence Interval
CoF	Centre of Force
CoM	Centre of Mass
CoP	Centre of Pressure
DCM	Direction Cosine Matrix
EMG	Electromyography/Electromyogram
FJC	Function Joint Centre
GCS	Global Coordinate System
GRF	Ground Reaction Force
HG	Heel-Gluteal
HJC	Hip Joint Center
IVD	Inverse Dynamics
KJC	Knee Joint Center
LCS	Local Coordinate System
LoA	Line of Action
ML	Medial/Lateral
MoI	Moment of Inertia
MRI	Magnetic Resonance Imaging
MSK	Musculoskeletal
MVC	Maximal Voluntary Contraction
OA	Osteoarthritis
PCSA	Physiological Cross Sectional Area
PSIS	Posterior Superior Illiac Spine
RMSD	Root Mean Squared Difference
SCoRE	Symmetric Centre of Rotation Estimation
SD	Standard Deviation
TC	Thigh-Calf

Chapter 1 – General Introduction

Habitual kneeling in high knee flexion postures is a risk factor for knee joint dysfunction yet critical parameters for modeling this range of motion remain unknown or untested in three dimensions (Coggon et al., 2000; Thompson et al., 2015). High flexion is defined as postures exceeding 120° at the knee joint (Hemmerich et al., 2006; Kobayashi et al., 2013) to a maximum of approximately 165° (Acker et al., 2011; Kingston and Acker, 2018a). At any given time, one in eight Canadian workers have diagnosable knee osteoarthritis (OA) with prevalence expected to increase to 1 in 4 as the population ages (Bombardier et al., 2011). Also, specific occupational and ethnic populations that habitually kneel have increased prevalence of degenerative diseases, such as OA (Baker et al., 2003; Kirkeshov Jensen, 2008), bursitis (Thun et al., 1987), and pain (Bombardier et al., 2011). This could suggest a causal relationship between habitual kneeling and increased degenerative disease prevalence resulting from repeated exposures. While self-report and physical exposure data has been collected from patients or workers, this retrospective method of data collection does not provide necessary detail for biomechanical modeling, exploration of disease mechanisms, or intervention planning.

This thesis was designed to explore two critical components for high knee flexion biomechanical modeling: intersegmental contact forces and lower limb muscular activation patterns across the full range of knee flexion. Ignoring these components would result in computational models lacking construct validity (Hicks et al., 2014) with estimations of tibial contact forces in high knee flexion being questionable. Therefore, intersegmental contact forces were incorporated to a three-dimensional (3D) musculoskeletal (MSK) model of the knee for estimating tibial contact forces with muscle activation data used as a qualitative assessment of model-estimated muscle force waveforms.

1.1 Objectives

Human MSK models provide researchers with tools that enable rapid testing of hypotheses and estimates of the mechanical processes in which our bodies produce movement. These estimates not only provide a deeper understanding of human kinesiology, but can assist clinical decisions and recovery (Zajac et al., 2003) or inform safe working guidelines (*Guidelines for Modified Work*, 2008). However, all models suffer a common limitation; estimates are only as good as the assumptions they have been built from. Generic MSK models verified for use in many different movements are rare as models are typically constrained to answer focused research questions. None of the most common knee joint contact models publicly available—notably Arnold et al. (2010), Carbone et al., (2015), or Halloran et al. (2010)—were designed for use in high knee flexion. Therefore, the global objective of this work was to develop a 3D MSK model of the knee to estimate tibial contact forces in high knee flexion postures for determining the effect of intersegmental contact on these estimations. Although there are implications of high knee flexion postures on the patellofemoral joint, such an investigation is outside the scope of this thesis. This model includes experimentally measured intersegmental contact forces and lower limb muscle activation patterns from high flexion movements as input and qualitative verification parameters respectively. Two experimental studies, verification against a 'gold-standard' dataset, and an application study supported this global objective (Figure 1.1). Their purposes were:

1. To measure total force magnitude and centre of force location of intersegmental contact during six high knee flexion movements (Chapter 3).

2. To define regression models based on participant anthropometrics for the estimation of intersegmental contact parameters (Chapter 3).

3. To measure surface and fine-wire EMG activation profiles in six high knee flexion movements (Chapter 4).

4. To determine if EMG from surface sites can be used as a proxy for fine-wire activation profiles (Chapter 4).

5. To quantify the error of the MSK model by comparing tibial compression force estimates to a gold standard (Chapter 5).

6. To quantify the effect of incorporating intersegmental contact on tibial contact force estimations (Chapter 6).

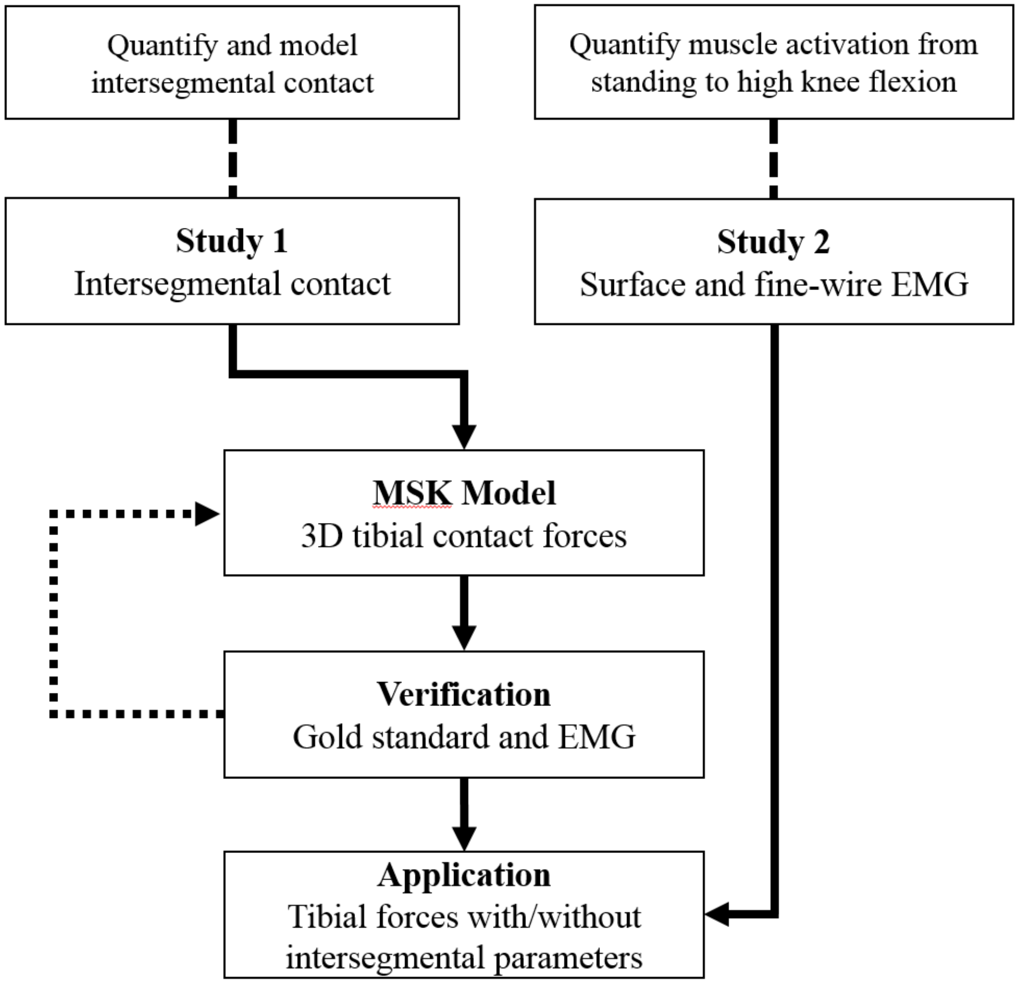

Figure 1.1 Flowchart of proposed studies. Dashed lines indicate research motivation. Solid lines indicate flow of outcomes. The dotted line indicates an iterative feedback loop. MSK model components are shown in Figure 1.2.

1.2 Intersegmental contact

Transitioning from standing to maximal knee flexion during squatting or kneeling results in soft tissue contact between the thigh and calf (TC) as well as heel and gluteal (HG) structures. Intersegmental contact begins at ~125º and increases in force magnitude until maximum knee flexion in young healthy adults (Kingston and Acker, 2018a; Pollard et al., 2011; Zelle et al., 2007). To date, no 3D MSK model has incorporated the effects of intersegmental contact forces on knee joint contact force estimations. Researchers have used sagittal plane 2D MSK models to estimate the reductions in muscle or joint contact forces that occur when considering TC force changes to the external flexion moment (Caruntu et al., 2003; Zelle et al., 2009). It should be noted that neither of the referenced studies directly measured TC contact, but estimated TC force using mass-spring systems (Caruntu et al., 2003) or used data from a previous dataset (Zelle et al., 2007). Even so, reductions of 700 N in quadriceps force (Caruntu et al., 2003) or 944 N in knee joint compressive forces (Zelle et al., 2009) have been reported. These planar studies highlight the importance of TC contact for tibial compression force estimation and the necessity for its inclusion in a 3D MSK model of high knee flexion.

Prior modeling efforts have acknowledged the need for incorporating TC contact data into future models, but considerable gaps remain. The most prolific TC contact dataset (Zelle et al., 2007) was collected from eight male and two female participants using a manually positioned pressure mat. The protocol used by Zelle et al. (2007) limits the applicability of their findings to a young healthy sample and suffers reliability issues when transforming contact forces to inputs for inverse dynamic (IVD) calculations due to not tracking the position of the pressure mat.

Therefore, the first study of this thesis measured TC and HG contact from 58 participants (28 males, 30 females) while synchronously measuring kinetics and kinematics. The main contributions of this study were the quantification of intersegmental contact through the full knee flexion range and evidence that regression equations—based on participant anthropometrics—

are unable to strongly estimate most intersegmental contact parameters except maximum knee flexion angle and TC CoF. For further details, refer to Chapter 3.

1.3 EMG in transitions to high knee flexion postures

There has been limited EMG measurement in the lower limb during high knee flexion movements (Gallagher et al., 2011; Kingston et al., 2017, 2016; Tennant et al., 2014). However, activation waveforms and discrete outcomes are well documented for musculature crossing the knee joint during gait (Dominici et al., 2011; Fregly et al., 2012; Hubley-Kozey et al., 2013) and activities of daily living (e.g. stair ambulation or rising from a chair) (Ciccotti et al., 1994; Heiden et al., 2009; Taylor et al., 2017). The lack of repeated studies to verify surface EMG measurements for high knee flexion movements suggests further assessment must be completed to provide a fulsome understanding of waveform patterns and provide verification data for the MSK modelling community. Despite this knowledge gap, there has not been any empirical work on the activation of deep muscles—notably vastus intermedius (VI), adductor magnus (AM), and semimembranosus (SM)—during high knee flexion movements, even though many MSK models incorporate their contribution to knee joint loading (Arnold et al., 2010; Carbone et al., 2015; Damsgaard et al., 2006; Lloyd and Besier, 2003; Modenese et al., 2011).

Therefore, the second study in this thesis recorded muscle activity, from the right lower limb, in eleven superficial sites and three indwelling sites while measuring the kinetics and kinematics of high knee flexion movements. This was the first study to measure this number of muscles in dynamic transitions into high knee flexion postures. The main contribution of Study 2 is that this study was the first to test the suitability of modeling deep muscle activity with surface EMG in high knee flexion activities. For further details, refer to Chapter 4. Additionally, the activation waveforms of this muscle set for six high knee flexion postures were used as a qualitative assessment of MSK model muscle force estimations (Chapter 6).

1.4 MSK model

A novel MSK model of the pelvis and right lower limb was coded in Matlab 9.2 (R2017a, The MathWorks, Natick, MA) to estimate tibial contact forces across the full range of knee flexion. External kinetics, kinematics, and anthropometric *in vivo* data were used as model inputs with EMG data used for verification (Figure 1.2). The geometric model consists of a pelvis, femur, patella, shank, and foot as well as 161 muscle elements (Appendix A) that actuate the hip, knee, and ankle joints (Horsman et al., 2007). Muscles included in this model that have *in vivo* data for verification are: vastus lateralis (VL), rectus femoris (RF), vastus medialis (VM), VI, biceps femoris (BF), semitendinosus (ST), SM, lateral gastrocnemius (LG), medial gastrocnemius (MG), tibialis anterior (TA), gluteus medius (GD), and AM. Muscular origin/insertion locations, lines of action (LoA), and physiological cross sectional area (PCSA) were taken from the most comprehensive lower limb cadaveric dataset available as of 2014 (Horsman et al., 2007). Finally, individual muscle force estimates were optimized to equal experimentally determined external knee joint moments (Carbone et al., 2015; Crowninshield and Brand, 1981; Miller et al., 2009).

This is the first 3D MSK model of the knee to incorporate intersegmental contact parameters which occur in high knee flexion postures. Therefore, this model is a unique tool which can estimate the magnitude of tibial contact forces in these exposures. While outside the scope of this thesis, this model could be used to provide insight on mechanisms of degenerative disease progression and improve our understanding of knee structure loading. For further details on model components, refer to Chapter 5.

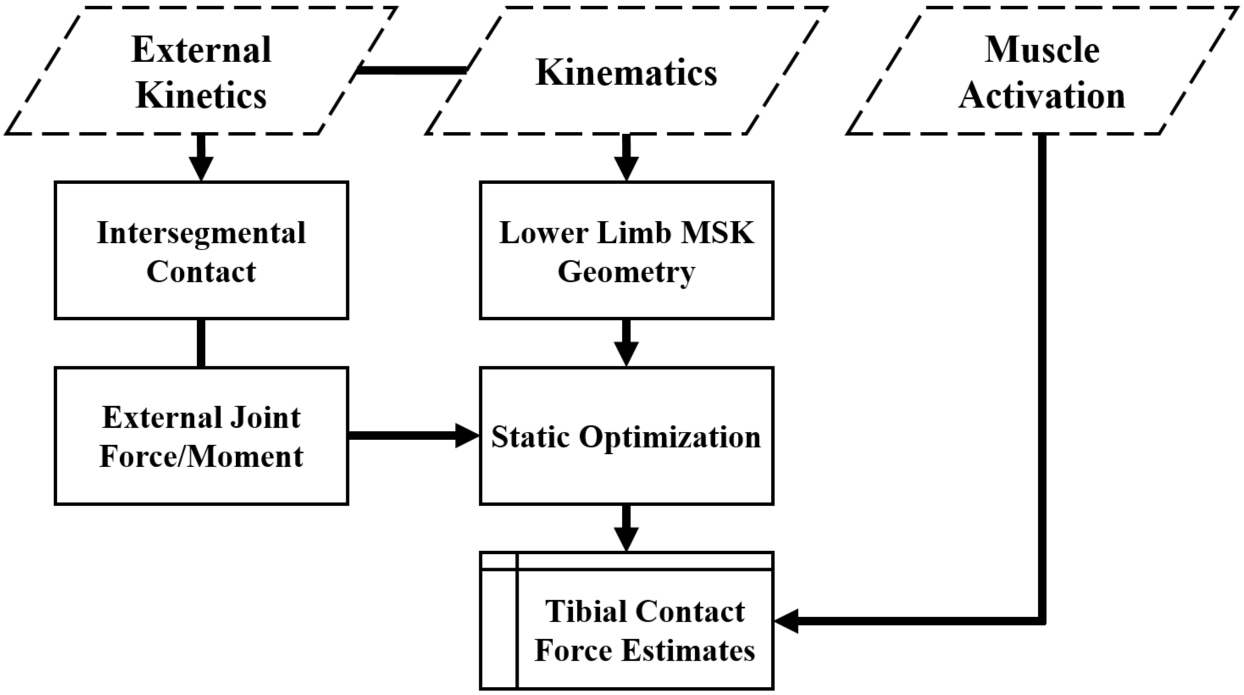

Figure 1.2 Data flow and computational modules of musculoskeletal model of the knee. Parallelograms indicate input data, square boxes indicate processes, and the square box with intersecting lines indicates internal storage (IBM, 1969).

1.4.1 Model verification

Verification is a critical step in any computational model development cycle. Verification of this model was completed by comparing estimates of tibial compression force to an instrumented knee implant, considered the 'gold standard' in this work. Verification data included kinematic, kinetic, and EMG data from a two-legged squat, 'bouncy' walking, and five normal walking trials provided in the 4th Grand Knee Challenge dataset (Fregly et al., 2012). It should be noted that verification data were limited to knee flexion ranges of 0-100°. Model performance was assessed using criteria defined by Grand Knee Challenge organizers: root mean squared difference (RMSD) and the coefficient of determination (R^2) of estimates compared to tibial compression measured from the instrumented implant. Surface EMG data was provided from fifteen muscles and used as a qualitative assessment to compare recorded muscle activations against estimated muscle force levels.

This verification procedure established a level of confidence in MSK model estimates and highlights areas for future improvements. The qualitative assessment against EMG waveforms suggest MSK model estimates are phenomenological in nature. For further details, refer to Chapter 5.

1.5 Model application

To address the global objective of this thesis, the MSK model was used to estimate changes in external knee joint moments and tibial contact forces from including intersegmental forces. This application is exploratory due to sample size (*n* = 16), but provided the most comprehensive kinetic evaluation of high knee flexion postures to date. There was an average RMSD reduction of 3.56, 0.16, and 0.06 %BW*HT in flexion/extension, ab/adduction, and int/external external moments respectively. This reduction in external moments resulted in the following average RMSD changes to tibial contact force estimates: 0.14 BW lower compression, 0.2 BW lower posterior shear, and 0.03 BW lower lateral shear. Significant reductions of posterior shear and increases of lateral shear was found in select movements when incorperating intersegmental contact. Muscle force estimates generally followed EMG waveforms in shape for vastii, GD, and AM with SM having better agreement with its idwelling signal compared to surface.

This body of work meaningfully contributes to the modelling community through advancing the number of high knee flexion movements assessed and providing foundational data for future verification and comparisons. As well, this application could provide critical input parameters for finite element (FE) modelling and other simulations useful for high knee flexion prosthesis design in future work. For further details, refer to Chapter 6.

Chapter 2 – Literature Review

This literature reviewed will briefly introduce knee OA as a disease with links to habitual exposure of high knee flexion postures. Then, a review of approaches and current data for modeling knee mechanics through *in vitro* and *in silico* methods will be completed. Finally, evidence will be provided to highlight the lack of fundamental data to support MSK modeling of high knee flexion postures.

2.1 Knee osteoarthritis and disease progression

On a global scale, lifetime knee OA prevalence among men 20-59 years of age is 54% (Baker et al., 2003) with incident rates of 250/100 000 people for both men and women (Cooper et al., 2000). Knee OA is a debilitating disease that decreases quality of life and can predispose individuals to future medical issues (Persson et al., 2017). Knee OA is multifactorial, but primary risk factors are aging and obesity (Arden and Nevitt, 2006; Bombardier et al., 2011). With disease progression, articular cartilage of the femur thins and/or develops into osseous tissue (Mithoefer et al., 2009). The meniscus of the tibia can also thin or tear due to pathological tribology as cartilage integrity diminishes and bone is exposed (Andriacchi and Mündermann, 2006). Osseous tissue may form around the joint or in connective tissue (Figure 2.1) with continued disease progression (Chu et al., 2012). These structural changes to joint tissues can result in friction during movement and a reduction in joint flexibility, which increases tissue stress, and stimulates biological responses such as inflammation and thinning of condylar cartilage (Andriacchi and Favre, 2014; Mündermann et al., 2008). An extreme representation of these changes is shown in Figure 2.2 with cadaveric examples in Figure 2.3. Radiographs comparing a healthy control to an occupational habitual kneeler with mild knee OA are shown in Figure 2.4.

Figure 2.1 Ossification of an occupational kneeler's posterior joint capsule (posterior) with a possible evulsion fracture at the tibial tuberosity or ossification of the patellar ligament. Image from a study that is not part of this thesis.

The most common location of knee OA is in the medial compartment (i.e. distal medial femoral condyle and medial tibial plateau) which accounts for approximately 68% of cases (Felson et al., 2002). This is unsurprising given that 60-70% of weight-bearing load is transmitted through the medial compartment (Andriacchi et al., 2004; Arden and Nevitt, 2006;

Kinney et al., 2013). Although medication, gait modification, or bracing can effectively reduce pain in some individuals, severe knee OA patients require unilateral or total knee arthroplasty (Banks et al., 2005; Kinney et al., 2013; Winby et al., 2009). These procedures generally improve knee joint alignment, tribology, and overall quality of life.

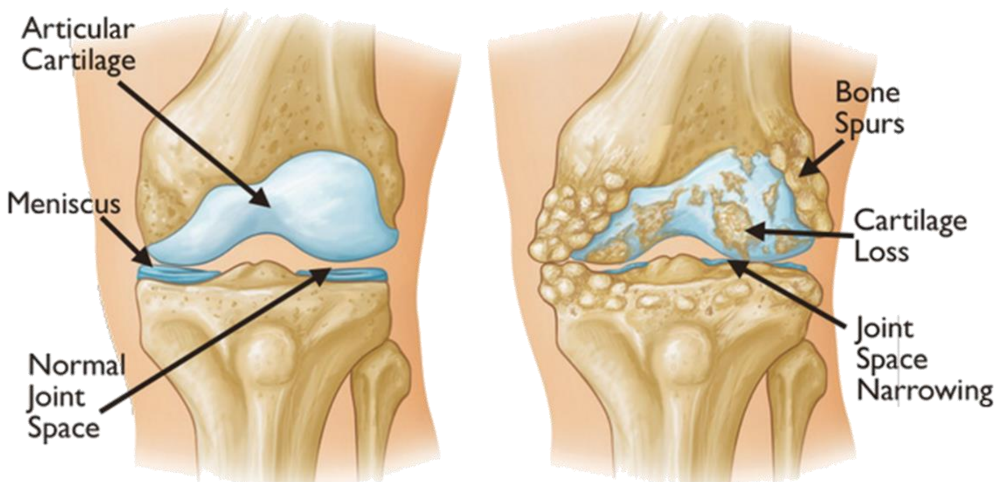

Figure 2.2 Healthy knee with complete articular cartilage covering underlying bone, intact meniscus, and normal joint spacing between the femur and tibial plateau (Left). Knee with Kellgren-Lawrence grade 4 osteoarthritis (Right) (Kellgren and Lawrence, 1957). Adapted from Foran & Fischer (2015).

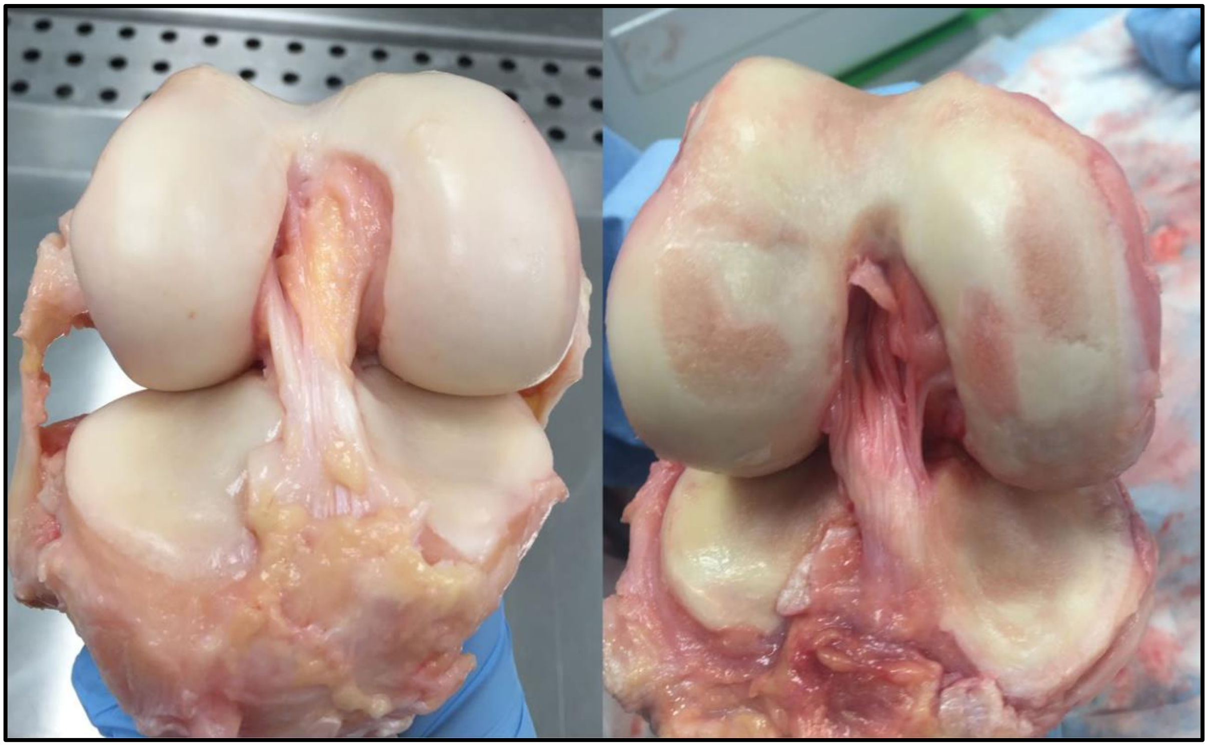

Figure 2.3 Young (43 years) healthy and old (88 years) osteoarthritic knee joint specimens (left and right respectively). Images from Peters et al. (2018).

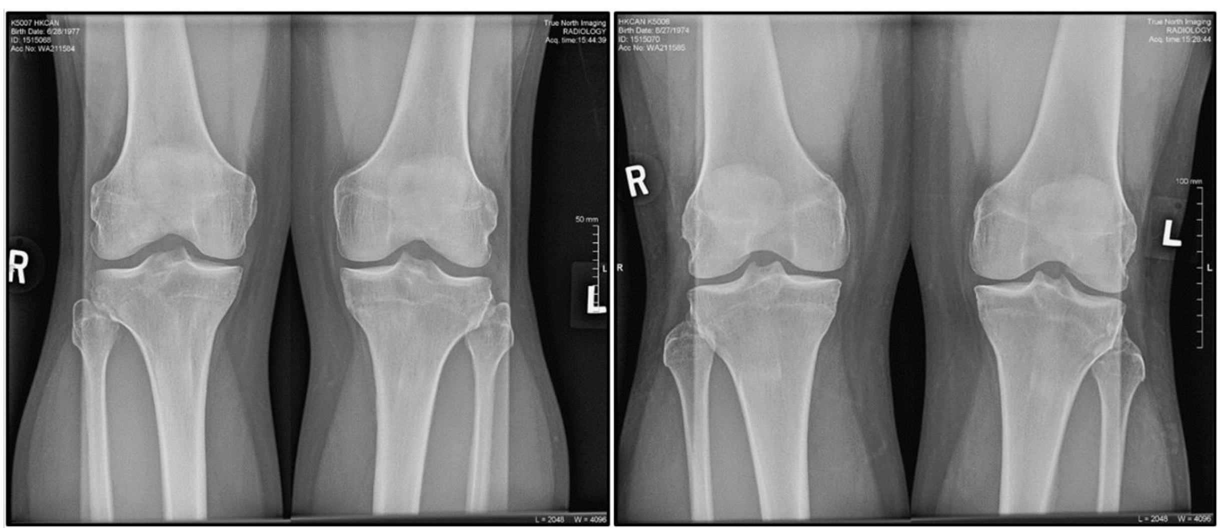

Figure 2.4 The left set of knee radiographs shows Kellgren-Lawrence grade 0 in both knees whereas the right set of knees have grade 2 in both knees, with minimal joint space narrowing but cupping of the tibial plateau resulting in spurs at the joint midline. Images from a non-thesis study.

2.2 Osteoarthritis development: Loading of unconditioned tissue

There is an increased prevalence of knee OA linked to high knee flexion exposure. Occupations which require kneeling more than thirty times a day or with heavy loads (>10 kg) have odds ratios of 2.3 and 2.9 for knee OA development (Coggon et al., 2000; Rytter et al., 2009). In addition, individuals who kneel for more than one hour per day have an odds ratio of 3.0 for knee OA development (Kirkeshov Jensen, 2008).

A theory of knee OA development resulting from high knee flexion exposure is that these postures stress “unconditioned” tissue with high joint contact forces (Andriacchi et al., 2004; Andriacchi and Favre, 2014). When the knee joint is in flexion between 30-120º there is a roughly linear increase in lateral femoral condyle posterior translation (Johal et al., 2005). This flexion range represents the common span over which most activities of daily living (ADL) occur (Kinney et al., 2013; Mündermann et al., 2008). However, above 120º of flexion, rapid posterior translation of both the medial and lateral femoral condyles occurs (Figure 2.5).

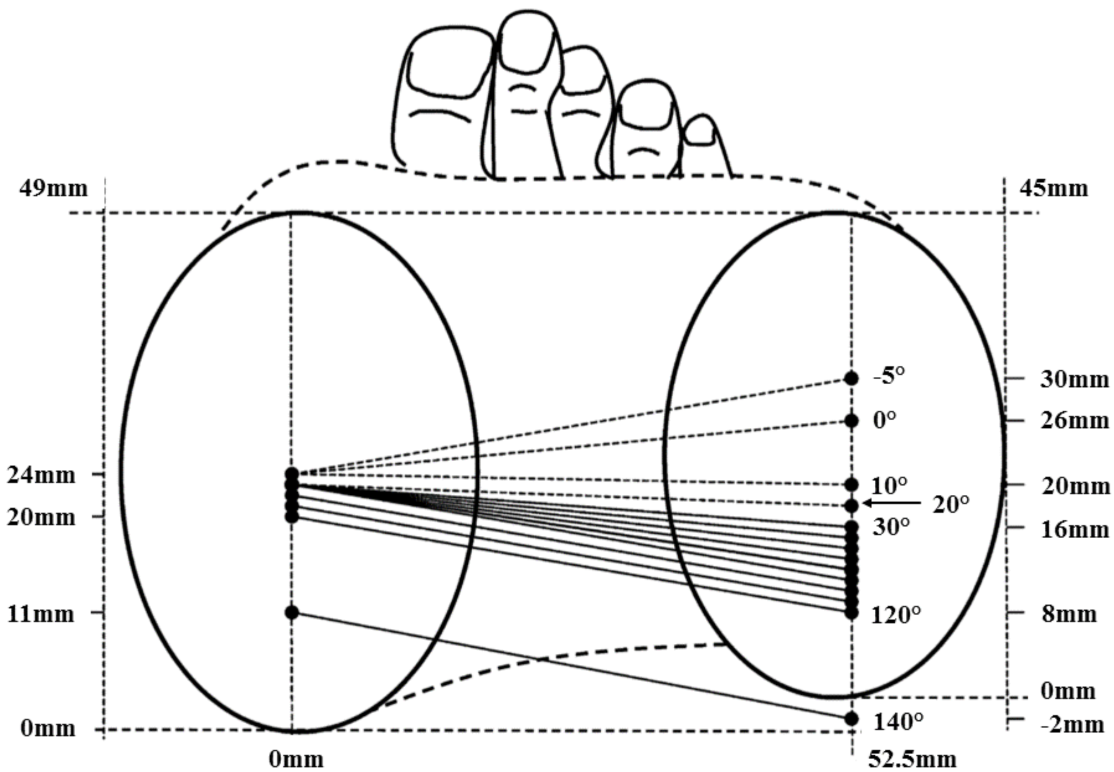

Figure 2.5 Movement of medial and lateral femoral condyles relative to tibia: right knee; weight bearing males; neutral tibial rotation. Broken lines depict adjusted values for transfer from the flexion facet center to the more anterior extension facet. Image reproduced from (Johal et al., 2005) under individual Elsevier (RightsLink) license #: 3723191122593.

For example, ten 20-40 year old Caucasian males performed knee flexion, in an open MRI, from -5-120º resulting in 21.1 ± 4.7 mm of posterior translation of the lateral femoral condyle, whereas from 121-140º, an additional 9.8 ± 2.1 mm occurred (Johal et al., 2005). These data agree with previous *in vivo* findings from ~30 year old Japanese males, where passive flexion to 162º was achieved with ~28mm of posterior translation occurring at the midpoint of the femoral condyles compared to standing (Nakagawa et al., 2000). Additionally, when the knee joint is in high flexion, condylar contact area decreases from 6.3 ± 1.4 mm^2 and 5.4 ± 0.7 mm^2 to 4.7 ± 0.9 mm^2 and 3.3 ± 0.7 mm^2 in the lateral and medial compartments compared to standing

(Yao et al., 2008). The posterior translation and decreased contact area resulting from high knee flexion causes loading of articular cartilage and meniscus in areas that are not stressed in most ADLs. Although knee OA patient data supports this theory of disease development, there is limited biomechanical data for modelling joint exposure in the high knee flexion range.

2.3 Joint and tissue damage of the knee joint

Cyclic compressive exposure is the most widely accepted cumulative mechanism for knee joint injury (Bevill et al., 2010; Seedhom, 2006). Healthy knee joint tribology generally results in minimal shear forces acting on articular cartilage in anterior-posterior (AP) or medial-lateral (ML) directions as low coefficients of friction exist between femoral condyles and the tibial plateau (Sasazaki et al., 2006; Swann and Seedhom, 1993). However, joint level injuries, such as anterior cruciate ligament (ACL) or meniscal tearing, commonly result from acute shear loading exposures in plant-pivot sports such as rugby and soccer (Gianotti et al., 2009), or in stair ambulation (Smith and Barrett, 2001; Tomatsu, 1992). In ACL deficient knees, the meniscus and cartilage is particularly susceptible to AP shear damage as meniscal suture tear out can occur at shear forces of ~108 N or cartilage fissures can result from shear loads of ~40 N applied directly to tissue (Atkinson et al., 1998; Fisher et al., 2002). Although these data are compelling for knee joint and tissue damage in typical activities of daily living, injury pathways could be different for high knee flexion exposure.

Shear loading of the knee joint in high knee flexion postures is poorly understood but has been identified as a likely cause of prosthetic loosening (Thambyah and Fernandez, 2014), and is a critical measure in tissue engineering and remodeling (De Sanctis et al., 2015; Whitney et al., 2017). Given the small tibiofemoral joint contact area in high knee flexion compared to standing (Yao et al., 2008), cartilage level shear forces could be substantially increased if model estimates of tibial compression augment frictional coefficients (Nagura et al., 2006). In addition, reported peak joint level shear forces during high knee flexion activities range from 0.27-0.34 BW (Thambyah, 2008; Thambyah and Fernandez, 2014) to 0.95 BW (Zelle et al., 2009) when muscle force contributions were or were not accounted for respectively. Given that both compressive and shear loads can result in injury or joint damage, accurate reporting of joint level compression and shear forces is necessary for future implant and tissue engineering design.

2.4 Musculoskeletal modeling of the knee

Motivated by a need for greater understanding of injury and disease progression, researchers have developed physical and computational models of knee function. Mechanical testing of human and animal tissue has provided many parameters required for simulating joint exposures *in vitro* and *in silico*. While there are assumptions in any modeling approach, the practical and ethical limitations of obtaining joint force data *in vivo* (other than telemetric implant data) present few alternatives. Animal models have been used to measure anterior cruciate ligament (ACL) injuries (Amiel et al., 1986; Mclean et al., 2015), meniscus damage (Proffen et al., 2012), bone remodeling (Zhang et al., 2006), and mechanical tissue testing (Chaudhari et al., 2008; Haut, 1989; Keller, 1994). However, cadaveric work remains a gold standard in tissue testing (Proffen et al., 2012).

2.4.1 Muscle geometry

Experiments and dissection of cadaveric muscles has been performed to obtain tissue architecture and geometry. Popular datasets used in computational modeling of the knee are Wickiewicz et al. (1984), Yamaguchi el at. (1990), Horsman et al. (2007), and Ward et al. (2009). From these sources, muscle parameters relevant to this thesis are reported in Appendix

A. A notable limitation of the Wickiewicz et al. (1984) dataset is that data is only provided for lumped groups (e.g. knee flexors) as opposed to individual muscles. These data do not allow scaling of separate muscles to allow for subject specific anthropometrics (Anderson et al., 2007; Damsgaard et al., 2006). The listed datasets were obtained from cadaveric samples which are typically elderly. This warrants caution on physiological cross sectional area (PCSA) parameters for modeling young populations (Delp et al., 1990). Functional MRI data will likely improve the detail and age appropriateness of muscle architecture parameters but, at present, these datasets are the most comprehensive available to researchers.

2.4.2 Patellar tendon kinematics

Cadaveric testing has defined relationships between knee flexion angle and skeletal kinematics for many structures. For example, altering separate vastii muscle force levels significantly affects patellar tendon kinematics and tension (Shalhoub, 2012; Steinbrück et al., 2013). Applying low force magnitudes (62, 44, and 70 N for the rectus femoris, vastus medialis, and vastus lateralis respectively) causes mediolateral shifts of the patella up to 6 mm from 0-120º of knee flexion (Shalhoub and Maletsky, 2014). Patellar tendon moment arm length has also been quantified by numerous researchers from 0-90º of knee flexion (see the review by Tsaopoulos, Baltzopoulos, & Maganaris 2006) with a recent study (Fiorentino et al., 2013) using real-time MRI to validate *in vivo* patellar tendon moment arms from prior work (3-4 cm over 0-90º range). This MRI study also reported the range of knee motion to 125º of flexion—still 20-40º below end range of high flexion postures (Acker et al., 2011; Nakagawa et al., 2000)—where the moment arm decreased to ~1 cm (Fiorentino et al., 2013). However, no patellar tendon moment arm data exists for high knee flexion postures.

2.4.3 Tibiofemoral impact

During ambulation the knee experiences impact forces at heel strike and sustained stress during the support phase of gait. When injury or disease is present in the knee, viscoelastic properties of tissues can be compromised and impact forces can increase. In an erect osteoligamentous knee specimen, compression increased 13% (radial cut of lateral and medial menisci), 21% (menisci removed), 35% (articular cartilage removed), and 79% (conventional total knee arthroplasty) due to respective tissue alterations (Hoshino and Wallace, 1987). This highlights the importance of tissue for cushioning impact loads in the non-pathologic knee. These magnitudes of tissue attenuation have been supported in porcine models; following meniscectomy compressive stress increased 2.2-5.2 times compared to intact testing depending on valgus or varus alignment in an un-flexed knee (Fukuda et al., 2000). The effects of OA tissue changes can increase knee impact data as much as 24% compared to a Kellgren-Lawrence (KL) scale 0 knee (Hoshino and Wallace, 1987; Kellgren and Lawrence, 1957). With increased stress due to reduced contact area in high knee flexion postures these effects could be further amplified, but no experimental testing to date has been completed.

2.4.4 Mechanical testing of cadaveric knees

Many *in vitro* knee testing devices are based off of the Oxford knee jig design (Zavatsky, 1997). The Oxford jig allowed flexion/extension and ab/adduction at the femoral and tibial attachment points as well as vertical translation of the femur relative to the tibia (Figure 2.6). However, the Oxford jig was designed for use with an osteoligamentous specimen, therefore, there are no considerations of muscle force. Modern Oxford-type simulators use pulley assemblies to simulate patellar tendon loads in knee specimens (Van Haver et al., 2013; Verstraete and Victor, 2015). Additionally, computer controlled servo-hydraulic simulators are currently in use; three research groups are noted in the following for reference.

The University of Kansas has mechanical simulators to assess quadriceps and hamstring muscle load influence on patellofemoral kinematics (Shalhoub and Maletsky, 2014) and dynamic activities with a five degree of freedom knee (Halloran et al., 2010). The simulator of Shalhoub & Maletsky (2014) tested quadriceps loads up to ~600 N from 15-120º of knee flexion with one degree of freedom. Alternatively, dynamic activities of walking and cutting maneuvers have been simulated up to knee flexion angles of ~45º with combined quadriceps loads of ~3 000 N (Halloran et al., 2010).

The University Hospital of Munich has a dynamic knee simulator which can replicate quadriceps and hamstring forces for total knee arthroplasty research (Steinbrück et al., 2013). This simulator produces a maximal quadriceps force of 400 N in flexion and 600 N in extension for surgical component testing. This simulator can apply muscle and hip moments within a 20-120º range of knee flexion.

Two groups in Belgium have simulators which are used to test surgical protocols for arthroplasty assessment (Heyse et al., 2014; Victor et al., 2009). Both simulators are designed for testing 10-120º of knee flexion with quadriceps and hamstring loads up to 180 N and 130 N.

Servo-hydraulic simulators can provide unparalleled experimental control to assess the influence of muscle activation patterns and loads on knee structures. These devices also provide critical data for design and surgical methods of total knee arthroplasty. Unfortunately, the physical size of mechanical controlling equipment makes many simulators unable to attain high knee flexion postures. Therefore, limited *in vitro* experimental testing has been completed in high knee flexion, none of which investigated tibiofemoral compressive loads (Shalhoub, 2012).

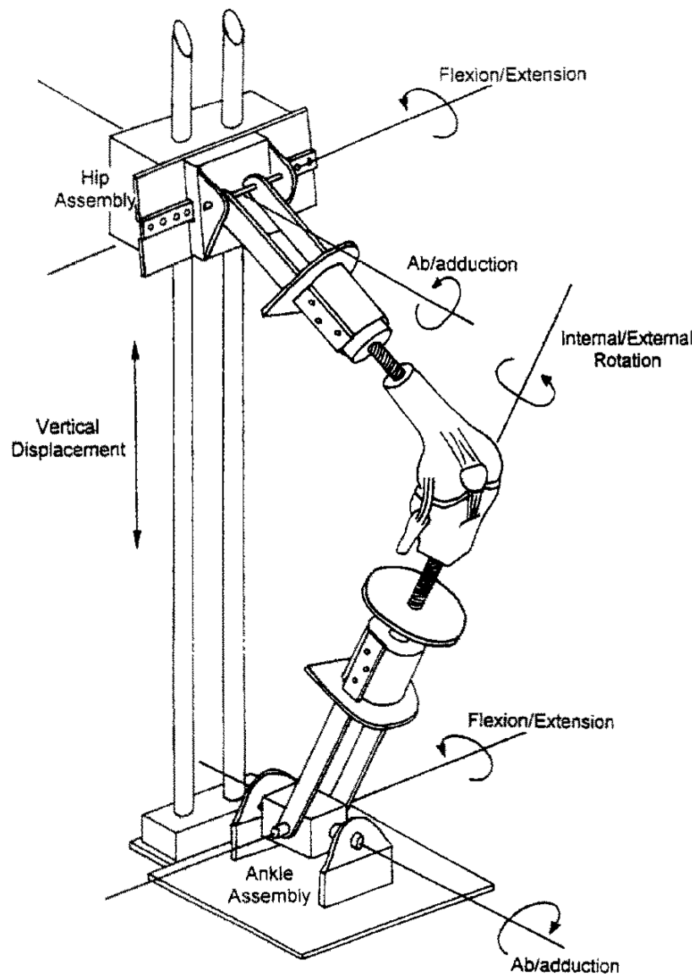

Fig. 1. The Oxford Knee-Testing Rig. The ankle assembly allows flexion/extension, abduction/adduction, and internal/external tibial rotation. The hip assembly allows flexion/extension and abduction/adduction. In addition, the hip assembly can move vertically relative to the ankle assembly.

Figure 2.6 Oxford style knee jig. Image reproduced from (Zavatsky, 1997) under individual Elsevier (RightsLink) license #: 3723191122593.

2.4.5 Computational models

Computational models provide researchers with a high level of control as individual parameters and model complexity can be tailored to best suit the research question. With the continuing increase of computational power, *in silico* approaches to human movement analysis have risen in popularity. *In silico* methods are also appealing due to the limited sample size and availability of gold standard *in vivo* telemetric datasets (Fregly et al., 2012; Taylor et al., 2017) and/or the monetary cost and biofidelity of pursing *in vitro* methodologies. The full knee flexion MSK model developed in this thesis, addressing the global objective of estimating tibial contact forces, uses static optimization (SO) to distribute muscle forces (Chapter 5). However, three generalized modeling approaches within the MSK space will be briefly discussed below: finite element (FE), Hill-type, and optimization approaches.

2.4.5.1 Finite element

Finite element models use 3D polygon meshes to represent tissue volumes (e.g. meniscus, cortical bone, ligaments) with each having defined material properties (Donahue et al., 2002). Knee FE models are primarily used for joint contact force modeling in implant design and testing (Halloran et al., 2010; Knight et al., 2007). A divergent feature of FE models, compared to Hill-type or optimization MSK models, is that they model the stress and deformation of tissues. Ideally, FE models would be applied in series with MSK joint force estimations to gain further insight into mechanical response of human tissue. For example, SO could be used as part of the computation for knee joint forces, then, an FE model could be used to characterize articular cartilage, bone, and meniscus loading.

Many industries and researchers use the commercially available software Abaqus (Dassault Systèmes, Cedex, France) to define and run FE models. Although FE methods can generate accurate results (< 2 mm translational and < 3º rotational root mean squared error compared to joint capsule cadaveric testing) they provide little understanding of the overall system kinesiology (Halloran et al., 2010). As well, quantification of external and internal loading exposure and skeletal kinematics are critical for accurate FE predictions. Currently there is insufficient foundational data available for FE use in high knee flexion ranges.

2.4.5.2 Hill-type

Hill-type models use EMG and muscle architecture parameters to estimate individual muscle forces based on a three element mechanical system (Figure 2.7 and Eq 2.1). When combined with geometric models of skeletal motion, muscle forces are applied about respective LoA and moment arms to generate internal forces and moments. A strong argument in favor of Hill-type or EMG-driven models is the data source; a participant's own muscle activation. Electromyographic data are collected 'downstream' from the CNS and contain additional sensory feedback in the signal (Cheung et al., 2005). This implies that individual muscular activation strategy is accounted for in muscle force estimates. However, Hill-type models require confidence in muscle fiber, tendon, and passive tissue length/force parameters for accurate estimations. Also, no reliability studies have been performed on EMG measurements in high flexion postures that likely result in considerable muscle length changes and motor unit shift. Many of these parameters have not been verified in high knee flexion postures and would require experimental validation prior to confident implementation.

$$F^{mt}(\theta, t) = f(a(t), l^{mt}, v^{mt}, \sigma_{max}, l_o^m, T_s^m, \phi_o) \qquad \textbf{Eq 2.1}$$

where F^{mt} is the musculotendinous force, θ is the angle of the joint of which the musculotendinous unit articulates, t is time, $a(t)$ is conditioned EMG with considerations for activation dynamics, l^{mt} is the length of the musculotendinous unit, v^{mt} is the velocity of musculotendinous unit fibers, σ_{max} is the maximal isometric muscle force, l_o^m is the musculotendinous unit's length at which optimal muscle fiber overlap occurs, T_s^m is the tendon slack length, and ϕ_o is the pennation angle between the muscle fiber and tendon (Buchanan et al., 2004).

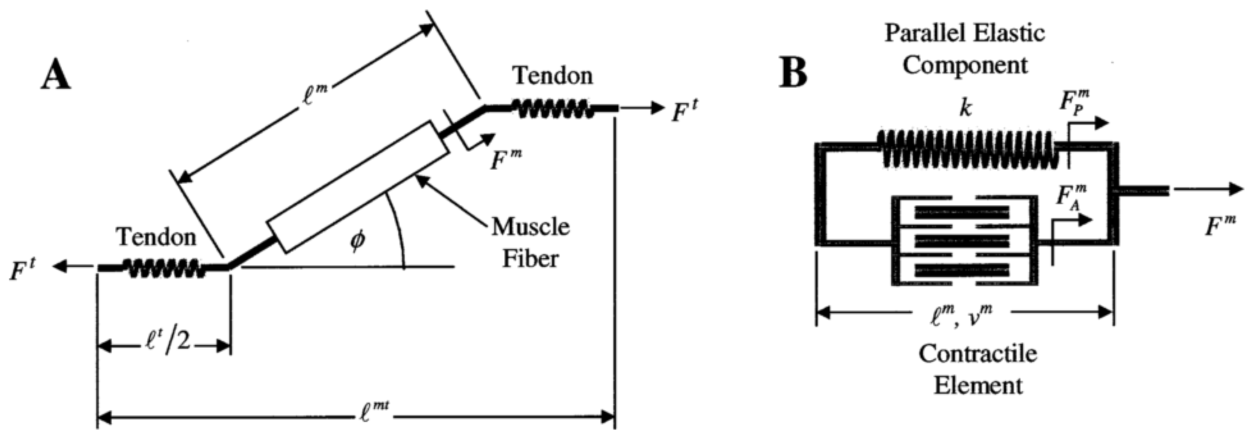

Figure 5 — (A) Schematic of muscle-tendon unit showing muscle fiber in series with the tendon. Note the pennation angle, ϕ, of the muscle fiber relative to the tendon and that the total tendon length, ℓ^t, is twice that of the tendon on either end of the muscle fiber, $\ell^t/2$. (B) Schematic of muscle fiber with the contractile element and parallel elastic component. The nonlinear tendon stiffness is given by k. The force produced by the contractile element, F^m, is a function of ℓ^m and v^m, while the tendon force, F^t, is a function of ℓ^t. The total muscle fiber force, F^m, is the sum of $F_A{}^m$ and $F_p{}^m$.

Figure 2.7 Schematic of muscle-tendon unit with Hill-type muscle model parameters highlighted in original caption. Image reproduced from Buchanan et al. (2004) under individual Human Kinetics license #: 3738370256215.

Many of the parameters required as inputs for Hill-type models are difficult to experimentally validate. Currently, there is no method that can simultaneously measure musculotendinous unit length, fiber pennation angle, motor unit activation, and filament overlap with respect to joint angles *in vivo*. Tendon stress/strain relationships also lack biofidelic testing as axial strain is the most common experimental protocol (Schatzmann et al., 1998; Yang et al., 2010). This ignores changes to tissue properties resulting from tendons wrapping around soft and osseous tissue (Charlton and Johnson, 2001; Herzog and Read, 1993; Horsman et al., 2007). No model exists which can account for connective tissue responses which occur during force production across individual muscle fibers, nor the interaction of fiber types and fascia.

2.4.5.3 Optimization

Optimization approaches contrast with EMG-driven models in that a constrained mathematical equation is solved to determine an 'optimal' distribution of muscle forces satisfying mechanical equilibrium or other cost function. Applications in kinesiology typically involve cost functions which minimize physiological or neuromechanical based quantities, such as metabolic cost or muscle stress (Anderson & Pandy, 2001; Crowninshield & Brand, 1981). Any number of muscles can be modeled using optimization—35 in Arnold et al. (2010) to over 80 in Damsgaard et al. (2006)—however this capability comes at a substantial cost; simplifying the central nervous system (CNS) control to a deterministic mathematical function.

Adjustments to constraints for specific tasks can increase component validation of optimization methods, but verification almost always requires comparison to EMG data (Dickerson, 2005; Dowling, 1997; Hicks et al., 2014). This begs the question, "why not use EMG as an input in the first place?" One must have confidence in muscle architecture parameters for an EMG-driven model to be accurate, and at present, this is not possible for high knee flexion postures. Additionally, typical EMG comparisons consist of onset/offset congruence more than magnitude comparisons (Hicks et al., 2014). Therefore, the model presented in this thesis for high knee flexion used SO to estimate muscle forces.

Optimization models for human movement generally consist of three types: static optimization (SO), modified static optimization (MSO), and dynamic optimization (DO) (Ackermann, 2007; Sharif Shourijeh, 2013). Static optimization is a computationally efficient approach which solves for the objective function instantaneously (i.e. no consideration for previous or future solution points). As a result, SO cannot be used for time-integral objective functions such as minimizing metabolic cost (Anderson and Pandy, 2001).

MSO is similar to SO, except that muscular contraction and activation dynamics are added to the optimization process (Ackermann, 2007). This allows for non-linear constraints to solution bounds for neural excitations and kinematics. However, MSO requires finite difference derivatives of the muscle force and activation in computing the muscle speed, activation, and excitation, which potentially leads to numerical issues, such as instability and truncation errors. Additionally, as previously mentioned, there is concern regarding the confidence one should have in using Hill-type parameters in high knee flexion postures.

Dynamic optimization is the most intensive approach used in simulation/predictions of human movement and requires numerical integration of dynamical systems of equations. This can also be referred to as 'forward dynamics' (Buchanan et al., 2004). Dynamic optimization uses time-integral objective functions to minimize error over the entire movement (Ackermann, 2007; Anderson and Pandy, 2001). The advantage of DO is that smooth transitions between solution points are paramount and non-physiological solutions, such as a muscle activation switching very low to very high activation within 1 ms, are avoided. Added biofidelity comes at a considerable complexity and computational cost; below is an example calculation time for one trial of walking Table 2-1.

Table 2-1 Approximate calculation times and number of variables for various approaches of optimization to solve a single walking trial for one participant (Ackermann, 2007).

Method	Computation Time	Optimization Variables
Static Optimization	5.3 s	8
Modified Static Optimization	12.9 s	8
Dynamic Optimization	Multi-day	+400

The strength of optimization based models, compared to EMG-driven, is their ability to simulate data and outcome testing compared to *in vivo* methods as models can be adjusted *in silico*. These benefits are compounded with a reduction in the level of complexity and time required for experimental data collection as EMG procedures are absent. Those critical of optimization argue that simplifying the central nervous system to a cost function is unreasonable and question their validity in corner case testing (e.g. toe-in gait modification (Shull et al., 2013)). Additionally, few cost functions solve with appropriate levels of co-contraction shown in experimental EMG studies unless constraints are applied (Dickerson et al., 2007).

2.5 Measurement and modelling of EMG

Improvements and availability of telemetric surface and fine-wire recording hardware have made it increasingly easier to attain high quality EMG data during dynamic movement. These hardware improvements reduce participant encumbrance and decrease experimental time as MVCs and movement trials are less prone to low-frequency wire movement artifact or pulling. The result is more repeatable trials, a wider range of testable movements, and improvements to signal quality. Despite these advancements, issues remain when using EMG as a data source, namely: noise (Clancy et al., 2002); cross-talk between muscles (Howard et al., 2015); and normalization method (Lehman and McGill, 1999; Rutherford et al., 2011). Between bi-polar electrode interfaces there is the concern of half-cell potentials, or the impedance of electron flow between each pickup. Modern electrodes consist of Ag-AgCl leads which has greatly improved electrical stability compared to stainless steel electrodes of the past (Ciccotti et al., 1994). Similarly, electrode impedance issues have been largely mitigated with modern hardware and standardized preparation/location protocols such as the SENIAM project (Hermens et al., 2005).

Cross-talk is unavoidable with surface EMG, but negligible with indwelling EMG (Bogey et al., 2000; Fuglevand et al., 1992). Due to the pickup volume of surface EMG, signal content from neighboring muscles will be measured in addition to the muscle of interest. In the relatively large muscles of the lower limb (Wren et al., 2006), this is less of an issue than in trunk (e.g. electrocardiogram interference (Drake and Callaghan, 2006)) or upper extremity muscles (Kamavuako et al., 2013). If cross-talk is a concern for the muscle of interest, cross-correlation between individual EMG sites is a standard method used to assess signal similarity (Winter, 2009). However, it is best to minimize cross-talk with careful electrode placement.

Controversy exists on normalization methods for EMG reporting during dynamic movement. Within this thesis, static MVC trials to attain normalization values for individual participants was used. This is an accepted procedure for dynamic EMG assessment by many researchers (Hermens et al., 2005; Lehman and McGill, 1999). Although peak or a mean of peak values from dynamic tasks can be used as a normalization method, evidence suggests that variance ratio, interclass correlations, and overall reproducibility of EMG signals is improved using isometric MVCs (Burden and Bartlett, 1999; Knutson et al., 1994; Rutherford et al., 2011).

The high knee flexion movements performed in this thesis were not performed quickly (~1 Hz) and do not require the normalization considerations inherent to rapid movements such as cycling or running (Ball and Scurr, 2013). Additionally, prior work in our laboratory (Kingston et al., 2016) has shown peak EMG values during high knee flexion activities to be below 100 %MVC during kneeling transitions using standardized isometric contractions (Appendix B).

2.6 Issues with current knee models for use in high flexion

A number of limitations in existing knee joint MSK models which prevent their use in high knee flexion postures: (1) thigh-calf contact; (2) lower limb EMG data; (3) muscle moment arm distances; and (4) tibiofemoral and patellar kinematics above 120º of flexion. Currently, four 2D models exists which consider force transfer between the thigh and shank (Caruntu et al., 2003; Hirokawa and Fukunaga, 2013; Pollard et al., 2011; Zelle et al., 2009). These studies had one or two high knee flexion postures—dorsiflexed kneeling (Hirokawa and Fukunaga, 2013; Zelle et al., 2009) and squatting (Caruntu et al., 2003; Pollard et al., 2011)—performed with ten or fewer subjects (Pollard et al., 2011; Zelle et al., 2007).

Outside of our research group, there is a single study which reports high knee flexion EMG data from a simulated low-seam mining task (Gallagher et al., 2011). This study only reports peak muscular activations from three vastii and two hamstring muscles when moving a 11.3 kg cinderblock, making these data inappropriate for unloaded or time series comparison. Therefore, there is a need for more fulsome time-series EMG data in high knee flexion postures.

Muscle moment arm data is limited in high knee flexion postures as the most comprehensive datasets only reported moment arms of a cadaveric specimen to ~130º of knee flexion (Buford et al., 1997; Herzog and Read, 1993). As well, *in vivo* moment arm data is only available for the rectus femoris at 20-120º of knee flexion through the use of real-time MRI (Fiorentino et al., 2013). However, there is a wealth of data from cadaveric samples at ~0-100º of knee flexion for major lower limb muscle moment arms (Gerus et al., 2013; Tsai et al., 2012; Tsaopoulos et al., 2007; Wilson and Sheehan, 2010). Until muscular moment arm data in high knee flexion postures are available through MRI or other imaging methods, geometric models of the lower limb are required to estimate tendon attachment sites using wrapping surfaces (An et al., 1984a; Pandy, 1999; Spoor and Leeuwen, 1992).

The most troubling issue which exists in current computational knee modeling is insufficient verification (Anderson et al., 2007; Hicks et al., 2014). Two situations currently exist: 1) *in vitro* models are tested without comparison to physiological loading magnitudes and data is extrapolated to *in vivo* conditions and 2) i*n silico* models are developed and used without comparison to gold standard, EMG activation profiles, or physiologically based muscle architecture parameters. Many *in vitro* models (Shalhoub & Maletsky, 2014; Steinbrück et al., 2013; Wünschel, Leichtle, Obloh, Wülker, & Müller, 2011) use tensile forces <300 N in quadriceps and <200 N in hamstrings muscles when simulating knee movements. These loads are below *in vivo* measured forces in the patellar tendon (~2200 N during a squat) and do not represent physiological magnitudes (Finni, Komi, & Lepola, 2000). Cadaveric tissue quality likely limits the tensile force applied, but a recent study applied ~1250 N through the patellar tendon (Verstraete and Victor, 2015). This quadriceps force was required to maintain mechanical equilibrium in an Oxford-type simulator when a specimen simulated a squat movement

(Verstraete and Victor, 2015). Therefore, the use of low tensile forces in some *in vitro* testing may not hold *in vivo* relevance.

A brief review of two of the most commonly used optimization and EMG-driven *in silico* knee models will highlight their limitations to high knee flexion postures. OpenSim was created from the work of Delp et al. (1990) and evolved into the first multi-institution MSK model heavily used in biomechanics. A popular knee model in the OpenSim architecture was developed by Arnold et al. (2010). Her lower limb model has 35 muscles with cylindrical wrapping surfaces for the gastrocnemii and quadriceps musculature about a 1 DoF knee (flexion/extension). Muscle activation predictions from this model have been verified against EMG in gait and the geometric model has been the foundation for many MSK models using OpenSim (Arnold et al., 2010; Hicks et al., 2014; Millard et al., 2013; Stylianou et al., 2013). For example, Sartori et al. (2013) assessed the ability of their EMG driven model, which used Arnold et al. (2010) MSK geometry and muscle parameters, to estimate knee flexion moments in gait with 0.98 R^2 and 0.08 normalized RMSD compared to telemetric *in vivo* knee data (Fregly et al., 2012). These contributions to the knee modeling community are substantial but issues exist for generalizing this application to other movements.

The AnyBody model (AnyBody Technology A/S, Salem, MA, USA) uses a polynomial SO objective function (Eq 2.2), similar to Crowninshield & Brand (1981), to estimate muscle forces without EMG data (Damsgaard et al., 2006). The ‘geometric knee’ model used in AnyBody software is a 6 DoF joint that results in marked differences when directly compared to Arnold et al. (2010). The AnyBody knee allows the use of subject specific 3D MRI data to scale bone and muscle attachments; unlike anatomical marker scaling in OpenSim. These differences contribute to an average increase in flexion moment of 58 Nm with peak differences occurring

18% of gait cycle earlier (stance phase) in OpenSim when compared to the AnyBody knee model (Sandholm et al., 2011). This occurred even though the AnyBody knee was imported into OpenSim to maintain generic model scaling and to provide consistency of optimized muscle forces. While there are no comparisons available between the OpenSim and AnyBody models using telemetric knee implant data, those critical of either software commonly point to inaccurate co-contraction predictions and/or underestimations of joint contact forces (Modenese et al., 2016).

$$G(F^M) = \sum_{i=1}^{n^M} \left(\frac{f_i^M}{N_i}\right)^P \qquad \textbf{Eq 2.2}$$

where G is the objective function (e.g. recruitment strategy of the central nervous system), F^M forces of all modeled muscles, f_i force of muscle M, N_i the strength of the muscle, and P is the *a priori* defined exponent; commonly 3 (Damsgaard et al., 2006).

Limitations of the Arnold et al. (2010) model are considerable for applications to high knee flexion: a 1 DoF knee joint, a knee flexion range of 0-100º, and a maximal muscle stress of 61 N/cm^2. This muscle stress value was taken from Delp et al. (1990) and justified as a scaled value to adjust for PCSA decrease in cadaveric specimens. Values used for maximal muscle stress vary within the modeling community from 30-88 N/cm^2 (Carbone et al., 2015; Dickerson, 2005), however physiological studies on mammalian tissue commonly report values closer to 22 N/cm^2 in guinea pigs (Powell et al., 1984) or 24 N/cm^2 in living humans (Fukunaga et al., 1996). Similarly, AnyBody applicability to high knee flexion is limited by its knee flexion range of 0-

100º, proprietary source code, and cost. Therefore, either the OpenSim or AnyBody models would ultimately require such heavy modification that a novel model was warranted.

Chapter 3 – Intersegmental contact during high knee flexion movements

Components of this chapter have been published (Kingston and Acker, 2018) or are currently accepted (Proceedings of the Institution of Mechanical Engineers, Part H: Journal of Engineering in Medicine, JOEIM-17-0153.R1), however, additional detail is provided in methodology and results sections.

3.1 Introduction

The magnitude and location of contact forces between thigh-calf (TC) and heel-gluteal (HG) structures in high knee flexion postures are critical input parameters for development of a high knee flexion joint contact model. Given the increased incidence of degenerative knee diseases in populations that regularly assume high knee flexion postures (Baker et al., 2003; Bombardier et al., 2011; Kirkeshov Jensen, 2008), further study to refine injury mechanisms by quantifying exposure is needed. A theoretical injury mechanism in high knee flexion postures is the exposure of under-conditioned tissues to high joint contact forces (Andriacchi et al., 2004; Andriacchi and Favre, 2014). However, this theory does not account for the potential unloading effect TC or HG contact may have on the joint. Therefore, the limited *in vitro* data available from testing knee joint compressive forces, up to 135º of flexion, likely over-estimate compressive forces when extrapolated to end range of motion (Hofer et al., 2012; Victor et al., 2009).

The issue of force over-estimation was first supported by Zelle et al. (2009), who used a finite element model of the knee with external TC contact forces (taken from Zelle (2007) *in vivo* data). Decreases from 4.37 to 3.07 times body weight (BW) in knee joint compression and 1.31

to 0.72 times BW in shear during a flatfoot squat movement were estimated as a result of including TC contact (Zelle et al., 2009). However, further verification of reported magnitude and location data is critical to improve estimates of joint contact forces in future computational models and to increase the variety of movements measured (Thompson et al., 2015).

A variety of high knee flexion postures exist in activities of daily living where intersegmental contact data could be used to improve estimates of loading exposure. Islamic religious practices and traditional East Asian cultural customs involve symmetric high flexion kneeling with the feet in dorsiflexion or plantarflexion (Hefzy et al., 1998; Hemmerich et al., 2006). High knee flexion squatting is also common during childcare, sport, and toileting in many cultures (Hemmerich et al., 2006; Kurosaka et al., 2002). Finally, single-leg (unilateral) kneeling is used during many occupational tasks (Gallagher et al., 2011) and is a primary shooting position used in military theater (Department of the Army, 2010).

During symmetric kneeling, TC contact force has been reported at up to 34% BW (Zelle et al., 2007) with a separate study reporting HG contact forces of approximately 11% BW (Pollard et al., 2011). However, only a dorsiflexed foot position was tested during kneeling, and there is no known intersegmental contact data for unilateral kneeling positions. Further investigation of HG contact is needed as the large moment arm results in similar knee extension moments as TC contact with considerably smaller forces (Pollard et al., 2011). Therefore, also including HG contact forces in future modelling efforts will improve the biofidelity of tibial contact force estimates.

Prior work on TC contact involved assessment only in the sagittal plane with pressure sensors not attached to segments. Small sample sizes (10 participants) also prevented the investigation of sex differences in prior work (Pollard et al., 2011; Zelle et al., 2007). Given the anthropometric (Power and Schulkin, 2008) and flexibility differences between sexes (Krivickas and Feinberg, 1996), females may be exposed to lower joint compressive loads as a result of increased TC and HG contact in high flexion postures. In addition, females generally have a higher distribution of body-fat in the pelvic and thigh region (Cnop et al., 2003; Nielsen et al., 2004) which may also result in different intersegmental loading when compared to males. Past studies have relied on manually positioning, or having participants hold, pressure sensors in place while performing movement trials (Pollard et al., 2011; Zelle et al., 2007). This could reduce repeatability between trials, and did not allow for unilateral postures as larger pressure sensors designed for seating applications (Conformat model #5330, Tekscan, South Boston, MA, USA) were used. Finally, prior studies used sensors with a low spatial resolution of 0.5 sensels per cm^2, and were collected at a maximum of 8 Hz (Pollard et al., 2011; Zelle et al., 2007).

It is assumed that variation in participant anthropometrics would partially explain variation in thigh-calf contact parameters. A single previous study reported moderate to strong bivariate correlations between TC contact parameters (onset, max angle, and total force) and anthropometrics (thigh and shank circumferences, BMI, and participant weight) during a heels-up squat and dorsiflexed kneel (Zelle et al., 2007). However, such variables have not been used in the estimation of TC contact forces and collinearity between variables was not reported. In addition, the participant sample was small and predominantly male (8 male and 2 female), which limits the applicability of such findings to other populations (Zelle et al., 2007). Because the strength of intersegmental contact estimation and the collinearity between various anthropometric measures is unknown an investigation of anthropometrics-based regressive models to estimate TC contact parameters is warranted.

Overall, this study was designed to accomplish two goals: 1) quantify five intersegmental contact parameters from six high knee flexion postures and 2) develop anthropometric based regression equations to estimate contact parameters.

3.1.1 Definition of intersegmental contact parameters

Five parameters were identified to represent critical inputs for inverse dynamic calculations in high knee flexion postures. These parameters were: 1) the knee flexion angle at which TC contact begins ('onset'), 2) maximum knee flexion range ('max angle'), 3) contact force magnitude ('force'), 4) contact force area ('area'), and 5) longitudinal CoF location. A secondary objective of this component was to investigate sex differences within these parameters.

3.1.2 Anthropometric regression of intersegmental contact parameters

There were two objectives in investigating the estimation accuracy of anthropometric variables: 1) to define Pearson correlations between several anthropometric measurements and TC contact parameters and 2) to assess the accuracy with which these parameters could be estimated using multiple linear anthropometric models. Anthropometric measures (predictor variables) were height, mass, BMI, and the following measurements for both the thigh and shank: length, circumferences (proximal, mid, distal), and skinfold thickness. Intersegmental contact parameters (outcome variables) were onset, max angle, and three parameters measured at maximum knee flexion: force, longitudinal CoF location, and area. For these last three parameters, max angle was also included as a predictor variable. Based on Pearson correlations reported previously (Zelle et al., 2007), we hypothesized that linear regressive models would: A) have a strong fit with onset, total force, CoF and contact area data; B) regressive models would have a moderate fit with max angle data.

3.2 Methodology

3.2.1 Participants

An *a-priori* power analysis was performed using mean and standard deviation data from Zelle et al. (2007). The analysis indicated that seventy two participants (36M/36F) would be required to achieve a 0.8 power level (beta) with: 5 predictor variables, an estimated effect size of 0.2 (0.15 medium - Cohen, 1992), and $\alpha = 0.05$. This sample size was determined using G*Power 3.1.7 software (Faul, 2013). During the study progression, it became apparent that the reported variability underestimated distributions present in this sample, likely due to the comparatively small sample in Zelle et al. (2007). Therefore, a total of twenty-eight male and thirty female participants (Table 3-1) were recruited from a sample of convenience in the university's student body. Exclusion criteria consisted of any low back, or lower limb injury within the past year that required medical intervention or time off from work for longer than three days, and any history of surgical interventions to the back or lower limb. Only one participant was not right leg dominant. Each participant read and signed an informed consent form approved by the university's research ethics board.

Table 3-1 Mean (SD) descriptive and anthropometric participant information of original sample.

Parameter	Female (n = 30)	Male (n = 28)	Total (n = 58)
Age (yrs)	21.00 (3.8)	23.70 (3.8)	22.33 (4.00)
Height (m)	1.63 (0.06)	1.77 (0.07)	1.70 (0.10)
Mass (kg)	61.67 (10.26)	77.15 (15.60)	69.15 (15.15)
BMI (kg/m^2)	23.25 (3.84)	24.57 (4.08)	23.89 (3.98)
Thigh Length (m)	0.39 (0.05)	0.40 (0.03)	0.40 (0.04)
Proximal Thigh Circumference (m)	0.56 (0.06)	0.58 (0.08)	0.57 (0.07)
Mid-Thigh Circumference (m)	0.51 (0.06)	0.54 (0.08)	0.52 (0.07)
Distal Thigh Circumference (m)	0.39 (0.05)	0.40 (0.03)	0.40 (0.04)
Thigh Skinfold (mm)	32 (12)	19 (13)	26 (14)
Shank Length (m)	0.37 (0.03)	0.40 (0.03)	0.39 (0.03)
Proximal Shank Circumference (m)	0.33 (0.03)	0.34 (0.03)	0.33 (0.03)
Mid Shank Circumference (m)	0.34 (0.03)	0.37 (0.04)	0.36 (0.04)
Distal Shank Circumference (m)	0.20 (0.02)	0.22 (0.02)	0.21 (0.02)
Shank Skinfold (mm)	18 (11)	13 (12)	16 (11)

3.2.2 Experimental protocol

Participant height and segmental anthropometrics (Table 3-1), from the right lower limb, were measured before instrumentation. Participant mass was calculated from force plate data during a static calibration trial. Thigh and shank skinfold measurements were taken at the midpoint between the inguinal fold and the anterior surface of the patella and the medial aspect of maximal shank girth respectively (International Society for the Advancement of Kinanthropometry, 2001) as a gross representation of adiposity. Thigh length was measured as the distance between the palpated greater trochanter and lateral femoral condyle. Thigh circumference measurements were taken at three distances from the greater trochanter: 10% (proximal), 50% (mid), and 90% (distal) of thigh length. Shank length was measured as the distance between the palpated lateral tibial condyle and malleolus with circumferences measured at the same distances, from the lateral tibial condyle, as the thigh. A generic measure of participant flexibility was not quantified as there are no verified and reliable protocols established for this measure.

Following preparations for kinematic tracking, participants completed a static standing trial, followed by knee and hip functional joint center trials (Besier et al., 2003b; Camomilla et al., 2006). Then, after conditioning (see section 3.2.3), a pressure sensor was attached to the posterior right thigh (Figure 3.1). Participants first observed the high knee flexion movements, performed by the researcher, and then practiced until they could perform each comfortably. Five repetitions of the following six movements (Figure 3.2) were completed in a fully randomized order: heels-up squat (HS), flatfoot squat (FS), dorsiflexed kneel (DK), plantarflexed kneel (PK), dorsiflexed unilateral kneel (DUK), and plantarflexed unilateral kneel (PUK). Each trial took 6 seconds to complete and consisted of stepping onto embedded force plates, descending to end range of motion, and statically holding the position. Participants moved at a self-selected speed with movement instructions of: step with the right foot first followed by the left (all movements); kneel onto the right knee during the transitional phase (Figure 3.1 for kneeling movements); then assume the final posture (Figure 3.2). When performing unilateral kneeling movements, participants were instructed to support the majority of their body weight on the right leg in the static phase of these positions similar to techniques used in military theater (Department of the Army, 2010).

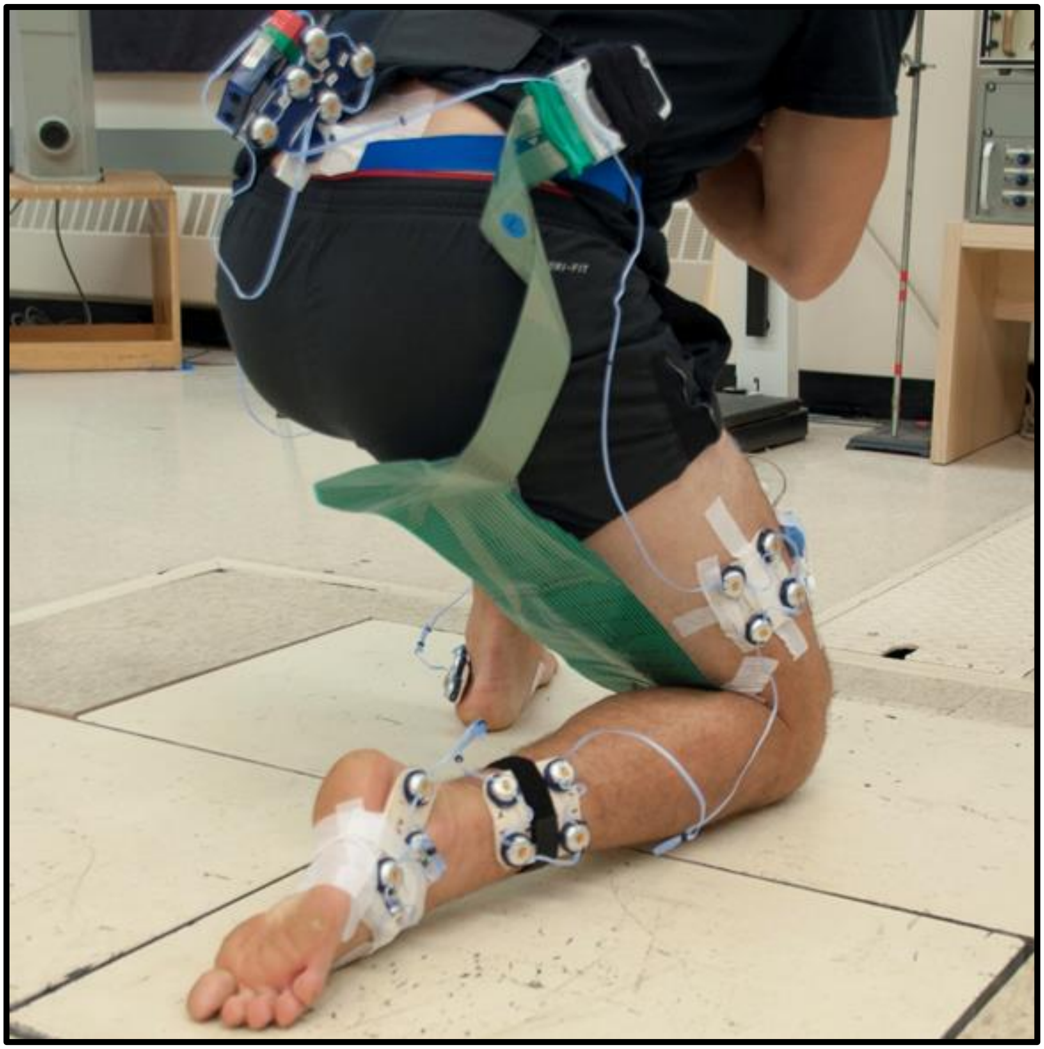

Figure 3.1 Participant performing a transition to kneeling with the pressure sensor (3005E) attached to the posterior thigh and positioned so the edge closest to the knee joint entered the popliteal fossa upon flexion.

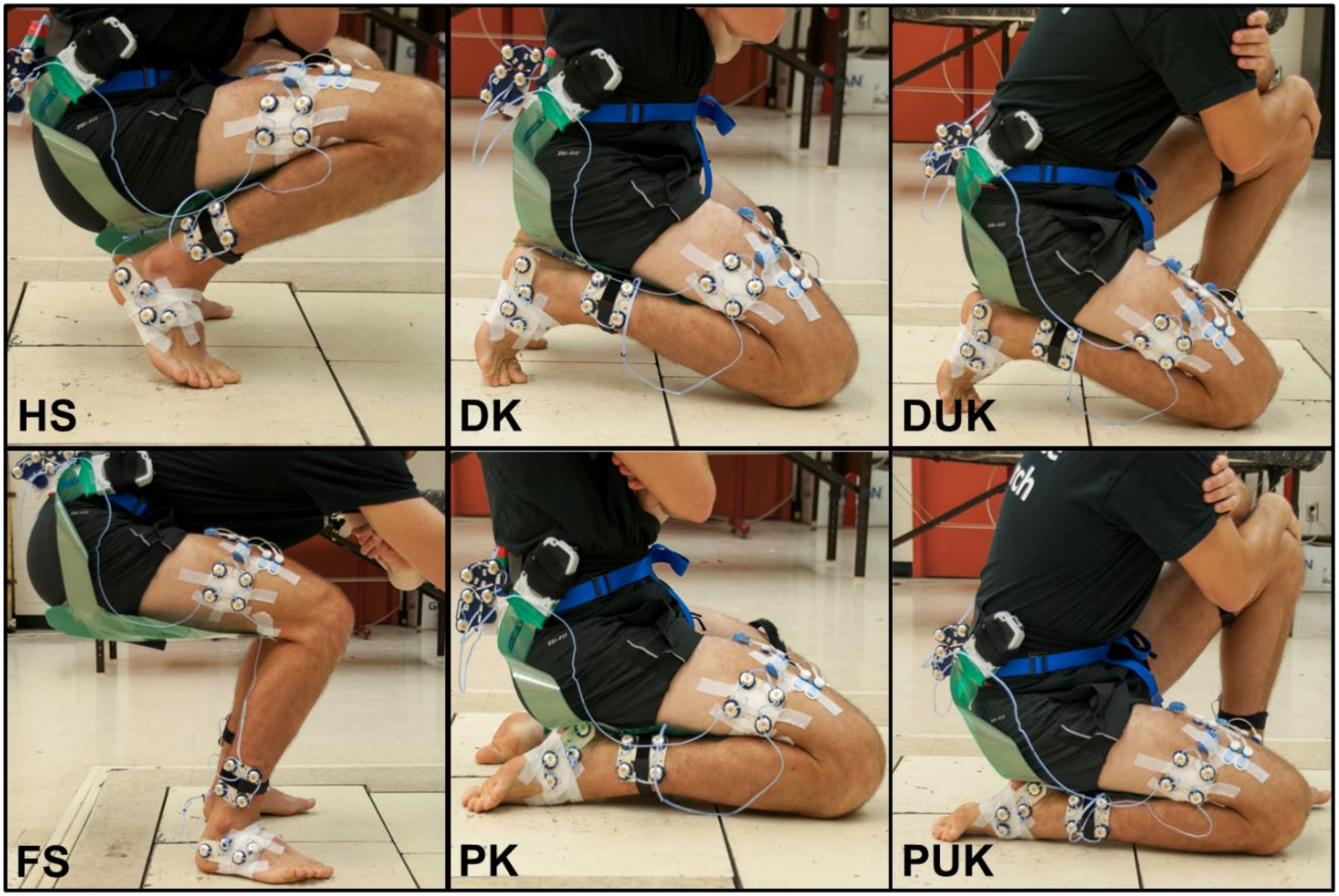

Figure 3.2 High knee flexion postures performed in this study: Heels-up squat (HS), flatfoot squat (FS), dorsiflexed kneel (DK), plantarflexed kneel (PK), dorsiflexed unilateral kneel (DUK), and plantarflexed unilateral kneel (PUK).

3.2.3 Instrumentation

Kinematic data were recorded at 64 Hz from rigid bodies attached to the right thigh, shank, foot, and the pelvis using an optoelectronic system (Certus, NDI, Waterloo, ON). Kinetic data were synchronously recorded at 2048 Hz from four embedded force plates (OR6-7, AMTI, Watertown, MA). Pressure data were synchronously recorded at 64 Hz (3005E-FScan, Tekscan, Boston, MA). This 8-bit resistive pressure sensor had a spatial resolution of 3.9 sensels/cm2 and a sensing region that was 15.75 cm wide by 39.62 cm long. It was conditioned to 103.4 kPa ten times in 3-second cycles, equilibrated for 30 seconds at three points (34.5 kPa, 68.9 kPa, and 103.4 kPa) then calibrated following the manufacturer's non-linear (power) procedure (Table 3-6). The power calibration is the most accurate calibration provided in Tekscan software for varying load applications (Brimacombe et al., 2009).

3.2.4 Data processing

Data processing was completed using Matlab 9.0 (The Mathworks, Release R2016a, Natick, MA). Kinematic and GRF data were low-pass filtered using a bidirectional 2nd-order Butterworth digital filter with a 6 Hz cut-off frequency (Longpré et al., 2013; Winter, 2009). Knee and hip joint centers were calculated from functional trials following established protocols (Besier et al., 2003b; Camomilla et al., 2006; Ehrig et al., 2007). Knee joint angles were decomposed in a Z-X-Y Cardan sequence. Data were then truncated, starting when the GRF under the right foot (always the first foot to contact a force plate) exceeded 10 N. The trial end point was manually identified as the frame where the knee flexion waveform plateaued (Figure 3.3). All data were then time normalized and averaged across the five repetitions of each movement.

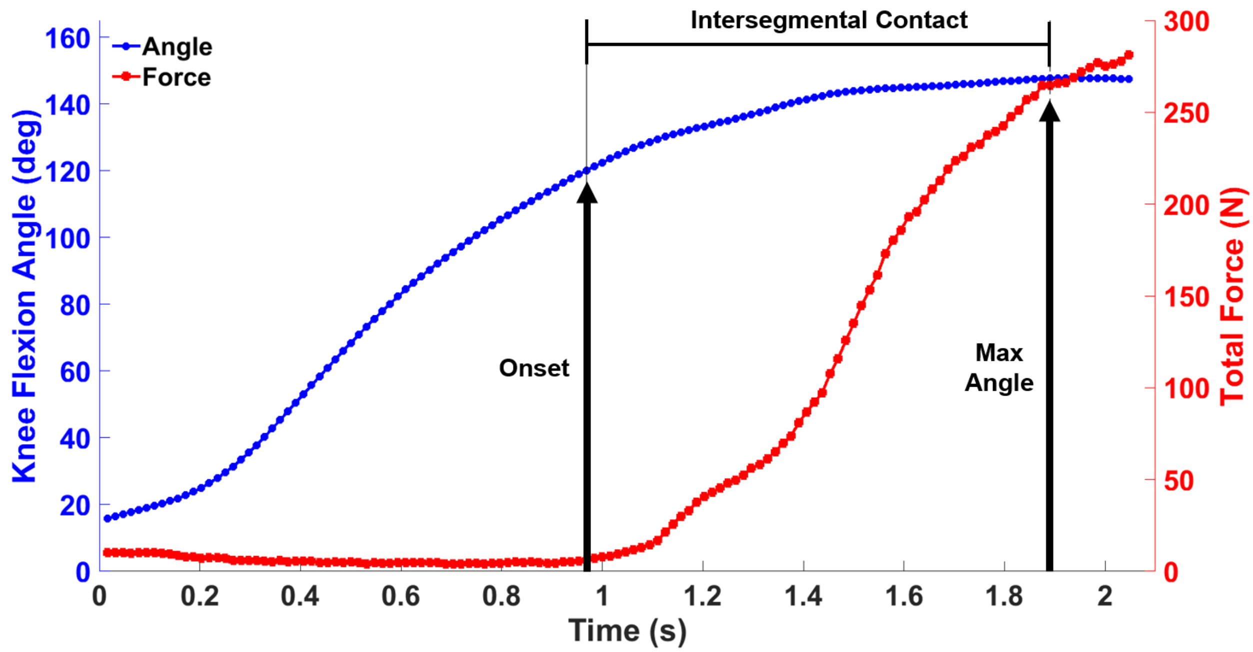

Figure 3.3 Intersegmental contact range definition. Onset was defined using the criteria shown in Figure 3.5 while Max Angle was manually defined for each trial at the plateau of the knee flexion waveform.

Raw pressure data, from the last frame of the truncated trial, underwent a 'masking' procedure to identify regions of TC and HG contact for every repetition (Figure 3.4). Masks were represented as matrices of 78 x 31 logical values (1 if element was in selected region, 0 if not) and multiplied by the raw data to omit the values of unselected sensels. This procedure was completed to reduce sensor noise as sensor deformation around the small circumference of the calcaneus resulted in pressure artifacts (Figure 3.4 – A vs D). Masking was completed on all trials for each participant (900 frames x 2 masks) twice (figure displayed maxima of 30 and 80 kPa) to allow for an intraclass correlation (ICC) of mask selection reliability, and then completed by two additional untrained raters, at 30 kPa, to estimate interrater reliability.

After masking, onset was calculated using knee flexion angle and total force from the pressure sensor. Mean and standard deviation were calculated from force data in a 10-frame window surrounding the frame when the knee flexion angle reached 110º. The onset threshold was defined as the mean plus two standard deviations. Onset (Figure 3.5 – data at the point of onset indicated by black circles) was defined as the flexion angle at the frame where force data exceeded this threshold (Hodges and Bui, 1996). Contact area values were calculated from both contact regions as the sum of sensel areas that had values greater than 0 kPa after masking.

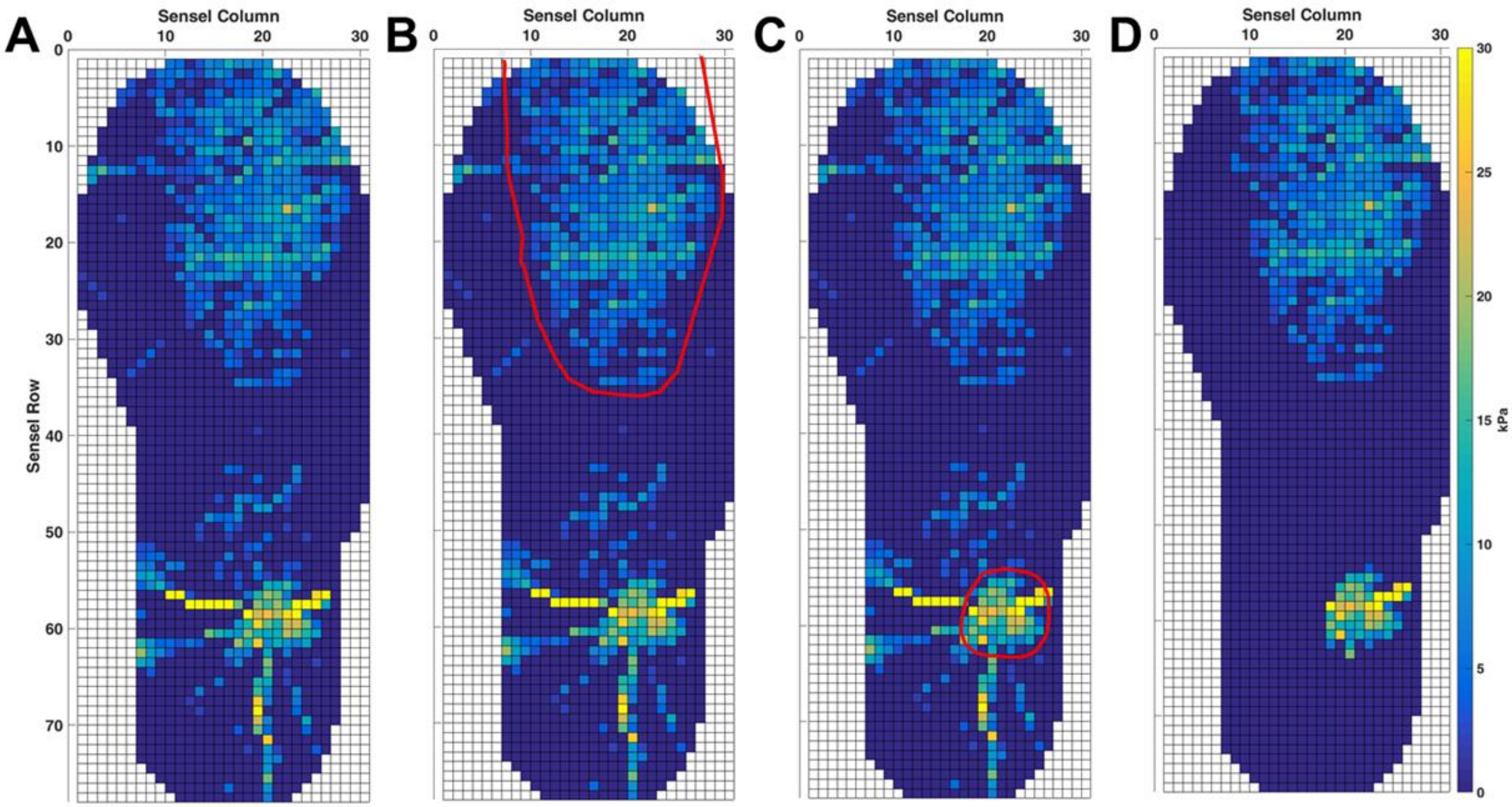

Figure 3.4 Raw (A) to masked (D) pressure sensor data completed through regional selections using a custom Matlab function. The frame of pressure data at Max Angle for every repetition was used to define masks for the thigh-calf and heel-gluteal (if applicable) contact regions. A is raw data, B is the selection of thigh-calf contact mask, C is the selection of heel-gluteal mask, and D is the masked data where raw data is multiplied by logical matrices (1 if element was in selected region, 0 if not) to omit the values of unselected sensels. For this example: total force in A = 175.4 N; total force in D = 123.5 N (51.9 N difference from A); thigh-calf force in D = 87.7 N; heel-gluteal force = 35.8 N.

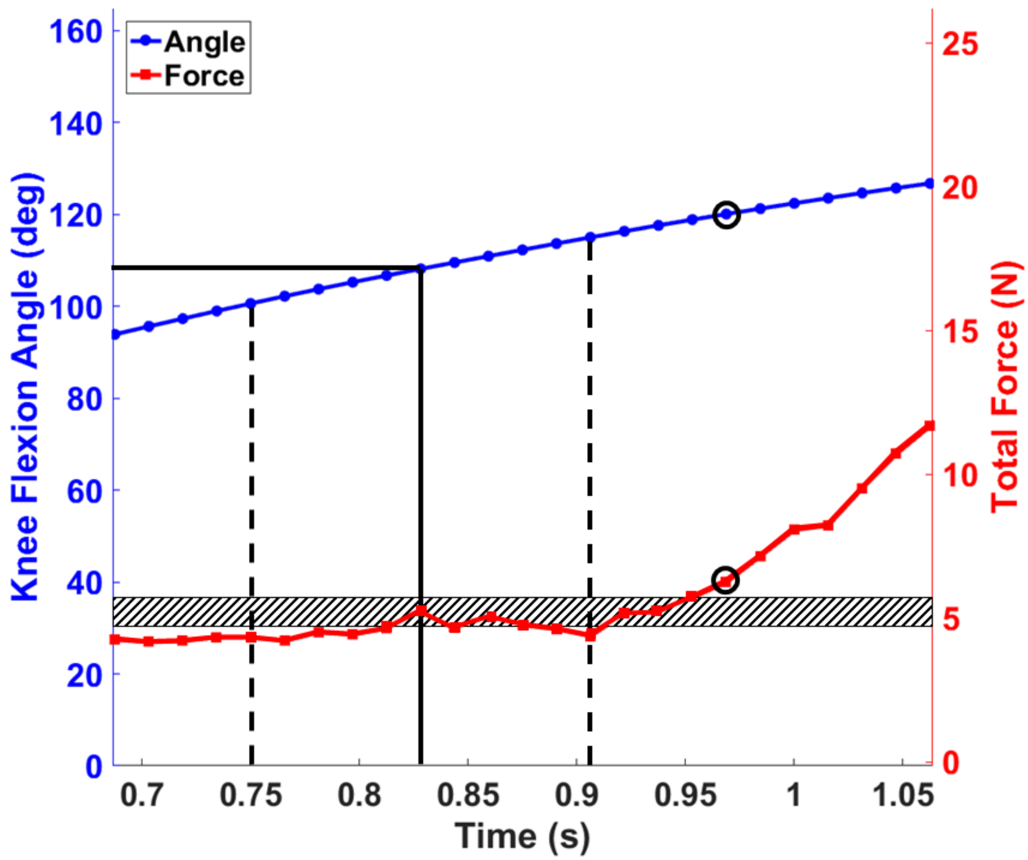

Figure 3.5 Thigh-calf contact onset criteria. The vertical dashed lines indicate a window of 10 data points surrounding the frame in which the participant reached 110° of knee flexion. The mean (bottom of shaded region) and standard deviation of the force values in this window were used to define the onset threshold (top of the shaded region at 2 SD above the mean). The circled red point indicates where force data exceeded onset threshold and the circled blue point indicates the knee flexion angle where onset of thigh-calf contact occurred.

Longitudinal CoF was calculated as the distance from the functional knee joint center, for both the TC and HG contact regions using a weighted-centroid approach (Verkerke et al., 2005). A fixed transformation used to position the pressure sensor (and thus the CoF) with respect to the thigh was defined (Figure 3.6). Points on the pressure sensor that were digitized in the global coordinate system—while the participant was standing upright—were used to define a local coordinate system (LCS) on the sensor. The sensor LCS was assumed to lay flat in the regions where contact occurred (Caruntu et al., 2003). The vertical-frontal plane of the sensor was positioned parallel to the frontal plane of the thigh segment (Figure 3.6). Anterior-posterior positioning of the sensor was accomplished by setting the perpendicular distance between these two planes (Figure 3.6 - A) such that sensor passed through the midpoint (O) of a vector between the most posterior points of the mid-thigh (Figure 3.6 - M) and distal thigh (Figure 3.6 - D) circumferences. The angle between the long axis of the pressure sensor and the long axis of the thigh in the plane of the sensor was then calculated using the dot product to convert CoF points from the sensor coordinate system into the thigh.

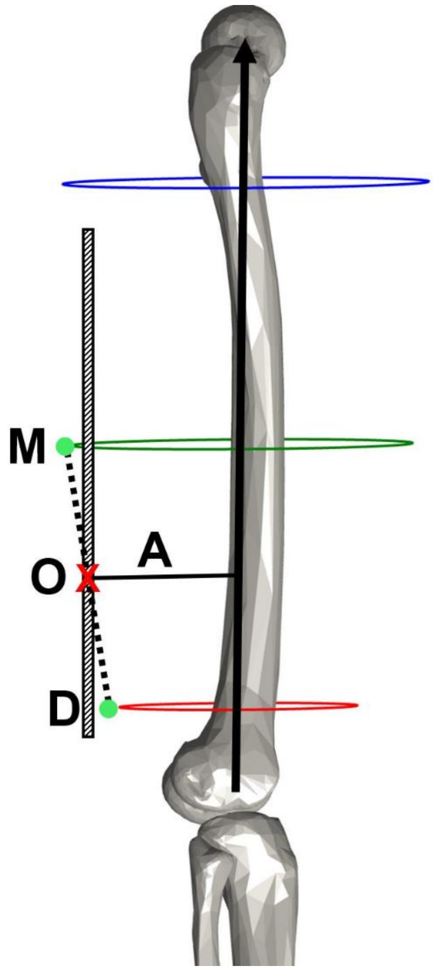

Figure 3.6 Sagittal view of the femur and shank depicting the position of the pressure sensor plane (hashed black rectangle) referenced to the thigh segment. Point M (green circle) is the posterior point on the mid-thigh circumference located at 50% of segment length. Point D (green circle) is the posterior point on the distal thigh circumference located at 90% of segment length. Point O (red X) is the mid-point between points M and D, which was used to define the anterior-posterior position of the pressure sensor that was a fixed perpendicular distance (A) from the long axis of the femur (vertical black arrow).

3.2.4.1 Statistical analyses

All statistical procedures were performed using SPSS (Version 20.0 – Released 2011, IBM Corp., Armonk, NY). To estimate trained rater reliability in mask selection, a two-way random ICC(2,1) was completed for 58 participants, using average absolute agreement between thigh-calf region CoF from the 30 and 80 kPa rounds of masking (Shrout and Fleiss, 1979). Similarly, a second two-way random ICC(2,3) was completed to estimate rater reliability between the trained and two untrained raters in selecting masks. To assess differences between high knee flexion contact parameters across the six postures, a linear mixed model was used with fixed effects of posture and sex, and *a priori* $\alpha = 0.05$. Dependent variables were onset, max angle, and measures taken at the last frame of the truncated trial (max angle): total force, TC force, TC CoF, TC area, HG force, HG CoF, and HG area. Bonferroni corrections were applied for post hoc pairwise comparisons to adjust α levels for multiple comparisons.

Pearson correlation coefficients were computed between thirteen anthropometric predictors (Table 3-1 – excluding age) and five outcome variables (onset, max angle, peak force, CoF, and contact area) for each of the six high knee flexion movements separately. In addition, max angle was used as a predictor variable for peak force, CoF, and contact area as these outcome variables were discrete points taken at the frame of maximum knee flexion. Typically this number of comparisons would require Bonferroni adjustments to α, however, to facilitate comparison with the findings from previous work (Zelle et al., 2007) an uncorrected $\alpha = 0.05$ was used to identify significant correlations. Correlation coefficient strengths were defined using the following criteria: 0.00-0.09 (none), 0.10-0.29 (weak), 0.3-0.59 (moderate), and 0.6-1.00 (strong) (Cohen et al., 2003; Field, 2009).

Multiple linear regressions were used to test associations between predictors, with random intercept and outcome variables, following backward stepwise procedures (Babyak, 2004; Steyerberg et al., 2001). Predictor inclusion and exclusion criteria levels were set at $p >$ 0.05 and 0.10 respectively. Thirty separate regression equations (5 thigh-calf contact parameters x 6 movements) were assessed for model fit, frequency of predictor inclusion, and variance explained. In line with previous work, Bonferroni *p*-value corrections adjusted for the number of statistical models, therefore, α = 0.0017 was used to identify significantly predictive regression models (Chehab et al., 2017). Models were evaluated using correlation strength using intervals indicated in the previous paragraph (Cohen et al., 2003; Field, 2009) If models for a pair of similar movements (e.g. HS and FS) had multiple predictors in common, exploratory regressions were computed for combined movement data. All models were assessed for compliance with serial correlation (Durbin-Watson statistic 1.5-2.5), heteroscedasticity (visual inspection), and multicollinearity (tolerance > 0.2 and variance inflation factor < 4.0) assumptions (Babyak, 2004; Field, 2009; Streiner, 1994). If an included predictor violated the above criteria hierarchical models were defined using variables resulting from stepwise regression, with suspect variables removed, until all criteria were met (Legendre and Legendre, 1998).

3.3 Results – Intersegmental contact parameters

ICC(2,1) estimates were excellent (lowest value 0.932) between masking attempts at different kPa display levels (Cicchetti, 1994). Likewise, ICC(2,3) values were excellent between raters (lowest single and mean values 0.873 and 0.954 respectively). A complete set of mean values and standard deviations for dependent variables is in Table 3-2. Notable differences are reported below.

Table 3-2 Mean values (± 1 SD) of high knee flexion parameters. † and ‡ indicate main effects of posture or sex respectively, * indicates an interaction of posture and sex (differences occurred in the DUK posture only). Values sharing lettered superscripts are not different within a column. HS is heels-up squat, FS is flatfoot squat, DK is dorsiflexed kneel, PK is plantarflexed kneel, DUK is dorsiflexed unilateral kneel, and PUK is plantarflexed unilateral kneel. TC is thigh-calf and HG is heel-gluteal contact. CoF is center of force.

Posture	Group	Onset†‡ (deg)	Max Angle†‡ (deg)	Total Force† (N)	TC Force† (N)	TC CoF†* (mm)	TC Area†* (cm^2)	HG Force† (N)	HG CoF† (mm)	HG Area† (cm^2)
	Female	126.0 (7.9)	153.0 (7.3)	68.47 (34.86)	68.47 (34.86)	60 (15)	92.14 (26.20)	-	-	-
HS	**Male**	123.9 (7.2)	146.2 (9.4)	78.91 (69.13)	78.91 (69.13)	54 (19)	88.79 (36.19)	-	-	-
	Total	125.0 (7.5) [a,b]	149.6 (9.0) [a]	73.59 (54.19)	73.59 (54.19)	57 (17) [a]	90.49 (31.25)	-	-	-
	Female	130.6 (9.0)	152.8 (6.6)	42.54 (19.01)	42.54 (19.01)	58 (15)	75.75 (20.65)	-	-	-
FS[1]	**Male**	125.5 (5.0)	145.9 (7.1)	60.37 (45.49)	60.37 (45.49)	48 (18)	78.51 (35.88)	-	-	-
	Total	128.1 (7.7) [a]	149.5 (7.5)	51.07 (34.70)	51.07 (34.70)	53 (17)	77.07 (28.29)	-	-	-
	Female	124.1 (7.4)	155.2 (7.5)	114.88 (55.17)	113.36 (55.09)	71 (21)	121.57 (36.73)	6.51 (6.17)	343 (18)	3.93 (2.37)
DK[2]	**Male**	119.9 (6.5)	148.2 (10.4)	122.65 (80.60)	122.34 (80.55)	63 (19)	120.98 (38.91)	-	-	-
	Total	122.1 (7.3) [b,c,d]	151.8 (9.6) [b,c]	118.63 (68.13) [a]	117.69 (68.11) [a]	67 (20) [b]	121.29 (37.47) [a]	6.51 (6.17) [a]	343 (18) [a,b]	3.93 (2.37)
	Female	121.1 (6.4)	156.0 (6.9)	105.16 (49.56)	99.44 (49.00)	62 (15)	110.92 (30.11)	14.28 (9.88)	306 (16)	8.44 (4.43)
PK[3]	**Male**	118.2 (6.2)	149.2 (9.2)	123.88 (72.74)	118.98 (68.80)	61 (20)	120.43 (38.51)	12.48 (12.52)	326 (22)	8.91 (4.94)
	Total	119.7 (6.4) [c]	152.7 (8.8) [b]	114.20 (62.01) [a]	108.88 (59.67) [a]	62 (17) [a]	115.51 (34.45) [a]	13.42 (11.00) [a]	315 (22) [a]	8.67 (4.58)
	Female	125.9 (6.9)	155.3 (7.1)	201.49 (89.16)	196.28 (87.66)	82 (27)	155.61 (41.03)	11.17 (11.91)	333 (24)	5.81 (3.89)
DUK[4]	**Male**	122.7 (8.5)	147.2 (11.9)	178.00 (110.30)	176.56 (109.07)	67 (22)	137.33 (51.10)	10.11 (4.33)	340 (20)	7.01 (3.16)
	Total	124.3 (7.8) [a]	151.4 (10.4) [a,b]	190.15 (99.74) [b]	186.76 (98.20)	75 (26) [b]	146.78 (46.67)	10.93 (10.58) [a]	335 (23) [b]	6.08 (3.68)
	Female	121.0 (6.0)	152.9 (7.5)	167.54 (94.43)	155.34 (92.06)	60 (18)	121.24 (40.88)	24.39 (23.24)	306 (20)	9.67 (4.73)
PUK[5]	**Male**	118.8 (6.9)	146.7 (12.3)	171.44 (106.28)	162.30 (101.31)	60 (23)	127.92 (48.82)	23.27 (19.57)	330 (21)	10.56 (4.94)
	Total	119.9 (6.5) [d]	149.9 (10.5) [a,c]	169.42 (99.46) [b]	158.70 (95.84)	60 (20) [a]	124.46 (44.61) [a]	23.92 (21.35)	316 (23) [a]	10.05 (4.75)

[1] Only 12 females and 11 males could achieve thigh-calf contact when performing the FS movement
[2] HG values in DK had 7 females
[3] HG values in PK had 12 females and 11 males
[4] HG values in DUK had 15 females and 11 males
[5] HG values in PUK had 14 females and 4 males

3.3.1 Range of flexion during thigh-calf contact

There was a main effect of posture and sex for both onset ($p < 0.001$ and $p = 0.01$) and max angle (both $p < 0.001$). These variables define the range of flexion over which thigh-calf contact occurred. For male participants, onset (121.0º) and max angle (147.4º) occurred on average 3.1º and 7.0º earlier than for females (onset: 124.1º and max angle: 154.4º). Onset occurred earliest in PK (119.7º) which was 8.4º earlier ($p < 0.001$) than the activity with the latest onset, FS (128.1º). The only posture-pair (e.g. squatting, symmetric kneeling, or unilateral kneeling) that had onset differences was unilateral kneeling; PUK (119.9º) had a 4.4º earlier onset ($p < 0.001$) than DUK (124.3º). In addition, the movement with the highest max angle was PK (152.7º) which was 3.2º higher ($p < 0.001$) than the activity with the lowest max angle, FS (149.5º).

3.3.2 Contact force

For the measured forces, there was a main effect of posture only for total force ($p < 0.001$), TC force ($p < 0.001$), and HG force ($p = 0.012$) at max angle. Individual participant and mean total force curves for each movement (normalized to percent body weight for comparison to previous data) are shown in Figure 3.7. Only two total force pairwise comparisons (Table 3-2) were not significantly different: DK vs. PK and DUK vs. PUK ($p = 1.00$ and 0.27 respectively). The range of mean total contact force at max angle was 139.08 N, from 51.07 N in FS to 190.15 N in DUK.

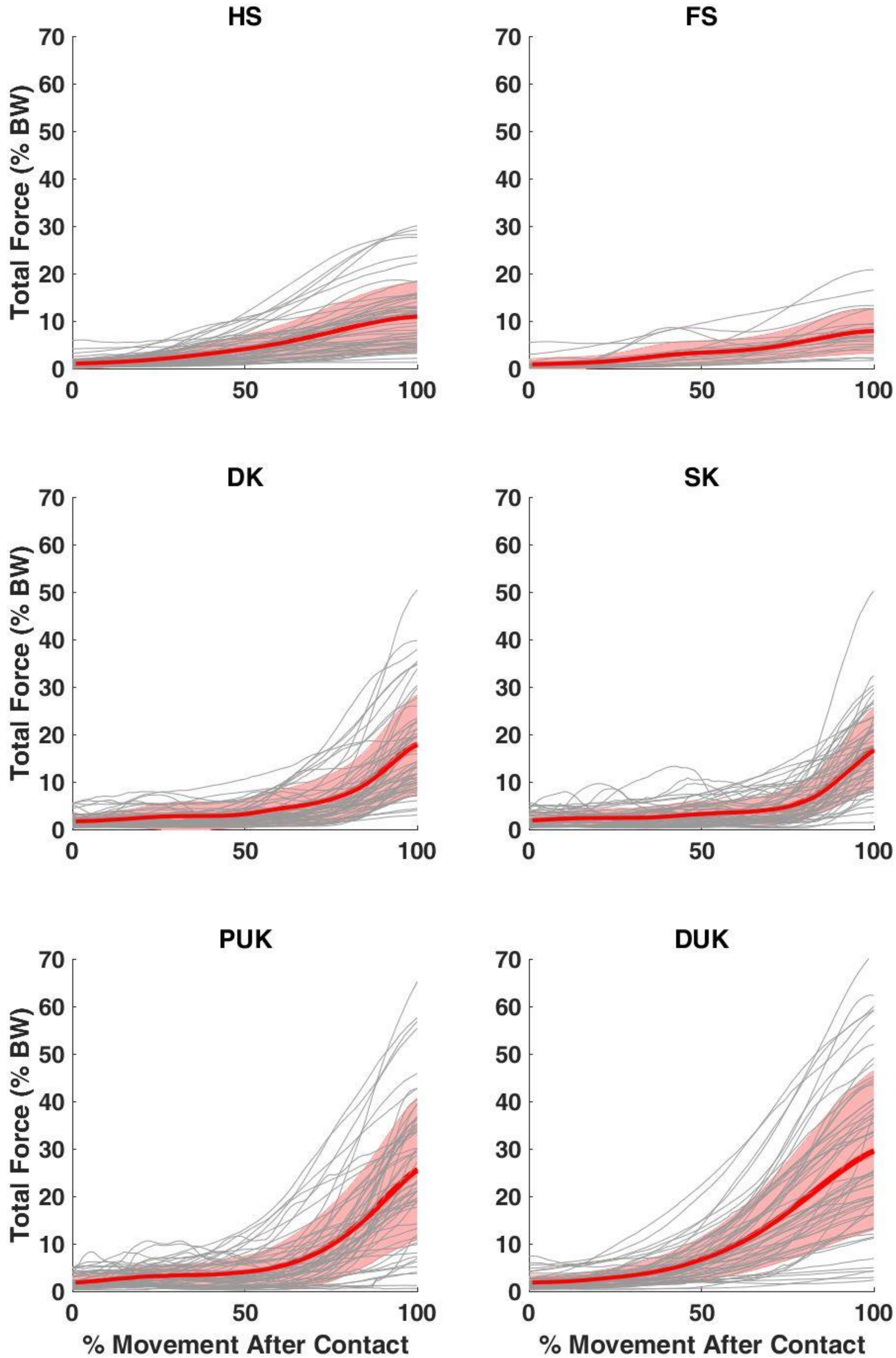

Figure 3.7 Participant (grey) and mean (red) with shaded ± 1 SD band total force values across movements. Percentage movement after contact represents the time from onset to max angle for each participant.

Similar to total force, all TC contact force pairwise comparisons (Table 3-2) were different ($p < 0.001$) except for symmetric kneeling (DK and PK, p = 1.00). The highest TC contact force was in DUK (186.76 N) which was 135.69 N more force than FS (51.07 N).

HG contact only occurred for 15 females and 11 males in DUK, 12 females and 11 males in PK, 14 females and 4 males in PUK, and 7 females in DK. Of this sub-sample, HG contact force was highest in PUK (23.92 N) which was 12.99 N higher ($p = 0.02$) than DUK (10.93 N) and 17.41 N higher ($p = 0.02$) than DK (6.51 N).

3.3.3 Center of force

An interaction was observed for the TC region CoF ($p = 0.002$). In DUK, the CoF was 15 mm farther from the knee joint center in females when compared to males (82 and 67 mm respectively). A main effect of posture ($p = 0.008$) was present for the HG region CoF, with a 19 mm difference ($p = 0.01$) occurring between PUK (316 mm) and DUK (335 mm).

3.3.4 Contact area

Similar to CoF, an interaction was observed for TC contact area ($p = 0.013$). In DUK, contact area was 18.28 cm^2 larger for females (155.61 cm^2) when compared to males (137.33 cm^2). A main effect of posture ($p = 0.023$) was present for heel-gluteal contact area, with PUK (10.05 cm^2) having a 3.97 cm^2 larger area ($p = 0.022$) than DUK (6.08 cm^2).

3.4 Results - Anthropometric regression

Pearson correlations of predictor variables with outcomes are reported in Table 7-1-7.5. Seventy-eight correlations (13 potential predictors x 6 movements) were computed for onset and max angle outcome variables. Eighty-four correlations were computed for total force, CoF, and area outcome variables. The additional correlations were due to the addition of max angle as an additional predictor. Significant Pearson correlations for onset were found in 27 of 78 comparisons; 6 weak and 21 moderate correlations were observed (Table 7-1). Max angle had the largest number of significant correlations with 47 of 78 comparisons being significant; 2 weak, 31 moderate, and 14 strong (Table 7-2). Total contact force at maximum flexion angle had only 3 weak and 2 moderate correlations (Table 7-3). Thigh-calf CoF had 5 weak, 14 moderate, and 4 strong correlations which mostly occurred in DK and DUK (Table 7-4). Thigh-calf contact area had 6 weak, 8 moderate, and 1 strong correlation which mostly occurred in DUK (Table 7-5).

Regression models shared similar trends to correlation findings in that the outcome variables with strong linear fits across all movements were max angle and CoF (Table 3-3). Max angle and CoF values from regression models are plotted against measured values in Figure 3.8 and Figure 3.9 respectively. While a strong fit was achieved for area during the DUK and PUK postures, the four remaining postures had poor to moderate fits (Table 3-3). Of the thirty regression models, seven contained two variables that violated VIF and tolerance criteria; 5 in max angle (all but FS) and 1 (HS) in total force and CoF. Proximal thigh circumference was the variable that most commonly violated multicollinearity criteria.

Table 3-3 Summary of linear regression model fit across six movements. Correlation coefficient (*R*) and coefficient of determination (R^2) values across separate regression models for each movement. Strong correlation coefficients are bolded.

Movements	Onset		Max Angle		Total Force		CoF		Area	
	R	R^2	***R***	R^2	***R***	R^2	***R***	R^2	***R***	R^2
Heels-up Squat (HS)	0.41	0.17	**0.77**	0.59	0.17	0.03	**0.61**	0.38	0.47	0.22
Flatfoot Squat (FS)	0.56	0.31	**0.77**	0.59	0.36	0.13	**0.63**	0.39	0.30	0.09
Dorsiflexed Kneel (DK)	0.39	0.15	**0.79**	0.62	0.24	0.06	**0.72**	0.52	0.54	0.30
Plantarflexed Kneel (PK)	0.46	0.21	**0.68**	0.46	0.44	0.20	**0.68**	0.38	0.49	0.24
Dorsiflexed Unilateral Kneel (DUK)	0.56	0.31	**0.79**	0.62	0.40	0.16	**0.77**	0.60	**0.60**	0.35
Plantarflexed Unilateral Kneel (PUK)	0.53	0.28	**0.65**	0.42	0.41	0.17	**0.75**	0.57	**0.67**	0.45

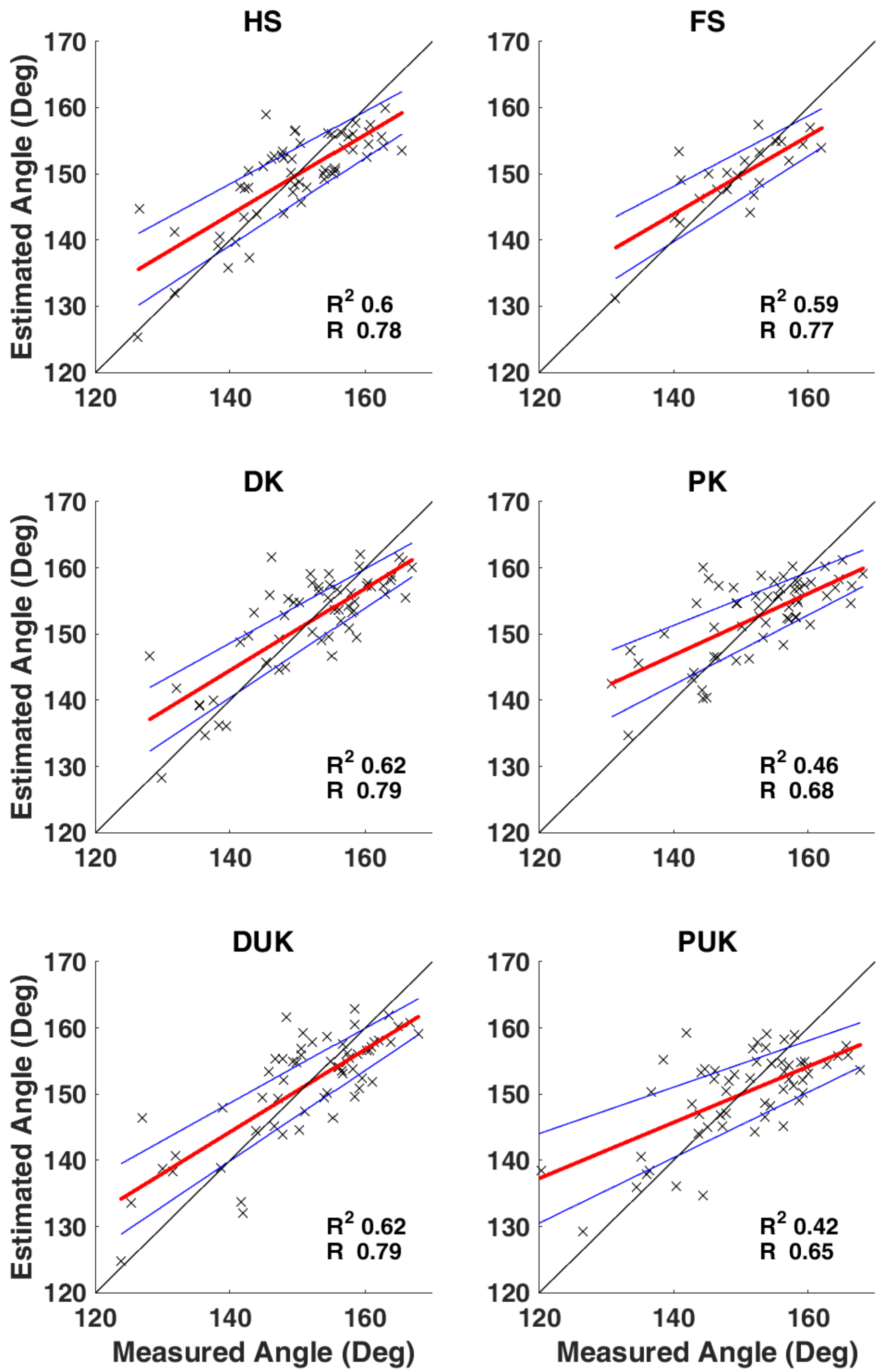

Figure 3.8 Mean estimated response (red lines) of maximum angle achieved during high flexion movements with 95% confidence interval bands from multiple linear regression (blue lines). Measured individual values are indicated with a black x. The solid black line indicates a perfect line of agreement. Pearson *R* and R^2 values are indicated for the fit and variance explained for each movement.

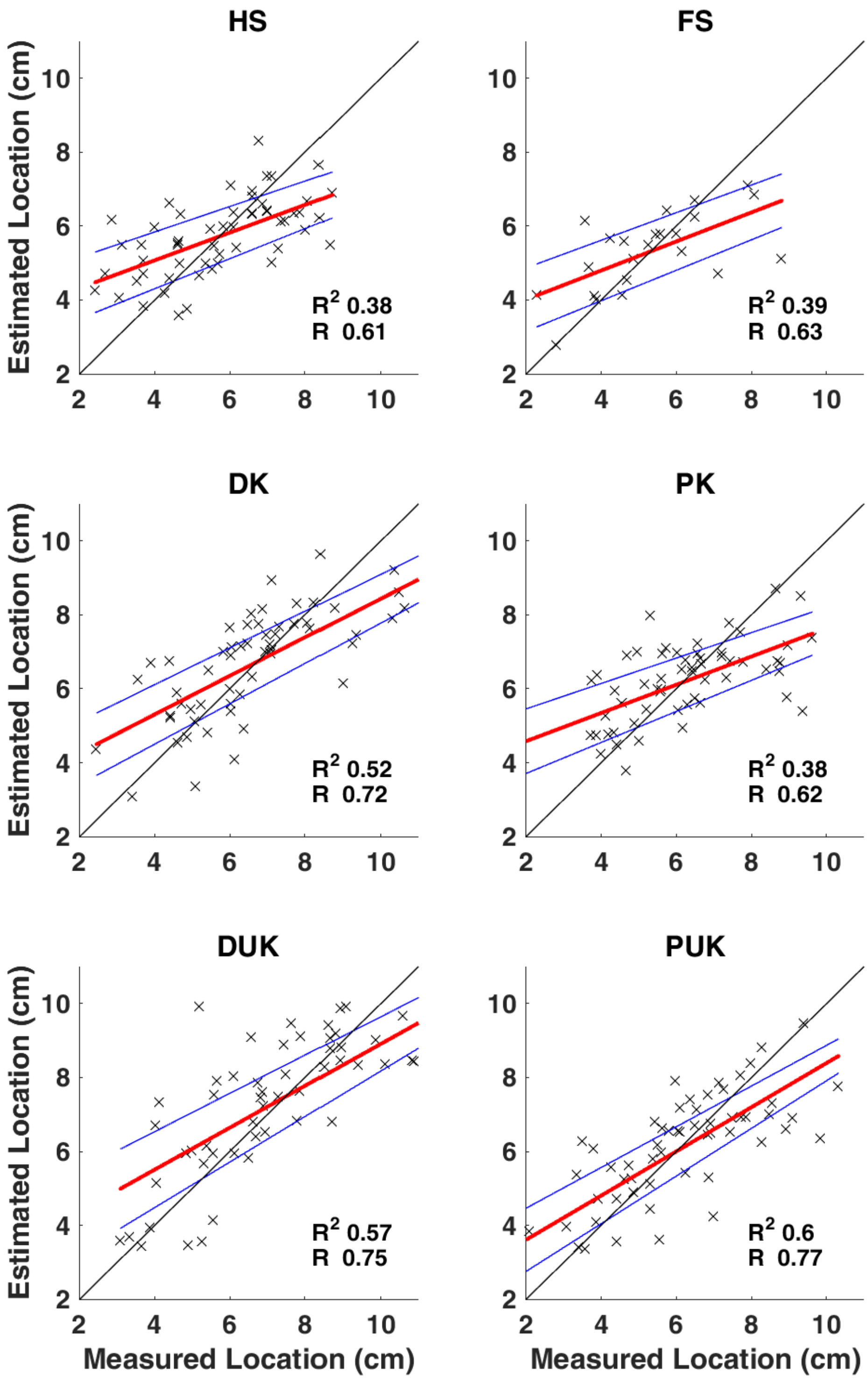

Figure 3.9 Mean estimated response (red lines) of longitudinal center of force (from the functional knee joint center) achieved during high flexion movements with 95% confidence interval bands from multiple linear regression (blue lines). Measured individual values are indicated with a black x. The solid black line indicates a perfect line of agreement. Pearson *R* and R^2 values are indicated for the fit and variance explained for each parameter.

The strong correlation coefficients and high coefficients of determination of max angle and CoF regressions resulted in an exploratory assessment by paired movements; squatting (FS and HS), kneeling (PK and DK), and unilateral kneeling (PUK and DUK). Combined models remained strongly fit for all paired movements in max angle and CoF except for a moderate fit of CoF squatting (Table 3-4). Comparisons of our findings to previously reported correlations are highlighted in Table 3-5.

Table 3-4 Summary of regression models structure and fit for grouped movement-pairs in estimating max knee flexion angle and center of force. Values for intercept and predictor variables are unstandardized β values (standard error). Dst is distal and Cir is circumference.

	Max Angle			Center of Force		
Predictors	**Squat**	**Kneel**	**Unilateral Kneel**	**Squat**	**Kneel**	**Unilateral Kneel**
R	0.78	0.74	0.72	0.59	0.72	0.74
R^2	0.60	0.55	0.58	0.35	0.52	0.55
Intercept	128.03 (10.79)	128.99 (9.60)	123.01 (10.92)	-172.36 (41.06)	-205.33 (32.61)	-240.82 (39.30)
Mass	-0.69 (0.08)	-0.67 (0.07)	-0.69 (0.08)	–	–	–
BMI	–	–	–	–	–	-1.16 (0.55)
Mid-Thigh Cir	–	11.15 (12.42)	19.00 (14.37)	–	–	–
Dst Thigh Cir	–	–	–	–	–	75.32 (40.21)
Thigh Skinfold	0.13 (0.05)	0.13 (0.05)	0.09 (0.06)	–	–	–
Shank Length	106.59 (34.15)	122.63 (28.04)	162.12 (31.13)	-47.97 (78.94)	–	–
Dst Shank Cir	116.28 (50.96)	61.65 (45.55)	–	308.35 (105.54)	239.61 (65.95)	323.05 (87.51)
Max Angle	–	–	–	1.23 (0.20)	1.45 (0.16)	1.59 (0.19)

Table 3-5 Comparison of Pearson correlations between Zelle et al. (2007) and the current study (bold italicized) for measured parameters that were common to both studies (onset, maximum flexion angle, and total force at maximum flexion). We have assumed that circumference measurements reported in previous work were defined in the same manner as the mid-thigh circumference and the mid-shank circumference in the current work.

Posture	Outcome Variable	Thigh Circumference	Calf Circumference	BMI	Weight
Heels-Up Squat	Onset	-0.54 ***-0.22***	-0.79 ***-0.17***	-0.42 ***-0.27***	- ***-0.27***
	Max Angle	-0.63 ***-0.40***	-0.68 ***-0.55***	-0.81 ***-0.68***	- ***-0.69***
	Total Force	0.73 ***0.14***	0.77 ***0.24***	0.57 ***0.19***	0.73 ***0.20***
Dorsiflexion Kneel	Onset	-0.70 ***-0.26***	-0.82 ***-0.32***	-0.69 ***-0.35***	- ***-0.42***
	Max Angle	-0.32 ***-0.40***	-0.27 ***-0.58***	-0.49 ***-0.69***	- ***-0.68***
	Total Force	0.93 ***0.08***	0.81 ***0.07***	0.74 ***0.02***	0.72 ***0.08***

3.5 Discussion – Intersegmental contact parameters

A purpose of this investigation was to define TC and HG contact parameters for six high knee flexion movements and to investigate potential sex differences. The results for total force, CoF, and contact area are reported in Newtons and not normalized to any participant anthropometric measures. Results indicate that unilateral kneeling movements have the highest TC contact forces occurring at CoF locations farthest from the knee joint center. These activities would therefore theoretically result in the greatest reduction of knee joint flexion moments for the right knee, although not necessarily the lowest compression force. Squatting movements had the lowest TC contact forces, with the majority of participants (35) unable to achieve TC contact when performing FS. Sex differences occurred in range of flexion parameters (onset and max angle), with males having lower TC contact onset and max angle. This difference effectively shifts the entire range of flexion during contact to lower flexion angles for males. Interactions of sex by movement occurred where sex had a significant effect on contact area and CoF location for the TC and HG regions for the DUK posture only. It should be noted that our results (specifically sex differences) reported in this study only relate to our sample of healthy, young, non-habitually kneeling participants and the reader is cautioned against generalizing these findings to a population level.

The knee flexion angle where the onset of TC contact occurred was approximately 10º to 15º earlier than values reported by Zelle et al. (2007), however, our max angles are also approximately 5º lower. This is likely attributed to differences in kinematic tracking as three markers were used to define thigh and shank motion in Zelle et al. (2007), as opposed to 3D reconstruction with functional joint centers (Besier et al., 2003b; Camomilla et al., 2006) used in our study. In addition, there is a non-sensing boarder around the perimeter of previously used sensors that may contribute to later onset angles. The sensor used in this study was more sensitive, therefore it enabled the use of onset criterion similar to established methods used in electromyographic work (Hodges and Bui, 1996). This threshold is different from the 5% bodyweight value used by Zelle et al. (2007).

The mean total contact force values reported in this study are considerably lower than prior work (Table 3-6). However, it should be noted that a small number of participants achieved similar contact force magnitudes in our sample population (Figure 3.7). While it appears to have been largely ignored in prior work, noise within pressure sensor technology can be considerable when performing high knee flexion movements due to the deformation of the segment and sensor. For example, noise represented 51.9 N ≈ 30% of the raw total force displayed in Figure 3.4 – A. Also, the approach used to calibrate Tekscan sensors can alter output substantially as the power calibration method (used in the current study) is almost ten times more accurate, across full scale output, when compared to linear methods (Brimacombe et al., 2009). Previous work used linear calibration methods (Pollard et al., 2011; Zelle et al., 2007). In addition, contact areas were less than 50% of those reported in Zelle et al. (2007) and thus lower total contact forces would be expected.

Differences in participant anthropometrics (e.g. thigh circumference/skinfold thickness) likely contributed to the differences in contact areas between these studies, but this theory is speculative as segment circumferences were not reported in previous work. As well, for the same TC contact area, the finer spatial resolution of the pressure sensor used in the current study would result in a smaller contact area measured, compared to a sensor with coarser resolution. Finally, it should be noted that prior work did not explicitly state if participants were barefoot or shod. Performing kneeling movements while shod can alter ankle flexion by up to 8º (Chong et al., 2017) and could result in increased contact area and pressure due to material of the shoe extending posteriorly from the heel. These issues, in addition to our study using a masking procedure to reduce noise, may help explain the differences in findings between studies.

Table 3-6 Summary of thigh-calf contact methods and findings from in vivo studies. All sensor models are from Tekscan (Tekscan Inc., South Boston, MA, USA). Mean (SD) contact force values are reported for the Heels-Up and Dorsiflexed Kneeling movements consistent across the listed studies. Dorsiflexed kneel values from Pollard et al. (2011) and the current study are reported with thigh-calf (left) and heel-gluteal (right) segregated values.

Study	Participants		Sensor					Heels-Up Squat (%BW)	Dorsiflexed Kneel (%BW)	
	Male	Female	Model	Spatial Accuracy (sensels/cm^2)	Calibration	Sample Rate (Hz)	Sensitivity (kPa)			
Zelle et al. (2007)	8	2	Conformat (5330)	0.5	Linear	8	0-33.3	34.20 (9.69)	30.90 (9.31)	
Pollard et al. (2011)	7	3	ClinSeat (5315)	1.0	Linear	4	41-207[2] 0-207[2]	39.00 (14)	28.00 (13)	11.00 (6)
Kingston & Acker (2018)	28	30	3005E	3.9	Power[1]	64	0-154[3]	10.98 (7.01)	17.88 (10.14)	1.13 (0.84)

[1] Point 1 – 22.72kg over ≈610 sensels, Point 2 – 114.94kg over ≈820 sensels, Exponent 0.87-1.27, Scaling Factor 0.502-0.84, Sensel Excitation (S) = 34.

[2] Pollard et al., (2011) report a 0-30 PSI range for their sensor, however, details available from the 5315 specification sheet note a 6-30 PSI sensitivity range.

[3] Specifications of the 3005E sensor state a 0-75 PSI or 0-120 PSI sensitivity range, but our F-Scan software allowed changing the excitation voltage of the sensor to lower the effective sensitivity range to ≈0-22 PSI.

Thigh-calf CoF values for HS are considerably lower in this study (≈5.7 ± 1.7 cm) compared to the findings of Zelle et al. (2007) (16.6 ± 2.64 cm), likely a result of smaller contact area measured. Our DK CoF values are separated into TC and HG components, as opposed to an overall CoF, limiting direct comparison to previous work. The difference in the reference points used to express the CoF locations in previous works—perpendicular distance between the posterior knee and the epicondylar axis (Zelle et al., 2007) or midway between the epicondyles of the femur (Pollard et al., 2011)—highlights that a reporting standard needs to be established. We feel that expressing the CoF with respect to the functional knee joint centre warrants consideration due to the ubiquity of its use in current 3D modeling (Hicks et al., 2014).

Limitations of this study include the manual selection of contact regions, the inability to account for shear loading or deformation in the pressure sensor, soft-tissue artifact, and the weight distribution instruction for unilateral kneeling. Although ICCs were excellent for the user-defined masks, mask selection is subjective and could influence comparisons between studies. As well, the tapered shape of this pressure sensor toward the popliteal fossa may have resulted in not measuring thigh-calf contact data in rare instances, similar to the non-sensing border of rectangular pressure sensors. Current pressure sensing technology remains limited in that shear forces cannot be separated from normal force. In addition, deformation of the sensor—especially in HG contact regions—manifests as pressure artifacts. Therefore, our assumption that the sensor was flat between contact areas likely results in systematically over-estimated force values. We acknowledge that soft tissue deformation of the thigh and shank segments is considerable during high knee flexion movements, and that this would affect both the calculation of knee flexion angle and confidence in pressure sensor location. Dual-plane fluoroscopic studies are needed in high knee flexion ranges before quantification of soft-tissue error can be estimated from surface tracking (Cereatti et al., 2017). In addition, the authors are not aware of a verified method for tracking sensor deformation during dynamic activities and future work is needed to establish movement between the pressure sensor and segments. Finally, we instructed participants to support the majority of their bodyweight on the flexed leg during unilateral kneeling. This posture was novel to all participants although commonly used in military populations (Department of the Army, 2010). Therefore, results for these postures could be interpreted as ‘worst-case’ in-vivo thigh-calf and heel-gluteal load magnitudes.

3.6 Discussion – Anthropometric regression

This study assessed the correlation of thirteen predictor variables (anthropometric measures and knee flexion angle) to parameters of TC contact and quantified their fit to outcome variables using multiple linear regression. We hypothesized that multiple linear regressions on thigh-calf contact onset, total force, center of force, and area would have a strong linear fit and moderate fit for max angle. Our findings suggest strong correlations and estimates of max angle and CoF from regression models but moderate to weak correlations and estimates for other outcome variables.

Person correlations did not support our hypotheses as the strength of trends were different than those reported in Zelle et al., (2007) (Table 3-5). The small samples used in prior work may have resulted in findings specific to a particular demographic that cannot be generalized to larger groups. Of note is the difference in correlations for total force outcomes across movements common to both studies (Table 3-5). We speculate that the wider range of anthropometrics, particularly due to a more balanced sex distribution in participants, is a major contributor to the lower correlations in the current study.

Of the thirteen anthropometric parameters used in this study, six were commonly retained in backward stepwise models: mass, proximal and mid-thigh circumferences, thigh skinfold, and shank length (Table 3-4). An interesting finding was that all CoF models (except for FS) retained distal shank circumference and max angle as predictors. We expected the small diameter and low variability in distal shank circumference to result in exclusion from most models, but further investigation of this relationship could be warranted. This effect is speculated to result from the relationship of shank circumferences and length where increased distal shank circumference results in a longer contact area due to soft tissue deformation. In addition, we provide support for the relationship that increased knee flexion angle results in a more distal CoF. A key consideration of these results is that collinearity was considered when developing regression models. Pearson bivariate correlations may imply estimation accuracy, but the unique variability captured from each predictor is not clear. For example, BMI was not included in the vast majority of regression models but was strongly correlated with outcome parameters across many movements Appendix C.

Due to the overall poor fit and variance explained by the linear regression models of onset, total force, and contact area further work is needed to provide waveform estimations of these parameters for use in clinical and modeling settings. While the onset of thigh-calf contact is not strongly estimated from this sample, prior works have established that onset occurs between ~125-135º of knee flexion (Kingston and Acker, 2018a; Zelle et al., 2007). This study has shown maximum knee flexion angle could be estimated based on anthropometrics. Therefore, other waveform assessment tools may be able to account for underlying sources of variation within the total force waveform, and could be used to model the magnitude of thigh-calf contact parameters within the range of motion establish in existing works.

Limitations of the regressive component of this study include limited sample size, lack of predictive testing, and the assumption of an underlying linear data structure. The procedures in this study assess the fit of a linear model based on anthropometric measures to TC contact parameters and provide guidance on whether anthropometric-based estimation of TC contact parameters is possible. Assessment of predictive ability on a new data set was not pursued due to the limited number of strong linear fits to the existing data. While these data were collected from the largest population measured for thigh-calf contact to date, this population consisted of healthy university aged participants who did not report habitual engagement in high flexion activities. Therefore, it requires further study to verify if parameter magnitudes, and regression results, found in the current study, would apply to older or habitually kneeling populations. Finally, only linear regressive models were used to fit these data and non-linear models may improve overall fit to the data.

3.7 Conclusions

Our results suggest that TC and HG contact can result in considerable force transfer between the thigh and shank segments during high knee flexion movements. While previous work has quantified these effects at the joint loading level (Pollard et al., 2011; Zelle et al., 2009) future work is required to incorporate TC contact parameters into a 3D MSK model. It is noteworthy that the population used in this study—consisting of young, generally active participants from many ethnic backgrounds—was largely unable to attain heel-gluteal contact in kneeling postures. Given our findings are markedly lower than previously published values in almost all contact parameters, it seems pertinent to recommend that future work on TC contact should include detailed information about calibration procedures, instrumentation, and participant anthropometrics to facilitate comparisons between studies. As well, data is needed from sufficiently sampled populations with specific cultural or occupational kneeling practices that are linked to increased risks of knee joint degenerative diseases.

Anthropometrics-based linear regression models for six high knee flexion movements strongly fit the maximum knee flexion angle and CoF using easily accessible anthropometric measurements (and maximum angle itself for the CoF equation). Regression estimates of TC onset, total force, and contact area were only weak to moderate. The identified predictor variables were robust to collinearity criteria from the largest currently available sample of TC contact data. Given the need to include TC contact forces in 3D MSK joint contact models of the knee in high flexion, waveform estimates of the studied parameters and other potential participant-specific explanatory variables should be explored to advance modeling of high knee flexion activities.

This study provides normative data for future modelling efforts investigating knee joint contact forces. Implementation of the reported total forces at appropriate CoF locations would improve the biofidelity and accuracy of inverse dynamics calculations or finite element simulations. We speculate that these data could be used to improve knee joint prosthetic design as overestimations of joint contact forces could result in excessive material deposition or rigidity in components. Although regression equations were only defined for two of the five intersegmental contact parameters, future work investigating regressions of these parameters after participant-specific normalization, or using nonlinear approaches, could provide stronger relationships.

3.8 Acknowledgments

I would like to formally recognize Dr. Paul Stratford (McMaster) for his guidance on statistical procedures and regression best-practices used in the anthropometric regression component of this study.

Chapter 4 – High knee flexion EMG

Components of this chapter have been published (Kingston and Acker, 2018b), however, additional detail is provided in methodology and results sections.

4.1 Introduction

Muscular activation waveforms of the vastus intermedius (VI), adductor magnus (AM), or semimembranosus (SM) during high knee flexion movements are unknown. High knee flexion is defined as movements where knee flexion exceeds 120º (Hemmerich et al., 2006; Kingston and Acker, 2018a; Zelle et al., 2009). Activation waveforms for these muscles are needed for muscle force modeling and verification in high knee flexion postures. Previous work, that did not measure deep musculature, represented the VI waveform as the average of vastus medialus (VM) and vastus lateralus (VL) or semitendinosus (ST) as identical to SM (Lloyd and Besier, 2003). Similarly, optimization based musculoskeletal (MSK) models currently have limited (Byrne et al., 2005; Montgomery et al., 1994; Saito et al., 2015) or no (Hamner et al., 2010; Martelli et al., 2015) verification data to assess biofidelity of predicted muscle activity in these muscles. These muscles were studied because they are the deep lower-limb muscles with the largest cross-sectional areas (and thus are the most likely to contribute to joint contact forces) that can be measured using fine wire insertion.

There have been previous attempts to represent fine-wire activation waveforms from surface EMG data. Jacobson et al. (1995) measured VM and biceps femoris (BF) activity during walking and running from 12 males with both surface and fine-wire electrodes. Between the two sites, there were similar variance ratios (< 0.4), reproduceability, and linear envelope shapes (R^2 > 0.5). McGill et al. (1996) reported that, in 5 males and 3 females, surface measured muscle activity could represent fine-wire measured activity of the quadratus lumborum, external oblique, internal oblique, and transverse abdominis muscles within 15% RMSD but stated their R^2 comparisons were not informative as phase misalignment of EMG peaks can lead to unexpectedly low values given good overall visual agreement. Byrne et al. (2005) found a modest linear correlation (R = 0.579, R^2 = 0.336) between surface and fine-wire recordings of the rectus femoris (RF) concluding that surface recordings might not be representative of RF activation levels due to vastii crosstalk. Finally, Allen et al. (2013) compared surface and fine-wire activity from supraspinatus and infraspinatus, in 10 males and females, during a number of isometric exertions. During external or internal axial humeral rotation trials, surface recordings overestimated supraspinatus by 32% (R^2 =.76) and 21% (R^2 = 0.72) and infraspinatus by 72% (R^2 = 0.64) and 500% (R^2 = 0.62) respectively (Allen et al., 2013). Although these previous studies have achieved varying levels of success in using surface recordings as proxies for fine-wire recordings, the promising results of Jacobson et al. (1995) motivated the current study.

The purpose of this study was to quantify the activation of VI, AM, and SM using fine-wire electrodes and to compare these signals to those acquired from easily accessible surface locations over VL, RF, VM, ST, and BF. We hypothesised that relationships exist in which fine-wire signals may be estimated reliably from surface sites. Two criteria were used to evaluate if the surface locations reliably represented fine-wire: Coefficient of determination (R^2) greater than 0.85 and RMSD less than 10 %MVC (McGill et al., 1996). These relationships, if robust, would simplify future work of muscular control in high knee flexion movements and could potentially improve MSK model estimates of knee joint contact forces.

4.2 Methodology

4.2.1 Participants

Sixteen participants, eight male and female, were recruited as a sample of convenience from the university's study body (Table 4-1). Exclusion criteria consisted of any low back or lower limb injury within the past year that required medical intervention or time off from work for longer than three days, and any history of surgical interventions to the back or lower limb. All participants self-reported right leg dominance and the ability to kneel to the ground without pain. Each participant read and signed an informed consent form approved by the university's research ethics board.

Table 4-1 Mean (standard deviation) descriptive and anthropometric participant information. Circumferences were measured distally from the greater trochanter towards the lateral femoral condyle: proximal circumference was measured at 10%, mid at 50%, and distal at 90% of thigh length.

Parameter	Females (*n* = 8)	Males (*n* = 8)	All (*n* = 16)
Age (yrs)	24.30 (4.5)	26.30 (3.2)	25.30 (3.9)
Height (m)	1.70 (0.1)	1.80 (0.1)	1.80 (0.1)
Mass (kg)	70.40 (10.7)	88.60 (16.5)	79.50 (16.4)
BMI (kg/m^2)	24.30 (3.8)	27.00 (3.4)	26.70 (3.8)
Thigh Length (m)	0.41 (0.04)	0.40 (0.04)	0.40 (0.04)
Proximal Thigh (m)	0.60 (0.04)	0.63 (0.09)	0.61 (0.07)
Mid-Thigh (m)	0.53 (0.04)	0.55 (0.12)	0.54 (0.09)
Distal Thigh (m)	0.41 (0.04)	0.42 (0.05)	0.41 (0.04)

4.2.2 Experimental protocol

Participant height and segmental anthropometrics (Table 4-1), from the right lower limb, were measured before instrumentation. Participant mass was calculated from force plate data during a static calibration trial. Thigh circumferences were measured distally from the greater trochanter towards the lateral femoral condyle: proximal circumference was measured at 10%, mid at 50%, and distal at 90% of thigh length.

Surface EMG electrode sites (Appendix D) were located and prepared following SENIAM guidelines (Hermens et al., 2005) in a similar configuration to a previous high knee flexion study (Kingston et al., 2016). Following surface EMG preparations, fine-wire electrodes were inserted into the VI, AM, and SM (Figure 4.1) of the right leg. After each insertion, participants firmly contracted against manual resistance 3-6 times in knee flexion/extension (VI and SM) or hip adduction (AM) to set fine-wires inside the muscle. Participants sat on the edge of a massage table (~90º knee flexion) for VI and AM insertions. Fine-wires for VI passed through the rectus femoris (RF) and terminated at the mid-point of the muscle belly (Figure 4.1 – A). Prior to the insertion at AM, Doppler ultrasound was used to identify femoral artery blood flow, then gentle adductions of the femur was monitored via ultrasound to identify the gracillis, AM, and adductor longus muscles (Figure 4.1 – B). Participants were able to stand and walk if cramping or discomfort occurred until they self-reported that discomfort had subsided. Fine-wires remained in muscles for approximately 1 (SM) and 1.75 (VI and AM) hours.

Participants then completed two 6 s isometric maximum voluntary contractions (MVC) for each muscle group with a minimum 60 s rest between trials. Vastii MVCs were performed with the right leg in a commercial leg extension exercise machine, under isometric conditions, with the knee joint positioned at 45º of flexion (Hermens et al., 2005; Kingston et al., 2016).

Adductor MVCs were performed with participants seated on a massage table where they isometrically adducted their hips to squeeze the thorax (~0.5 m diameter) of the investigator.

Participants were then asked to assume a prone position for SM insertions. Prior to the insertion of SM the popliteal artery was identified with Doppler ultrasound medial to the semitendinosus tendon, then gentle knee flexion contractions were performed to find the border between SM and the flexor head of AM (Figure 4.1 – C). Semimembranosus MVCs were performed isometrically against manual resistance with the knee at 65º of flexion (Hermens et al., 2005; Kingston et al., 2016).

After EMG preparations, rigid bodies were attached to the right thigh, shank, foot, and the pelvis for kinematic tracking (Figure 3.2). Participants then completed a static standing trial, followed by knee and hip functional joint center trials (Besier et al., 2003b; Camomilla et al., 2006; Ehrig et al., 2007). The high knee flexion movements in this study were the same as those used in study 1 (Figure 3.2). Participants first observed all movements being performed by the investigator, then practiced until they could perform each movement comfortably. One repetition of each movement and a single walking trial were completed in a fixed order block. Movement order was then fully randomized for four more repetitions (a total of 5 repetitions) of: heels-up squat (HS), flatfoot squat (FS), dorsiflexed kneel (DK), plantarflexed kneel (PK), dorsiflexed unilateral kneel (DUK), plantarflexed unilateral kneel (PUK), and walking (WK). The fixed order block was used to ensure that at least a single trial of each movement was recorded as quickly as possible in case of accidental fine-wire shift or discomfort. Each squatting or kneeling trial took 6 s to complete and consisted of stepping onto an embedded force plate, descending to maximal knee flexion, and holding the position. Walking trials began with participants two steps away from the force plates such that their third step was contact of the right foot on a single force plate. Participants moved at a self-selected pace in all trials, with the following movement restrictions during high flexion movements: step with the right foot first; kneel onto the right knee (kneeling trials); then hold the final posture until instructed to stand. During performance of DUK or PUK, participants were instructed to shift the most of their bodyweight onto the right leg to resemble firing positions used in military theater (Department of the Army, 2010).

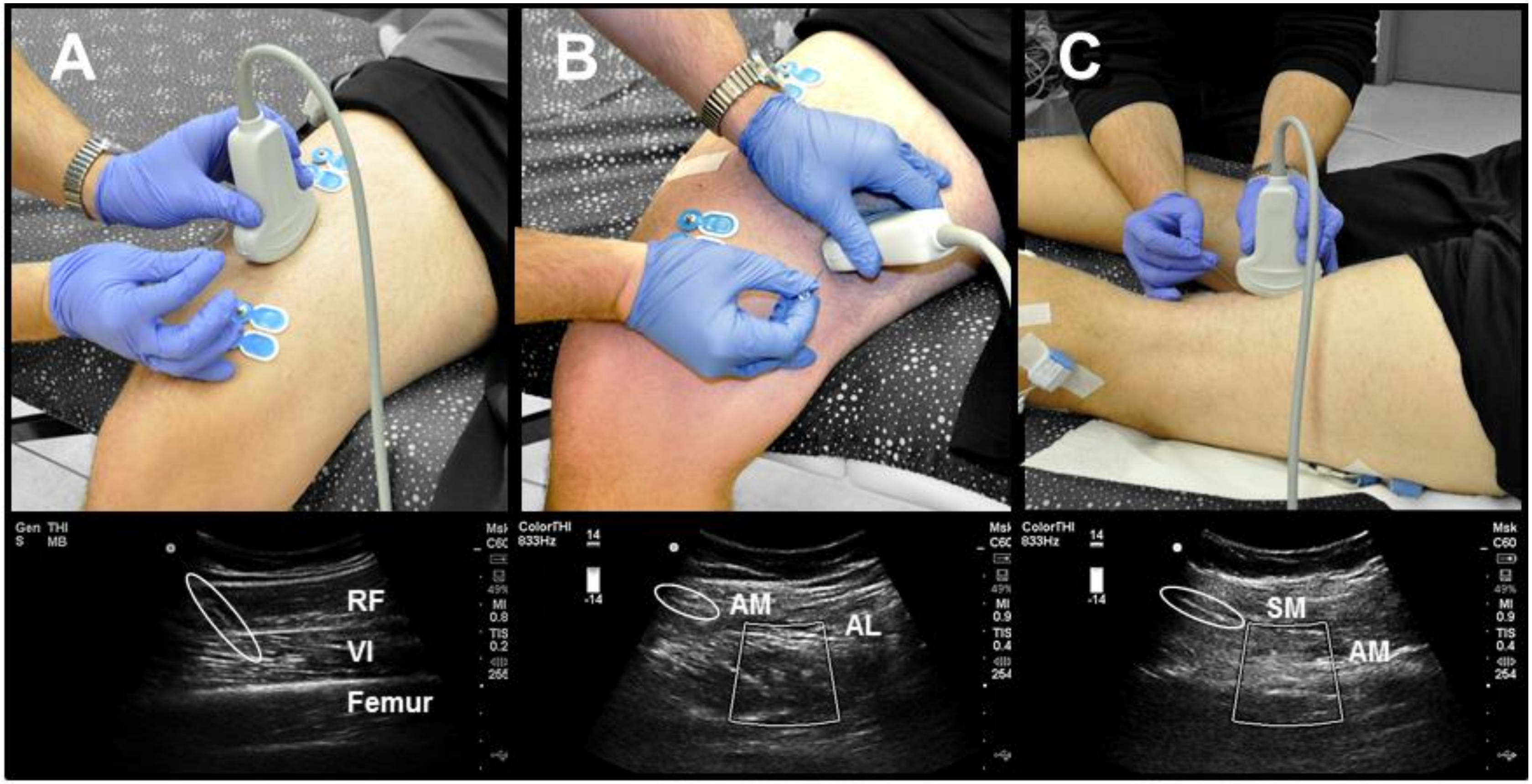

Figure 4.1 Fine-wire insertion locations and needle positioning during preparation of participant P16. Top row: Ultrasound probe placement and needle positioning for insertion. Bottom row: Needle location (circled) within muscles before the cannula was removed. RF is rectus femoris, VI is vastus intermedius, AM is adductor magnus, AL is adductor longus, and SM is semimembranosus.

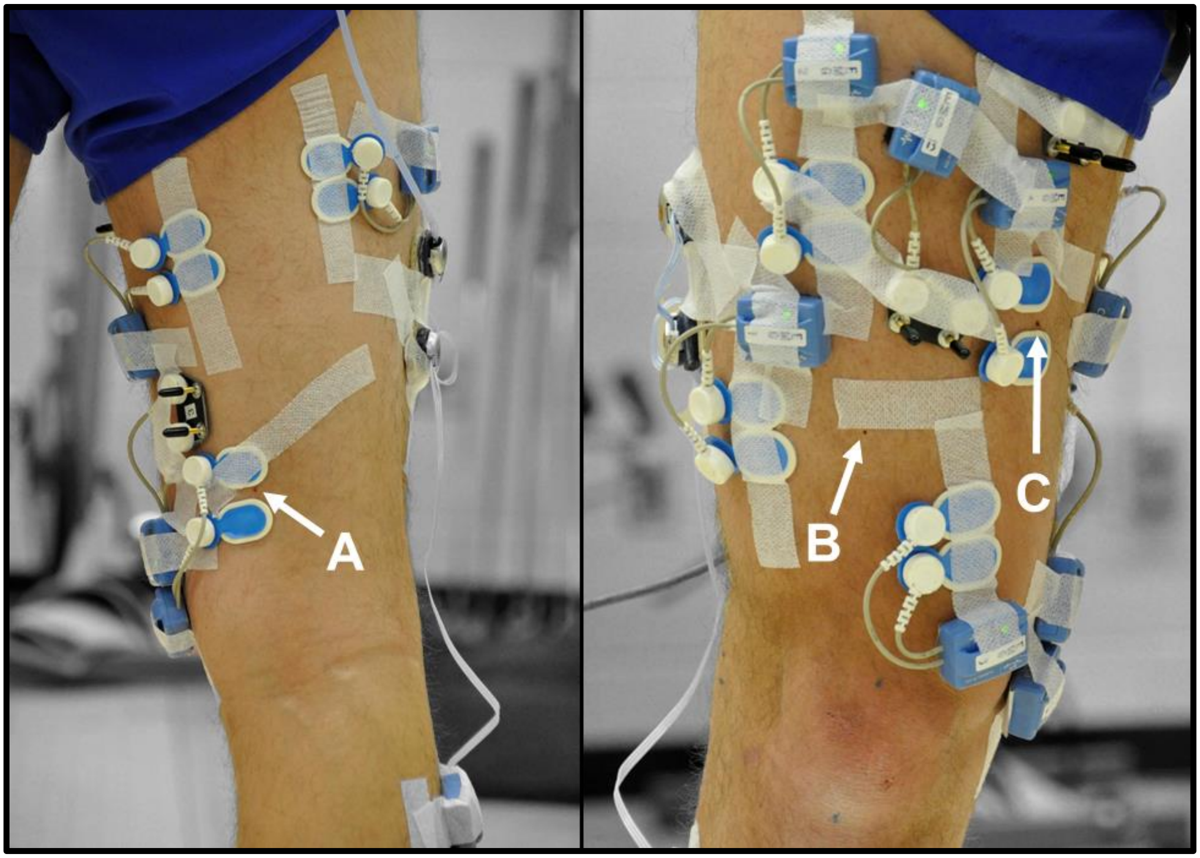

Figure 4.2 Fine-wire and surface EMG instrumentation from the posterior (left) and anterior (right) thigh of participant P04. Arrows indicate fine-wire insertion sites. A) Fine-wire location of semimembranosus (SM) with surface electrodes spanning the insertion site. B) Fine-wire location of vastus intermedius (VI). C) Fine-wire location of adductor magnus (AM) with surface electrodes spanning the insertion site.

4.2.3 Instrumentation

The participant's right leg was instrumented with wireless surface EMG equipment (Wave Plus, Cometa srl, Milan, IT; input impedance = 20 MΩ, common mode rejection ratio = 120 dB at 60 Hz, bandpass filter 10-1000 Hz) to measure activity of the VL, RF, VM, ST, and BF at 2100 Hz. Bipolar Ag/AgCl electrodes (BlueSensor N, Ambu Inc., Glen Burnie, MD, USA) were adhered, with 2 cm inter-electrode spacing, after shaving, abrading, and cleaning of the skin. Surface electrodes with 2-2.5 cm inter-electrode spacing were attached over the AM and SM insertion sites to avoid interference with fine-wires.

Fine-wire measurement of VI, AM, and SM was recorded at 2100 Hz using the same hardware as surface signals. Researchers wore new nitrile gloves for each insertion and used isopropyl alcohol to create a 2 cm^2 sterile field at the insertion site. Sterile single-use 50 mm long 25 gauge (0.55 mm) hypodermic needles (Motion Lab Systems, Inc., Baton Rouge, LA) were used to insert bipolar fine-wire electrodes using guidelines from Perotto (2011) and real-time ultrasonography (M-Turbo, Sonosite Inc., WA, USA; Figure 4.1). Each needle contained two nylon insulated 304 series stainless steel wires (0.051 mm x 200 mm), which were insulated except for a 2 mm exposed sensor inside the muscle and 5 mm bare-wire termination for connection to spring leads. Fine-wires extended > 8 cm above the skin surface (Figure 4.2).

Kinematic data were recorded at 100 Hz using an optoelectronic system (Optotrak, NDI, Waterloo, ON). Kinetic data were recorded at 2100 Hz from two embedded force plates (OR6-7, AMTI, Watertown, MA). All data were synchronized via collection software with a fixed 14 ms telemetric delay in EMG data accounted for in data processing.

4.2.4 Data processing

Processing was completed using Matlab 9.2 (R2017a, The Mathworks, Natick, MA). Kinematic and ground reaction force (GRF) data were low-pass filtered using a bidirectional 2nd-order Butterworth digital filter with a 6 Hz cut-off frequency (Longpré et al., 2013; Winter, 2009). Knee and hip joint centres were calculated from functional trials using the Symmetrical Centre of Rotation Estimation (SCoRE) algorithm (Ehrig et al., 2007, 2006) which provides accurate hip joint centre predictions from skin markers when compared to dual-plane fluoroscopy (Fiorentino et al., 2016). Knee joint angles were decomposed in a flexion/extension-ab/adduction-axial rotation (Z-X-Y) Cardan sequence (Wu and Cavanagh, 1995).

Data were then truncated from when vertical GRF component exceeded 10 N to a manually identified frame where the knee flexion waveform plateaued in high flexion movements (Kingston and Acker, 2018a) and from heel-strike to toe-off in walking. Activation waveforms were visually screened for motion and/or electrode contact artifacts, then processed using a 2 Hz low-pass single-pass Butterworth filter to produce a linear envelope and normalized to isometric MVCs (Kingston et al., 2016; Shultz et al., 2001). The activation waveform of VI was compared to three surface vastii sites (VL, RF, VM), with SM compared to three surface hamstring sites (surface SM, BF, ST), and AM compared to its surface site.

Time normalized trials were averaged within-participant with RMSD calculated between fire-wire and surface activation waveforms. RMSD were averaged across participants (Chapman et al., 2010; McGill et al., 1996). Regression was performed within-participant—between fine-wire and respective surface sites—using a least-squares quadratic polynomial to define our R^2 criterion and then averaged across participants (Byrne et al., 2005; McGill et al., 1996).

4.3 Results

Based on mean RMSD and R^2 values, no surface sites satisfied either of our criteria (< 10 %MVC RMSD or R^2 > 0.85) to act as a proxy for fine-wire sites in these movements. Mean RMSD and R^2 in each movement are reported in Table 4-2. The best matched surface and indwelling signals from our sample, as per our stated criteria, are shown in Figure 4.3. Across participant mean fine-wire activation profiles for each movement, normalized to knee flexion angle, are reported in Appendix E.

Table 4-2 Mean (standard deviation) of RMSD and R^2 values across participants for high flexion movement comparisons of surface to respective fine-wire signals. Movements listed in the leftmost column are: heels-up squat (HS), flatfoot squat (FS), dorsiflexed kneel (DK), plantarflexed kneel (PK), dorsiflexed unilateral kneel (DUK), plantarflexed unilateral kneel (PUK), and walking (WK). Muscles are vastus intermedius (VI), vastus lateralis (VL), rectus femoris (RF), vastus medialis (VM), adductor magnus (AM), semimembranosus (SM), biceps femoris (BF), and semitendinosus (ST).

Indwelling	VI						AM		SM					
Surface	VL		RF		VM		AM		BF		ST		SM	
Movement	RMSD	R^2	RMSD	R^2	RMSD	R^2	RMSD	R^2	RMSD	R^2	RMSD	R^2	RMSD	R^2
HS	15.6 (14.8)	0.40 (0.24)	16.3 (15.0)	0.29 (0.25)	14.7 (14.6)	0.39 (0.22)	40.7 (20.7)	0.39 (0.19)	27.3 (26.4)	0.29 (0.18)	26.6 (26.8)	0.36 (0.19)	26.9 (27.9)	0.31 (0.19)
FS	19.7 (17.3)	0.36 (0.33)	25.3 (23.5)	0.37 (0.34)	18.5 (16.6)	0.37 (0.35)	49.0 (23.0)	0.29 (0.20)	29.2 (29.3)	0.22 (0.21)	26.0 (26.9)	0.35 (0.2)	40.3 (63.9)	0.30 (0.22)
DK	17.2 (13.5)	0.46 (0.26)	17.7 (14.2)	0.45 (0.32)	15.4 (13.6)	0.45 (0.26)	43.0 (25.3)	0.32 (0.20)	21.6 (19.6)	0.18 (0.15)	20.8 (18.7)	0.30 (0.21)	35.5 (63.4)	0.39 (0.19)
PK	20.6 (20.6)	0.38 (0.22)	19.6 (20.2)	0.37 (0.27)	17.4 (19.7)	0.34 (0.17)	45.7 (24.6)	0.32 (0.16)	21.8 (17.8)	0.18 (0.14)	22.5 (19.9)	0.31 (0.19)	37.7 (63.8)	0.35 (0.22)
DUK	21.2 (19.4)	0.45 (0.26)	20.1 (18.7)	0.40 (0.29)	18.0 (18.9)	0.42 (0.25)	41.9 (22.5)	0.32 (0.15)	23.2 (22.2)	0.30 (0.20)	18.9 (12.5)	0.31 (0.22)	18.6 (12.2)	0.45 (0.19)
PUK	18.6 (15.8)	0.40 (0.32)	18.7 (15.6)	0.43 (0.33)	17.0 (15.1)	0.41 (0.30)	49.6 (34.3)	0.24 (0.16)	23.7 (26.8)	0.23 (0.15)	16.7 (13.0)	0.25 (0.25)	19.7 (19.1)	0.33 (0.24)
WK	39.3 (37.9)	0.43 (0.31)	36.3 (39.0)	0.34 (0.29)	35.2 (39.8)	0.43 (0.29)	76.1 (48.0)	0.45 (0.27)	33.5 (21.0)	0.38 (0.27)	32.8 (20.2)	0.52 (0.26)	34.7 (21.3)	0.48 (0.29)

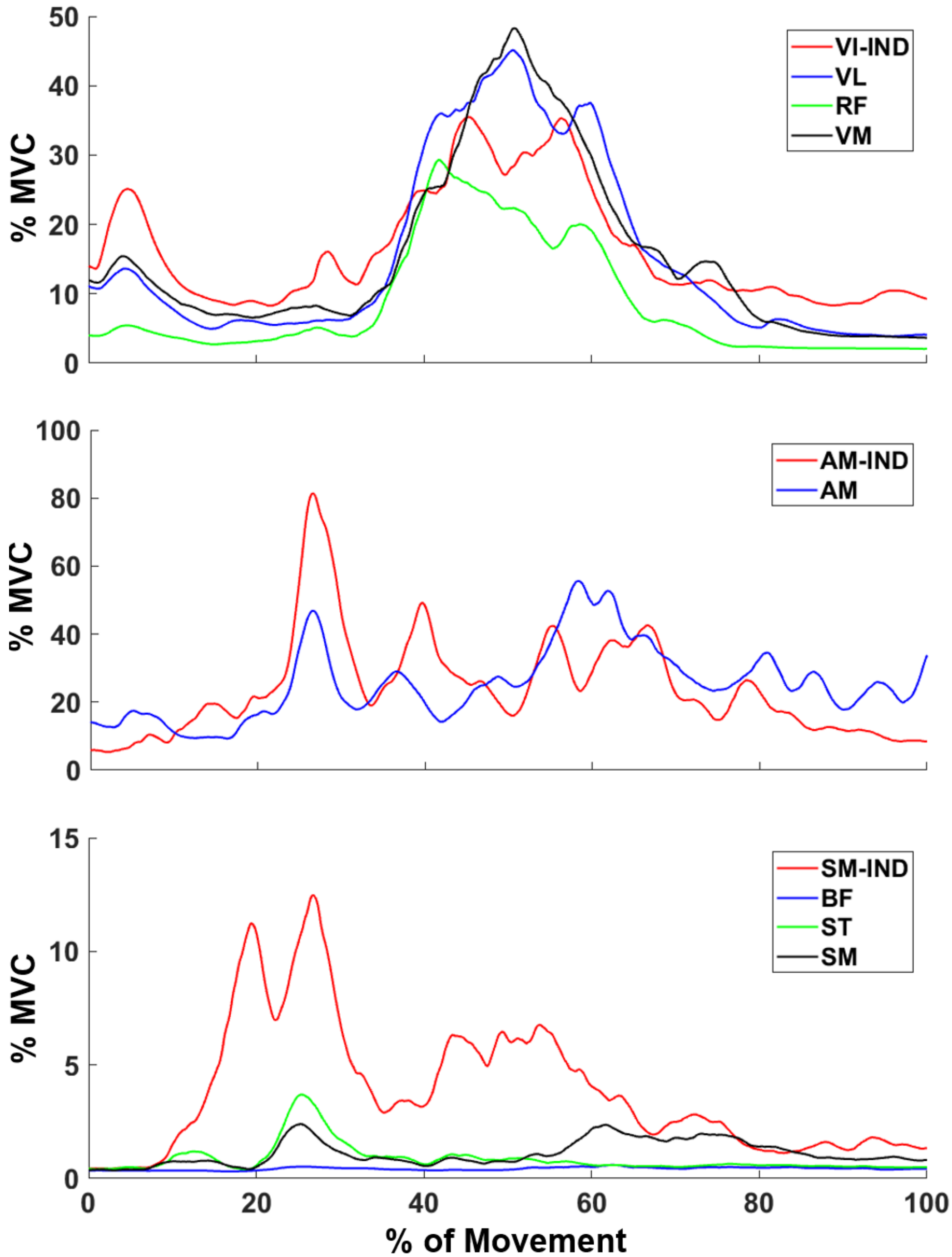

Figure 4.3 Muscle activation waveforms normalized to percentage of movement across five repetitions. Top: Vastii waveforms from participant P01 performing a dorsiflexed kneel. Middle: Adductor waveforms from participant P05 performing a heels-up squat. Bottom: Hamstrings from participant P04 performing a flat-foot squat. Muscle sites are: fine-wire vastus intermedius (VI-IND), vastus lateralis (VL), rectus femoris (RF), vastus medialis (VM), fine-wire adductor magnus (AM-IND), adductor magnus (AM), fine-wire semimembranosus (SM-IND), semimembranosus (SM), semitendinosus (ST), and biceps femoris (BF).

4.4 Discussion

The purpose of this study was to quantify the activation of VI, AM, and SM using fine-wire electrodes for comparison to easily accessible surface sites. These comparisons took place for six high knee flexion activities and level walking using criteria of < 10 %MVC RMSD and >0.85 R^2 to indicate a reliable surface to fine-wire relationship. None of the surface sites satisfied our criteria in this healthy young sample. This was largely due to the considerable variability of surface-indwelling comparisons between participants (Table 4-2 and Appendix E). Our findings suggest that the measurement of VI, AM, and SM muscles during high knee flexion movements cannot be accurately represented by surface sites and that fine-wire EMG may be required if isolated muscle/motor unit activity is desired.

Although vastii musculature did not meet our criteria, some participants met both criteria in select movements (primarily squatting activities). At a sample level, results would suggest that VM is the only muscle that could be modeled if a more relaxed RMSD and R^2 criterion could be accepted. For 5 of our 16 participants, VM satisfied our RMSD criterion across all high flexion movements with 2 also satisfying our R^2 criterion in select cases. Interestingly, of the surface vastii comparisons, RF activation was the least representative of VI activation even though its line of action, and assumed mechanical function, is the most similar to VI.

The surface site for AM, confirmed appropriate via ultrasound, was below 20 %MVC for most participants while the fine-wire site was ~50 %MVC. We were surprised that the surface signal was lower than the indwelling given the influence of crosstalk from neighboring muscles due to the larger pick-up volume of surface compared to fine-wire approaches (Basmajian and De Luca, 1985; Clancy et al., 2002; Winter et al., 1994). Even so, AM comparisons were consistently the worst of the fine-wire sites assessed in this study and is rarely reported in lower limb EMG studies. Therefore, limited comparisons can be made to previous work.

The RMSD results of SM comparisons should be viewed with caution as the descent phase of high flexion activities generally requires less than 20 %MVC from hamstring muscles (Kingston et al., 2016). The small magnitude of the signals could allow this criterion to be met despite a poor fit in terms of pattern. Therefore, R^2 outcomes may be the more meaningful metric for this muscle group in this study. Across this sample, these muscles did not meet our R^2 criterion nor the more relaxed 0.5 R^2 criterion used by Jacobson et al. (1995).

The largest difference between surface and fine-wire sites, across all movements, occurred during the weight bearing phase of our walking trial. We speculate that this is due to the localized pick-up volume of our fine-wire sites as the motor units with exposed sensors present may have been, by chance, more active than the holistic representation surface sites provide (Clancy et al., 2002; Winter et al., 1994). The low physical demand of walking, compared to squatting or kneeling, may support this theory as site agreement would likely be higher if more motor units were recruited (Fuglevand et al., 1992; Henneman et al., 1965; Yao et al., 2000).

Limitations of this study include muscle fibre/motor unit movement relative to surface locations, the muscle fibre/motor unit type that was measured from fine-wire electrodes, and the relative novelty of some of these high knee flexion movements to most participants. Participants performed movements using their entire range of knee flexion, therefore, the signal measured from surface EMG was not from the same volume of muscle fibers throughout the trial. Surface EMG pickup volume would also be influenced by soft-tissue artifact as local displacement of electrodes is unavoidable in high knee flexion postures. However, fine-wire measurements would be minimally influenced by such artifact. While fine-wire EMG provides a precise representation of muscle activity, we are not aware of any assessment (or the practicality) of the day-to-day repeatability in these measures for the muscles investigated. Finally, this sample of convenience consisted of young healthy individuals who do not commonly perform these high knee flexion movements. Therefore, the applicability of these findings to habitually kneeling populations (e.g. construction workers, practicing Muslims) requires further investigation.

4.5 Conclusion

The results of this study suggest that variability in %MVC RMSD and R^2 is high when comparing surface EMG activation waveforms to fine-wire measurement of VI, AM, and SM during high knee flexion activities and walking. Therefore, representative surface locations were not identified for the high knee flexion movements investigated in this study. Future modelling efforts using EMG based muscle force estimation may benefit from fine-wire measurement of the activity of these muscles, as crosstalk would be eliminated, but researchers should be cautious of electrode site specificity being unrepresentative of a musculotendinous unit.

These data will support verification of future high knee flexion models as they are the first report of activation waveforms for high knee flexion movements in general, but also for four newly investigated postures. As described in the limitations, the reported fine-wire signals are site specific and should be interpreted with caution if being used for comparative purposes. Future work is needed on combining multiple surface measurements to assess weighted fit with fine-wire signals and the investigation of regional variability of EMG signals in the large muscles of the lower limb. Should regional variability exist within this musculature, there would be empirical support for variable activation of muscle partitions in musculoskeletal modelling approaches.

4.6 Acknowledgements

We would like to formally recognize Dr. Linda McLean (University of Ottawa) for fine-wire EMG training and Geena Frew (University of Waterloo) for her dedicated assistance during data collection.

Chapter 5 – Full flexion musculoskeletal knee joint model

This chapter will detail modules and assumptions which were part of the first stage of development for a full range of motion 3D MSK model of the knee designed to estimate tibial contact forces in high knee flexion postures.

5.1 Introduction

There is no current 3D MSK model of the knee that can incorporate the effects of intersegmental contact during high knee flexion postures. Sagittal plane models have been previously reported (Hirokawa and Fukunaga, 2013), as have finite element models (Caruntu et al., 2003; Zelle et al., 2009), but none of these studies incorporated 3D intersegmental contact force orientation. In addition, these models used lumped muscle parameters to simplify MSK geometry to the sagittal plane. The model used by Zelle et al. (2009) consisted of tibia and femur segments only and was not verified for use in lower ranges of knee flexion (closer to standing). Caruntu et al. (2003) used a spring-damping model to estimate thigh-calf contact forces, but did not report magnitudes nor verify their predictions against empirical intersegmental contact data. Hirokawa and Fukunaga (2013) used thigh-calf contact parameters reported from Zelle et al. (2007), but were limited to a seven muscle sagittal plane model. Therefore, development of new model using more fulsome MSK geometry and 3D intersegmental parameters was warranted.

Intersegmental contact is a critical parameter when modelling high knee flexion movements. Omitting intersegmental contact may result in model overestimations of tibial compression and shear as high as 1.99 and 0.54 BW respectively (Zelle et al., 2009). The importance of including intersegmental contact was also highlighted by Nagura et al. (2006) as their 2D high knee flexion model did not consider these forces and predicted tibial compression as high as 5 kN or 7.3 BW during a full squat. In our own work (Kingston and Acker, 2018a), it became apparent that direct tracking of a pressure sensor with a known measurement plane would be advantageous compared to assuming a sagittal plane force vector. This would allow for a more accurate tibial contact force orientation and provide the first 3D report of these forces in high knee flexion movements.

Other modelling considerations specific to high knee flexion movements exist. There are no known reports of musculotendinous moment arms—for knee flexor and extensor muscles—in the high knee flexion range as current *in vitro* studies report from 0-120° (Buford et al., 1997; Wagner et al., 2013) or from 40-110º *in vivo* (Fiorentino et al., 2013). Therefore, estimates of moment arms must be computed using knowledge of regional anatomy during these movements. There is a wide range of muscle specific tension values used in the modelling literature that have not been assessed for sensitivity in high knee flexion ranges. Many modern MSK model specific tensions exceed the 15-30 N/cm^2 values reported for mammalian and human tissue (Erskine et al., 2011, 2009; Fukunaga et al., 1996; O'Brien et al., 2010). For example, Carbone et al. (2015) used 30 N/cm^2, Arnold et al. (2010) and Delp et al. (1990) used 61 N/cm^2, and Dickerson et al. (2007) used 88 N/cm^2. Therefore, model sensitivity to specific tension must be assessed.

Verification of MSK model predictions is a critical aspect in any computational model development cycle. Although there is no known instrumented implant data available from high knee flexion ranges, publicly available gold-standard datasets are available for ~0-100º of knee flexion (Fregly et al., 2012; Taylor et al., 2017). The Grand Knee Challenge was a semi-annual modelling competition where kinematic, kinetic, EMG, and tibial compression data were provided to researchers. Similarly, Orthoload datasets will provide triaxial tibial forces—in addition to kinematic, kinetic, and EMG data—but fulsome datasets are not yet publicly available (personal communication with Dr. William Taylor-ETH Zurich).

Therefore, the purpose of this study was to define and quantify prediction error of a full range of motion 3D MSK model of the right lower limb that incorporated 3D intersegmental contact parameters. Component verification consisted of comparing estimates of tibial compressive force to instrumented implant values during activities in the ~0-100º knee flexion range and to qualitatively compare EMG waveforms to muscle force estimates of *in vivo* data from the 4th Grand Knee Challenge dataset (Fregly et al., 2012).

5.2 Methods

5.2.1 Overview

This model contains 13 DoF across three joints: a 6 DoF ankle, 4 DoF knee, and 3 DoF hip and was coded in Matlab 9.2 (R2017a, The MathWorks, Natick, MA). Required inputs are kinematic, kinetic, and anthropometric data which is detailed below. This model was designed in modular format to facilitate future development and is presented in that layout. Data collected from sixteen participants—reported in section 4.2.1—were used as inputs to the model. In addition, ten participants who took part in both studies 1 and 2, were used as a sub-sample for repeatability of intersegmental contact parameter measurement (section 5.2.4).

5.2.2 Anatomical Geometry

Kinematic data of the lower limb was recorded from rigid body marker clusters on the pelvis, femur, shank, and foot. Three-dimensional displacement of rigid bodies from an Optotrak system (Certus/3020, NDI, Waterloo) was output with digitized landmarks in a GCS. A standardized set of anatomical points was used across all studies for segmental LCS definitions (Appendix F).

5.2.2.1 Functional joint centers

Functional joint centres (CoR in Eq 5.1) were defined for the hip and knee using the Symmetrical Centre of Rotation Estimation (SCoRE) algorithm (Ehrig et al., 2007, 2006) written as a linear least-squares problem (Eq 5.1). Functional definition of the hip joint center location improves point estimates by 14-62 mm (Camomilla et al., 2006) when compared to geometric scaling (Bell et al., 1989) in simulated data. The SCoRE algorithm was shown to be the best predictor (10.8 ± 3.2 mm) of hip joint center locations when compared to dual-plane fluoroscopy from *in vivo* data (Fiorentino et al., 2016). Similarly, Besier, Lloyd, & Ackland (2003) found increased landmark repeatability using functional hip joint centers and averaged helical knee axes, similar to the Gillette algorithm, used in Visual 3D software (Schwartz and Rozumalski, 2005). Functional joint trials were cyclic knee flexion extension and star-arc movements (Camomilla et al., 2006).

$$\begin{pmatrix} pR_1 & -dR_1 \\ \vdots & \vdots \\ pR_n & -dR_n \end{pmatrix} \begin{pmatrix} pCoR_{loc} \\ dCoR_{loc} \end{pmatrix} = \begin{pmatrix} dLCS_{o_1} - pLCS_{o_1} \\ \vdots \\ dLCS_{o_n} - pLCS_{o_n} \end{pmatrix} \qquad \textbf{Eq 5.1}$$

pR_n is the LCS of the proximal segment for frame n, dR_n is the LCS of the distal segment for frame n, $pCoR_{loc}$ is the locally expressed centre of rotation estimation from the proximal segment, $dCoR_{loc}$ is the locally expressed centre of rotation estimation from the distal segment, $dLCS_{o_n}$ is the translation vector from GCS origin to the distal segment's LCS origin for frame n, $pLCS_{o_n}$ is the translation vector from GCS origin to the proximal segment's LCS origin for frame n.

5.2.2.2 Bone Scaling

Bone surfaces were obtained from vertex based object files of a single Japanese male patient (BodyParts3D, © The Database Center for Life Science licensed under CC Attribution-Share Alike 2.1 Japan). Hip and knee joint spacing was calculated from source bone models by manually selecting vertices on the acetabulum and femoral head (hip), medial tibial and femoral plateaus (knee), and distal tibial plateau and talus (ankle).

After establishing source model joint spacing, rigid affine scaling (Umeyama, 1991) was used to modify each bone separately by minimizing the 3D Euclidean distance between the following bone vertex locations and measured anatomical points: pelvis) right ASIS, right PSIS, left ASIS, and left PSIS; thigh) GT, lateral and medial femoral epicondyles; shank) lateral and medial tibial epicondyles, tibial tuberosity, and lateral and medial malleoli; foot) heel, 1st and 5th metatarsals (Figure 5.1 and Figure 5.2). Mean 3D scaling errors, for each participant and segment, were calculated to assess reconstruction error. Joint spacing was also re-assessed post scaling and segmental translations were used to position scaled bone models with less than 1mm 3D error compared to pre-scaling values.

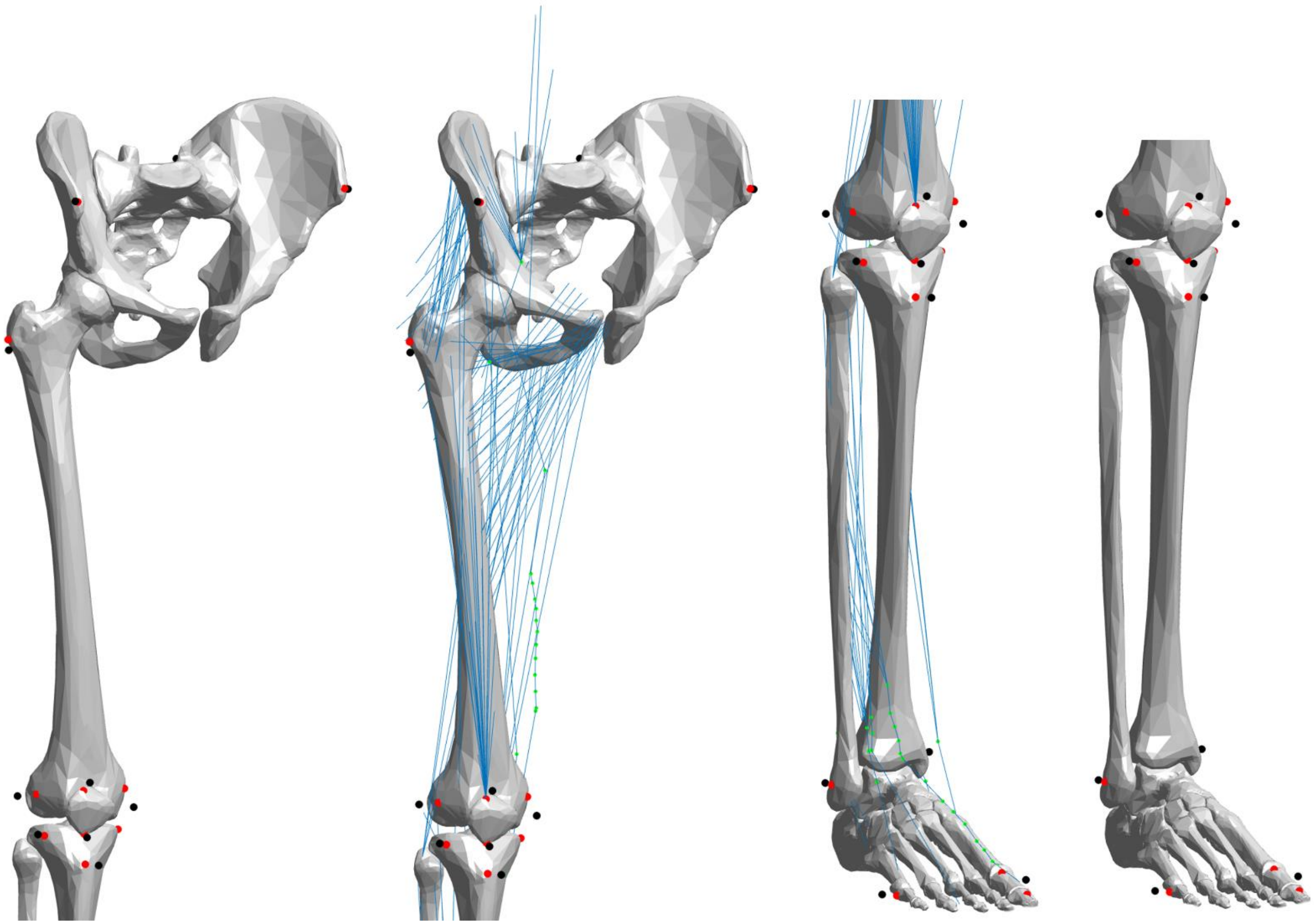

Figure 5.1 Anterior view of bone and muscle geometry of musculoskeletal (MSK) model. Red spheres are manually selected landmarks matching those from Horsman et al. (2007). Black spheres are the scaled positions of source MSK geometry with blue lines indicating muscle paths. Green spheres within a muscle path are scaled VIA points. 3D bone models are from BodyParts3D, © The Database Center for Life Science licensed under CC Attribution-Share Alike 2.1 Japan.

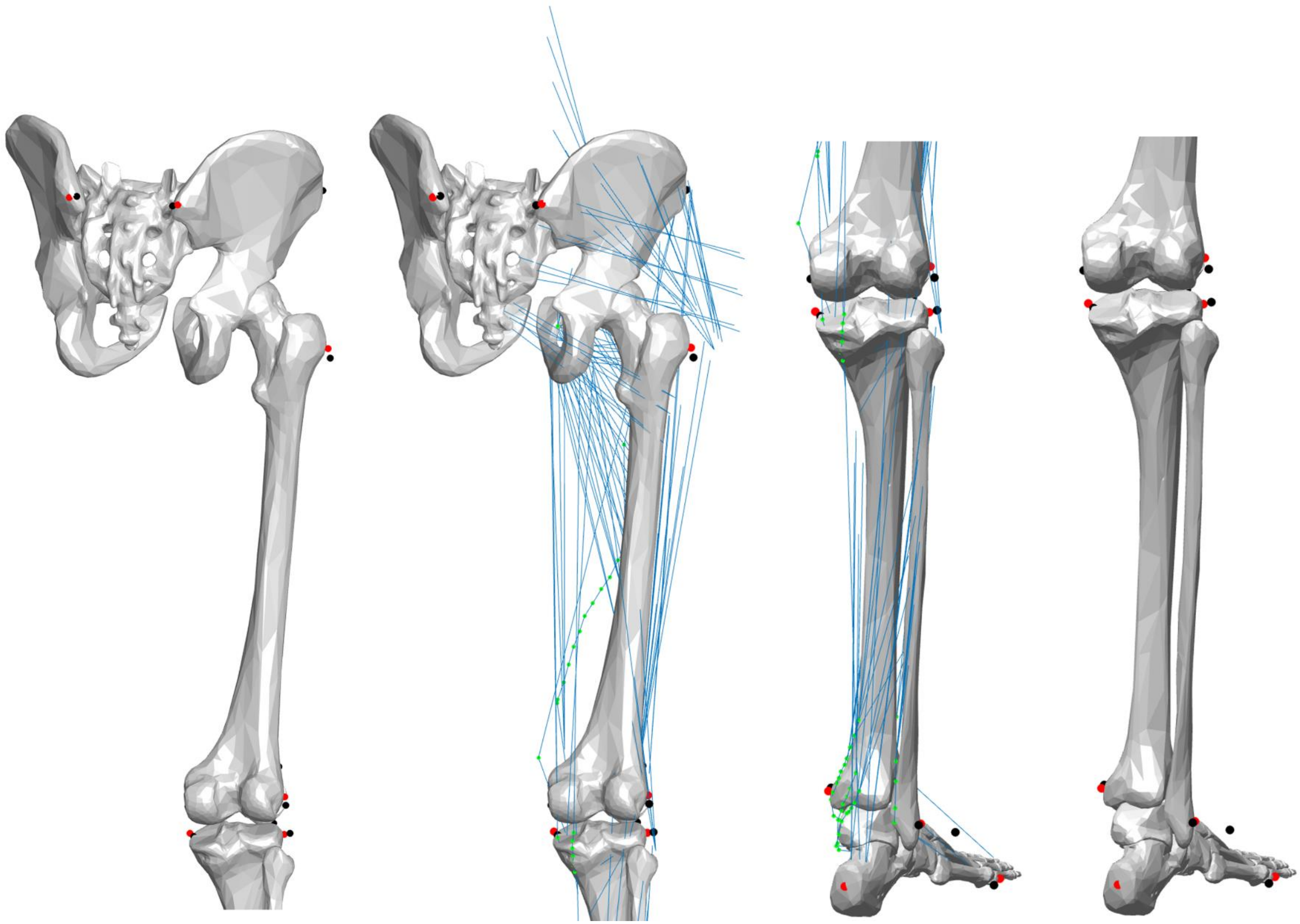

Figure 5.2 Posterior view of Figure 5.1.

5.2.2.3 Muscle parameters and moment arms

Muscle origin and insertion locations were defined using coordinate data from Horsman et al. (2007). These data were taken from the right leg of an embalmed male (age 77 yrs, height 1.74 m, mass 105 kg) sectioned at the superior aspect of the L1 spinal body (Horsman et al., 2007). Muscle parameters (e.g. PCSA, pennation angle, fibre length) and origin/insertion locations—with respect to the hip joint center—are listed in Appendix A. This data set included 56 muscle partitions (38 muscles in total) that were further segmented into 161 muscle elements. Muscle attachment and VIA points were provided in relation to specific segments (Appendix A).

Quadriceps muscles have a confluence at the proximal patella. Therefore, knee extensor muscles passing the knee joint were forced to conform to a participant specific spherical wrapping surface (Figure 5.3 – B & C) if the perpendicular distance to a LoA from the sphere origin was less than its radius (Charlton and Johnson, 2001; Damsgaard et al., 2006). The engagement of wrapping was determined using the vector quadruple product to determine 3D point-line distance each frame (Figure 5.4 and Eq 5.2). The wrapping sphere radius (Figure 5.3 - A) was determined as the perpendicular distance between the femoral groove and an axis defined between vertices of the medial and lateral femoral condyles (Iwaki et al., 2000).

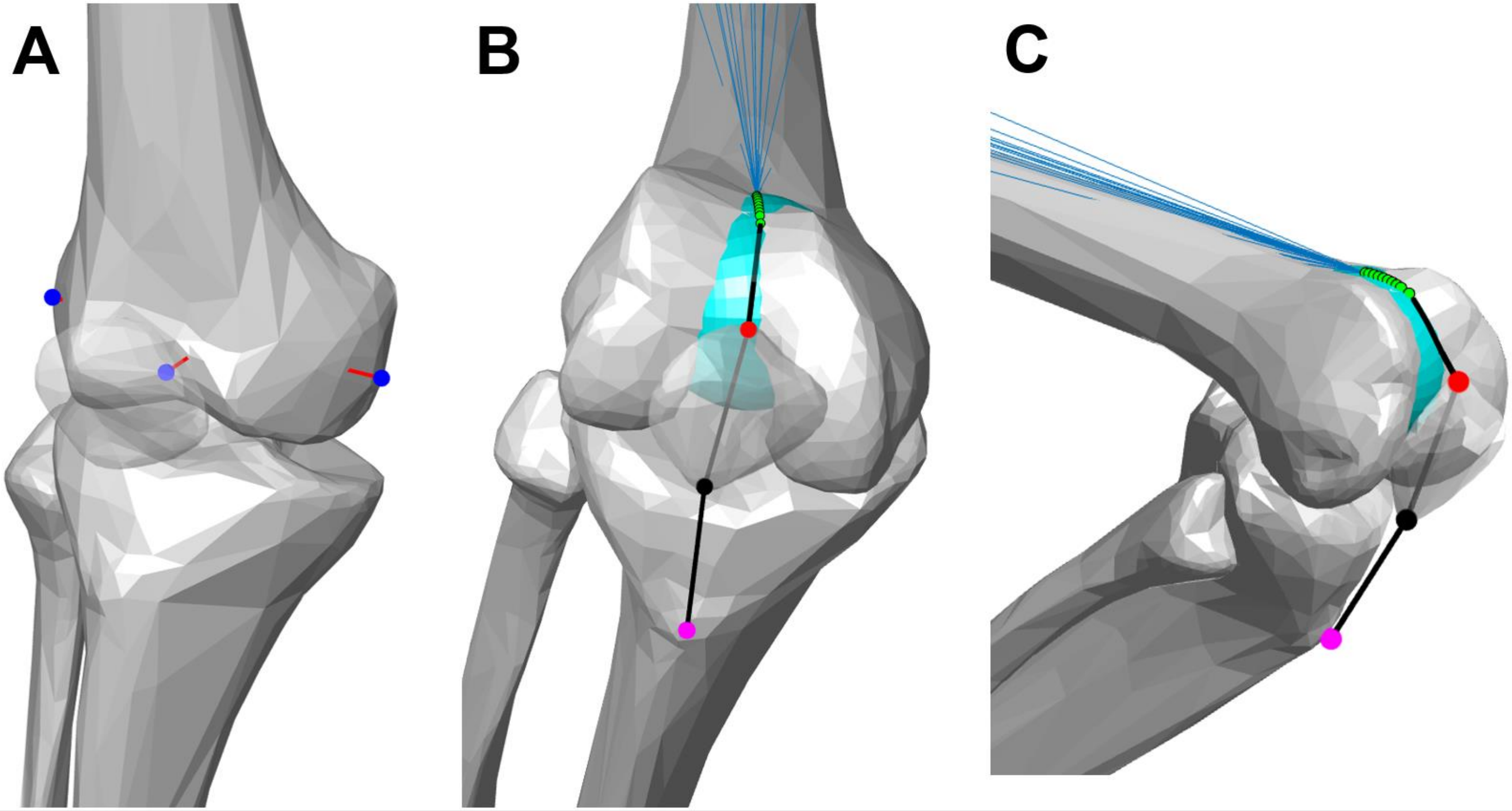

Figure 5.3 Determination of wrapping surface size and path of common knee extensor musculature. A) blue points represent vertices of the medial and lateral femoral condyles and femoral groove (perpendicular to the condylar axis); B) anterior view of wrapping sphere (cyan) with curved path (green points) connecting to the proximal patella (red point), distal patella (black point) and tibial tuberosity (magenta point); C) anterior-sagittal view of wrapping surface depicting orientation of quadriceps and patellar tendons.

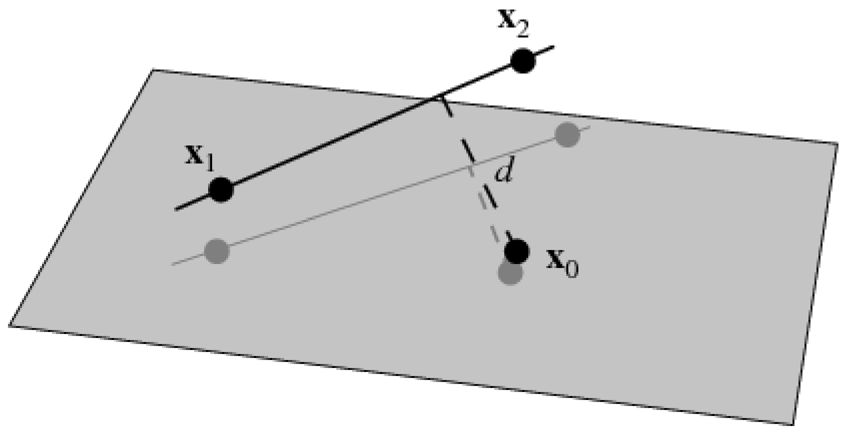

Figure 5.4 Visual depiction of the vector quadruple product. In this application, x_0 is the wrapping sphere centroid, x_1 is the origin of a muscle element, x_2 is the common insertion of knee extensors on the proximal patella, and d is the shortest perpendicular distance to line between $x_1$and x_2. See Eq 5.2 for further details. (Weisstein, n.d.).

$$d = \frac{|(x_0 - x_1) \times (x_0 - x_2)|}{|x_2 - x_1|} \qquad \textbf{Eq 5.2}$$

where x_0 is the wrapping sphere centroid, x_1 is the origin of a muscle element, x_2 is the common insertion of knee extensors on the proximal patella, and d is the perpendicular distance to the line between $x_1$and x_2 from x_0.

The tendon-excursion method (An, 2007; An et al., 1984; Pandy, 1999) was used to populate a muscle Jacobian matrix for each muscle element allowing an estimate of time varying musculotendinous moment arms (Eq 5.3). This method involves iterations of positively and negatively rotating a distal segment about a joint's degree of freedom by a small (e.g. 5º) angular perturbations. The derivative of musculotendinous unit length between the perturbed states, with respect to angle, is equivalent to the perpendicular moment arm about that degree of freedom (An et al., 1984; Pandy, 1999).

$$J_{ij} = \frac{\partial l_i}{\partial \theta_j} \qquad \textbf{Eq 5.3}$$

where $J_{i,j}$ is the moment arm for muscle element i about the j degree of freedom, l_i is the length of muscle element i, θ is the angular perturbation, and j represents the degree of freedom.

5.2.3 Segmental kinematics

Linear kinematic calculations were completed using standard procedures with angular kinematics determined from segmental LCS (Appendix F) (Winter, 2009; Zatsiorsky, 1998). Segmental angular velocities (ω) were determined by correcting for intermittent 3D axial rotations following the Euler decomposition sequence used (Eq 5.4-Eq 5.7). Segmental angular accelerations (α) were derived as the finite difference of ω values. Joint kinematics were determined using a Cardan flexion/extension, ab/adduction, and int/external (Z-X-Y) rotation sequence (Eq 5.8). Direction cosine matrices (DCM) were decomposed into Euler angles using elemental relationships defined in Eq 5.9.

$$\omega_z = \begin{bmatrix} 0 \\ 0 \\ \dot{\theta}_3 \end{bmatrix} \qquad \textbf{Eq 5.4}$$

$$\omega_x = \begin{bmatrix} \dot{\theta}_1 \\ 0 \\ 0 \end{bmatrix} + \begin{bmatrix} 1 & 0 & 0 \\ 0 & c_1 & s_1 \\ 0 & -s_1 & c_1 \end{bmatrix} \begin{bmatrix} 0 \\ 0 \\ \dot{\theta}_3 \end{bmatrix} = \begin{bmatrix} \dot{\theta}_1 \\ \dot{0} \\ 0 \end{bmatrix} + \begin{bmatrix} 1 \\ s_1\dot{\theta}_3 \\ c_1\dot{\theta}_3 \end{bmatrix} = \begin{bmatrix} \dot{\theta}_1 \\ s_1\dot{\theta}_3 \\ c_1\dot{\theta}_3 \end{bmatrix} \qquad \textbf{Eq 5.5}$$

$$\omega_y = \begin{bmatrix} 0 \\ \dot{\theta}_2 \\ 0 \end{bmatrix} + \begin{bmatrix} c_2 & 0 & -s_2 \\ 0 & 1 & 0 \\ s_2 & 0 & c_2 \end{bmatrix} \begin{bmatrix} \dot{\theta}_1 \\ s_1\dot{\theta}_3 \\ c_1\dot{\theta}_3 \end{bmatrix} = \begin{bmatrix} 0 \\ \dot{\theta}_2 \\ 0 \end{bmatrix} + \begin{bmatrix} c_2\dot{\theta}_1 - s_2c_1\dot{\theta}_3 \\ s_1\dot{\theta}_3 \\ s_2\dot{\theta}_1 + c_2c_1\dot{\theta}_3 \end{bmatrix} = \begin{bmatrix} c_2\dot{\theta}_1 - s_2c_1\dot{\theta}_3 \\ \dot{\theta}_2 + s_1\dot{\theta}_3 \\ s_2\dot{\theta}_1 + c_2c_1\dot{\theta}_3 \end{bmatrix} \qquad \textbf{Eq 5.6}$$

$$\omega = \begin{bmatrix} \omega_x \\ \omega_y \\ \omega_z \end{bmatrix} = \begin{bmatrix} c_2 & 0 & -s_2c_1 \\ 0 & 1 & s_1 \\ s_2 & 0 & c_2c_1 \end{bmatrix} \begin{bmatrix} \dot{\theta}_1 \\ \dot{\theta}_2 \\ \dot{\theta}_3 \end{bmatrix} \qquad \textbf{Eq 5.7}$$

where ω is angular velocity, θ is the segmental angle in global space, s is sin, c is cosine, and dots represent a finite difference.

$$DCM = R_{Y_3}R_{X_2}R_{Z_1} = \begin{bmatrix} c_yc_z - s_xs_ys_z & -c_xs_z & c_zs_y + c_ys_xs_z \\ c_zs_xs_t + c_ys_z & c_xc_z & -c_yc_zs_x + s_ys_z \\ -c_xs_y & s_x & c_xc_y \end{bmatrix} \qquad \textbf{Eq 5.8}$$

where c_i represents the cosine of the i axis, s_j represents the sine of the j axis, R_k is the rotation sequence for axis k, and DCM is the direction cosine matrix.

$$\begin{aligned} \theta_X &= \arcsin(D_{3,2}) \\ \theta_Y &= \operatorname{atan2}(-D_{3,1}, D_{3,3}) \\ \theta_Z &= \operatorname{atan2}(-D_{1,2}, D_{2,2}) \end{aligned} \qquad \textbf{Eq 5.9}$$

where θ_Z is the rotation about the flexion/extension axis, θ_X is the rotation about the abduction/adduction axis, θ_Y is the rotation about the internal/external axis, and $D_{i,j}$ refers to the element of matrix D from Eq 5.8.

Patellar kinematics were modeled at this stage of MSK model development as our lab did not have the capability to track patellar movement *in vivo*. Participants assumed three knee flexion angles (0º, 90º, and end range of motion in HS) while the tibial tuberosity, distal, and proximal patellar points were manually palpated and digitized with respect to the shank LCS. Patellar points were piecewise linearly interpolated—in 0.5º knee flexion increments—to provide reference locations for MSK attachment points and LoA of knee extensor muscles.

Femoral anterior-posterior (AP) translation with respect to the tibial plateau was modeled as a linear function of knee flexion angle. Values from active and passive range of motion tests *in vivo* report posterior translations up to 2.8 cm at 162º of knee flexion using MRI (Nakagawa et al., 2000). Therefore, a posterior shift was applied to the femoral LCS origin of 0-3 cm through the 0-180º knee flexion range to approximate *in vivo* data. This reduced the knee to a 4 DoF joint as medial-lateral (ML) and axial translations of the femur with respect to the tibia were fixed.

The hip joint was limited to a 3 DoF joint to maintain joint spacing imposed during bone scaling. After initial bone scaling and positioning was completed, the centroid of the femoral head was determined. This point was used to establish a rotation point, local to the pelvis, which fixed the distance of the pelvis LCS origin from the femoral head and allowed only rotations.

5.2.4 Intersegmental contact

A *post hoc* addition to the experimental protocol used in Chapter 4 was measurement of thigh-calf (TC) and heel-gluteal (HG) contact during one trial of all six high knee flexion movements. The pressure sensor was attached to a polycarbonate sheet and manually positioned by a research assistant (Figure 5.5) which limited participant movement to approximately half speed. This protocol was used to measure 3D orientation, CoF, magnitude, and active area of intersegmental contact as a function of knee flexion angle. Participants started movements from standing (HS and FS), kneeling on hands and knees (DK and PK), or with hands on the floor and the non-measured leg raised to simulate the end position of DUK or PUK movements (Figure 3.2). The DUK and PUK starting position was similar to that of a sprinter in track blocks.

When incorporating intersegmental contact as an external force, these data were rounded to the nearest 0.25º of knee flexion each frame and averaged if more than one value was present at a given angle. This assumes that when participants were statically resting in a high knee flexion posture, a constant intersegmental exposure was applied. Intersegmental contact data were not collected during the ascending phase of movement using the protocol outlined above. Therefore, it was assumed that forces during the ascending phase of movement were identical to those measured in descent. This assumption was made as Tekscan (Tekscan Inc., South Boston, MA, USA) resistive pressure sensors are susceptible to drift during sustained loading (Nicolopoulos et al., 2000; Wilson et al., 2003).

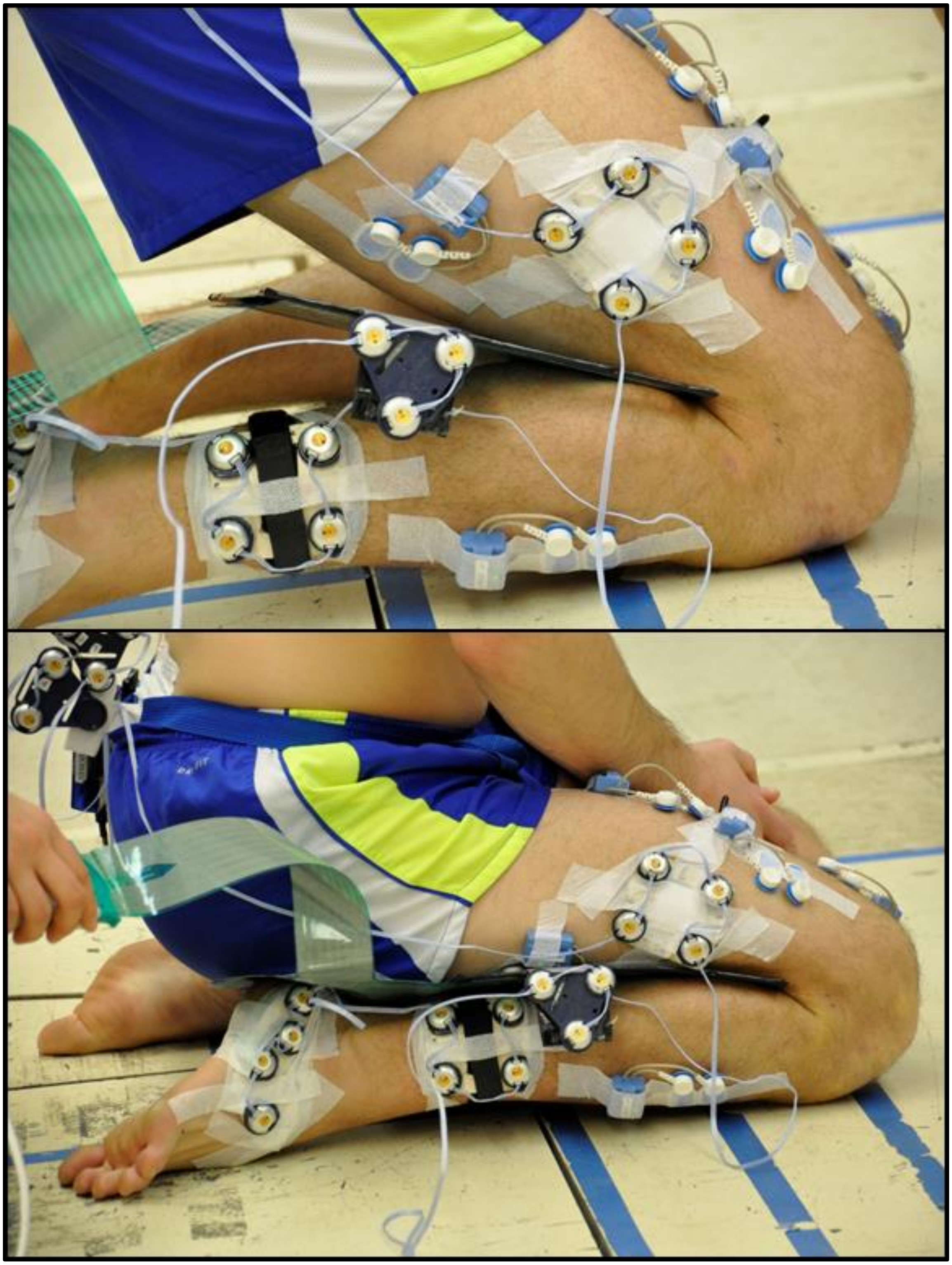

Figure 5.5 Positioned pressure sensor (top) during transition to a plantarflexed kneel (PK). Participant at maximal knee flexion during PK (bottom).

Following calibration (section 3.2.3), the pressure sensor was attached to a 4 mm thick 23 x 19 cm polycarbonate sheet (Figure 5.6) and a motion trial was collected synchronously with pressure data. Using the tip of a digitizing probe to activate a small cluster of sensels (1-4), four locations were used to define a LCS in pressure sensor coordinates originating at point 3 (Figure 5.6 and Figure 5.7). Locally defined pressure locations were used to transform planar distances of pressure outputs into global space (Figure 5.7). The exterior corners of the sheet were digitized, with respect to the attached marker cluster, for global positioning of pressure outputs. Total force, onset, max angle, and contact area were computed identically to section 3.2.4.

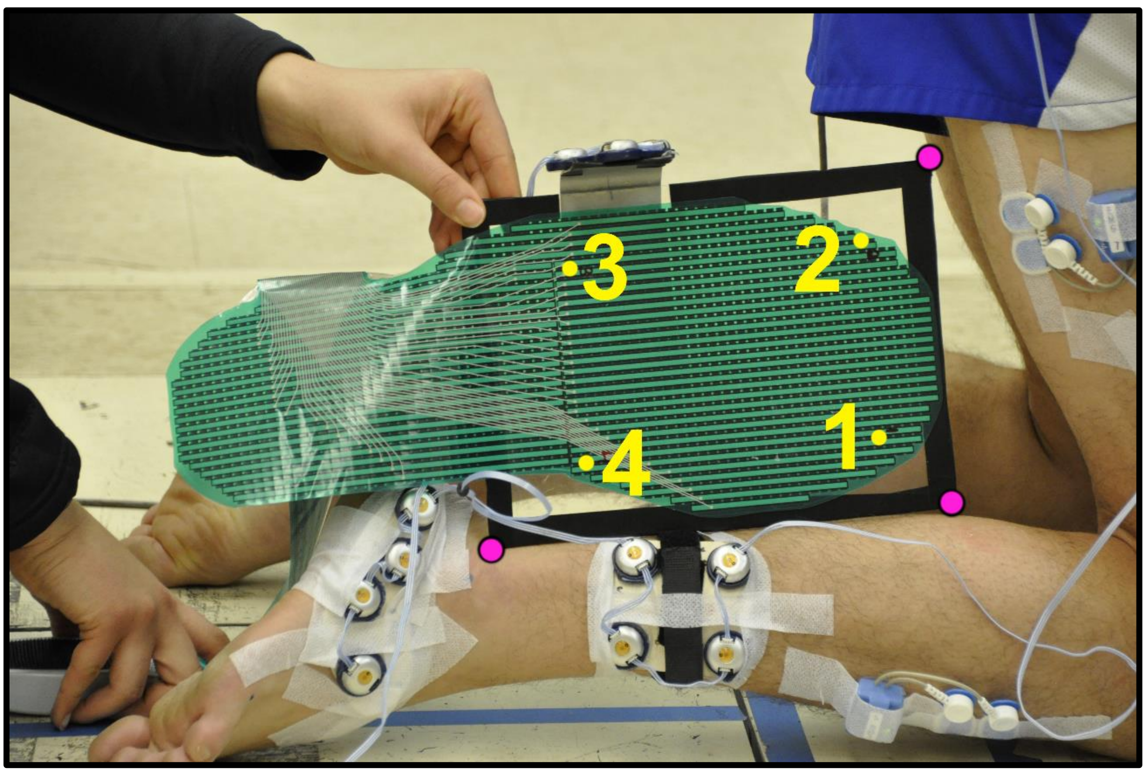

Figure 5.6 3005E sensor attached to the polycarbonate sheet. Points 1-4 used for transforming pressure sensor data to global space are highlighted for clarity in square pattern on the sensor in yellow. Digitized corners are highlighted in magenta (and under the assistant's thumb).

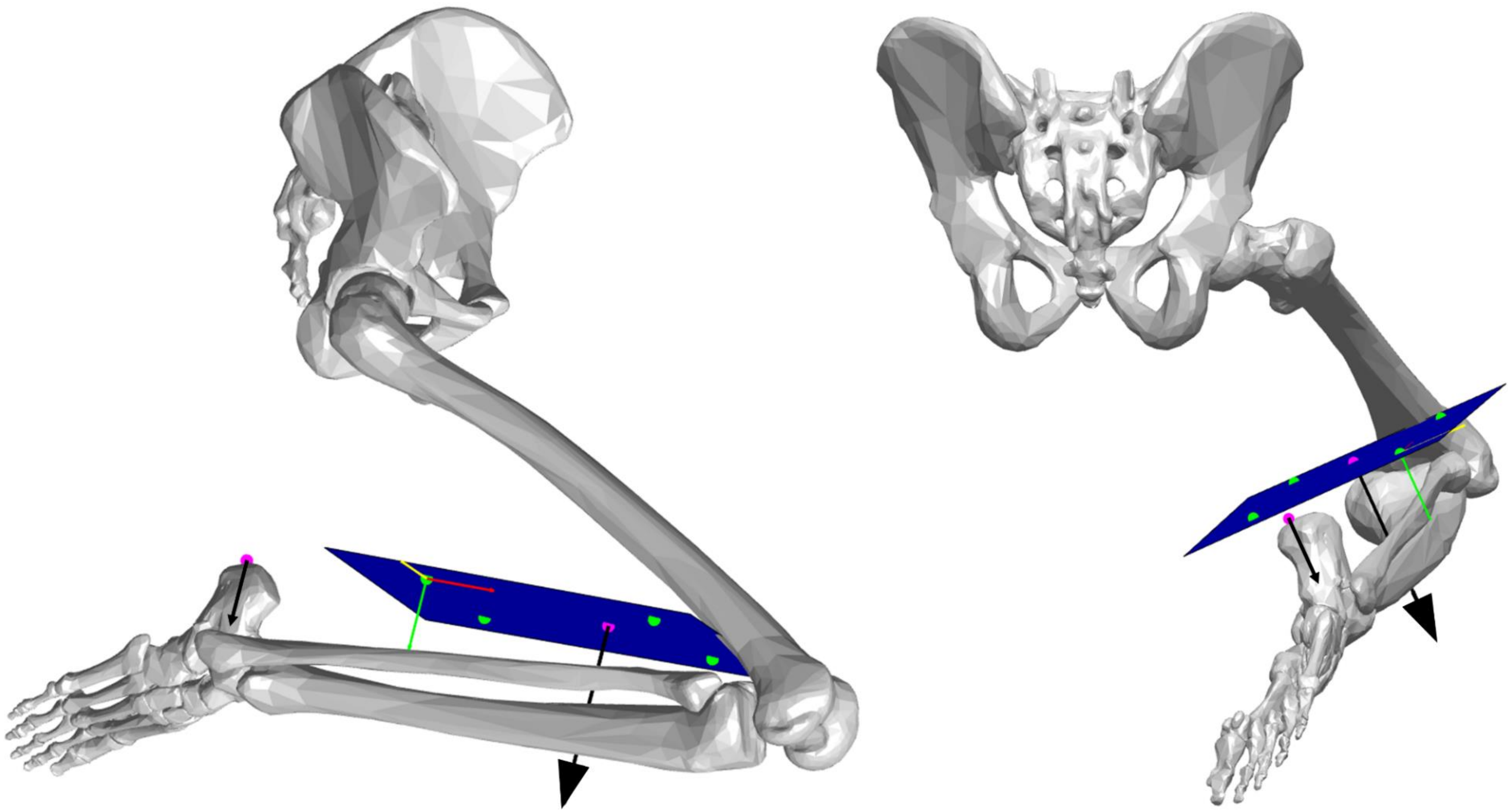

Figure 5.7 A participant performing a plantarflexed kneel with a blue rectangle representing the reconstructed polycarbonate sheet in sagittal (left) and posterior (right) views. Green spheres indicate fixed transformation points (1-4) in Figure 5.6. Magenta spheres are the instantaneous center of force location for thigh-calf and heel-gluteal contact with black arrows indicating the direction and scaled magnitude of total force normal to the sheet.

The novel approach used to measure intersegmental contact in this chapter was tested for repeatability of intersegmental contact parameter measurements made in Chapter 3 as the compressive surfaces—posterior thigh versus a polycarbonate sheet—differed. A sample of ten participants took part in both *in vivo* data collections (Table 5-1). Participant means were taken from the protocol used in Chapter 3 and compared to single trials detailed above.

Table 5-1 Mean (SD) descriptive and anthropometric participant information of reliability sample.

Parameter	Female (n = 3)	Male (n = 7)	Total (n = 10)
Age (yrs)	23.67 (5.51)	25.14 (3.85)	24.40 (1.04)
Height (m)	1.67 (0.03)	1.81 (0.09)	1.74 (0.10)
Mass (kg)	66.34 (2.05)	91.19 (17.54)	78.77 (17.57)
BMI (kg/m^2)	23.82 (1.04)	27.58 (3.75)	25.70 (2.66)
Thigh Length (m)	0.38 (0.05)	0.40 (0.04)	0.39 (0.02)
Proximal Thigh Circumference (m)	0.59 (0.01)	0.63 (0.09)	0.61 (0.03)
Mid-Thigh Circumference (m)	0.54 (0.02)	0.55 (0.13)	0.55 (0.01)
Distal Thigh Circumference (m)	0.38 (0.05)	0.40 (0.04)	0.39 (0.02)
Thigh Skinfold (mm)	36 (1)	30 (19)	33 (4)
Shank Length (m)	0.39 (0.01)	0.41 (0.03)	0.40 (0.01)
Proximal Shank Circumference (m)	0.34 (0.00)	0.36 (0.04)	0.35 (0.02)
Mid Shank Circumference (m)	0.36 (0.01)	0.39 (0.04)	0.37 (0.02)
Distal Shank Circumference (m)	0.20 (0.01)	0.23 (0.03)	0.21 (0.02)
Shank Skinfold (mm)	19 (7)	22 (20)	21 (3)

5.2.5 Inverse dynamics

External reaction forces acting at joint centers were calculated using Eq 5.10 (Hof, 1992; Zatsiorsky, 2002). Segmental mass and moments of inertia were estimated using segmental length ratios adjusted from Zatsiorsky et al. (1990) to joint center locations (de Leva, 1996).

External forces considered in this approach were gravity, GRF measured from force plates, and intersegmental contact forces.

$$F_{JC} = -\sum_{r=1}^{f} F_r - \sum_{s=1}^{k} m_s g + \sum_{s=1}^{k} m_s L_s \qquad \textbf{Eq 5.10}$$

where f is the number of external forces, k is the number of segments, F_r are external forces, m_s is the mass of segment s, and g is the vertical acceleration due to gravity, and L_s is the linear acceleration of segment s.

External joint moments about the ankle, knee, and hip were calculated using an inverse approach (Hof, 1992; Plamondon et al., 1996; Zatsiorsky, 2002). Knee joint forces were not separated into medial and lateral compartments at this stage of model development. External joint moments were calculated in four components: reaction (Eq 5.11), segmental (Eq 5.12), linear acceleration (Eq 5.13) and angular acceleration (Eq 5.14) (Hof, 1992; Plamondon et al., 1996). These terms were summed to obtain the overall external joint moment.

$$M_{GRF} = -\sum_{r=1}^{f} (p_r - p_{CoM}) \times F_r - \sum_{r=1}^{m} M_r \qquad \textbf{Eq 5.11}$$

where f is the number of external forces, m is the number of external moments, p_r is the global point of ground reaction force application, p_{CoM} is the global location of the foot segment center of mass, F_r are the external forces applied to the foot from the force plate, M_r are the external moments applied to the foot from the force plate, and M_{GRF} is the moment due to external reaction forces.

$$M_{Seg} = -\sum_{s=1}^{k}\left[\left(p_s - p_p\right) \times m_s g\right] \qquad \textbf{Eq 5.12}$$

where k is the number of segments, p_s is the global point of segment s's center of mass, p_p is the global location of the segment proximal endpoint, m_s is the mass of segment s, g is the vertical acceleration due to gravity, and M_{Seg} is the moment due to segmental mass.

$$M_{Lin} = \sum_{s=1}^{k}\left(p_s - p_p\right) \times m_s L_s \qquad \textbf{Eq 5.13}$$

where k is the number of segments, p_s is the global point of segment s's center of mass, p_p is the global location of the functional knee joint center, m_s is the mass of segment s, L_s is the linear acceleration of segment s CoM, and M_{Lin} is the moment due to linear acceleration of the segment.

$$M_{Ang} = \sum_{s=1}^{k}\frac{d}{dt} I_s \omega_s \qquad \textbf{Eq 5.14}$$

where k is the number of segments, I_s is the moment of inertia about segment s CoM, ω_s is the angular velocity of segment s, and M_{Ang} is the moment due to angular acceleration of the segment.

5.2.6 Static optimization

Muscle forces were estimated using static optimization for each frame of motion data. A cost function (*CF*, Eq 5.15) was minimized to solve for muscle forces which incorporates the minimization of muscular fatigue and co-contraction (Collins, 1994; Crowninshield and Brand, 1981; Dul et al., 1984; Monaco et al., 2011). This optimization problem minimized CF using 161 individual muscle elements and was solved using the generalized non-linear solver 'fmincon' from the Matlab Optimization Toolbox (R2017a, The MathWorks, Natick, MA). Possible muscle element force estimations were limited between zero and a predicted upper bound UB_m determined by multiplying the specific tension of a muscle by its PCSA (Eq 5.16). An equality constraint required that the muscles crossing each joint produced equivalent forces to oppose the joint moments computed by inverse dynamics at each frame (Eq 5.17) (Miller et al., 2009).

$$CF = \sum_{m=1}^{161} \left(\frac{F_m}{PCSA_m}\right)^3 \qquad \textbf{Eq 5.15}$$

where CF is the instantaneous cost function, F_m is the force estimate of muscle element m, and $PCSA_m$ is the physiological cross sectional area of muscle element m.

$$0 \leq F_m \leq UB_m \qquad \textbf{Eq 5.16}$$

where F_m is a muscle element force estimate and UB_m is the maximum force of a muscle element determined by multiplying the specific tension of a muscle by its PCSA.

$$\sum_{m=1}^{161} r_{mj} F_m = M_j \qquad \textbf{Eq 5.17}$$

where r_{mj} is the moment arm of muscle element m at joint j and M_j is the external joint moment at joint j computed from inverse dynamics.

Linear equality and inequality constraints are defined in Eq 5.18 and Eq 5.19. Inequality constraints consisted of limiting the force estimation between elements in the same muscle partition to within 15% (Balice-Gordon and Thompson, 1988; Crago et al., 1980; Huijing and Baan, 2001). Similarly, a 15% limit on force estimation differences between the medial and lateral gastrocnemii was assumed due to selective recruitment of these muscles being unlikely.

$$Ax = b \qquad \textbf{Eq 5.18}$$

where A is a 9x161 matrix containing the moment arms of muscle elements (columns) for every DoF of each joint (rows), x is a 161x1 vector for the unknown force for each muscle element, and b is a 1x9 vector containing net external moments for every DoF of each joint.

$$A_i x = b_i \qquad \textbf{Eq 5.19}$$

where A_i is a 106x161 matrix containing muscle force disparity limits for muscle elements within a partition and between muscle partitions, x is the same 161x1 vector for unknown muscle forces in Eq 5.18, and b_i is a 106x1 zero vector.

The optimization solver required an initial guess to drive the search algorithm, however, solutions using this approach are to be sensitive to the initial guess (Neptune, 1999; Wu and Zhu, 2001). Given that muscle force estimates are unknown for this set of muscle elements in these postures the 'MultiStart' solver was used from the Matlab Global Optimization Toolbox (R2017a, The MathWorks, Natick, MA) to generate 1000 random initial guesses of F_m within estimate bounds. Once an optimal solution was found for the first frame of data, following iterations used the preceding solution as the initial guess (Miller et al., 2009).

5.2.7 Verification

Estimates of tibial compression from the MSK model were compared to *in vivo* data from the 4th Grand Knee Challenge dataset (Fregly et al., 2012). These data were collected from an elderly male participant (height: 1.68 m, mass: 66.7 kg) who had undergone a total hip and knee arthroplasty where the knee contained an instrumented tibial plateau. Vertex based object files of participant bones and CAD files of the implant were available. Manually selected landmarks were used to scale MSK origin and insertion points from the Horsman et al. (2007) dataset using the procedure described in section 5.2.2.2 (Figure 5.8 and Figure 5.9).

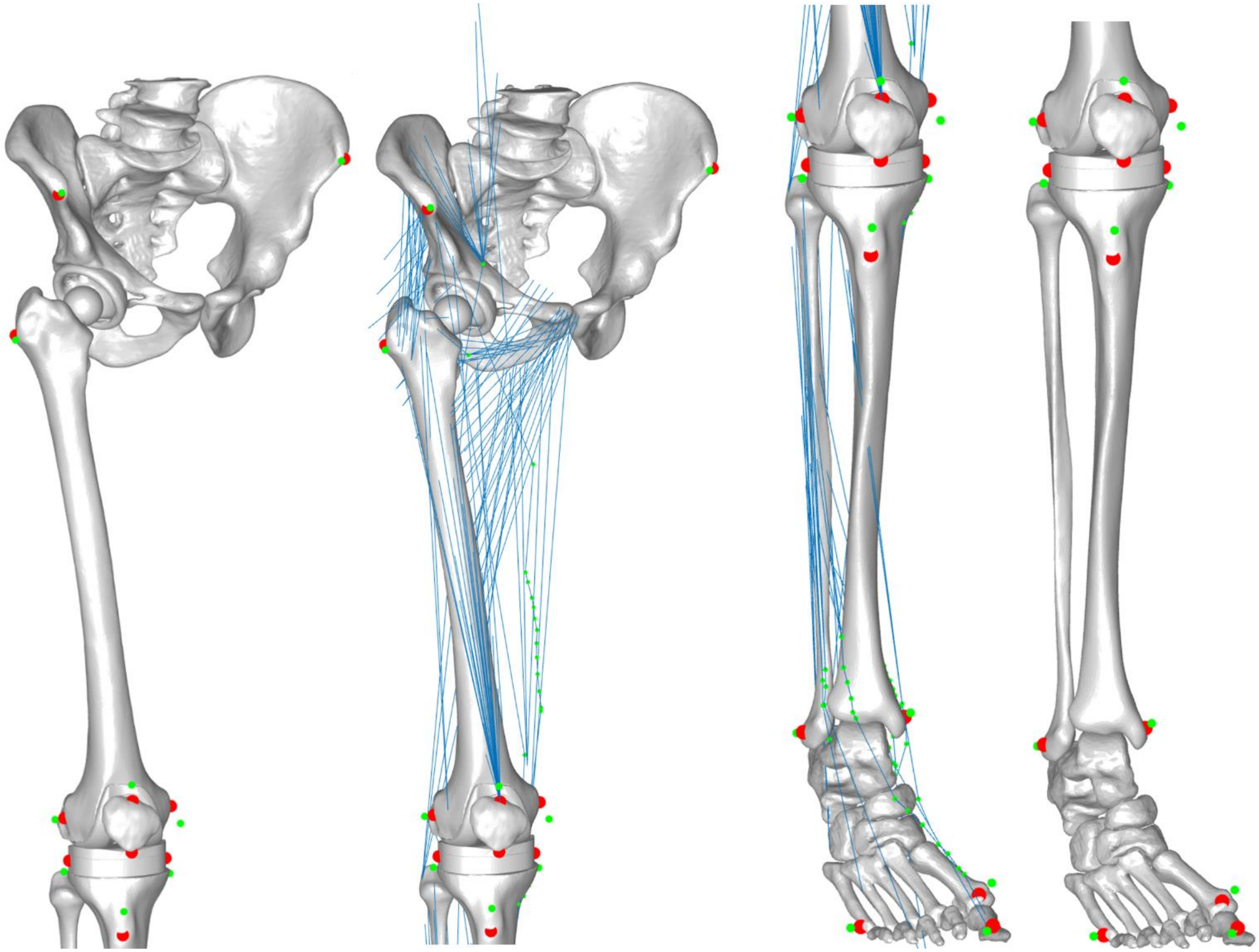

Figure 5.8 Anterior view of bone and muscle geometry from the 4th Grand Knee Challenge dataset (Fregly et al., 2012). Red spheres are manually selected landmarks matching those from Horsman et al. (2007). Green spheres are the scaled positions of source MSK geometry with blue lines indicating muscle paths. Spheres within a muscle path are scaled VIA points.

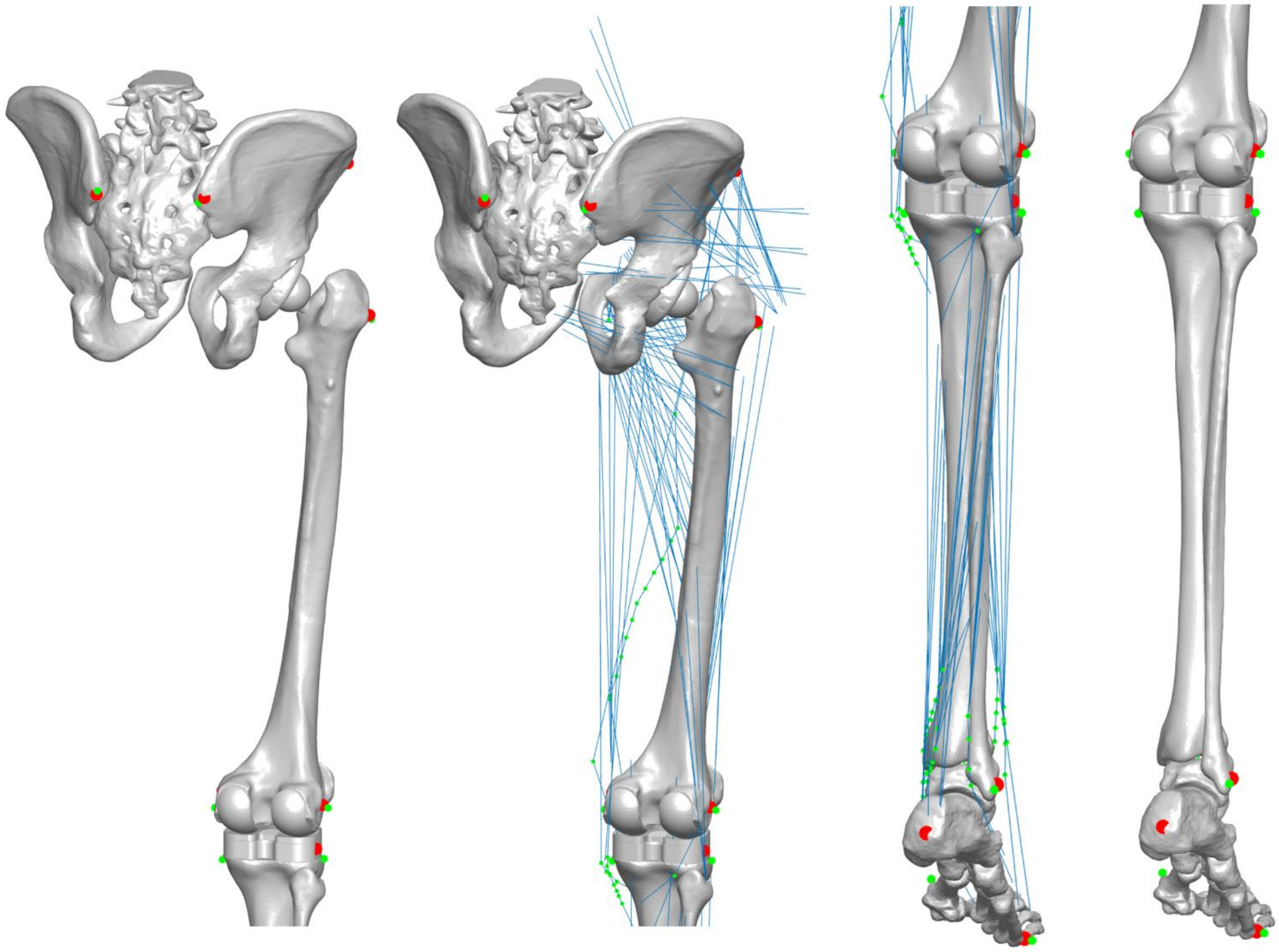

Figure 5.9 Posterior view of Figure 5.8.

Time synchronized data were provided for marker trajectories, surface EMG, tibia compression (eKnee), and GRF. Kinematic variables were calculated identically to previously defined methods except for the foot segment as the participant was shod. This resulted in the same points for the long axis of the foot (heel and toe), but a 'lateral mid-foot' marker was used in place of the distal head of the 5^{th} metatarsal (Figure 5.10). Anatomical landmarks were extracted from a static pose trial with functional joint centers determined (flexion-extension trial for the knee and star-arc pattern for the hip) using the SCoRE method (Ehrig et al., 2007, 2006). EMG data were provided from 15 muscles: SM, BF, VM, VL, RF, MG, LG, tensor fascia lata (TL), TA, peroneus longus (PL), soleus (SL), AM, gluteus maximus (GX), GM, and sartorius (SA). Data from MVC trials were provided and all EMG data were processed using the same linear envelope as detailed in section 4.2.4. eKnee data were converted to a single compression force using validated regression equations for this implant (Zhao et al., 2007).

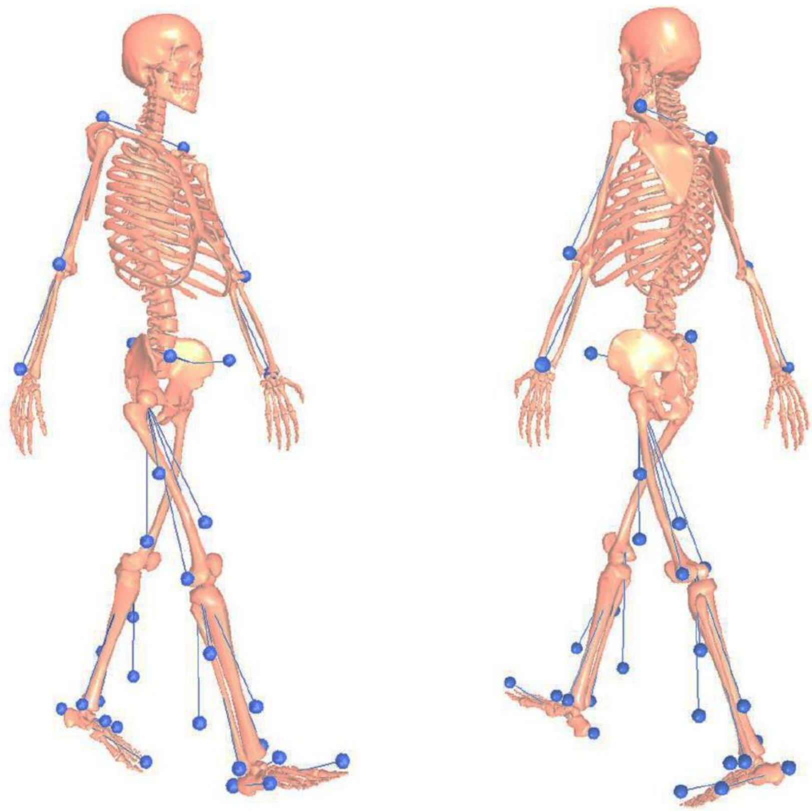

Figure 5.10 Representation of surface marker locations during dynamic trials from the Grand Knee Challenge manual (Fregly et al., 2012). Additional markers were present during pose providing similar markers to kinematic procedures detailed in Appendix F.

External kinetics were calculated (section 5.2.5) and used as inputs to the static optimization procedure (section 5.2.6) to estimate tibial compression in three different exposures; two-legged squatting, walking, and 'bouncy' walking. Model performance was assessed by RMSD and R^2 between MSK compression estimates and eKnee data as these were the outcome measures used to evaluate Grand Knee Challenge models (Fregly et al., 2012).

A qualitative comparison of EMG to estimated muscle force was also completed to provide insight on the biofidelity of muscle force estimates. Muscle force estimates were computed by taking the mean of element force estimations within a muscle partition. These estimates were expressed as a percentage of maximal force capacity (% Max) and directly compared to %MVC EMG.

5.2.8 Statistical analyses

Statistical procedures were performed using SPSS (IBM Corp. Released 2011. IBM SPSS Statistics for Windows, Version 20.0, Armonk, NY). For reliability testing between intersegment contact measurement approaches used in Chapter 3 and those outlined in section 5.2.4 outcome parameters listed in Table 3-2 were compared using paired-sample t-tests. An *a priori* α level was set at 0.05 for each statistical model.

5.3 Results

5.3.1 Anatomical geometry

Hip and knee joint spacing, prior to scaling, was found to be within healthy population ranges; 6.5 mm medial compartment knee joint space (Anas et al., 2013; Marsh et al., 2013) and 4 mm femoral head to acetabular wall (Im and Kim, 2010; Kashimoto and Friedenberg, 1977; Lequesne et al., 2004; Ratzlaff et al., 2014). After bone scaling, mean 3D error of anatomical points was calculated per participant (Table 5-2).

Table 5-2 Mean 3D error (m) between all bone vertex and corresponding anatomical points after rigid affine scaling.

Participant	Foot	Shank	Femur	Pelvis
P01	0.004	0.012	0.017	0.020
P02	0.007	0.011	0.010	0.021
P03	0.004	0.016	0.010	0.019
P04	0.004	0.015	0.011	0.007
P05	0.009	0.009	0.009	0.013
P06	0.006	0.011	0.006	0.020
P07	0.003	0.012	0.009	0.014
P08	0.004	0.012	0.011	0.017
P10	0.004	0.014	0.009	0.010
P11	0.006	0.017	0.013	0.018
P12	0.006	0.011	0.006	0.015
P13	0.007	0.010	0.004	0.011
P14	0.003	0.012	0.008	0.018
P15	0.000	0.013	0.008	0.016
P16	0.004	0.011	0.013	0.017

5.3.1.1 Muscle parameters and moment arms

Participant musculotendinous moment arms were within 1 SD for knee flexion ranges where cadaveric data is available (Wagner et al., 2013). However, it should be noted that the quadriceps/patellar tendon is the primarily reported moment arm and no *in vitro* data are available to compare the vast majority of moment arm estimates.

5.3.2 Intersegmental contact

A summary of significant differences is listed in Table 5-3. There were no significant differences between intersegmental contact parameters for FS or PK movements. Of note: contact force magnitudes were an average 34% higher when using the polycarbonate sheet and participants were able to achieve an average 6% higher maximum flexion angle.

Table 5-3 Significant differences in pressure measurement outcomes between approaches. Mean values were computed as sensor attached to participant (approach 1) minus sensor attached to the polycarbonate sheet (approach 2). Therefore, negative values indicates approach 2 was larger in magnitude. Postures are: heels-up squat (HS), dorsiflexed kneel (DK), dorsiflexed unilateral kneel (DUK), and plantarflexed unilateral kneel (PUK). TC is thigh-calf with CoF reported as difference in axial (with respect to shank LCS) distance from the functional knee joint center.

Posture	Measure	Paired Differences					t	df	Sig
		Mean	SD	SE Mean	95% CI				
					Lower	Upper			
HS[1]	Max Angle (deg)	-12.50	9.24	2.92	-19.11	-5.89	-4.278	9	.002
	Total Force (N)	-98.08	67.49	22.50	-149.96	-46.19	-4.359	8	.002
	TC CoF (mm)	49.66	19.99	6.66	34.29	65.02	-7.450	8	.000
	TC Area (cm^2)	-28.81	29.77	9.92	-51.70	-5.92	-2.903	8	.020
DK	Onset (deg)	-8.96	5.05	1.60	-12.57	-5.34	-5.607	9	.000
	TC CoF (mm)	-21.32	15.46	4.89	-32.38	-10.26	-4.360	9	.002
DUK	Onset (deg)	-7.88	6.13	1.94	-12.26	-3.49	-4.063	9	.003
	Max Angle (deg)	-6.64	8.94	2.83	-13.04	-0.24	-2.349	9	.043
	Total Force (N)	-121.00	133.38	42.18	-216.42	-25.59	-2.869	9	.019
	TC Force (N)	-132.90	144.98	45.85	-236.62	-29.19	-2.899	9	.018
	TC CoF (mm)	-29.60	13.58	4.53	-40.04	-19.16	-6.539	9	.000
	TC Area (cm^2)	-25.45	32.11	10.15	-48.42	-2.48	2.506	9	.034
PUK	Max Angle (deg)	-11.06	12.61	3.99	-20.08	-2.04	-2.774	9	.022
	Total Force (N)	-163.85	219.12	69.29	-320.60	-7.10	-2.365	9	.042

[1] Total force and TC force were equivalent as no heel-gluteal contact occurred

5.3.3 Verification

Mean tibial compression estimations from five walking trials was compared to eKnee data in Figure 5.11. Model estimates strongly fit implant data shape (R^2 0.83) with an overall RMSD of 0.47 BW. Effects of changing specific tension for walking, cyclic squatting, and 'bouncy' walking trials is reported in Table 5-4 and shown in Figure 5.12-Figure 5.14.

Table 5-4 Tibial compression force estimate error and fit when comparing MSK model to implant data from the 4th Grand Knee Challenge. RMSD values are reported in BW.

Specific Tension (N/cm^2)	Walking		Squatting		'Bouncy' Walking	
	RMSD	R^2	RMSD	R^2	RMSD	R^2
30	0.44	0.82	0.16	0.93	0.58	0.74
61	0.50	0.79	0.17	0.94	0.65	0.66
88	0.45	0.83	0.35	0.94	0.87	0.61

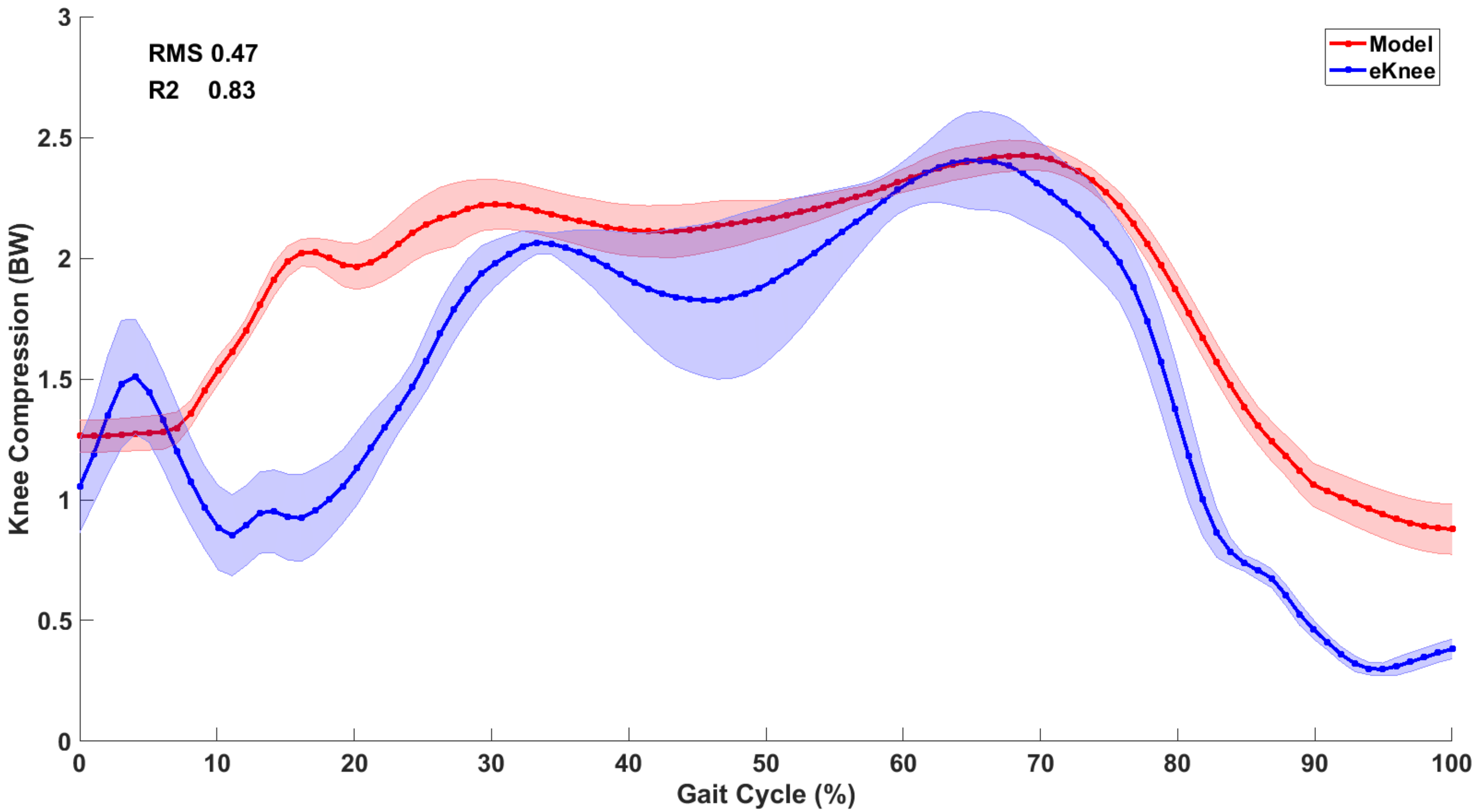

Figure 5.11 Model estimated tibial compression compared to eKnee data from the 4th Grand Knee Challenge dataset during five normal walking trials with a specific tension of 30 N/cm^2. Shaded bands represent ± 1 SD. RMS is the root mean squared difference (BW) and R2 is the corrected coefficient of determination between estimates and implant data.

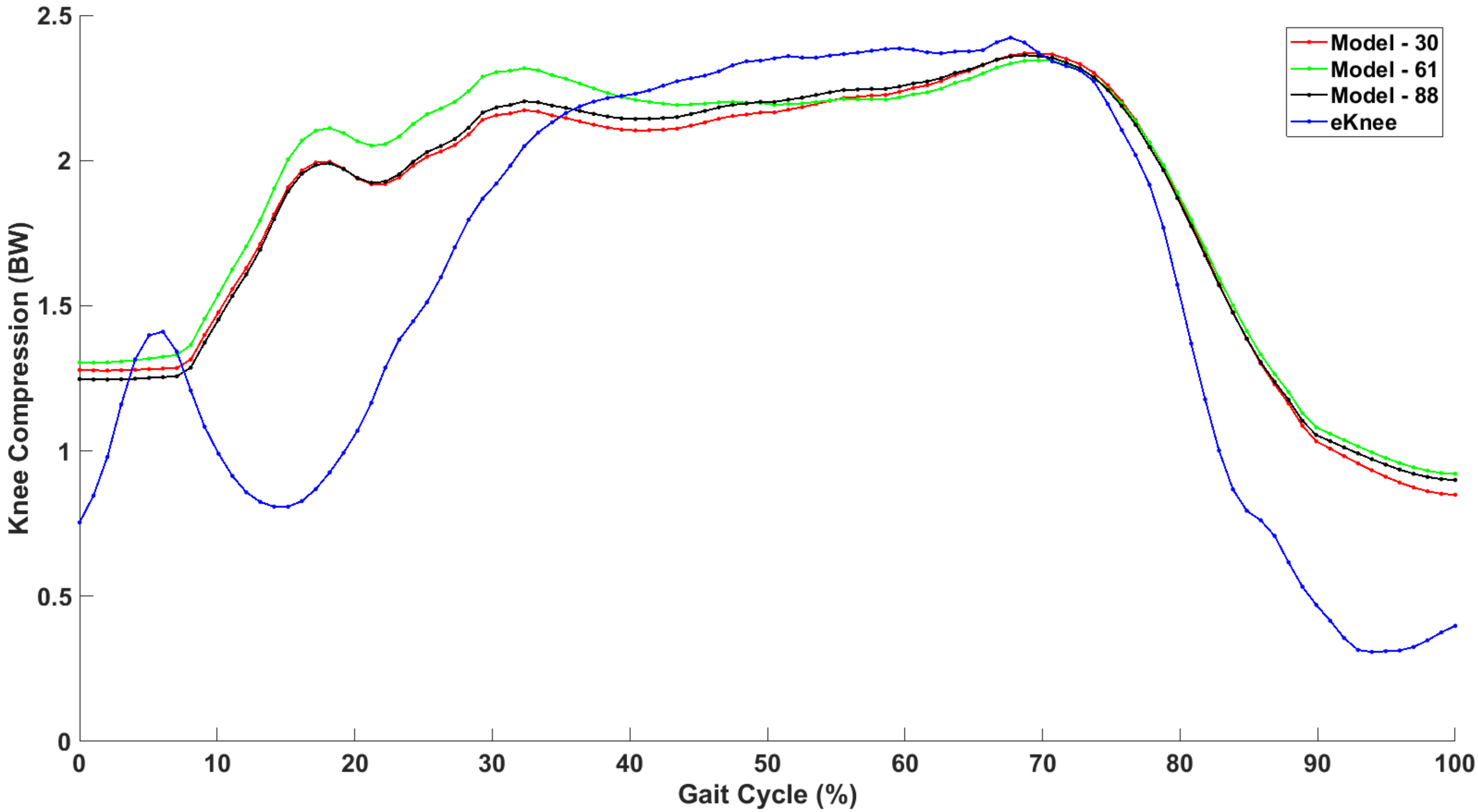

Figure 5.12 Model estimated tibial compression compared to eKnee data from the 4th Grand Knee Challenge dataset from a single walking trial when altering the specific tension (i.e. maximal muscle force) to 30, 61, or 88 N/cm^2.

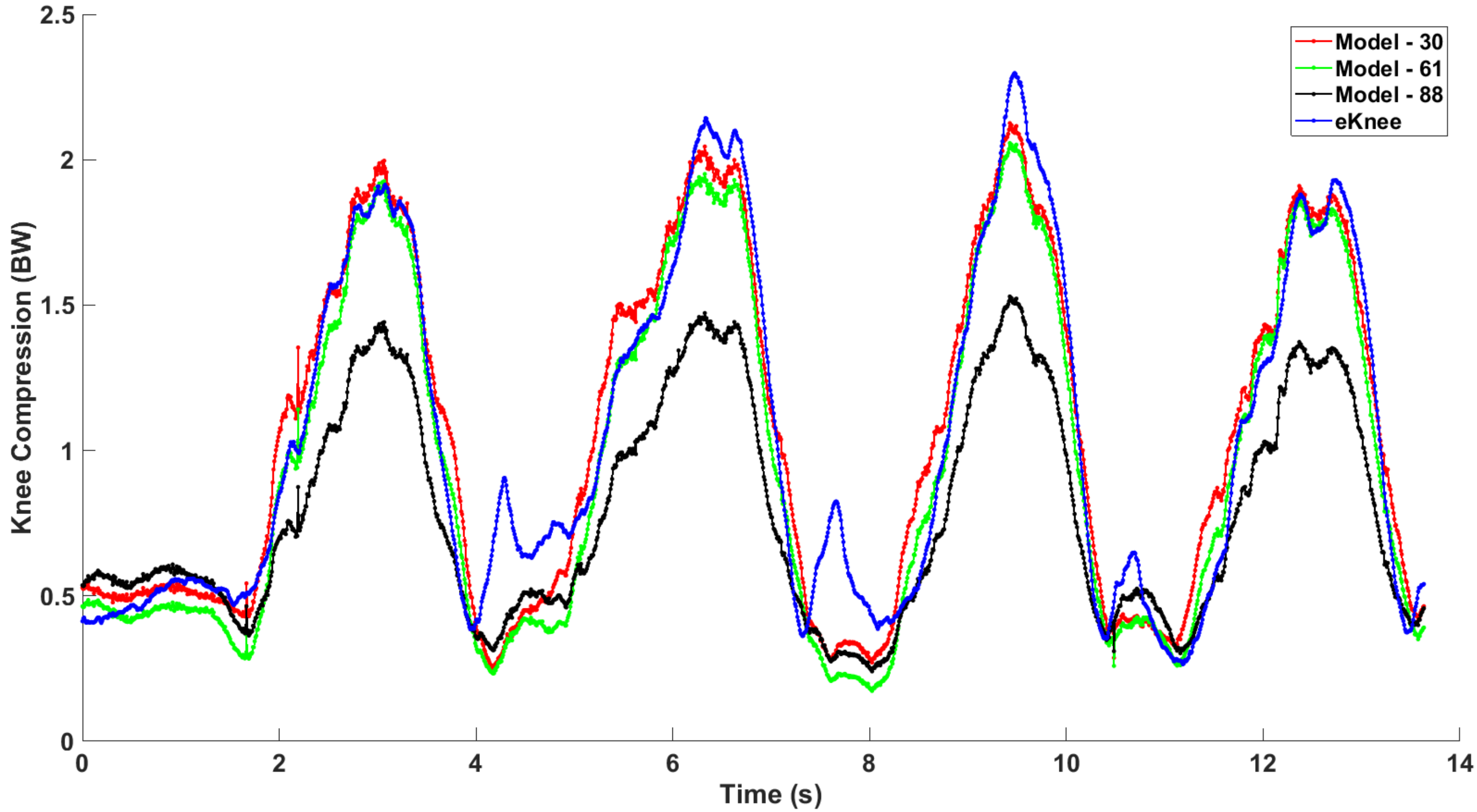

Figure 5.13 Model estimated tibial compression compared to eKnee data from the 4th Grand Knee Challenge dataset from a cyclic squatting trial when altering the specific tension (i.e. maximal muscle force) to 30, 61, or 88 N/cm^2.

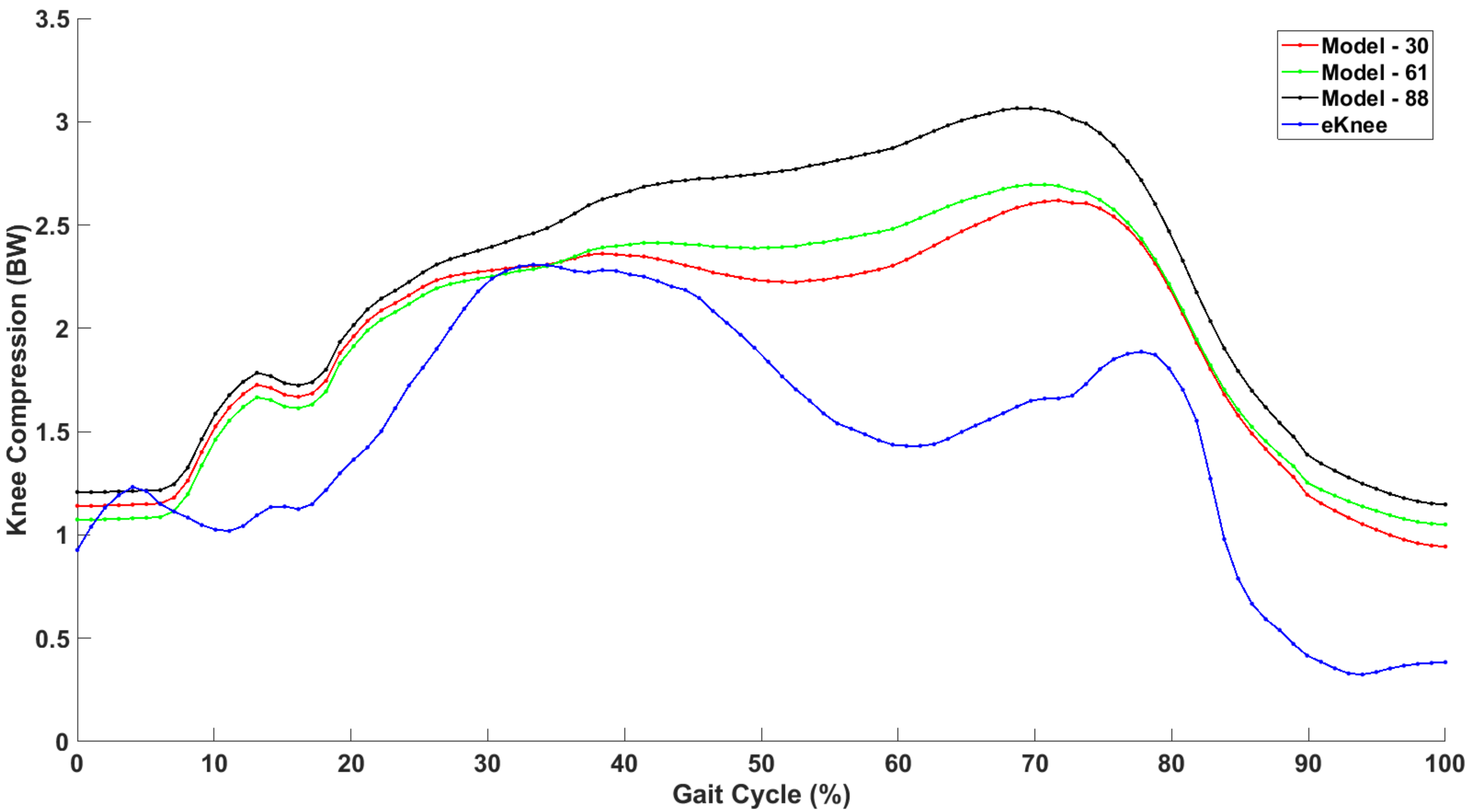

Figure 5.14 Model estimated tibial compression compared to eKnee data from the 4th Grand Knee Challenge dataset from a 'bouncy' walking trial when altering the specific tension (i.e. maximal muscle force) to 30, 61, or 88 N/cm^2.

EMG data from the 4th Grand Knee Challenge walking trials had some signals which exceeded 100 %MVC. Of note are VM, TF, and SA waveforms during a walking trial (Figure 5.15). Remaining figures depicting EMG to muscle force comparisons is provided in Appendix G. Overall, model estimates of muscle force did not follow general visual trends of EMG activation waveforms. GM and SA were the only muscles which showed general alignment of increasing muscle force with EMG activity (Figure 5.15).

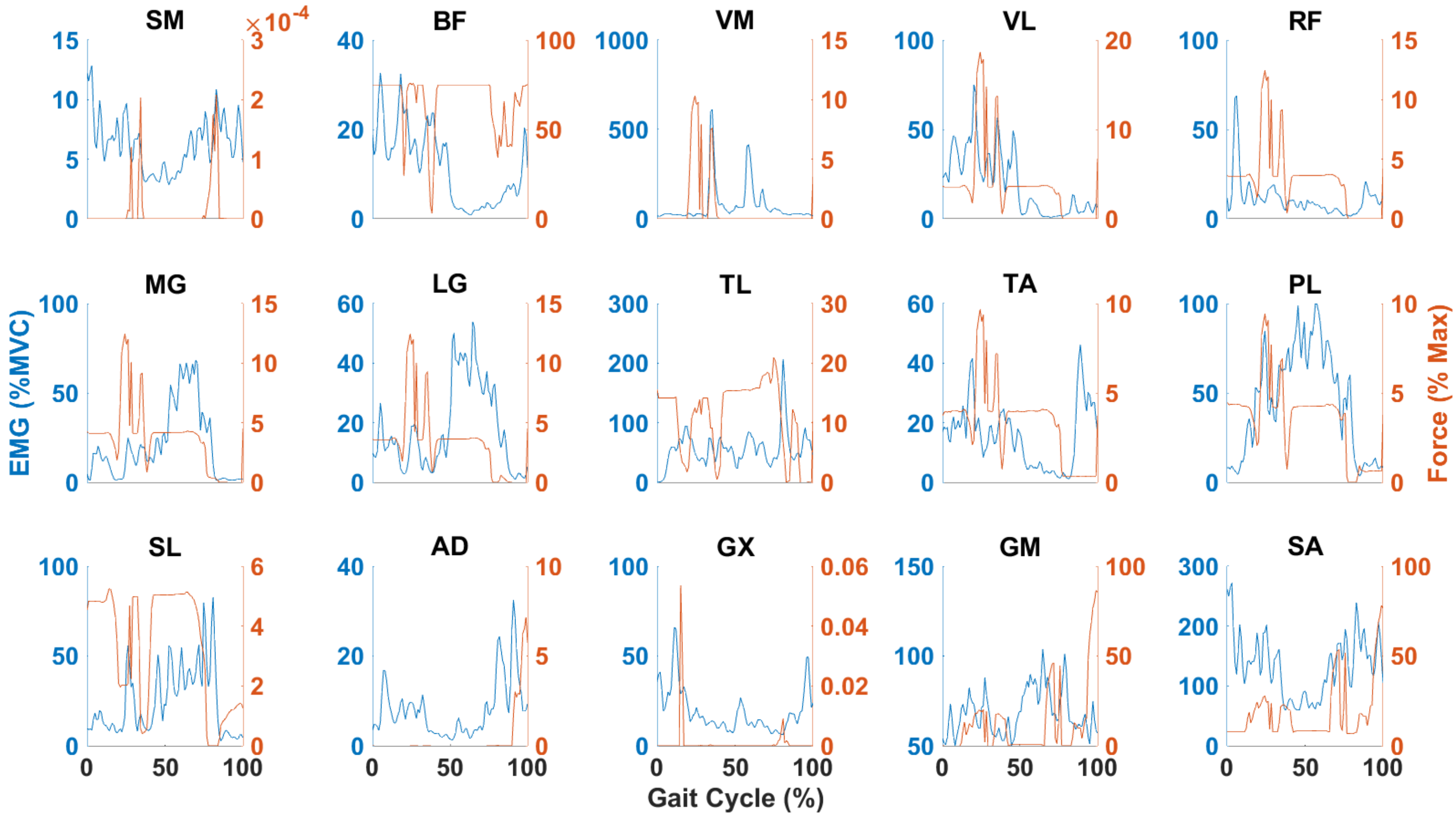

Figure 5.15 Muscle activations (blue) compared to mean muscle forces (orange) for a walking trial with a specific muscle tension of 30 N/cm^2. Muscles are: semimembranosus (SM), biceps femoris (BF), vastus medialis (VM), vastus lateralis (VL), rectus femoris (RF), medial gastrocnemius (MG), lateral gastrocnemius (LG), tensor fascia lata (TL), tibialis anterior (TA), peroneus longus (PL), soleus (SL), adductor magnus (AM), gluteus maximus (GX), gluteus medius (GM), and sartorius (SA).

5.4 Discussion

The purpose of this study was to define and verify a full range of motion 3D MSK model of the right lower limb that incorporated 3D intersegmental contact parameters. Component verification consisted of comparing estimates of tibial compression and qualitative comparisons of EMG waveform to predicted muscle force estimates of *in vivo* data from the 4th Grand Knee Challenge dataset (Fregly et al., 2012). Error between instrumented implant compression forces and MSK model estimations was highest during early and late stance in normal and 'bouncy' gait resulting in approximately 0.5-1 BW overestimations. Model estimations during cyclic squatting was superior to walking with the lowest RMSD of 0.16 BW. The use of 30 N/cm^2 as a specific muscle tension was supported as it had the lowest RMSD across all movements. The overall poor agreement of EMG to muscle force estimate comparisons suggests that the MSK model is phenomenological in nature.

Model estimations of tibial compression has lower RMSD during squatting movements when compared to walking or bouncy gait. This is a curious result given that model predictions at moderate compressive magnitudes (0.5-1.5 BW) were well matched during squatting but poor in gait. A feasible explanation could be issues of model predictive ability at lower knee flexion angles. Compressive estimates were worst near standing in cycle squatting or early/late stance phase in gait and best when the knee was flexed during descent/ascent of squatting or mid-stance in gait. A plausible explanation could be the poor biofidelity of using straight lines of action gastrocnemii and gluteal muscles, as these "primary movers" have been highlighted as influential on model force estimations (Carbone et al., 2015, 2012). Incorporating cylindrical or additional spherical wrapping surfaces would result in curvilinear insertions and increase the mechanical advantage of these muscles. However, compressive estimates were underestimated during squatting and overestimated during gait. Although the intended application of this model is high knee flexion postures where intersegmental contact occurs, this inconsistency in model prediction near standing requires future investigation.

The qualitative assessment of EMG data to muscle force estimations suggests that this model does not represent muscle activation measurements taken during these activities. However, it is difficult to make comparisons without more intimate knowledge of EMG collection protocol (e.g. specific electrode placements, MVC protocol) since protocols can vary widely and affect signal outcomes (Clancy et al., 2002; Hermens et al., 2005; Lehman and McGill, 1999). This was highlighted by the finding that some muscles far exceeded 100% MVC during a walking task. Inspection of video recordings of participant trials did not reveal any contact of visible electrodes/leads. Although gross qualitative assessments of EMG to muscle force estimations are common within the modelling literature (Durandau et al., 2018; Modenese et al., 2011; Mohammadi et al., 2015; Sartori et al., 2014; Winby et al., 2009) the direct relationship of EMG to force is far more complicated (Buchanan et al., 2004; Guimaraes et al., 1994; Nussbaum and Chaffin, 1998; Walter et al., 2014).

The bone and MSK scaling procedure used in this model had a varying level of error for each participant—maximal mean 3D errors of 0.9 cm (foot), 1.7 cm (shank/femur), and 2.1 cm (pelvis)—but used a segment specific scaling approach as opposed to a whole body scaling factor common in OpenSim software. This approach was selected as segmental scaling would be required to alter source MSK geometry for future subject specific models. However, this approach likely introduces geometric errors on origin and insertion locations between single or multi-joint muscles. In addition muscle origin and insertion points were obtained from a single cadaver and participants' ages, body composition, ethnicity, and in some cases sex differed from the donor. Due to considerable variability in muscle size and geometry between individuals Carbone et al. (2012) completed a fulsome sensitivity analysis of the MSK geometry used in this model for a gait ranges of knee flexion. Unsurprisingly, Carbone et al. (2012) reported that small errors in MSK geometry can have a significant effect on muscle force predictions, specifically in "primary movers" (e.g. muscles attaching through the Achilles tendon, gluteal muscles, and vastii). The separation of larger muscles into partitions (e.g. superior/mid/inferior gluteus maximus) and further separation the further separation of partitions to multiple elements, would theoretically reduce the effect of poorly positioned origin and insertion points.

Rigid body mechanics was assumed for all segments which has implications on kinematic and kinetic outcomes. High flexion postures result in thigh and shank soft tissue deformation causing marker deflection. This introduces uncertainty in the coordinates of anatomical points reconstructed from technical coordinate systems. Bone pin rigid bodies could be used in high flexion postures to quantify soft tissue artifact. However, the invasiveness of this approach and variance in lean mass between participants make the use of bone pins ethically and logistically problematic. Similarly, accurate patellar tracking was not feasible in our laboratory. Inaccurate patellar positioning would alter knee extensor wrapping paths and LoA, but a first attempt of modelling patellar movement with a piecewise linear fit was performed (section 5.2.3).

Soft tissue artifact would also alter segmental kinematic outcomes. Internal/external axis rotations are disproportionally influenced by this soft tissue artifact—even in gait ranges of knee flexion (Sangeux et al., 2017)—and would likely be highest for the thigh rigid body due to lean and fat mass concentrations. This issue was the primary motivation for limiting the DoF of the knee to reduce distal translations of the modeled femur. Although this MSK model contains two joints with constrained movement—4 DoF knee and a 3 DoF hip—limiting biofidelity it should be noted some researchers use a 1 DoF (flexion/extension) knee joint (Arnold et al., 2010). Until surface measurement approaches/corrections are robust to soft tissue artefact, mechanical simplifications are required to maintain joint spacing and ensure plausible muscle and ligament length/LoA estimates.

Joint center locations were defined using an algorithm verified for ranges of motion below 100° of knee flexion (Ehrig et al., 2007, 2006), therefore, the accuracy of the SCoRE method has not been tested for use in high knee flexion postures. Given that the femur posteriorly translates relative to the tibia (Nakagawa et al., 2000), the KJC estimate would only be computed across the flexion range input to the algorithm. The functional knee joint trial used in sections 3.2.2 and 4.2.2 is the current standard (Besier et al., 2003b), but is completed during standing with an unloaded limb. This limitation requires future investigation.

This iteration of the MSK model does not contain joint capsular ligaments. Basing joint surface geometry on a scaled model results in less confidence in knee joint congruency than when directly-measured joint surface geometry is used. Thus, the scaling in our current approach limits our ability to estimate ligament forces as the toe regions of knee joint ligaments is below 2 mm (Yang et al., 2010). This limitation is somewhat attenuated by the low force contributions, measured *in vitro*, of the ACL (< 40 N), PCL (< 20 N), MCL (< 10 N), and LCL (< 5 N) ligaments above 90º of knee flexion (Yang et al., 2010).

Total force measured from the pressure mat was expressed as external forces acting through the calculated CoP (section 5.2.4). This simplifies the external tissue loading environment. While outside the scope of this thesis, an FE model could use a matrix of 3D force vectors to more accurately model tissue response. Current pressure mat technology only measures forces normal to its surface, resulting in under predicted shear force magnitudes between the thigh and shank segments and ultimately shear force estimates at the joint. These considerations would likely result in increased knee flexor activation responses and ultimately change tibial contact force predictions.

Caution is warranted when interpreting muscle force predictions from any MSK model. The SO procedure used in the MSK model simplifies the CNS and peripheral system to a three term cost function. As well, a fixed 30 N/cm^2 specific tension was applied to all muscle elements even though a range of tissues and fibre types exist within the musculature used in this model. Given the mechanical constraint of external force equilibrium, there is no consideration for heat liberation, or energy storage in tissues. Additionally, few computational models account for joint tribology and frictionless surfaces were assumed. The instantaneous objective function used may produce non-physiological results as muscle contraction/relaxation time is not accounted for. Finally, linear relationships are assumed within the listed constraints due to mathematical simplicity over viscoelastic models (Fung, 1994).

5.5 Conclusions

The RMSD magnitudes between MSK model predictions and *in vivo* data from the 4th Grand Knee Challenge dataset (Fregly et al., 2012) suggest that this model could be confidently used to predict tibial compression forces from ~0-100^{o} of knee flexion. However, qualitative comparisons of EMG to muscle force estimates imply this model is phenomenological. Model details and assumptions made in general, and with respect to high knee flexion activities, were presented. Intersegmental contact parameters were measured using a novel approach and expressed in relation to knee flexion angle to allow incorporation to future inverse dynamic calculations.

This model is currently the most fulsome representation of anatomical geometry available that is capable of modeling high knee flexion ranges of activity. In addition, this model can be used to estimate tibial contact forces to gain further insight into joint loading during high knee flexion activities. The inclusion of 3D intersegmental contact parameters in this model results in a more accurate representation of joint loading than has previously been available. Although model estimates of tibial compression during a squatting activity were quite accurate, further investigations are need into the comparatively poor accuracy in gait estimations. Further verification of tibial contact force estimations is required in high knee flexion postures, but estimates from this model could be used to guide prosthetic design and improve our understanding of knee joint tissue loading in this exposure.

Chapter 6 – Influence of intersegmental contact on tibial contact forces during high knee flexion movements

6.1 Introduction

High knee flexion postures result in intersegmental contact in the lower limb but the effect of these external forces on modeled muscle and internal joint force estimates has not been assessed in 3D. High knee flexion is defined as movements where knee flexion exceeds 120º (Hemmerich et al., 2006; Kingston and Acker, 2018a; Zelle et al., 2009). There is an increased incidence of knee tissue degeneration in populations that regularly use high knee flexion postures (Baker et al., 2003; Bombardier et al., 2011; Kirkeshov Jensen, 2008). Therefore, accurately representing the exposure of knee joint structures to loading is critical. One explanation of disease progression in high knee flexion postures is the exposure of under-conditioned tissues to high joint contact forces (Andriacchi et al., 2004; Andriacchi and Favre, 2014). However, this theory did not consider the effect intersegmental contact has on tibial contact force estimates as current 3D musculoskeletal (MSK) models are not designed for use in high knee flexion ranges (Arnold et al., 2010; Carbone et al., 2015; Modenese et al., 2011). In this study, a 3D MSK model (Chapter 5) designed for use in the full range of knee flexion was used to assess the effect of including intersegmental contact on tibial contact force estimates.

The effect of incorperating intersegmental contact on knee joint compressive force estimates was investigated by Zelle et al. (2009) when performing a flatfoot squat. Their finite element model of the knee, which included sagittal plane external thigh-calf contact forces (Zelle et al., 2007), reported a decrease of 1.3 BW (from 4.37 to 3.07 BW) in knee joint compression. However, Zelle et al. (2009) used primarily sagittal plane inputs, only a partial femur and tibia, and potentially inflated intersegmental force magnitudes (Kingston and Acker, 2018a). Prior sagitttal plane high knee flexion models—which did not account for intersegmental contact—have predicted markedly higher knee joint compressive forces of 7.3 ± 1.9 BW or 4470 ± 1825 N during a full squat (Nagura et al., 2006). While the Nagura et al. (2006) model included cruciate ligaments, their peak estimations were over 2 BW higher than a preceding sagitttal plane model in similar flexion ranges (Dahlkvist et al., 1982). Therefore, this study used a more fulsome model of the lower limb, 3D intersegmental contact parameters, and a variety of high knee flexion movements to provide a range of exposures (Chapter 3 & Chapter 4).

Tibial anterior-posterior (AP) and midal-lateral (ML) shear is not as well understood as compression largely due to few instrumented tibial implants having this measurement capability (Heinlein et al., 2007; Zhao et al., 2007). Data reported from studies using multi-axis instrumented implants are in knee flexion ranges of ~0-100º but can still provide meaningful insight for verification of model predictions (Bergmann et al., 2014; Kutzner et al., 2010; Mündermann et al., 2008; Taylor et al., 2017; Zhao et al., 2007). The only known 3D MSK study which estimated tibial AP shear forces in high knee flexion—and included sagittal plane thigh-calf contact estimates—predicted a peak decrease of 0.54 BW from 0.95 BW (Zelle et al., 2009). However, only a quadriceps force was modeled in this simulation (Zelle et al., 2009). Thambyah (2008) estimated peak AP shear forces during a flatfoot squat and found maximal anterior forces of 0.27 BW during descent and 0.34 BW during ascent phases. Although these magnitudes are far lower than compression, there is a rapid change from posterior to anterior shear during transitional movements to high knee flexion postures and finite element analyses have suggested this is a primary cause of femoral implant loosening (Thambyah, 2008; Thambyah and Fernandez, 2014). The lack of any ML shear predictions in high knee flexion postures, in addition to a single report of AP shear changes from intersegmental contact, warranted investigating these forces using our model.

Currently, there is limited information on electromyographic (EMG) activity of lower limb musculature when performing high knee flexion postures (Gallagher et al., 2011; Kingston and Acker, 2018b; Kingston et al., 2017). While the relationship of EMG activity to the force generating capacity of a muscle is complex (Jia et al., 2011; Manal and Buchanan, 2013; Nussbaum and Chaffin, 1998) a comparison between these two parameters can provide a qualitative assessment of muscle force estimations (Modenese et al., 2016; Walter et al., 2014; Winby et al., 2009). Therefore, should muscle force estimations follow general trends of EMG activity, this model could be used to garner insights of neuromuscular control during high knee flexion movements.

Therefore, the primary purpose of this study was to quantify the effect of including intersegmental contact on tibial compression, AP, and ML shear estimations during the static phase of six high knee flexion movements. We hypothesized that the inclusion of intersegmental contact would significantly decrease tibial compression, anterior shear, and medial shear forces. We speculated that this would result from a reduction in knee joint external moments when including intersegmental contact to inverse dynamic calculations. A secondary objective of this study was to qualitatively compare EMG waveforms to muscle force estimates.

6.2 Methodology

This study is a secondary assessment of data collected in Chapter 4 (Kingston and Acker, 2018b). For brevity, please see details on participants, experimental protocol, and general methodology of data collection in section 4.2. Aspects new to this study are detailed below.

6.2.1 Data processing

High knee flexion trials were truncated into three movement phases: descending from standing to kneeling (descent), resting in a static posture (static), and ascending from kneeling to standing (ascent). The beginning of the descent phase was defined similar to section 3.2.4; once the knee flexion angle exceeded a 10 frame threshold in standing and continued to a manually identified frame where the knee flexion angle plateaued in high flexion movements (Kingston and Acker, 2018a). The static phase was defined from the end of the descent phase to a manually identified point where a rapid change in knee flexion moment could be visually identified. The ascent phase was defined identically to descent but in reverse order.

External joint moments and forces were calculated for the ankle, knee, and hip (section 5.2.5) (Hof, 1992; Zatsiorsky, 2002) and expressed with respect to distal segment LCS (e.g. knee forces and moments are expressed with respect to the shank). External moments and forces were calculated with and without incorporating intersegmental contact magnitude, CoF, and orientation obtained from the protocol defined in section 5.2.4. Truncated knee flexion and external moment data were then intra-participant averaged and a representative trial was selected using the lowest RMSD value from their mean curve. Joint moments and muscle element moment arms (section 5.2.2.3) from the representative trial were fit to 100 points representing 100% of movement phase. This was necessary due to the 1.5 hour runtime required to solve a single 1500 frame trial with available hardware (dual-core Intel Core i3-3220 CPU at 3.30 GHz with 8 GB of RAM) using the protocol detailed in section 5.2.6.

Tibial contact force estimates were computed, with and without intersegmental contact, using methods defined in Chapter 5. Quantification of intersegmental contact effect on tibial contact forces was performed using RMSD for each high knee flexion movement and phase (Hicks et al., 2014; Modenese et al., 2011; Sartori et al., 2014). Inter-participant RMSD averages were then computed for each high knee flexion movement and phase.

Muscle force estimates were computed as an average representation of all muscle elements for comparison to EMG signals. For example, VL has two partitions—superior and inferior—which contain two and six elements respectively (Appendix A). Force estimates for each element were expressed as a percentage of its maximum force generating capacity (% Max). A mean of all elements—from all partitions—that were part of the VL muscle was computed and directly compared to %MVC EMG (section 4.2.2) for qualitative assessment of waveform trends. This procedure was completed for all 14 muscles which had EMG measurements for comparisons. Inter-participant averages of muscle force estimates and EMG signals were completed and with mean curves reported in Figure 6.8 and Appendix H.

6.2.2 Statistical analysis

All statistical procedures were performed using SPSS (IBM Corp. Released 2011. IBM SPSS Statistics for Windows, Version 20.0, Armonk, NY). To test the hypothesis that the inclusion of intersegmental contact would significantly decrease tibial contact forces three 6 x 2 two-way repeated measures ANOVA—with fixed effects of movement

(HS/FS/DK/PK/DUK/PUK) and intersegmental contact (none/included) and a random effect of participant—were used across mean tibial compression, AP, and ML shear values from the static phase of high knee flexion movements. The α level for all comparisons was preset at 0.05 with Bonferroni adjustment to account for multiple comparisons and simple main-effect analysis performed on significant interaction terms.

6.3 Results

6.3.1 External knee joint moments

There was a consistent reduction in external knee moments for all high knee flexion movements when intersegmental contact was considered (Table 6-1). A representative waveform of the effect of incorporating intersegmental contact on an external knee flexion moment is provided in Figure 6.1.

Table 6-1 Mean changes in peak external moments resulting from the inclusion of intersegmental contact parameters. All values are reported in %BW*HT. Movements are: heels-up squat (HS), flatfoot squat (FS), dorsiflexed kneel (DK), plantarflexed kneel (PK), dorsiflexed unilateral kneel (DUK), plantarflexed unilateral kneel (PUK). Brackets indicate 1 SD. Negative values indicate a decrease.

Axis	HS	FS	DK	PK	DUK	PUK
Flex/Extension	-2.77 (1.48)	-2.11 (1.36)	-2.69 (1.53)	-3.40 (1.98)	-5.12 (3.06)	-5.29 (3.40)
Ab/Adduction	-0.18 (0.37)	-0.24 (0.35)	-0.06 (0.17)	-0.08 (0.18)	-0.13 (0.29)	-0.25 (0.63)
Int/External Rotation	-0.03 (0.04)	-0.02 (0.02)	-0.04 (0.07)	-0.10 (0.09)	-0.06 (0.10)	-0.12 (0.12)

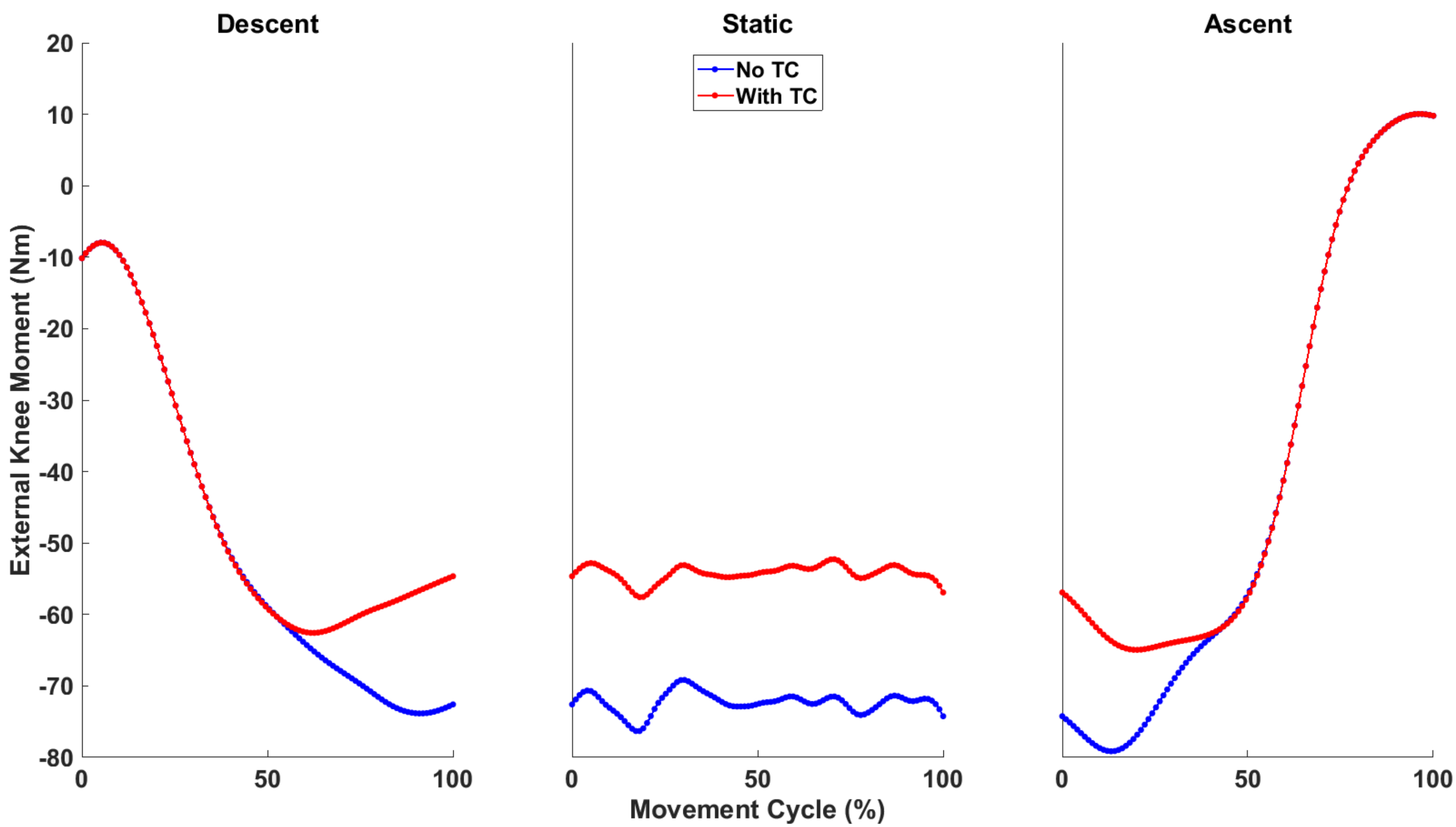

Figure 6.1 Changes to the external knee flexion (+)/extension (-) moment during a flatfoot squat when considering intersegmental contact parameters for participant P01. TC is thigh-calf contact.

6.3.2 Estimated tibial contact forces

Tibial compression had a main effect of movement ($p = 0.001$) with post hoc tests indicating a 2.01 BW lower compression during the FS movement when compared to PUK ($p = 0.008$) (Table 6-2). No other significant differences were found in axial forces. Tibial AP shear had an interaction effect between movement and intersegmental contact ($p < 0.001$) (Table 6-2). Simple main effects revealed that with intersegmental contact there were decreases in posterior shear of 0.25 BW in HS ($p = 0.017$), 0.21 BW in PK ($p = 0.024$), 0.42 BW in DUK ($p = 0.008$), and 0.42 BW in PUK ($p < 0.001$). Finally, tibial ML shear also had an interaction effect between movement and intersegmental contact ($p < 0.001$) (Table 6-2). Simple main effects revealed increases in lateral shear of 0.05 BW in DK ($p = 0.39$) and 0.08 BW in DUK ($p = 0.014$) with intersegmental contact.

In addition to statistical findings, peak RMSD between tibial force estimates that did or did not include intersegmental forces are reported in Table 6-3 with inter-participant mean tibial force waveforms provided in Figure 6.2-Figure 6.7.

Table 6-2 Mean tibial contact forces—in BW—during the static phase of high knee flexion movements. Brackets indicate 1 SD. Movements are: heels-up squat (HS), flatfoot squat (FS), dorsiflexed kneel (DK), plantarflexed kneel (PK), dorsiflexed unilateral kneel (DUK), and plantarflexed unilateral kneel (PUK). This data resulted from calculations that did not include intersegmental contact (NO) and those that did (TC). † indicates a main effect of movement with bold italicized pairs indicating interaction effects of movement and intersegmental contact identified at a movement level by simple main effects. Tibial compression (+) is COMP, anterior (+)/posterior (-) shear is AP, and medial (-)/lateral (+) shear is ML.

	COMP†		**AP**		**ML**	
Movement	**NO**	**TC**	**NO**	**TC**	**NO**	**TC**
HS	3.23 (1.49)	2.96 (1.52)	***-0.27 (0.13)***	***0.02 (0.29)***	0.05 (0.08)	0.06 (0.07)
FS	1.98 (1.48)	1.99 (1.43)	-0.09 (0.24)	0.00 (0.22)	0.03 (0.06)	0.03 (0.04)
DK	4.50 (2.25)	4.38 (2.32)	-0.26 (0.31)	-0.05 (0.28)	***0.07 (0.08)***	***0.12 (0.07)***
PK	3.25 (2.14)	3.26 (2.16)	***-0.28 (0.20)***	***0.07 (0.31)***	0.10 (0.07)	0.13 (0.05)
DUK	4.13 (2.09)	4.18 (1.92)	***-0.48 (0.22)***	***-0.06 (0.30)***	***0.01 (0.14)***	***0.10 (0.09)***
PUK	4.02 (2.03)	3.97 (2.00)	***-0.47 (0.20)***	***-0.05 (0.41)***	0.07 (0.10)	0.09 (0.07)

Table 6-3 Mean RMSD of tibial contact force estimates—in BW—for each high knee flexion movement and movement phase when intersegmental contact was included in MSK model calculations. Brackets indicate 1 SD. Movements are: heels-up squat (HS), flatfoot squat (FS), dorsiflexed kneel (DK), plantarflexed kneel (PK), dorsiflexed unilateral kneel (DUK), and plantarflexed unilateral kneel (PUK).

Axis	Phase	HS	FS	DK	PK	DUK	PUK
Tension Compression	Descent	0.13 (0.10)	0.12 (0.18)	0.09 (0.07)	0.08 (0.07)	0.08 (0.06)	0.10 (0.06)
	Static	0.27 (0.26)	0.17 (0.25)	0.17 (0.23)	0.11 (0.09)	0.16 (0.15)	0.18 (0.12)
	Ascent	0.13 (0.10)	0.10 (0.17)	0.08 (0.08)	0.08 (0.08)	0.08 (0.06)	0.09 (0.06)
Anterior Posterior	Descent	0.12 (0.08)	0.05 (0.06)	0.10 (0.09)	0.12 (0.06)	0.16 (0.08)	0.18 (0.12)
	Static	0.29 (0.19)	0.10 (0.12)	0.22 (0.19)	0.36 (0.22)	0.42 (0.22)	0.43 (0.26)
	Ascent	0.14 (0.08)	0.06 (0.08)	0.11 (0.09)	0.14 (0.07)	0.22 (0.14)	0.23 (0.14)
Medial Lateral	Descent	0.02 (0.02)	0.02 (0.02)	0.02 (0.03)	0.01 (0.02)	0.03 (0.03)	0.02 (0.02)
	Static	0.04 (0.05)	0.03 (0.03)	0.05 (0.06)	0.03 (0.04)	0.08 (0.10)	0.05 (0.06)
	Ascent	0.02 (0.02)	0.02 (0.02)	0.03 (0.03)	0.02 (0.02)	0.04 (0.05)	0.03 (0.04)

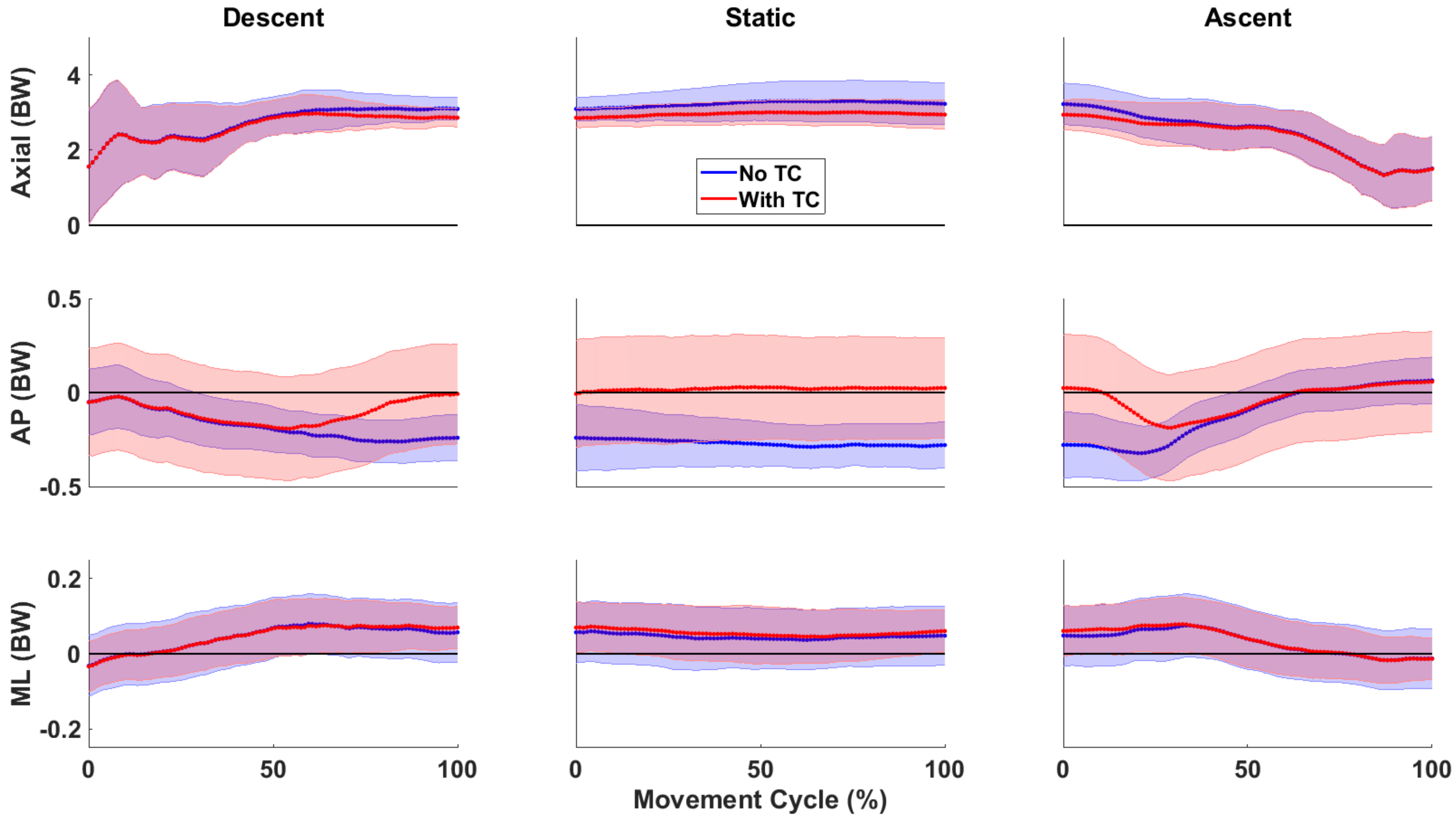

Figure 6.2 Mean model estimates of tibial compression (+), anterior (+)/posterior (-) shear, and medial (-)/lateral (+) shear forces during a heels-up squat. Shaded regions represent ±1 SD.

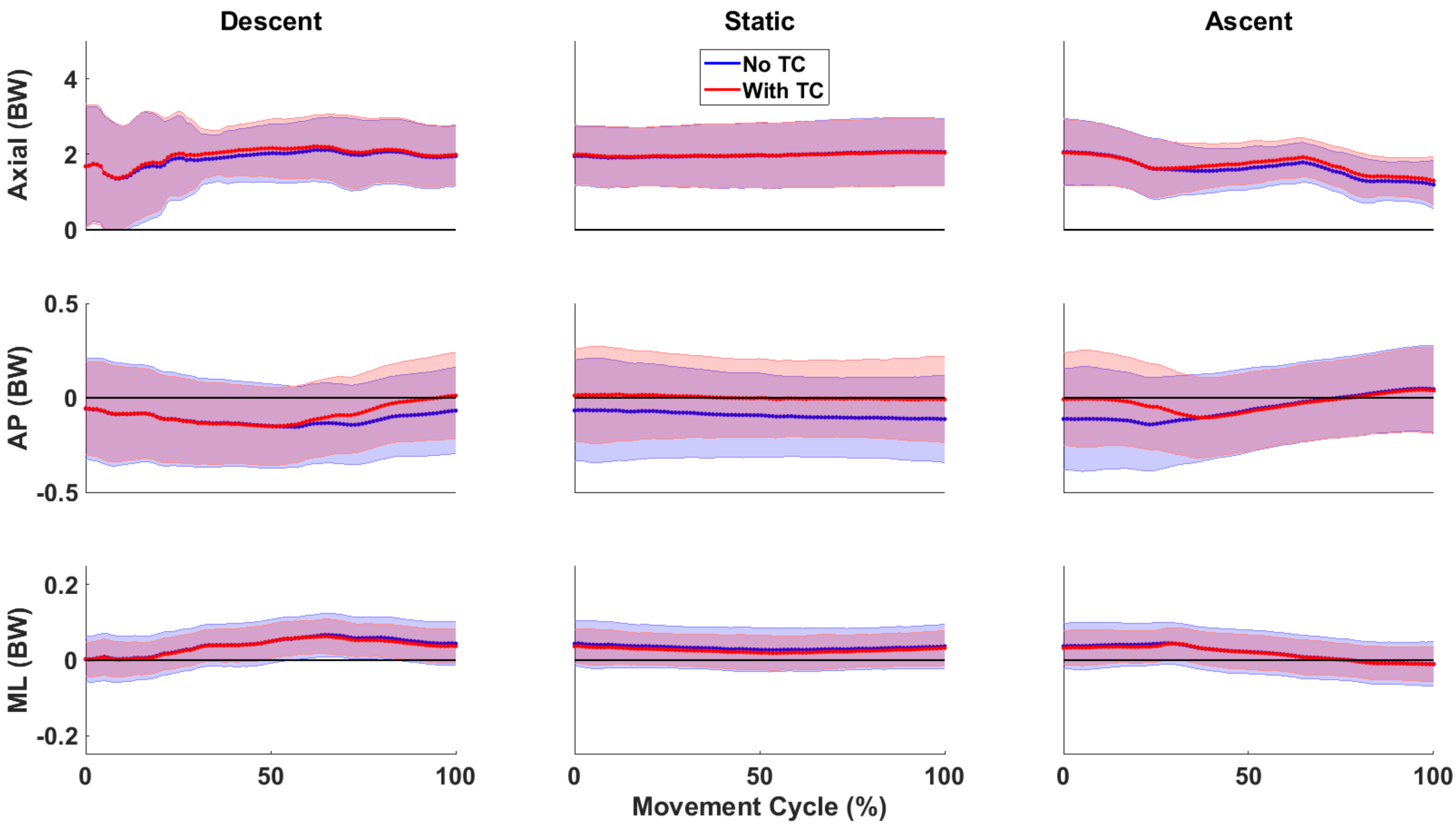

Figure 6.3 Mean model estimates of tibial compression (+), anterior (+)/posterior (-) shear, and medial (-)/lateral (+) shear forces during a flatfoot squat. Shaded regions represent ±1 SD.

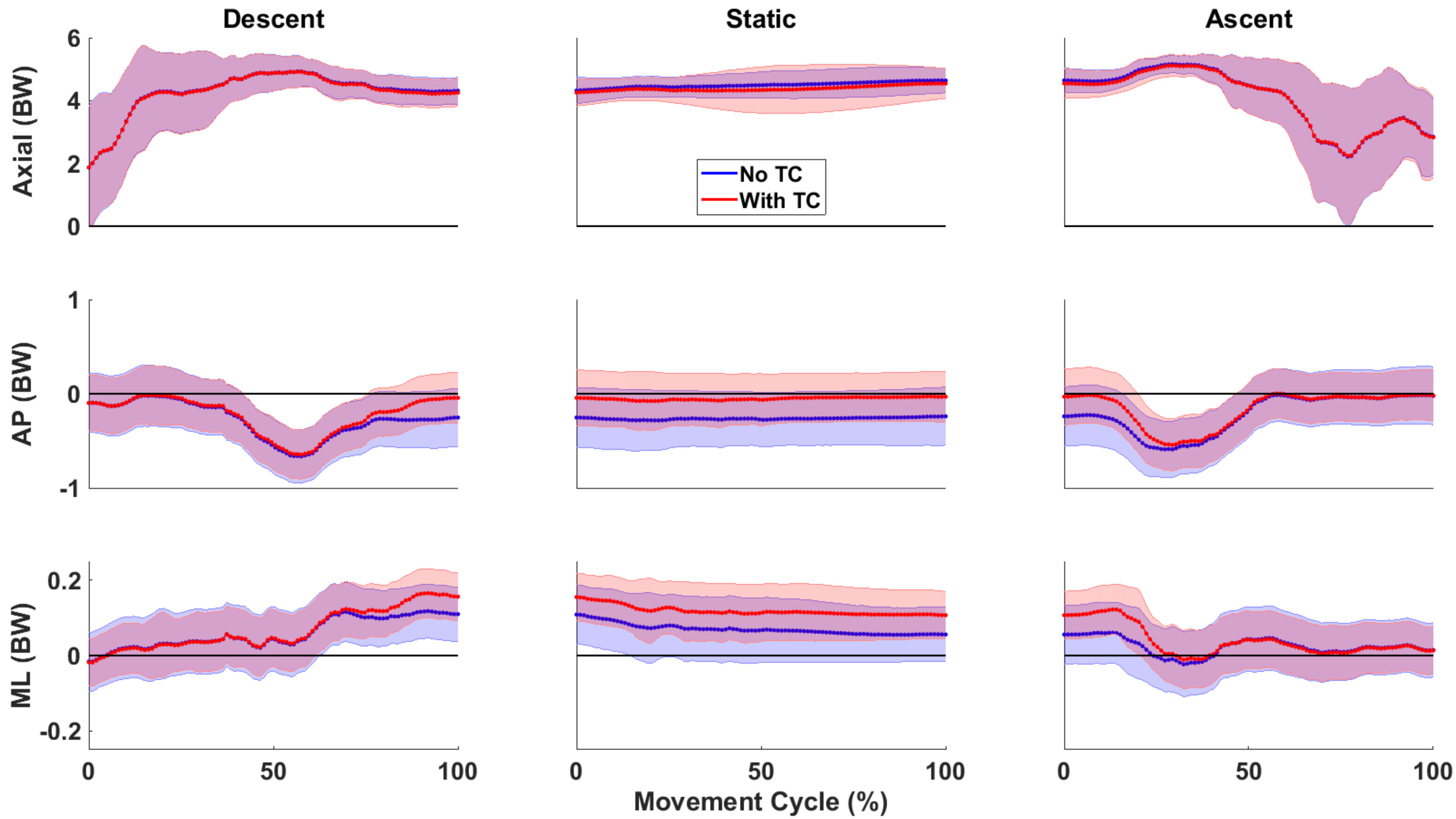

Figure 6.4 Mean model estimates of tibial compression (+), anterior (+)/posterior (-) shear, and medial (-)/lateral (+) shear forces during a dorsiflexed kneel. Shaded regions represent ±1 SD.

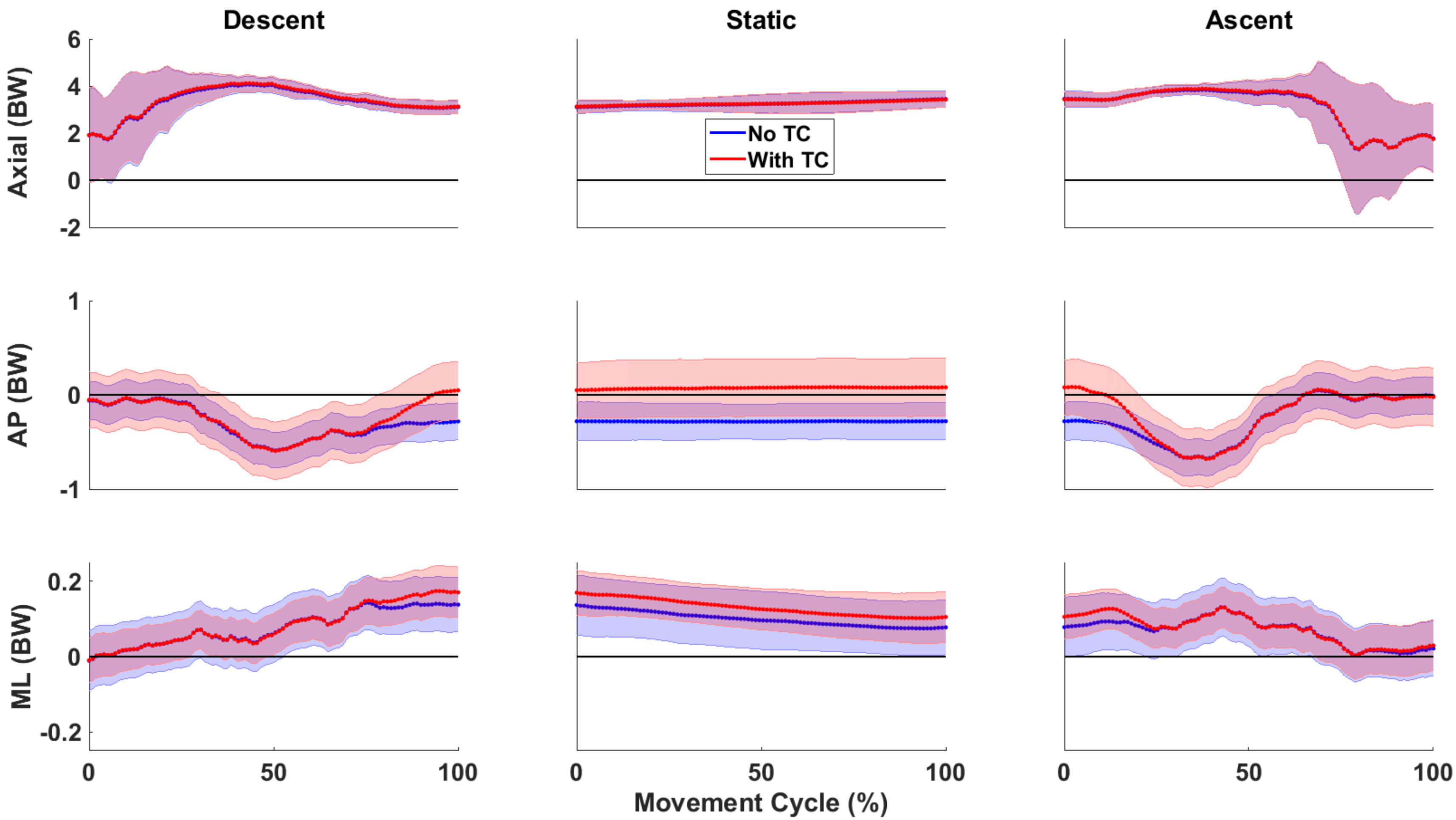

Figure 6.5 Mean model estimates of tibial compression (+), anterior (+)/posterior (-) shear, and medial (-)/lateral (+) shear forces during a plantarflexed kneel. Shaded regions represent ±1 SD.

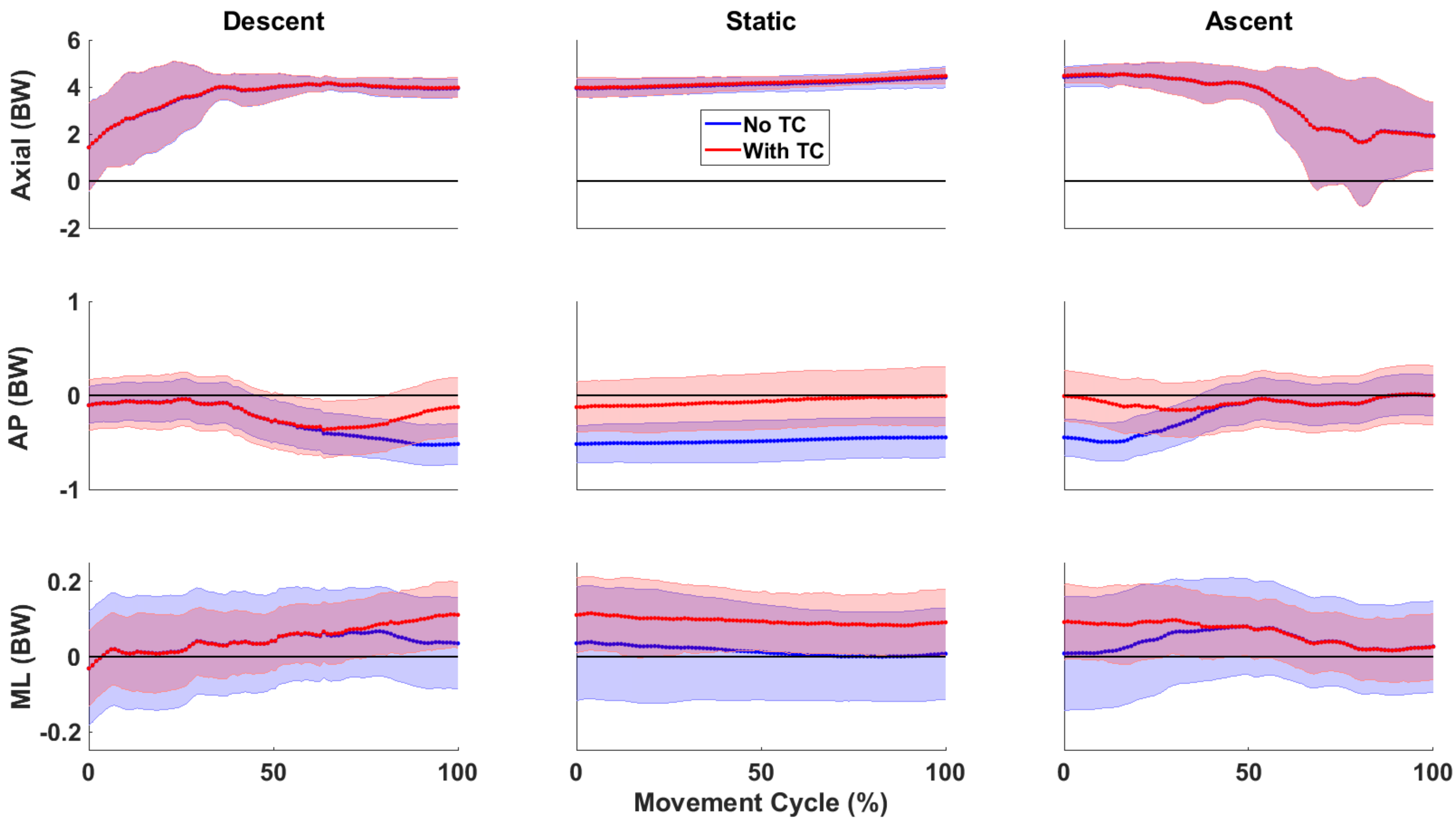

Figure 6.6 Mean model estimates of tibial compression (+), anterior (+)/posterior (-) shear, and medial (-)/lateral (+) shear forces during a dorsiflexed unilateral kneel. Shaded regions represent ±1 SD.

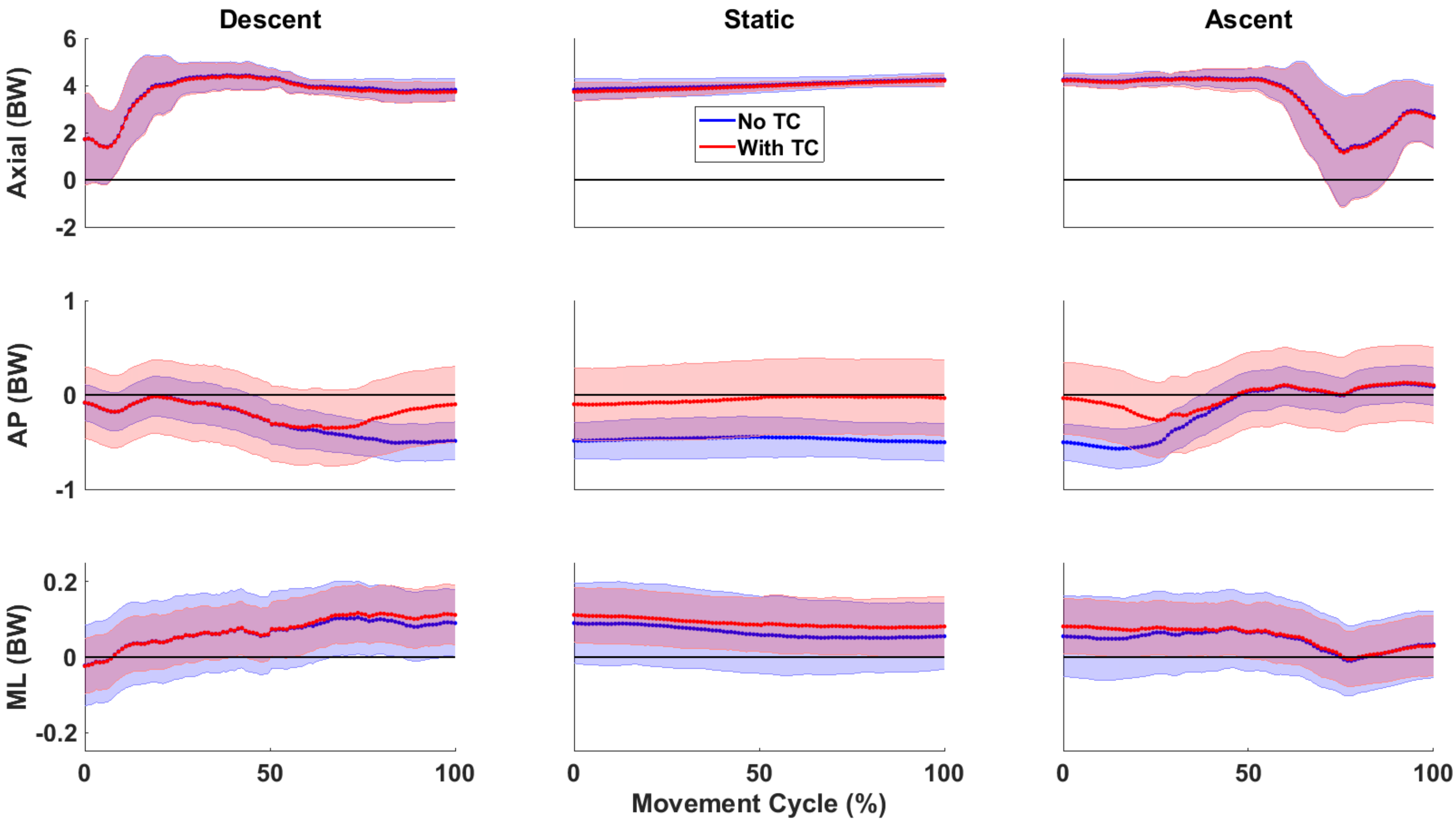

Figure 6.7 Mean model estimates of tibial compression (+), anterior (+)/posterior (-) shear, and medial (-)/lateral (+) shear forces during a plantarflexed unilateral kneel. Shaded regions represent ±1 SD.

Model estimates of muscle force that generally had the best visual agreement with mean EMG waveforms were vastii, GD, AM (surface site), ST, and SM (fine-wire site) (Figure 6.8 and Appendix H). There was a poor overall agreement with hamstrings and gastrocnemii (Figure 6.8 and Appendix H). Mean muscle force predictions had notably worse visual agreement during the PK movement (Appendix H) as force magnitudes were elevated during the static phase of movement (33-66 % movement cycle) compared to transitional periods, 0-32 % (descent) and 67-100% (ascent) of movement cycle.

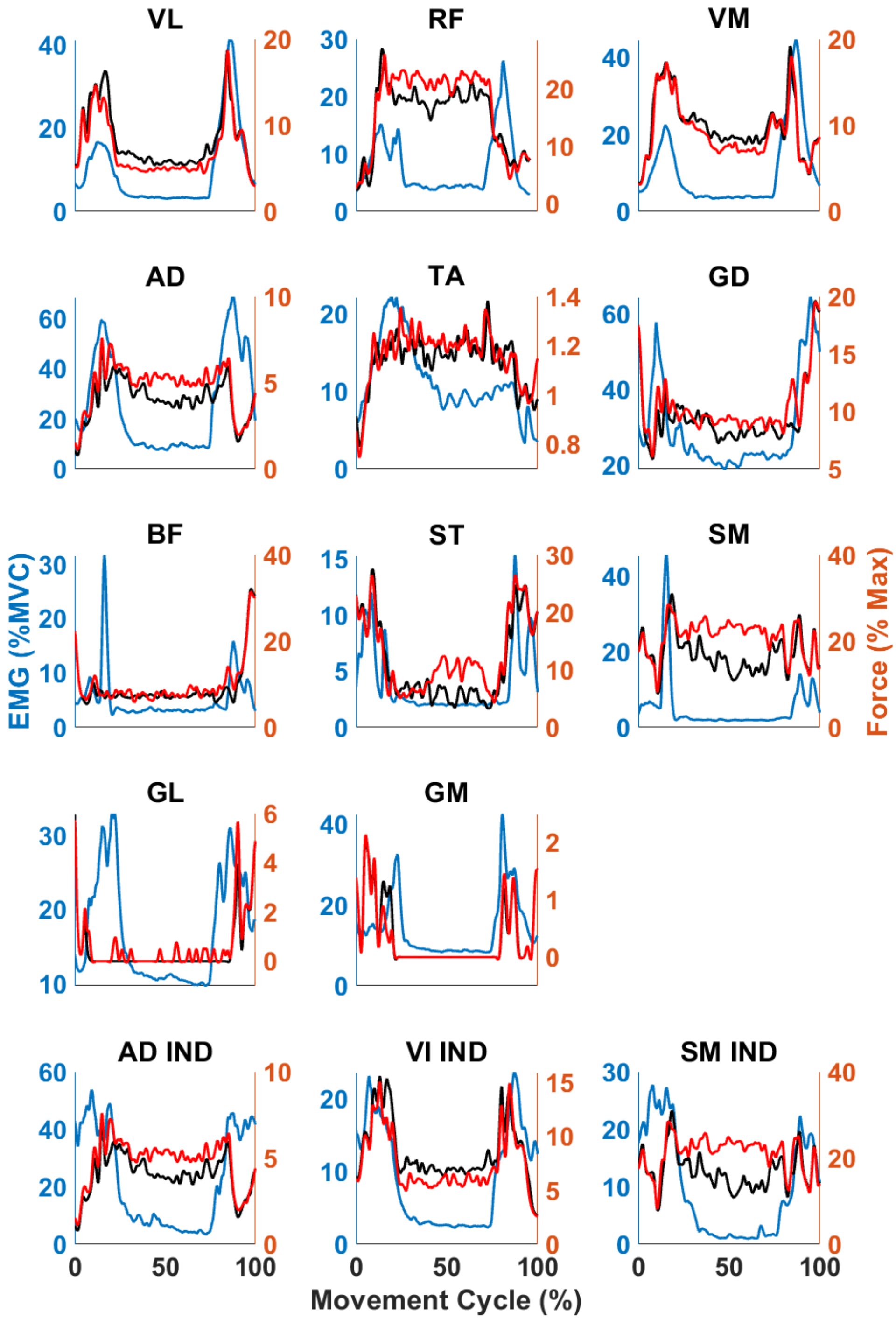

Figure 6.8 Mean muscle activations (blue) compared to mean muscle forces with (orange) and without intersegmental contact (black) for heels-up squat. Muscles are: vastus lateralis (VL), rectus femoris (RF), vastus medialis (VM), adductor magnus (AM), tibialis anterior (TA), gluteus medius (GD), biceps femoris (BF), semitendinosus (ST), semimembranosus (SM), lateral gastrocnemius (GL), medial gastrocnemius (GM), with indwelling recordings of adductor magnus (AD IND), vastus intermedius (VI IND), and semimembranosus (SM IND).

6.4 Discussion

The primary purpose of this study was to quantify the effect of including intersegmental contact on tibial compression, AP, and ML shear estimations during the static phase of six high knee flexion movements. Due to an average RMSD of 3.56, 0.16, and 0.06 %BW*HT in flexion/extension, ab/adduction, and int/external external moments from including intersegmental contact parameters, significant reductions in posterior shear were observed for HS (0.25 BW), PK (0.21 BW), DUK (0.42 BW), and PUK (0.42 BW). Also, significant increases in tibial lateral shear were found when including intersegmental contact parameters during DK (0.05 BW) and DUK (0.08 BW) movements. The secondary objective of this study was to qualitatively compare EMG waveforms to muscle force estimates. Muscle force estimates generally followed EMG waveforms in shape for vastii, GD, and AM with SM having an improved agreement using its indwelling signal compared to surface measurements.

External moments have previously been reported for transitional and static phases of some kneeling activities (Chong et al., 2017) with similar flexion/extension magnitudes reported (0-6 %BW*HT) as our DK and PK movements. As well, Pollard et al. (2011) reported 3D external knee joint moments for symmetric squatting and kneeling tasks of 3-5, 0.5-1.3, and 0.25-0.4 %BW*HT for flexion/extension, ab/adduction, and int/external axes respectively. Given the 30-40% reduction in flexion moment resulting from incorporating intersegmental contact, one could expect the largest reduction to occur in tibial compression. However, AP shear had the largest magnitude and highest number of significant reductions.We speculate that there could be two fesible explanations: 1) the current MSK model geometry and cost function are insensitive to changes in external flexion moments or 2) high levels of tibial compression occur in high knee flexion postures. Unfortunately, there is no instrumented implant data available beyond ~100º of knee flexion to verify our reported tibial compression magnitudes. Therefore, future work is required to assess model sensitivity for these estimations.

Tibial contact force estimations are within reported instrumented implant values for a variety of low to mid range knee flexion activities (Bergmann et al., 2014; Kutzner et al., 2010; Mündermann et al., 2008; Taylor et al., 2017; Zhao et al., 2007). For example, average MSK model predictions of all tibial contact forces were slightly above magnitudes observed during stair abulation (Kutzner et al., 2010) and 1-2 BW higher than peak loading when standing from a chair at a knee flexion angle of ~80º (Taylor et al., 2017). The only known study which estimated tibial contact forces in high knee flexion—and modeled thigh-calf contact—predicted peak decreases of 1.99 BW in compression and 0.54 BW in posterior shear (Zelle et al., 2009). Our maximum mean RMSD compressive force reduction was considerably smaller (0.27 BW), but we reported similar changes in posterior shear with a maximum mean RMSD of 0.30 BW.

Tibial contact force estimates from this model appear to be more biologically feasible than prior 2D reports. Our peak tibial compression and shear estimates are almost half (Nagura et al., 2006) or 1-3 BW (Dahlkvist et al., 1982) lower than sagitttal plane high knee flexion models which did not account for intersegmental contact. Using joint contact areas measured in prostheses (Thambyah et al., 2005; Zhao et al., 2007), the peak compressive and shear force magnitudes reported by Nagura et al. (2006) are in excess of 21 MPa tensile yield stress of both ultra high molecular weight (UHMW) polyethylene (Chapman-Sheath et al., 2003) and 15-20 MPa range known to damage cartilage and kill chondrocytes (Clements et al., 2001). Defining a knee joint contact model for high knee flexion postures was outside the scope of this thesis, but our peak tibial compression and AP shear estimates were comparable to Zelle et al. (2009) and mid-range implant data (Fregly et al., 2012; Taylor et al., 2017).

We speculate that the tibial contact force magnitudes estimated in the current study support a theory that intersegmental contact could be a protective mechanism for knee joint articular cartilage in high knee flexion postures. The superficial tangential zone of knee articular cartilage acts as a callous to resist shear forces; which this tissue is more sensitive to than compression (Bevill et al., 2010). Given the susceptability of cartilage to damage after sustained compression (Kim et al., 2012), individuals who regularly assume high knee flexion postures may be predisposed to injury. This would support the cascade of OA initiation (Andriacchi et al., 2006, 2004; Bevill et al., 2010) and the inability of treatment due to loss of tissue integrity. Since individuals can regularly perform high knee flexion activities with negligible acute tissue damage, we feel the inclusion of intersegmental contact is necessary in future tissue and joint contact models of the knee.

Based on visual inspection, muscle force estimates generally followed EMG waveform profiles for vastiis, GD, AM, and SM (Figure 6.8 and Appendix H). This style of comparison is subjective, but common within the modelling literature (Durandau et al., 2018; Modenese et al., 2011; Mohammadi et al., 2015; Sartori et al., 2014; Winby et al., 2009). PK had more instances of poor agreement between EMG and mean muscle force estimations than other activities; specifically in the static phase of movement where estimated muscle forces increased when EMG activity was consistantly low. The most kinematically similar movement, PUK, had much better agreement. This outcome requires further investigation.

Limitations of this study include soft tissue artifact, the exclusion of knee capsular ligaments, assumptions of intersegmental contact parameters, and no estimation of knee joint contact area. Soft tissue deformation is considerable in the thigh segment during high knee flexion postures which lowers confidence in kinematic measurements. There is no data currently available to quantify error of surface markers compared to skeletal structures in high knee flexion movements. Although external force and moment calculations—which are inputs to the MSK model—would be affected by this error, it would be consistent between our tibial contact force calculations. Noted in section 5.4 was the exclusion of knee capsule ligaments. This limitation is somewhat attenuated by the low force contributions, measured *in vitro*, of the ACL (< 40 N), PCL (< 20 N), MCL (< 10 N), and LCL (< 5 N) ligaments have above 90º of knee flexion (Yang et al., 2010). However, *in vivo* response of these tissues in high knee flexion movements could alter capsular ligament contribution to tibial forces as *in vitro* studies are commonly osteoligamentous (Yang et al., 2010) or contain limited simulated muscle forces (Steinbrück et al., 2013; Victor et al., 2009). Intersegmental contact pressure distributions used in this study were measured against a polycarbonate sheet and modeled as a function of knee flexion angle. This assumes an approximately constant external force during the static phase of movements and 'mirrored' loading during the ascending phase as only the descent phase was measured. This was a limitation of measurement approach detailed in section 5.2.4. Finally, the current model does not have the capability to estimate contact area between femoral condyles and the tibial plateau. This does not allow us to comment on stress of knee joint tissues resulting from estimated tibial contact forces as contact area between femoral and tibial structures is unknown in this model.

6.5 Conclusion

Including 3D intersegmental contact forces when estimating tibial contact forces using a high knee flexion 3D MSK model resulted in a significant decrease in posterior shear and increase in lateral shear in select movements. Tibial posterior shear had peak forces of approximately 0.5 BW but was reduced by a peak mean RMSD of 0.43 BW in unilateral kneeling movements. Although tibial lateral shear was significantly increased in dorsiflexed kneeling movements, the biological effect of a 0.08 BW change is presumed to be negligible. There was no significant differences in tibial compression as a result of including intersegmental contact. These results suggest that intersegmental contact could significantly reduce the exposure of knee tissues to AP shear stress, however estimates of tibiofemoral contact area would be required to confirm this possibility. Although qualitative agreement between EMG and estimated muscle force measurement was improved when compared to section 5.3.3, this model does not represent underlying physiology.

Prior work has highlighted the need for accurate tibial compressive and shear force magnitudes to improve tissue engineering of knee joint structures (De Sanctis et al., 2015; Moroni et al., 2007) and robustness to prosthetic loosening (Thambyah, 2008; Thambyah and Fernandez, 2014). Further verification of our reported magnitudes are needed as, unlike some biological tissues, conservative estimates of tissue loading is as detrimental as overestimates in terms of menisci and cartilage growth (Orsi et al., 2016; Seedhom, 2006). Therefore, the findings from this study are a substantial step forward in improving our understanding of the tibial loading environment during high knee flexion exposures. Future work is needed to address soft tissue artifact as confidence in femoral and tibial plateau surface geometry is needed to implement realistic finite element models of tissue strain. These simulations could then be used to predict tissue injury and identify mechanisms of disease progression.

Chapter 7 – Contributions

The series of experimental and modelling efforts detailed in this document supported the global objective of this work: to develop a 3D MSK model of the knee to estimate tibial contact forces in high knee flexion postures for determining the effect of intersegmental contact on tibial contact forces. This section is separated into novel contributions and novel findings presented in a listed format.

7.1 Novel contributions

1) Intersegmental contact data were collected from the largest sample to date during six high knee flexion movements, four of which had never been previously measured (Chapter 3). These data were calculated using a newly defined artifact reduction process (Kingston and Acker, 2018a) and measured with approximately four times the spatial accuracy and eight times the sampling frequency of previous efforts (Pollard et al., 2011; Zelle et al., 2007). Mounting a pressure sensor to a polycarbonate sheet with kinematic markers enabled the first experimentally collected 3D position and orientation data of intersegmental contact forces (section 5.3.2).
2) Time-series waveforms of surface and indwelling EMG data were collected during six high knee flexion movements with many of the measured muscles being reported for the first time (Chapter 4). In addition, this was the first known attempt to model fine-wire recordings of three large PCSA muscles based on surface EMG signals.
3) A full flexion 3D MSK model of the pelvis and lower limb was defined that incorporated a 4 DoF knee joint, posterior translation as a function of knee flexion angle, and 161 muscle elements (Chapter 5). This statically determinant phenomenological model was

capable of matching tibial compression measurements from instrumented implant data within 0.16, 0.44, and 0.58 RMSD during cyclic squatting, walking, and 'bouncy' walking respectively (section 5.3.3).

7.2 Novel findings

1) Strong linear regression models were developed—based on participant anthropometrics—to estimate maximum knee flexion angle and TC CoF location at maximum knee flexion (section 3.4).
2) Strong linear regression models—based on participant anthropometrics—could not be formulated for thigh-calf contact onset angle, total force at maximum knee flexion, or contact area at maximum knee flexion (section 3.4).
3) Fine-wire EMG recordings of vastus intermedius, adductor magnus, and semimembranosus could not be modeled using surface EMG recordings from vastus lateralis, rectus femoris, vastus medialis, semitendinosus, and biceps femoris using criteria of $R^2 > 0.85$ and RMSD < 10 %MVC for the high knee flexion activities studied (Chapter 4). This was attributed to the considerable variability of surface to fine-wire comparisons between participants (Table 4-2 and Appendix D).
4) Intersegmental contact significantly reduced posterior shear and increased lateral shear contact force estimates but had little effect on compression (section 6.3.2). This could suggest that intersegmental contact acts as a protective mechanism for knee articular cartilage during high knee flexion movements as this tissue is less tolerant to shear than compressive loading.

7.3 Future work

Considerable work is still required to understand the motor control of high knee flexion movements and to assess the relation of our results to habitual kneeling populations. This should involve more high-quality studies of lower limb EMG during a variety of tasks as well as investigating balance and movement patterns. Additionally, cultural or ethnic considerations could be a promising line of questioning as anthropological versus anatomical capabilities may help explain the prominent use of high knee flexion postures in some cultures (Hemmerich et al., 2006). Occupational kneelers need to be assessed as this population commonly performs manual material handling tasks during high knee flexion and is a prominent group in North America exposed to these postures. Occupational kneelers would likely be the most receptive to assistive devices designed to reduce knee loading which could also provide case-control studies for the investigation of acute tissue responses to high knee flexion movements.

A limitation of using skin-mounted instrumentation in the study of high knee flexion activities—be it motion capture or EMG—is the issue of soft tissue artifact. Deformation of soft and lean tissue of the thigh is visually apparent in high knee flexion movements and would result in measurement error. Characterization of this artifact could be completed using a matrix of servomotors to simulate intersegmental loading pattern and experimentally perturb these tissues to measure response. Given the limitations of current pressure sensing technology, this could be the most feasible near-term approach. Similarly, functional joint center algorithms need to be assessed for robustness to soft tissue artifact for use in high flexion ranges as current approaches were verified for use in sub 100º knee flexion ranges.

Implants used in total knee arthroplasty are not commonly designed for high knee flexion ranges of motion (Thomsen et al., 2013). Although prosthetics exist which can restore function for cross-legged sitting or some kneeling tasks (Jain et al., 2013; Sancheti et al., 2013) lifespan of these implants is still under investigation as well as the multitude of rehabilitative factors which dictate ultimate range of motion. Specific to this body of work is results which may be used to inform implant design criteria. Although FE models have been developed to guide some aspects of prosthesis design (Zelle et al., 2009) our refinement on the external loading of the lower limb provides 3D force data not previously considered. The utility of these studies for such design choices is speculative, but improvements to FE simulations of external loading conditions is a feasible outcome.

The model defined within this thesis is an initial step towards improving tibial contact force estimations. Although it is able to estimate tibial compression and some muscle activation waveforms well, computational redundancies exist which add complexity to troubleshooting and sensitivity analyses. Elimination of muscle elements minimally contributing to joint contact force estimations will simplify the model in its next iteration. Further investigation of using EMG waveforms to dynamically modify limits on muscle force estimations could improve concordance with a participant's muscle activity. Using the existing inverse dynamics module, implementation of a neuromechanical or Hill-type model could be a useful investigation for comparative and learning purposes as question-specific muscle force estimations—beyond altering objective functions—could be facilitated.

Finally, although the reliability of the developed masking procedure (section 3.2.4) was determined to be excellent, the influence this procedure had on TC parameters or regression equations requires further investigation. The use of masks would reduce overall total force magnitude and contact area, and would alter CoF locations. Using intersegmental contact data collected as part of study 2 (section 5.2.4) as 'novel' data, regression equations determined from raw and masked data in study 1 could be evaluated. This investigation would also provide comparative data to determine the magnitude of differences between posterior thigh and polycarbonate sheet attachment methods of the pressure sensor which could guide future studies using this measurement technology.

Bibliography

Acker, S.M., Cockburn, R. a, Krevolin, J., Li, R.M., Tarabichi, S., Wyss, U.P., 2011. Knee kinematics of high-flexion activities of daily living performed by male Muslims in the Middle East. J. Arthroplasty 26, 319–27. https://doi.org/10.1016/j.arth.2010.08.003

Ackermann, M., 2007. Dynamics and Energetics of Walking. University of Stuttgart.

Allen, T.R., Brookham, R.L., Cudlip, A.C., Dickerson, C.R., 2013. Comparing surface and indwelling electromyographic signals of the supraspinatus and infraspinatus muscles during submaximal axial humeral rotation. J. Electromyogr. Kinesiol. 23, 1343–1349. https://doi.org/10.1016/j.jelekin.2013.08.002

Amiel, D., Kleiner, J.B., Roux, R.D., Harwood, F.L., Akeson, W.H., 1986. The phenomenon of “ligamentization”: anterior cruciate ligament reconstruction with autogenous patellar tendon. J. Orthop. Res. 4, 162–172. https://doi.org/10.1002/jor.1100040204

An, K., 2007. Tendon excursion and gliding: Clinical impacts from humble concepts. J. Biomech. 40, 713–718. https://doi.org/10.1016/j.jbiomech.2006.10.008

An, K., Kwak, B., Chao, E., Morrey, B., 1984a. Determination of muscle and joint forces: a new technique to solve the indeterminate problem. J. Biomech. Eng. 106, 364–7.

An, K., Takahashi, K., Harrigan, T., Chao, E., 1984b. Determination of Muscle Orientations and Moment Arms. J. Biomech. Eng. 106, 280. https://doi.org/10.1115/1.3138494

Anas, I., Musa, T.A., Kabiru, I., Yisau, A.A., Kazaure, I.S., Abba, S.M., Kabir, S.M., 2013. Digital radiographic measurement of normal knee joint space in adults at Kano, Nigeria. Egypt. J. Radiol. Nucl. Med. 44, 253–258. https://doi.org/10.1016/j.ejrnm.2013.03.005

Anderson, A., Ellis, B., Weiss, J., 2007. Verification, validation and sensitivity studies in computational biomechanics. Comput. Methods Biomech. Biomed. Engin. 10, 171–184. https://doi.org/10.1080/10255840601160484

Anderson, F., Pandy, M., 2001. Dynamic Optimization of Human Walking. J. Biomech. Eng. 123, 381. https://doi.org/10.1115/1.1392310

Andriacchi, T.P., Briant, P.L., Bevill, S.L., Koo, S., 2006. Rotational Changes at the Knee after ACL Injury Cause Cartilage Thinning. Clin. Orthop. Relat. Res. 442, 39–44. https://doi.org/10.1097/01.blo.0000197079.26600.09

Andriacchi, T.P., Favre, J., 2014. The Nature of In Vivo Mechanical Signals That Influence Cartilage Health and Progression to Knee Osteoarthritis. Curr. Rheumatol. Rep. 16, 1–8. https://doi.org/10.1007/s11926-014-0463-2

Andriacchi, T.P., Mündermann, A., 2006. The role of ambulatory mechanics in the initiation and progression of knee osteoarthritis. Curr. Opin. Rheumatol. 18, 514–518. https://doi.org/10.1097/01.bor.0000240365.16842.4e

Andriacchi, T.P., Mündermann, A., Smith, R.L., Alexander, E.J., Dyrby, C.O., Koo, S., 2004. A framework for the in vivo pathomechanics of osteoarthritis at the knee. Ann. Biomed. Eng. 32, 447–57.

Arden, N., Nevitt, M.C., 2006. Osteoarthritis: Epidemiology. Best Pract. Res. Clin. Rheumatol. 20, 3–25. https://doi.org/10.1016/j.berh.2005.09.007

Arnold, E.M., Ward, S.R., Lieber, R.L., Delp, S.L., 2010. A model of the lower limb for analysis of human movement. Ann. Biomed. Eng. 38, 269–79. https://doi.org/10.1007/s10439-009-

9852-5

Atkinson, T., Haut, R., Altiero, N., 1998. An investigation of biphasic failure criteria for impact-induced fissuring of articular cartilage. J Biomech Eng 120, 536–537.

Babyak, M., 2004. What you see may not be what you get: a brief, nontechnical introduction to overfitting in regression-type models. Psychosom. Med. 66, 411–421. https://doi.org/10.1097/01.psy.0000127692.23278.a9

Baker, P., Reading, I., Cooper, C., Coggon, D., 2003. Knee disorders in the general population and their relation to occupation. Occup. Environ. Med. 60, 794–797. https://doi.org/10.1136/oem.60.10.794

Balice-Gordon, R.J., Thompson, W.J., 1988. The organization and development of compartmentalized innervation in rat extensor digitorum longus muscle. J. Physiol. 398, 211–231.

Ball, N., Scurr, J., 2013. Electromyography normalization methods for high-velocity muscle actions: Review and recommendations. J. Appl. Biomech. 29, 600–608.

Banks, S., Fregly, B., Boniforti, F., Reinschmidt, C., Romagnoli, S., 2005. Comparing in vivo kinematics of unicondylar and bi-unicondylar knee replacements. Knee surgery, Sport. Traumatol. Arthrosc. 13, 551–6. https://doi.org/10.1007/s00167-004-0565-x

Basmajian, J., De Luca, C., 1985. Muscles Alive: Their Functions Revealed by Electromyography, 5th ed. Williams & Wilkins, Baltimore.

Bell, A.L., Brand, R.A., Pedersen, D.R., 1989. Prediction of hip joint centre location from external landmarks. Hum. Mov. Sci. 8, 3–16. https://doi.org/10.1016/0167-9457(89)90020-

1

Bergmann, G., Bender, A., Dymke, J., Duda, G., Damm, P., 2014. Standardized loads acting in knee implants. PLoS One 9, 1–12. https://doi.org/10.1371/journal.pone.0155612

Besier, T., Lloyd, D., Ackland, T., 2003a. Muscle activation strategies at the knee during running and cutting maneuvers. Med. Sci. Sports Exerc. 35, 119–27. https://doi.org/10.1249/01.MSS.0000043608.79537.AB

Besier, T., Sturnieks, D., Alderson, J., Lloyd, D., 2003b. Repeatability of gait data using a functional hip joint centre and a mean helical knee axis. J. Biomech. 36, 1159–1168. https://doi.org/10.1016/S0021-9290(03)00087-3

Bevill, S.L., Thambyah, A., Broom, N.D., 2010. New insights into the role of the superficial tangential zone in influencing the microstructural response of articular cartilage to compression. Osteoarthr. Cartil. 18, 1310–1318. https://doi.org/10.1016/j.joca.2010.06.008

Bogey, R., Perry, J., Bontrager, E., Gronley, J., 2000. Comparison of across-subject EMG profiles using surface and multiple indwelling wire electrodes during gait. J. Electromyogr. Kinesiol. 10, 255–259. https://doi.org/10.1016/S1050-6411(00)00015-8

Bombardier, C., Hawker, G., Mosher, D., 2011. the Impact of Arthritis in Canada: Today and Over the Next 30 Years, Arthritis Alliance of Canada.

Brimacombe, J.M., Wilson, D.R., Hodgson, A.J., Ho, K.C.T., Anglin, C., 2009. Effect of Calibration Method on Tekscan Sensor Accuracy. J. Biomech. Eng. 131, 034503. https://doi.org/10.1115/1.3005165

Buchanan, T.S., Lloyd, D.G., Manal, K., Besier, T.F., 2004. Neuromusculoskeletal Modeling:

Estimation of Muscle Forces and Joint Moments and Movements from Measurements of Neural Command. J. Appl. Biomech. 20, 367–395.

Buford, W., Ivey, F., Malone, J., Patterson, R., Peare, G., Nguyen, D., Stewart, A., 1997. Muscle balance at the knee - Moment arms for the normal knee and the ACL-minus knee. IEEE Trans. Rehabil. Eng. 5, 367–379. https://doi.org/10.1109/86.650292

Burden, A., Bartlett, R., 1999. Normalisation of EMG amplitude: an evaluation and comparison of old and new methods. Med. Eng. Phys. 21, 247–257.

Byrne, C., Lyons, G., Donnelly, A., O'Keeffe, D., Hermens, H., Nene, A., 2005. Rectus femoris surface myoelectric signal cross-talk during static contractions. J. Electromyogr. Kinesiol. 15, 564–575. https://doi.org/10.1016/j.jelekin.2005.03.002

Camomilla, V., Cereatti, A., Vannozzi, G., Cappozzo, A., 2006. An optimized protocol for hip joint centre determination using the functional method. J. Biomech. 39, 1096–106. https://doi.org/10.1016/j.jbiomech.2005.02.008

Carbone, V., Fluit, R., Pellikaan, P., van der Krogt, M.M., Janssen, D., Damsgaard, M., Vigneron, L., Feilkas, T., Koopman, H.F.J.M., Verdonschot, N., 2015. TLEM 2.0 - A comprehensive musculoskeletal geometry dataset for subject-specific modeling of lower extremity. J. Biomech. 48, 734–741. https://doi.org/10.1016/j.jbiomech.2014.12.034

Carbone, V., van der Krogt, M.M., Koopman, H.F.J.M., Verdonschot, N., 2012. Sensitivity of subject-specific models to errors in musculo-skeletal geometry. J. Biomech. 45, 2476–2480. https://doi.org/10.1016/j.jbiomech.2012.06.026

Caruntu, D.I., Hefzy, M.S., Goel, V.K., Goitz, H.T., Dennis, M.J., Agrawal, V., 2003. Modeling the Knee Joint in Deep Flexion : “ Thigh and Calf ” Contact, in: Summer Bioengineering Conference. Key Biscayne, Florida, pp. 4–5.

Cereatti, A., Bonci, T., Akbarshahi, M., Aminian, K., Barré, A., Begon, M., Benoit, D.L., Charbonnier, C., Maso, F.D., Fantozzi, S., Lin, C.-C., Lu, T.-W., Pandy, M.G., Stagni, R., van den Bogert, A.J., Camomilla, V., 2017. Standardization proposal of soft tissue artefact description for data sharing in human motion measurements. J. Biomech. https://doi.org/10.1016/j.jbiomech.2017.02.004

Chapman-Sheath, P.J., Bruce, W.J.M., Chung, W.K., Morberg, P., Gillies, R.M., Walsh, W.R., 2003. In vitro assessment of proximal polyethylene contact surface areas and stresses in mobile bearing knees. Med. Eng. Phys. 25, 437–443. https://doi.org/10.1016/S1350-4533(03)00016-X

Chapman, A.R., Vicenzino, B., Blanch, P., Knox, J.J., Hodges, P.W., 2010. Intramuscular fine-wire electromyography during cycling: Repeatability, normalisation and a comparison to surface electromyography. J. Electromyogr. Kinesiol. 20, 108–117. https://doi.org/10.1016/j.jelekin.2008.11.013

Charlton, I.W., Johnson, G.R., 2001. Application of spherical and cylindrical wrapping algorithms in a musculoskeletal model of the upper limb. J. Biomech. 34, 1209–1216. https://doi.org/10.1016/S0021-9290(01)00074-4

Chaudhari, A.M.W., Briant, P.L., Bevill, S.L., Koo, S., Andriacchi, T.P., 2008. Knee kinematics, cartilage morphology, and osteoarthritis after ACL injury. Med. Sci. Sports Exerc. 40, 215–22. https://doi.org/10.1249/mss.0b013e31815cbb0e

Chehab, E.F., Andriacchi, T.P., Favre, J., 2017. Speed, age, sex, and body mass index provide a rigorous basis for comparing the kinematic and kinetic profiles of the lower extremity during walking. J. Biomech. 58, 11–20. https://doi.org/10.1016/j.jbiomech.2017.04.014

Cheung, V.C.K., d'Avella, A., Tresch, M.C., Bizzi, E., 2005. Central and sensory contributions to the activation and organization of muscle synergies during natural motor behaviors. J. Neurosci. 25, 6419–6434. https://doi.org/10.1523/JNEUROSCI.4904-04.2005

Chong, H.C., Tennant, L.M., Kingston, D.C., Acker, S.M., 2017. Knee joint moments during high flexion movements: Timing of peak moments and the effect of safety footwear. Knee 24, 271–279. https://doi.org/10.1016/j.knee.2016.12.006

Chu, C.R., Williams, A. a, Coyle, C.H., Bowers, M.E., 2012. Early diagnosis to enable early treatment of pre-osteoarthritis. Arthritis Res. Ther. 14, 212. https://doi.org/10.1186/ar3845

Ciccotti, M.G., Kerlan, R.K., Perry, J., Pink, M., 1994. An electromyographic analysis of the knee during functional activities. I. The normal profile. Am. J. Sports Med. 22, 645–650. https://doi.org/10.1177/036354659402200512

Clancy, E., Morin, E., Merletti, R., 2002. Sampling, noise-reduction and amplitude estimation issues in surface electromyography. J. Electromyogr. Kinesiol. 12, 1–16.

Clements, K.M., Bee, Z.C., Crossingham, G. V., Adams, M.A., Sharif, M., 2001. How severe must repetitive loading be to kill chondrocytes in articular cartilage? Osteoarthr. Cartil. 9, 499–507. https://doi.org/10.1053/joca.2000.0417

Cnop, M., Havel, P.J., Utzschneider, K.M., Carr, D.B., Sinha, M.K., Boyko, E.J., Retzlaff, B.M., Knopp, R.H., Brunzell, J.D., Kahn, S.E., 2003. Relationship of adiponectin to body fat distribution, insulin sensitivity and plasma lipoproteins: evidence for independent roles of age and sex. Diabetologia 46, 459–469. https://doi.org/10.1007/s00125-003-1074-z

Coggon, D., Croft, P., Kellingray, S., Barrett, D., McLaren, M., Cooper, C., 2000. Occupational physical activities and osteoarthritis of the knee. Arthritis Rheum. 43, 1443–9. https://doi.org/10.1002/1529-0131(200007)43:7<1443::AID-ANR5>3.0.CO;2-1

Cohen, J., Cohen, P., West, S., Aiken, L., 2003. Applied Multiple Regression/Correlation Analysis for the Behavioral Sciences, 3rd ed. Lawrence Erlbaum Associates, Inc., Mahwah, New Jersey.

Collins, J., 1994. THE REDUNDANT NATURE OPTIMIZATION OF LOCOMOTOR OPTIMIZATION LAWS. J. Biomech. 28, 251–267.

Cooper, C., Snow, S., McAlindon, T., 2000. Risk factors for the incidence and progression of radiographic knee osteoarthritis. Arthritis Rheum. 45, 995–1000.

Crago, P.E., Peckham, P.H., Thrope, G.B., 1980. Modulation of Muscle Force by Recruitment During Intramuscular Stimulation. IEEE Trans. Biomed. Eng. BME-27, 679–684. https://doi.org/10.1109/TBME.1980.326592

Crowninshield, R.D., Brand, R. a, 1981. A physiologically based criterion of muscle force prediction in locomotion. J. Biomech. 14, 793–801.

Dahlkvist, N.J., Mayo, P., Seedhom, B.B., 1982. Forces during squatting and rising from a deep squat. Eng. Med. 11, 69–76. https://doi.org/10.1243/EMED_JOUR_1982_011_019_02

Damsgaard, M., Rasmussen, J., Christensen, S.T., Surma, E., de Zee, M., 2006. Analysis of musculoskeletal systems in the AnyBody Modeling System. Simul. Model. Pract. Theory 14, 1100–1111. https://doi.org/10.1016/j.simpat.2006.09.001

De Sanctis, V., Soliman, A., Bernasconi, S., Bianchin, L., Bona, G., Bozzola, M., Buzi, F., De Sanctis, C., Tonini, G., Rigon, F., Perissinotto, E., 2015. Primary dysmenorrhea in adolescents: Prevalence, impact and recent knowledge. Pediatr. Endocrinol. Rev. 13, 512–520. https://doi.org/10.1002/term

Delp, S.L., Loan, P., Hoy, M.G., Zajac, F.E., Topp, E.L., Rosen, J.M., 1990. An Interactiv Gaphics-Based Model of the Lower Extremity to Study Orthopaedic Surgical Procedures. IEEE Trans. Biomed. Eng. 37, 757–67.

Department of the Army, 2010. Technical Manual No. 3-22.31. US Army, Washington, DC.

Dickerson, C.R., 2005. A biomechanical analysis of shoulder loading and effort during load transfer tasks. University of Michigan.

Dickerson, C.R., Chaffin, D.B., Hughes, R.E., 2007. A mathematical musculoskeletal shoulder model for proactive ergonomic analysis. Comput. Methods Biomech. Biomed. Engin. 10, 389–400. https://doi.org/10.1080/10255840701592727

Dominici, N., Ivanenko, Y.P., Cappellini, G., d'Avella, a., Mondi, V., Cicchese, M., Fabiano, a., Silei, T., Di Paolo, a., Giannini, C., Poppele, R.E., Lacquaniti, F., 2011. Locomotor Primitives in Newborn Babies and Their Development. Science (80-.). 334, 997–999. https://doi.org/10.1126/science.1210617

Donahue, T.L.H., Hull, M.L., Rashid, M.M., Jacobs, C.R., 2002. A finite element model of the human knee joint for the study of tibio-femoral contact. J. Biomech. Eng. 124, 273–280. https://doi.org/10.1115/1.1470171

Dowling, J., 1997. The Use of Electromyography for the Noninvasive Prediction of Muscle

Forces. Sport. Med. 24, 82–96. https://doi.org/10.2165/00007256-199724020-00002

Drake, J.D.M., Callaghan, J.P., 2006. Elimination of electrocardiogram contamination from electromyogram signals: An evaluation of currently used removal techniques. J. Electromyogr. Kinesiol. 16, 175–187. https://doi.org/10.1016/j.jelekin.2005.07.003

Dul, J., Townsend, M., Shiavi, R., Johnson, G., 1984. Muscular synergism—I. On criteria for load sharing between synergistic muscles. J. Biomech. 17, 663–673.

Durandau, G., Farina, D., Sartori, M., 2018. Robust Real-Time Musculoskeletal Modeling Driven by Electromyograms. IEEE Trans. Biomed. Eng. 65, 556–564. https://doi.org/10.1109/TBME.2017.2704085

Ehrig, R.M., Taylor, W.R., Duda, G.N., Heller, M.O., 2007. A survey of formal methods for determining functional joint axes. J. Biomech. 40, 2150–2157. https://doi.org/10.1016/j.jbiomech.2006.10.026

Ehrig, R.M., Taylor, W.R., Duda, G.N., Heller, M.O., 2006. A survey of formal methods for determining the centre of rotation of ball joints. J. Biomech. 39, 2798–2809. https://doi.org/10.1016/j.jbiomech.2005.10.002

Erskine, R.M., Jones, D.A., Maffulli, N., Williams, A.G., Stewart, C.E., Degens, H., 2011. What causes in vivo muscle specific tension to increase following resistance training? Exp. Physiol. 96, 145–155. https://doi.org/10.1113/expphysiol.2010.053975

Erskine, R.M., Jones, D.A., Maganaris, C.N., Degens, H., 2009. In vivo specific tension of the human quadriceps femoris muscle. Eur. J. Appl. Physiol. 106, 827–838. https://doi.org/10.1007/s00421-009-1085-7

Felson, D.T., Nevitt, M.C., Zhang, Y., Aliabadi, P., Baumer, B., Gale, D., Li, W., Yu, W., Xu, L., 2002. High prevalence of lateral knee osteoarthritis in Beijing Chinese compared with Framingham Caucasian subjects. Arthritis Rheum. 46, 1217–1222. https://doi.org/10.1002/art.10293

Field, A., 2009. Discovering Statistics Using SPSS, 3rd ed. Sage, London.

Finni, T., Komi, P., Lepola, V., 2000. In vivo human triceps surae and quadriceps femoris muscle function in a squat jump and counter movement jump. Eur J Appl Physiol 416–426.

Fiorentino, N.M., Kutschke, M.J., Atkins, P.R., Foreman, K.B., Kapron, A.L., Anderson, A.E., 2016. Accuracy of Functional and Predictive Methods to Calculate the Hip Joint Center in Young Non-pathologic Asymptomatic Adults with Dual Fluoroscopy as a Reference Standard. Ann. Biomed. Eng. 44, 2168–2180. https://doi.org/10.1007/s10439-015-1522-1

Fiorentino, N.M., Lin, J.S., Ridder, K.B., Guttman, M. a, McVeigh, E.R., Blemker, S.S., 2013. Rectus femoris knee muscle moment arms measured in vivo during dynamic motion with real-time magnetic resonance imaging. J. Biomech. Eng. 135, 044501. https://doi.org/10.1115/1.4023523

Fisher, S.R., Markel, D.C., Koman, J.D., Atkinson, T.S., 2002. Pull-out and shear failure strengths of arthroscopic meniscal repair systems. Knee Surgery, Sport. Traumatol. Arthrosc. 10, 294–299. https://doi.org/10.1007/s00167-002-0295-x

Foran, J., Fischer, S., 2015. Total Knee Replacement [WWW Document]. OrhtoInfo - Your Connect. to Expert orthopeadic Inf. URL http://orthoinfo.aaos.org/topic.cfm?topic=A00389&webid=24DAE153 (accessed 9.18.15).

Fregly, B., Besier, T., Lloyd, D., Delp, S., Banks, S., Pandy, M., D'Lima, D., 2012. Grand challenge competition to predict in vivo knee loads. J. Orthop. Res. 30, 503–13. https://doi.org/10.1002/jor.22023

Fuglevand, A., Winter, D., Patla, A., Stashuk, D., 1992. Detection of motor unit action potentials with surface electrodes: influence of electrode size and spacing. Biol. Cybern. 67, 143–153.

Fukuda, Y., Takai, S., Yoshino, N., Murase, K., Tsutsumi, S., Ikeuchi, K., Hirasawa, Y., 2000. Impact load transmission of the knee joint-influence of leg alignment and the role of meniscus and articular cartilage. Clin. Biomech. 15, 516–521. https://doi.org/10.1016/S0268-0033(00)00013-9

Fukunaga, T., Roy, R.R., Shellock, F.G., Hodgson, J.A., Edgerton, V.R., 1996. Specific tension of human plantar flexors and dorsiflexors. J. Appl. Physiol. 80, 158–65. https://doi.org/10.1152/jappl.1996.80.1.158

Fung, Y., 1994. A First Course in Continuum Mechanics, 3rd ed. Prentice Hall, New Jersey.

Gallagher, S., Pollard, J., Porter, W.L., 2011. Electromyography of the thigh muscles during lifting tasks in kneeling and squatting postures. Ergonomics 54, 91–102. https://doi.org/10.1080/00140139.2010.535025

Gerus, P., Sartori, M., Besier, T.F., Fregly, B.J., Delp, S.L., Banks, S. a, Pandy, M.G., D'Lima, D.D., Lloyd, D.G., 2013. Subject-specific knee joint geometry improves predictions of medial tibiofemoral contact forces. J. Biomech. 46, 2778–86. https://doi.org/10.1016/j.jbiomech.2013.09.005

Gianotti, S.M., Marshall, S.W., Hume, P.A., Bunt, L., 2009. Incidence of anterior cruciate ligament injury and other knee ligament injuries: A national population-based study. J. Sci. Med. Sport 12, 622–627. https://doi.org/10.1016/j.jsams.2008.07.005

Guidelines for Modified Work, 2008. , Worksafe BC.

Guimaraes, A., Herzog, W., Hulliger, M., Zhang, Y., Day, S., 1994. EMG-force relationship of the cat soleus muscle studied with distributed and non-periodic stimulation of ventral root filaments. J. Exp. Biol. 186, 75–93.

Halloran, J.P., Clary, C.W., Maletsky, L.P., Taylor, M., Petrella, A.J., Rullkoetter, P.J., 2010. Verification of predicted knee replacement kinematics during simulated gait in the Kansas knee simulator. J. Biomech. Eng. 132, 081010. https://doi.org/10.1115/1.4001678

Hamner, S.R., Seth, A., Delp, S.L., 2010. Muscle contributions to propulsion and support during running. J. Biomech. 43, 2709–16. https://doi.org/10.1016/j.jbiomech.2010.06.025

Haut, R.C., 1989. Contact Pressures in the Patellofemoral Joint During Impact Loading on the Human Flexed Knee. J. Orthop. Res. 7, 272–280.

Hefzy, M.S., Kelly, B.P., Cooke, T.D., 1998. Kinematics of the knee joint in deep flexion: a radiographic assessment. Med. Eng. Phys. 20, 302–7.

Heiden, T., Lloyd, D., Ackland, T., 2009. Knee extension and flexion weakness in people with knee osteoarthritis: is antagonist cocontraction a factor? J. Orthop. Sports Phys. Ther. 39, 807–15. https://doi.org/10.2519/jospt.2009.3079

Heinlein, B., Graichen, F., Bender, A., Rohlmann, A., Bergmann, G., 2007. Design, calibration and pre-clinical testing of an instrumented tibial tray. J. Biomech. 40, 4–10. https://doi.org/10.1016/j.jbiomech.2007.02.014

Hemmerich, A., Brown, H., Smith, S., Marthandam, K., Wyss, U., 2006. Hip, Knee, and Ankle Kinematics of High Range of Motion Activities. J. Orthop. Res. 24, 770–781. https://doi.org/10.1002/jor.20114

Henneman, E., Somjen, G., Carpenter, D.O., 1965. EXCITABILITY AND INHIBITIBILITY OF MOTONEURONS OF DIFFERENT SIZES. J. Neurophysiol. 28, 599–620. https://doi.org/10.1152/jn.1965.28.3.599

Hermens, H., Freriks, B., Merletti, R., Rau, G., Disselhorst-Klug-Aachen, C., Stegeman, D., Haag, G., Hermens, H., Freriks, B., 2005. The SENIAM Project [WWW Document]. SENIAM Proj. URL http://www.seniam.org/

Herzog, W., Read, L.J., 1993. Lines of action and moment arms of the major force-carrying structures crossing the human knee joint. J. Anat. 182 (Pt 2, 213–30.

Heyse, T.J., El-Zayat, B.F., De Corte, R., Scheys, L., Chevalier, Y., Fuchs-Winkelmann, S., Labey, L., 2014. Biomechanics of medial unicondylar in combination with patellofemoral knee arthroplasty. Knee 21, S3–S9. https://doi.org/10.1016/S0968-0160(14)50002-6

Hicks, J.L., Uchida, T.K., Seth, a, Rajagopal, a, Delp, S., 2014. Is my model good enough? Best practices for verification and validation of musculoskeletal models and simulations of human movement. J. Biomech. Eng. 137. https://doi.org/10.1115/1.4029304

Hirokawa, S., Fukunaga, M., 2013. Knee Joint Forces When Rising from Kneeling Positions. J. Biomech. Sci. Eng. 8, 27–39. https://doi.org/10.1299/jbse.8.27

Hodges, P.W., Bui, B.H., 1996. A comparison of computer-based methods for the determination of onset of muscle contraction using electromyography. Electroencephalogr. Clin.

Neurophysiol. 101, 511–519. https://doi.org/10.1016/S0921-884X(96)95190-5

Hof, A., 1992. An explicit expression for the moment in multibody systems. J. Biomech. 25, 1209–1211.

Hofer, J., Gejo, R., McGarry, M., Lee, T., 2012. Effects of kneeling on tibiofemoral contact pressure and area in posterior cruciate-retaining and posterior cruciate-sacrificing total knee arthroplasty. J. Arthroplasty 27, 620–4. https://doi.org/10.1016/j.arth.2011.07.011

Horsman, K., Koopman, H., van der Helm, F., Prosé, L.P., Veeger, H., 2007. Morphological muscle and joint parameters for musculoskeletal modelling of the lower extremity. Clin. Biomech. 22, 239–247. https://doi.org/10.1016/j.clinbiomech.2006.10.003

Hoshino, A., Wallace, W., 1987. impact-absortbing properties of the human knee. Br. Editor. Soc. Bone Jt. Surg. 69, 807–811.

Howard, R.M., Conway, R., Harrison, A.J., 2015. An Exploration of Eliminating Cross-Talk in Surface Electromyography using Independent Component Analysis, in: Signals and Systems Conference. IEEE, Carlow, Ireland, pp. 2–7. https://doi.org/10.1109/ISSC.2015.7163754

Hubley-Kozey, C.L., Robbins, S.M., Rutherford, D.J., Stanish, W.D., 2013. Reliability of surface electromyographic recordings during walking in individuals with knee osteoarthritis. J. Electromyogr. Kinesiol. 23, 334–341. https://doi.org/10.1016/j.jelekin.2012.12.002

Huijing, P.A., Baan, G.C., 2001. Myofascial Force Transmission Causes Interaction between Adjacent Muscles and Connective Tissue: Effects of Blunt Dissection and Compartmental Fasciotomy on Length Force Characteristics of Rat Extensor Digitorum Longus Muscle.

Arch. Physiol. Biochem. 109, 97–109. https://doi.org/10.1076/apab.109.2.97.4269

IBM, C., 1969. IBM Data Processing Techniques - Flowcharting Techniques. https://doi.org/http://dx.doi.org/10.1016/B0-12-227240-4/00071-X

Im, G.I., Kim, J.Y., 2010. Radiological joint space width in the clinically normal hips of a Korean population. Osteoarthr. Cartil. 18, 61–64. https://doi.org/10.1016/j.joca.2009.08.001

International Society for the Advancement of Kinanthropometry, 2001. International Standards for Anthropometric Assessment. The international society for the advancement of kinanthropometry, Underdale, AUS.

Iwaki, H., Pinskerova, V., Freeman, M.A.R., 2000. Tibiofemoral movement 1: the shapes and relative movements of the femur and tibia in the unloaded cadaver knee. J. Bone Jt. Surg. 82, 1189–1195. https://doi.org/10.1302/0301-620X.82B8.10717

Jacobson, W.C., Gabel, R.H., Brand, R.A., 1995. Surface vs. fine-wire electrode ensemble-averaged signals during gait. J. Electromyogr. Kinesiol. 5, 37–44. https://doi.org/10.1016/S1050-6411(99)80004-2

Jain, S., Pathak, A.C., Kanniyan, K., Kulkarni, S., Tawar, S., Mane, P., 2013. High-Flexion Posterior-Stabilized Total Knee Prosthesis: Is It Worth the Hype? Knee Surg. Relat. Res. 25, 100–105. https://doi.org/10.5792/ksrr.2013.25.3.100

Jia, B., Kim, S., Nussbaum, M. a., 2011. An EMG-based model to estimate lumbar muscle forces and spinal loads during complex, high-effort tasks: Development and application to residential construction using prefabricated walls. Int. J. Ind. Ergon. 41, 437–446. https://doi.org/10.1016/j.ergon.2011.03.004

Johal, P., Williams, a., Wragg, P., Hunt, D., Gedroyc, W., 2005. Tibio-femoral movement in the living knee. A study of weight bearing and non-weight bearing knee kinematics using “interventional” MRI. J. Biomech. 38, 269–276. https://doi.org/10.1016/j.jbiomech.2004.02.008

Kamavuako, E.N., Rosenvang, J.C., Horup, R., Jensen, W., Farina, D., Englehart, K.B., 2013. Surface versus untargeted intramuscular EMG based classification of simultaneous and dynamically changing movements. IEEE Trans. Neural Syst. Rehabil. Eng. 21, 992–998. https://doi.org/10.1109/TNSRE.2013.2248750

Kashimoto, T., Friedenberg, Z.B., 1977. A study of radiographic variations of the hip joint. Acta Orthop. 48, 487–493. https://doi.org/10.3109/17453677708989736

Keller, T.S., 1994. Predicting the compressive mechanical behavior of bone. J. Biomech. 27, 1159–1168. https://doi.org/10.1016/0021-9290(94)90056-6

Kellgren, J.H., Lawrence, J.S., 1957. Radiological Assessment of Osteo-Arthrosis. Ann. Rheum. Dis. 16, 494–502. https://doi.org/10.1136/ard.16.4.494

Kim, W., Thambyah, A., Broom, N., 2012. Does prior sustained compression make cartilage-on-bone more vulnerable to trauma? Clin. Biomech. 27, 637–645. https://doi.org/10.1016/j.clinbiomech.2012.03.007

Kingston, D., Acker, S., 2018a. Thigh-calf contact parameters for six high knee flexion postures: Onset, maximum angle, total force, contact area, and center of force. J. Biomech. 67, 46–54.

Kingston, D., Acker, S., 2018b. Representing fine-wire EMG with surface EMG in three thigh muscles during high knee flexion movements. J. Electromyogr. Kinesiol. 43, 55–61.

https://doi.org/10.1016/j.jelekin.2018.08.006

Kingston, D.C., Tennant, L.M., Chong, H.C., Acker, S.M., 2017. Lower Limb Muscular Activation During Transitions to Symmetric High Knee Flexion Postures in Young Females. IISE Trans. Occup. Ergon. Hum. Factors 5, 82–91. https://doi.org/10.1080/24725838.2017.1326988

Kingston, D.C., Tennant, L.M., Chong, H.C., Acker, S.M., 2016. Peak activation of lower limb musculature during high flexion kneeling and transitional movements. Ergonomics 59, 1215–1223. https://doi.org/10.1080/00140139.2015.1130861

Kinney, A.L., Besier, T.F., Silder, A., Delp, S.L., D'Lima, D.D., Fregly, B.J., 2013. Changes in in vivo knee contact forces through gait modification. J. Orthop. Res. 31, 434–40. https://doi.org/10.1002/jor.22240

Kirkeshov Jensen, L., 2008. Knee osteoarthritis: influence of work involving heavy lifting, kneeling, climbing stairs or ladders, or kneeling/squatting combined with heavy lifting. Occup. Environ. Med. 65, 72–89. https://doi.org/10.1136/oem.2007.032466

Knight, L. a, Pal, S., Coleman, J.C., Bronson, F., Haider, H., Levine, D.L., Taylor, M., Rullkoetter, P.J., 2007. Comparison of long-term numerical and experimental total knee replacement wear during simulated gait loading. J. Biomech. 40, 1550–8. https://doi.org/10.1016/j.jbiomech.2006.07.027

Knutson, L.M., Soderberg, G.L., Ballantyne, B.T., Clarke, W.R., 1994. A Study of Various Normalization Procedures Day Electromyographic Data for Within day electromyographic data. J. Electromyogr. Kinesiol. 4, 47–59.

Kobayashi, K., Hosseini, A., Sakamoto, M., Qi, W., Rubash, H., Li, G., 2013. In vivo kinematics of the extensor mechanism of the knee during deep flexion. J. Biomech. Eng. 135, 81002. https://doi.org/10.1115/1.4024284

Krivickas, L.S., Feinberg, J.H., 1996. Lower extremity injuries in college athletes: Relation between ligamentous laxity and lower extremity muscle tightness. Arch. Phys. Med. Rehabil. 77, 1139–1143. https://doi.org/10.1016/S0003-9993(96)90137-9

Kurosaka, M., Yoshiya, S., Mizuno, K., Yamamoto, T., 2002. Maximizing flexion after total knee arthroplasty: the need and the pitfalls. J. Arthroplasty 17, 59–62. https://doi.org/10.1054/arth.2002.32688

Kutzner, I., Heinlein, B., Graichen, F., Bender, A., Rohlmann, A., Halder, A., Beier, A., Bergmann, G., 2010. Loading of the knee joint during activities of daily living measured in vivo in five subjects. J. Biomech. 43, 2164–2173. https://doi.org/10.1016/j.jbiomech.2010.03.046

Legendre, P., Legendre, L., 1998. Numerical Ecology, Volume 24, 2nd ed, Developments in Environmental Modelling. Elsevier B.V., Amsterdam. https://doi.org/10.1017/CBO9781107415324.004

Lehman, G., McGill, S., 1999. The Importance of Normalization in the Interpretation of Surface Electromyography: A Proof of Principal. J. Manip. Physiol. Ther. 22, 444–446.

Lequesne, M., Malghem, J., Dion, E., 2004. The normal hip joint space: Variations in width, shape, and architecture on 223 pelvic radiographs. Ann. Rheum. Dis. 63, 1145–1151. https://doi.org/10.1136/ard.2003.018424

Lloyd, D.G., Besier, T.F., 2003. An EMG-driven musculoskeletal model to estimate muscle forces and knee joint moments in vivo. J. Biomech. 36, 765–776. https://doi.org/10.1016/S0021-9290(03)00010-1

Longpré, H., Potvin, J., Maly, M., 2013. Biomechanical changes at the knee after lower limb fatigue in healthy young women. Clin. Biomech. 28, 441–7. https://doi.org/10.1016/j.clinbiomech.2013.02.010

Manal, K., Buchanan, T.S., 2013. An electromyogram-driven musculoskeletal model of the knee to predict in vivo joint contact forces during normal and novel gait patterns. J. Biomech. Eng. 135, 021014. https://doi.org/10.1115/1.4023457

Marsh, M., Souza, R.B., Wyman, B.T., Hellio Le Graverand, M.P., Subburaj, K., Link, T.M., Majumdar, S., 2013. Differences between X-ray and MRI-determined knee cartilage thickness in weight-bearing and non-weight-bearing conditions. Osteoarthr. Cartil. 21, 1876–1885. https://doi.org/10.1016/j.joca.2013.09.006

Martelli, S., Calvetti, D., Somersalo, E., Viceconti, M., 2015. Stochastic modelling of muscle recruitment during activity. Interface Focus 5, 20140094–20140094. https://doi.org/10.1098/rsfs.2014.0094

McGill, S., Juker, D., Kropf, P., 1996. Appropriately placed surface EMG electrodes reflect deep muscle activity (psoas, quadratus lumborum, abdominal wall) in the lumbar spine. J. Biomech. 29, 1503–1507. https://doi.org/10.1016/0021-9290(96)84547-7

Mclean, S.G., Mallett, K.F., Arruda, E.M., 2015. Deconstructing the Anterior Cruciate Ligament : What We Know and Do Not Know About Function , Material Properties , and Injury Mechanics. J. Biomech. Eng. 137, 1–19. https://doi.org/10.1115/1.4029278

Millard, M., Uchida, T., Seth, A., Delp, S.L., 2013. Flexing computational muscle: modeling and simulation of musculotendon dynamics. J. Biomech. Eng. 135, 021005. https://doi.org/10.1115/1.4023390

Miller, R.H., Gillette, J.C., Derrick, T.R., Caldwell, G.E., 2009. Muscle forces during running predicted by gradient-based and random search static optimisation algorithms. Comput. Methods Biomech. Biomed. Engin. 12, 217–225. https://doi.org/10.1080/10255840802430579

Mithoefer, K., McAdams, T., Williams, R.J., Kreuz, P.C., Mandelbaum, B.R., 2009. Clinical efficacy of the microfracture technique for articular cartilage repair in the knee: an evidence-based systematic analysis. Am. J. Sports Med. 37, 2053–63. https://doi.org/10.1177/0363546508328414

Modenese, L., Ceseracciu, E., Reggiani, M., Lloyd, D.G., 2016. Estimation of musculotendon parameters for scaled and subject specific musculoskeletal models using an optimization technique. J. Biomech. 49, 141–148. https://doi.org/10.1016/j.jbiomech.2015.11.006

Modenese, L., Phillips, A.T.M., Bull, A.M.J., 2011. An open source lower limb model: Hip joint validation. J. Biomech. 44, 2185–2193. https://doi.org/10.1016/j.jbiomech.2011.06.019

Mohammadi, Y., Arjmand, N., Shirazi-Adl, A., 2015. Comparison of trunk muscle forces, spinal loads and stability estimated by one stability- and three EMG-assisted optimization approaches. Med. Eng. Phys. 37, 792–800. https://doi.org/10.1016/j.medengphy.2015.05.018

Monaco, V., Coscia, M., Micera, S., 2011. Cost function tuning improves muscle force estimation computed by static optimization during walking. Conf. Proc. ... Annu. Int. Conf.

IEEE Eng. Med. Biol. Soc. IEEE Eng. Med. Biol. Soc. Annu. Conf. 2011, 8263–6. https://doi.org/10.1109/IEMBS.2011.6092037

Montgomery, W.H., Pink, M., Perry, J., 1994. Electromyographic analysis of hip and knee musculature during running. Am. J. Sports Med. 22, 272–278. https://doi.org/10.1177/036354659402200220

Moroni, L., Lambers, F., Wilson, W., van Donkelaar, C., de Wijn, J., Huiskes, R., van Blitterswijk, C., 2007. Finite element analysis of meniscal anatomical 3D scaffolds: Implications for tissue engineering. Open Biomed. Eng. J. 1, 23–34.

Mündermann, A., Dyrby, C.O., D'Lima, D.D., Colwell, C.W., Andriacchi, T.P., 2008. In vivo knee loading characteristics during activities of daily living as measured by an instrumented total knee replacement. J. Orthop. Res. 26, 1167–72. https://doi.org/10.1002/jor.20655

Nagura, T., Matsumoto, H., Kiriyama, Y., Chaudhari, A., Andriacchi, T., 2006. Tibiofemoral joint contact force in deep knee flexion and its consideration in knee osteoarthritis and joint replacement. J. Appl. Biomech. 22, 305–13.

Nakagawa, S., Kadoya, Y., Todo, S., Kobayashi, A., Sakamoto, H., Freeman, M. a, Yamano, Y., 2000. Tibiofemoral movement 3: full flexion in the living knee studied by MRI. J. bone Jt. Surg. 82, 1199–1200. https://doi.org/10.1302/0301-620X.82B8.10718

Neptune, R.R., 1999. Optimization algorithm performance in determining optimal controls in human movement analyses. J. Biomech. Eng. 121, 249–252. https://doi.org/10.1115/1.2835111

Nicolopoulos, C.., Anderson, E.., Solomonidis, S.., Giannoudis, P.., 2000. Evaluation of the gait analysis FSCAN pressure system: clinical tool or toy? Foot 10, 124–130. https://doi.org/10.1054/foot.1999.0536

Nielsen, S., Guo, Z., Johnson, C.M., Hensrud, D.D., Jensen, M.D., 2004. Splanchnic lipolysis in human obesity. J. Clin. Invest. 113, 1582–1588. https://doi.org/10.1172/JCI200421047

Nussbaum, M. a., Chaffin, D.B., 1998. Lumbar muscle force estimation using a subject-invariant 5-parameter EMG-based model. J. Biomech. 31, 667–672. https://doi.org/10.1016/S0021-9290(98)00055-4

O'Brien, T.D., Reeves, N.D., Baltzopoulos, V., Jones, D.A., Maganaris, C.N., 2010. In vivo measurements of muscle specific tension in adults and children. Exp. Physiol. 95, 202–210. https://doi.org/10.1113/expphysiol.2009.048967

Orsi, A.D., Chakravarthy, S., Canavan, P.K., Peña, E., Goebel, R., Vaziri, A., Nayeb-Hashemi, H., 2016. The effects of knee joint kinematics on anterior cruciate ligament injury and articular cartilage damage. Comput. Methods Biomech. Biomed. Engin. 19, 493–506. https://doi.org/10.1080/10255842.2015.1043626

Pandy, M.G., 1999. Moment arm of a muscle force. Exerc. Sport Sci. Rev. https://doi.org/10.1249/00003677-199900270-00006

Perotto, A., 2011. Anatomical Guide for the Electromyographer: The Limbs and Trunk, 5th ed. Charels C. Thomas, Springfeild, Il.

Persson, F., Turkiewicz, A., Bergkvist, D., Neuman, P., Englund, M., 2017. The risk of symptomatic knee osteoarthritis after arthroscopic meniscus repair vs partial meniscectomy vs the general population. Osteoarthr. Cartil. 26, 195–201.

https://doi.org/10.1016/j.joca.2017.08.020

Peters, A.E., Akhtar, R., Comerford, E.J., Bates, K.T., 2018. The effect of ageing and osteoarthritis on the mechanical properties of cartilage and bone in the human knee joint. Sci. Rep. 8, 1–13. https://doi.org/10.1038/s41598-018-24258-6

Plamondon, A., Gagnon, M., Desjardins, P., 1996. Validation of two 3-D segment models to calculate the net reaction forces and moments at the L(5)/S(1) joint in lifting. Clin. Biomech. 11, 101–110.

Pollard, J.P., Porter, W.L., Redfern, M.S., 2011. Forces and moments on the knee during kneeling and squatting. J. Appl. Biomech. 27, 233–41.

Powell, P.L., Roy, R.R., Kanim, P., Bello, M. a, Edgerton, V.R., 1984. Predictability of skeletal muscle tension from architectural determinations in guinea pig hindlimbs. J. Appl. Physiol. 57, 1715–1721. https://doi.org/10.1152/jappl.1984.57.6.1715

Power, M.L., Schulkin, J., 2008. Sex differences in fat storage, fat metabolism, and the health risks from obesity: possible evolutionary origins. Br. J. Nutr. 99, 931–940. https://doi.org/10.1017/S0007114507853347

Proffen, B.L., McElfresh, M., Fleming, B.C., Murray, M.M., 2012. A comparative anatomical study of the human knee and six animal species. Knee 19, 493–9. https://doi.org/10.1016/j.knee.2011.07.005

Ratzlaff, C., Van Wyngaarden, C., Duryea, J., 2014. Location-specific hip joint space width for progression of hip osteoarthritis - Data from the Osteoarthritis Initiative. Osteoarthr. Cartil. 22, 1481–1487. https://doi.org/10.1016/j.joca.2014.05.017

Rutherford, D.J., Hubley-Kozey, C.L., Stanish, W.D., 2011. Maximal voluntary isometric contraction exercises: A methodological investigation in moderate knee osteoarthritis. J. Electromyogr. Kinesiol. 21, 154–160. https://doi.org/10.1016/j.jelekin.2010.09.004

Rytter, S., Egund, N., Jensen, L.K., Bonde, J.P., 2009. Occupational kneeling and radiographic tibiofemoral and patellofemoral osteoarthritis. J. Occup. Med. Toxicol. 4, 19. https://doi.org/10.1186/1745-6673-4-19

Saito, A., Watanabe, K., Akima, H., 2015. Coordination among thigh muscles including the vastus intermedius and adductor magnus at different cycling intensities. Hum. Mov. Sci. 40, 14–23. https://doi.org/10.1016/j.humov.2014.11.010

Sancheti, K., Sancheti, P., Shyam, A., Joshi, R., Patil, K., Jain, A., 2013. Factors affecting range of motion in total knee arthroplasty using high flexion prosthesis: A prospective study. Indian J. Orthop. 47, 50–6. https://doi.org/10.4103/0019-5413.106901

Sandholm, A., Schwartz, C., Pronost, N., De Zee, M., Voigt, M., Thalmann, D., 2011. Evaluation of a geometry-based knee joint compared to a planar knee joint. Vis. Comput. 27, 161–171. https://doi.org/10.1007/s00371-010-0538-7

Sangeux, M., Barré, A., Aminian, K., 2017. Evaluation of knee functional calibration with and without the effect of soft tissue artefact. J. Biomech. 62, 53–59. https://doi.org/10.1016/j.jbiomech.2016.10.049

Sartori, M., Farina, D., Lloyd, D.G., 2014. Hybrid neuromusculoskeletal modeling to best track joint moments using a balance between muscle excitations derived from electromyograms and optimization. J. Biomech. 47, 3613–3621. https://doi.org/10.1016/j.jbiomech.2014.10.009

Sartori, M., Gizzi, L., Lloyd, D.G., Farina, D., 2013. A musculoskeletal model of human locomotion driven by a low dimensional set of impulsive excitation primitives. Front. Comput. Neurosci. 7, 79. https://doi.org/10.3389/fncom.2013.00079

Sasazaki, Y., Shore, R., Seedhom, B.B., 2006. Deformation and failure of cartilage in the tensile mode. J. Anat. 208, 681–694. https://doi.org/10.1111/j.1469-7580.2006.00569.x

Schatzmann, L., Brunner, P., Stäubli, H., 1998. Effect of cyclic preconditioning on the tensile properties of human quadriceps tendons and patellar ligaments. Knee surgery, Sport. Traumatol. Arthrosc. 6 Suppl 1, S56–S61. https://doi.org/10.1007/s001670050224

Schwartz, M., Rozumalski, A., 2005. A new method for estimating joint parameters from motion data. J. Biomech. 38, 107–116. https://doi.org/10.1016/j.jbiomech.2004.03.009

Seedhom, B.B., 2006. Conditioning of cartilage during normal activities is an important factor in the development of osteoarthritis. Rheumatology 45, 146–149. https://doi.org/10.1093/rheumatology/kei197

Shalhoub, S., 2012. The Effects of Variable Quadriceps and Hamstring Loading Configurations on Knee Joint Kinematics During In Vitro Testing By Sami Shalhoub. University of Kansas.

Shalhoub, S., Maletsky, L.P., 2014. Variation in patellofemoral kinematics due to changes in quadriceps loading configuration during in vitro testing. J. Biomech. 47, 130–136. https://doi.org/10.1016/j.jbiomech.2013.09.019

Sharif Shourijeh, M., 2013. Optimal Control and Multibody Dynamic Modelling of Human Musculoskeletal Systems. University of Waterloo.

Shrout, P.E., Fleiss, J.L., 1979. Intraclass correlations: Uses in assessing rater reliability. Psychol. Bull. 86, 420–428. https://doi.org/10.1037/0033-2909.86.2.420

Shull, P.B., Shultz, R., Silder, A., Dragoo, J.L., Besier, T.F., Cutkosky, M.R., Delp, S.L., 2013. Toe-in gait reduces the first peak knee adduction moment in patients with medial compartment knee osteoarthritis. J. Biomech. 46, 122–8. https://doi.org/10.1016/j.jbiomech.2012.10.019

Shultz, S., Perrin, D., Adams, M., 2001. Neuromuscular response characteristics in men and women after knee perturbation in a single-leg, weight-bearing stance. J. Athl. Train. 36, 37–43.

Smith, J., Barrett, G., 2001. Medial and lateral meniscal tear patterns in anterior cruciate ligament-deficient knees: a prospective analysis of 575 tears. Am. J. Sports Med. 29, 415–419.

Spoor, C., Leeuwen, J. Van, 1992. Knee muscle moment arms from MRI and from tendon travel. J. Biomech. 25, 201–206.

Steinbrück, A., Schröder, C., Woiczinski, M., Fottner, A., Müller, P.E., Jansson, V., 2013. Patellofemoral contact patterns before and after total knee arthroplasty: an in vitro measurement. Biomed. Eng. Online 12, 58. https://doi.org/10.1186/1475-925X-12-58

Steyerberg, E.W., Eijkemans, M.J., Harrell Jr., F.E., Habbema, J.D., 2001. Prognostic modeling with logistic regression analysis: in search of a sensible strategy in small data sets. Med.Decis.Making 21, 45–56. https://doi.org/10.1177/0272989X0102100106

Streiner, D.L., 1994. Regression in the service of the superego: The do’s and don’ts of stepwise multiple regression. Can. J. Psychiatry 39, 191–196.

Stylianou, A.P., Guess, T.M., Kia, M., 2013. Multibody muscle driven model of an instrumented prosthetic knee during squat and toe rise motions. J. Biomech. Eng. 135, 041008. https://doi.org/10.1115/1.4023982

Swann, A.C., Seedhom, B.B., 1993. The stiffness of normal articular cartilage and the predominant acting stress levels: Implications for the aetiology of osteoarthrosis. Rheumatology 32, 16–25. https://doi.org/10.1093/rheumatology/32.1.16

Taylor, W.R., Schütz, P., Bergmann, G., List, R., Postolka, B., Hitz, M., Dymke, J., Damm, P., Duda, G., Gerber, H., Schwachmeyer, V., Hosseini Nasab, S.H., Trepczynski, A., Kutzner, I., 2017. A comprehensive assessment of the musculoskeletal system: The CAMS-Knee data set. J. Biomech. 65, 32–39. https://doi.org/10.1016/j.jbiomech.2017.09.022

Tennant, L., Maly, M., Callaghan, J., Acker, S., 2014. Analysis of muscle activation patterns during transitions into and out of high knee flexion postures. J. Electromyogr. Kinesiol. 24, 711–717. https://doi.org/10.1016/j.jelekin.2014.06.011

Thambyah, A., 2008. How critical are the tibiofemoral joint reaction forces during frequent squatting in Asian populations? Knee 15, 286–294. https://doi.org/10.1016/j.knee.2008.04.006

Thambyah, A., Fernandez, J., 2014. Squatting-related tibiofemoral shear reaction forces and a biomechanical rationale for femoral component loosening. Sci. World J. 2014. https://doi.org/10.1155/2014/785175

Thambyah, A., Goh, J.C.H., De, S. Das, 2005. Contact stresses in the knee joint in deep flexion.

Med. Eng. Phys. 27, 329–35. https://doi.org/10.1016/j.medengphy.2004.09.002

Thompson, W.K., Gallo, C.A., Crentsil, L., Lewandowski, B.E., Humphreys, B.T., Dewitt, J.K., Fincke, R.S., 2015. Digital Astronaut Project Biomechanical Models Biomechanical Modeling of Squat , Single-Leg Squat and Heel Raise Exercises on the Hybrid Ultimate Lifting Kit (HULK). Hampton, VA.

Thomsen, M.G., Husted, H., Otte, K.S., Holm, G., Troelsen, A., 2013. Do patients care about higher flexion in total knee arthroplasty? A randomized, controlled, double-blinded trial. BMC Musculoskelet. Disord. 14, 4–9. https://doi.org/10.1186/1471-2474-14-127

Thun, M., Tanaka, S., Smith, a B., Halperin, W.E., Lee, S.T., Luggen, M.E., Hess, E. V, 1987. Morbidity from repetitive knee trauma in carpet and floor layers. Br. J. Ind. Med. 44, 611–620. https://doi.org/10.1136/oem.44.9.611

Tomatsu, T., 1992. Experimentally Produced Fractures of Articular Cartilage and Bone. The Effects of Shear Forces on the Pig Knee. J Bone Jt. Surg. 74, 457–62.

Tsai, L.-C., Colletti, P.M., Powers, C.M., 2012. Magnetic resonance imaging-measured muscle parameters improved knee moment prediction of an EMG-driven model. Med. Sci. Sports Exerc. 44, 305–12. https://doi.org/10.1249/MSS.0b013e31822dfdb3

Tsaopoulos, D.E., Baltzopoulos, V., Maganaris, C.N., 2006. Human patellar tendon moment arm length: Measurement considerations and clinical implications for joint loading assessment. Clin. Biomech. 21, 657–667. https://doi.org/10.1016/j.clinbiomech.2006.02.009

Tsaopoulos, D.E., Baltzopoulos, V., Richards, P.J., Maganaris, C.N., 2007. In vivo changes in the human patellar tendon moment arm length with different modes and intensities of muscle contraction. J. Biomech. 40, 3325–3332. https://doi.org/10.1016/j.jbiomech.2007.05.005

Umeyama, S., 1991. Least-squares estimation of transformation parameters between two point patterns. IEEE Trans. Pattern Anal. Mach. Intell. https://doi.org/10.1109/34.88573

Van Haver, A., De Roo, K., Claessens, T., De Beule, M., Verdonk, P., De Baets, P., 2013. Pilot validation study on a quasi-static weight-bearing knee rig. Proc. Inst. Mech. Eng. Part H J. Eng. Med. 227, 229–233. https://doi.org/10.1177/0954411912472595

Verkerke, G.J., Hof, A.L., Zijlstra, W., Ament, W., Rakhorst, G., 2005. Determining the centre of pressure during walking and running using an instrumented treadmill. J. Biomech. 38, 1881–1885. https://doi.org/10.1016/j.jbiomech.2004.08.015

Verstraete, M. a., Victor, J., 2015. Possibilities and limitations of novel in-vitro knee simulator. J. Biomech. 48, 3377–3382. https://doi.org/10.1016/j.jbiomech.2015.06.007

Victor, J., Van Glabbeek, F., Vander Sloten, J., Parizel, P.M., Somville, J., Bellemans, J., 2009. An experimental model for kinematic analysis of the knee. J. bone Jt. Surg. 91 Suppl 6, 150–163. https://doi.org/10.2106/JBJS.I.00498

Wagner, D.W., Stepanyan, V., Shippen, J.M., Demers, M.S., Gibbons, R.S., Andrews, B.J., Creasey, G.H., Beaupre, G.S., 2013. Consistency among musculoskeletal models: caveat utilitor. Ann. Biomed. Eng. 41, 1787–99. https://doi.org/10.1007/s10439-013-0843-1

Walter, J., Kinney, A., Banks, S., D’Lima, D., Besier, T., Lloyd, D., Fregly, B., 2014. Muscle synergies may improve optimization prediction of knee contact forces during walking. J. Biomech. Eng. 136, 021031. https://doi.org/10.1115/1.4026428

Ward, S., Eng, C., Smallwood, L., Lieber, R., 2009. Are current measurements of lower extremity muscle architecture accurate? Clin. Orthop. Relat. Res. 467, 1074–82. https://doi.org/10.1007/s11999-008-0594-8

Weisstein, E., n.d. Point-Line Distance--3-Dimensional [WWW Document]. From MathWorld--A Wolfram Web Resour. URL http://mathworld.wolfram.com/Point-LineDistance3-Dimensional.html (accessed 11.5.18).

Whitney, A., Jayaraman, K., Dennis, J., Mansour, J., 2017. Scaffold-free cartilage subjected to frictional shear stress demonstrates damage by cracking and surface peeling. J. Tissue Eng. Regen. Med. 11, 412–424. https://doi.org/10.1002/term.1925

Wickiewicz, T.L., Roy, R.R., Powell, P.L., Perrine, J.J., Edgerton, V.R., 1984. Muscle architecture and force-velocity relationships in humans. J. Appl. Physiol. 57, 435–43.

Wilson, D.R., Apreleva, M. V., Eichler, M.J., Harrold, F.R., 2003. Accuracy and repeatability of a pressure measurement system in the patellofemoral joint. J. Biomech. 36, 1909–1915. https://doi.org/10.1016/S0021-9290(03)00105-2

Wilson, N., Sheehan, F., 2010. Dynamic in vivo quadriceps lines-of-action. J. Biomech. 43, 2106–2113. https://doi.org/10.1016/j.jbiomech.2010.04.002

Winby, C., Lloyd, D., Besier, T., Kirk, T., 2009. Muscle and external load contribution to knee joint contact loads during normal gait. J. Biomech. 42, 2294–300. https://doi.org/10.1016/j.jbiomech.2009.06.019

Winter, D., 2009. Biomoechanics and Motor Control of Human Movement, 4th ed. John Wiley & Sons, Inc., Hoboken.

Winter, D., Fuglevand, A., Archer, S., 1994. Crosstalk in surface electromyography: theoretical and practical estimates. J. Electromyogr. Kinesiol. 4, 15–26.

Wren, T., Patrick Do, K., Rethlefsen, S., Healy, B., 2006. Cross-correlation as a method for comparing dynamic electromyography signals during gait. J. Biomech. 39, 2714–2718. https://doi.org/10.1016/j.jbiomech.2005.09.006

Wu, G., Cavanagh, P., 1995. ISB recommendations for standardization in the reporting of kinematic data. J. Biomech. 28, 1257–1261.

Wu, X., Zhu, Y., 2001. A global optimization method for three-dimensional conformal radiotherapy treatment planning. Phys Med Biol 46, 107–119.

Wünschel, M., Leichtle, U., Obloh, C., Wülker, N., Müller, O., 2011. The effect of different quadriceps loading patterns on tibiofemoral joint kinematics and patellofemoral contact pressure during simulated partial weight-bearing knee flexion. Knee Surgery, Sport. Traumatol. Arthrosc. 19, 1099–1106. https://doi.org/10.1007/s00167-010-1359-y

Yamaguchi, G., Sawa, A., Moran, D., Fessler, M., Winters, J., 1990. A Survey of Human Musculotendon Actuator Paramters, Multiple Muscle Systems: Biomechanics and Movement Organization. Spinger-Verlag, New York.

Yang, Z., Wickwire, A.C., Debski, R.E., 2010. Development of a subject-specific model to predict the forces in the knee ligaments at high flexion angles. Med. Biol. Eng. Comput. 48, 1077–85. https://doi.org/10.1007/s11517-010-0653-7

Yao, J., Lancianese, S.L., Hovinga, K.R., Lee, J., Lerner, A.L., 2008. Magnetic resonance image analysis of meniscal translation and tibio-menisco-femoral contact in deep knee flexion. J.

Orthop. Res. 26, 673–84. https://doi.org/10.1002/jor.20553

Yao, W., Fuglevand, R., Enoka, R., 2000. Motor-unit synchronization increases EMG amplitude and decreases force steadiness of simulated contractions. J. Neurophysiol. 83, 441–52.

Zajac, F., Neptune, R., Kautz, S., 2003. Biomechanics and muscle coordination of human walking: part II: lessons from dynamical simulations and clinical implications. Gait Posture 17, 1–17.

Zatsiorsky, V., 2002. Kinetics of Human Motion. Human Kinetics, Windsor, ON.

Zatsiorsky, V.M.M., 1998. Kinematics of Human Motion. Human Kinetics, Windsor, ON. https://doi.org/99.1998/zatsiorsky.0880116765

Zavatsky, A., 1997. A kinematic-freedom analysis of a flexed-knee-stance testing rig. J. Biomech. 30, 277–80. https://doi.org/10.1016/S0021-9290(96)00142-X

Zelle, J., Barink, M., De Waal Malefijt, M., Verdonschot, N., 2009. Thigh-calf contact: Does it affect the loading of the knee in the high-flexion range? J. Biomech. 42, 587–593. https://doi.org/10.1016/j.jbiomech.2008.12.015

Zelle, J., Barink, M., Loeffen, R., De Waal Malefijt, M., Verdonschot, N., 2007. Thigh-calf contact force measurements in deep knee flexion. Clin. Biomech. 22, 821–826. https://doi.org/10.1016/j.clinbiomech.2007.03.009

Zhang, P., Su, M., Tanaka, S.M., Yokota, H., 2006. Knee loading stimulates cortical bone formation in murine femurs. BMC Musculoskelet. Disord. 7, 73. https://doi.org/10.1186/1471-2474-7-73

Zhao, D., Banks, S.A., D’Lima, D.D., Jr, C.W.C., Fregly, B.J., 2007. In Vivo Medial and Lateral

Tibial Loads during Dynamic and High Flexion Activities. J. Orthop. Res. 25, 593–602.

https://doi.org/10.1002/jor

Appendix A – Musculoskeletal Model Muscle Parameters

#	Muscle (part)	Element	Origin X (cm)	Origin Y (cm)	Origin Z (cm)	O. Seg	Insertion X (cm)	Insertion Y (cm)	Insertion Z (cm)	I. Seg	Fibre Length (cm ± SD)	Sarcomere Length (cm ± SD)	Pennation Angle (deg ± SD)	Muscle PCSA (cm^2)	Tendon PCSA (cm^2)
1	Adductor Brevis (proximal)	1	4.62	-1.3	-6.92	5	-1.85	-8.34	1.81	4	10.7 ± 0.6	3 ± 0.2	-	3.8	0
		2	5.07	-1.32	-7.12	5	-1.32	-9.52	1.92	4					
2	Adductor Brevis (mid)	1	4.57	-1.82	-7.61	5	-0.96	-10.75	1.99	4	11.7 ± 0.6	3 ± 0.2	-	3.5	0
		2	4.93	-1.84	-7.78	5	-0.68	-12.02	2.01	4					
3	Adductor Brevis (distal)	1	3.86	-2.57	-8.34	5	-0.39	-13.28	1.97	4	12.6 ± 0.6	3 ± 0.2	-	3.2	0
		2	4.09	-2.58	-8.45	5	0.02	-14.52	1.87	4					
4	Adductor Longus	1	5.25	-0.92	-6.64	5	1.54	-17.44	1.68	4	11.5 ± 0.5	2.9 ± 0.2	-	15.1	0
		2	5.44	-1.16	-6.89	5	1.84	-18.64	1.52	4					
		3	5.57	-1.37	-7.19	5	2.16	-19.86	1.44	4					
		4	5.63	-1.56	-7.51	5	2.49	-21.09	1.39	4					
		5	5.61	-1.73	-7.85	5	2.8	-22.31	1.29	4					
		6	5.5	-1.88	-8.2	5	3.07	-23.52	1.1	4					
5	Adductor Magnus (distal)	1	-2.1	-7.1	-4.85	5	5.66	-36.31	-2.54	2	9.7 ± 0.9	2.4 ± 0.3	-	26.5	0.11
		2	-1.51	-6.71	-5.57	5	5.66	-36.31	-2.54	2					
		3	0.21	-5.78	-7.03	5	5.66	-36.31	-2.54	2					
6	Adductor Magnus (mid)	1	-2.79	-6.9	-4.94	5	1.82	-19.92	1.43	4	8.6 ± 0.9	2.2 ± 0.2	-	22.1	0
		2	-2.5	-6.68	-4.53	5	1.82	-19.92	1.43	4					
		3	-2.12	-6.6	-5.53	5	2.65	-23.01	0.99	4					
		4	-1.87	-6.42	-5.18	5	2.65	-23.01	0.99	4					
		5	-1.25	-6.21	-6.24	5	3.41	-26.12	0.9	4					
		6	-1.06	-6.07	-5.98	5	3.41	-26.12	0.9	4					
7	Adductor Magnus (proximal)	1	1.86	-4.5	-7.74	5	0.03	-10.75	1.54	4	8.8 ± 0.8	2.2 ± 0.2	-	5	0
		2	0.39	-5.33	-6.76	5	0.55	-12.77	1.52	4					
		3	1.13	-4.92	-7.25	5	1.07	-14.8	1.5	4					
		4	1.86	-4.5	-7.74	5	1.58	-16.82	1.48	4					
8	Biceps Femoris Longus	1	-3.78	-6.09	-1.71	5	1.63	-45.15	4.62	2	7.1 ± 0.3	2.3 ± 0.2	29.9 ± 3.5	27.2	0.51
9	Biceps Femoris Brevis	1	0.58	-19.35	1.77	4	1.63	-45.15	4.62	2	11.2 ± 0.4	3.3 ± 0.3	-	11.8	0.51
		2	1.81	-23.83	1.34	4	1.63	-45.15	4.62	2					
		3	2.68	-28.65	1.6	4	1.63	-45.15	4.62	2					
10	Extensor Digitorum Longus	1	2.49	-51.38	3.75	2	17.36	-96.59	6.79	1	8.1 ± 1.2	3.7 ± 0.2	8.3 ± 2.6	5.4	0.12
		2	2.9	-47.38	4.5	2	17.36	-96.59	6.79	1					
		3	3.39	-44.82	5.18	2	17.36	-96.59	6.79	1					
11	Extensor Hallucis Longus	1	4.12	-66.43	3.48	2	21.52	-93.48	4.97	1	7.3 ± 0.3	3.3 ± 0.2	14.4 ± 3.3	6.1	0.08
		2	3.45	-61.01	3.27	2	21.52	-93.48	4.97	1					
		3	2.89	-55.52	3.48	2	21.52	-93.48	4.97	1					
12	Flexor Digitorum Longus	1	6.4	-54.9	0.81	2	17.58	-96.88	5.87	1	2.9 ± 0.5	2 ± 0.2	28.5 ± 7.4	6.6	0.09
		2	7.16	-60.18	0.93	2	17.58	-96.88	5.87	1					
		3	7.24	-64.27	1.11	2	17.58	-96.88	5.87	1					

13	Flexor Hallucis Longus	1	2.22	-58.59	2.83	2	22	-94.84	4.55	1	2.1 ± 0.3	2.2 ± 0.2	30.1 ± 5.2	31.1	0.2
		2	3.01	-63.93	2.81	2	22	-94.84	4.55	1					
		3	3.8	-69.41	2.81	2	22	-94.84	4.55	1					
14	Gastrocnemius Lateralis	1	3.43	-37.75	2.21	4	2.9	-81.98	-1.89	1	4.8 ± 0.3	2.3 ± 0.2	25.4 ± 1.6	24	1.06
15	Gastrocnemius Medialis	1	5.04	-36.71	-1.48	4	3.01	-82.21	-2.74	1	5.7 ± 0.3	2.6 ± 0.2	10.8 ± 3.2	43.8	1.06
16	Gluteus Maximus (superior)	1	-7.91	7.77	-1.57	5	-4.04	5.7	7.47	4	11.5 ± 1.7	2.6 ± 0.4	-	49.7	0
		2	-8.98	5.51	-3.46	5	-4.31	2.63	7.74	4					
		3	-9.64	2.73	-5.01	5	-4.73	-0.44	7.99	4					
		4	-9.13	8.91	-2.68	5	-2.4	5.45	7.74	4					
		5	-10.33	6.77	-4.69	5	-2.6	2.37	8.02	4					
		6	-10.94	3.94	-6.19	5	-3.09	-0.69	8.26	4					
17	Gluteus Maximus (inferior)	1	-10.74	-0.83	-7.52	5	-5.61	-7.16	4.07	4	14.1 ± 0.8	2.5 ± 0.3	-	22.5	0
		2	-9.87	-1.49	-7.31	5	-5.07	-8.47	3.75	4					
		3	-9.05	-2.56	-7.35	5	-3.66	-10.78	3.38	4					
		4	-10.25	-0.16	-6.86	5	-5.61	-7.16	4.07	4					
		5	-9.38	-0.82	-6.65	5	-5.07	-8.47	3.75	4					
		6	-8.65	-2	-6.8	5	-3.66	-10.78	3.38	4					
18	Gluteus Medius (anterior)	1	0.4	9.48	4.46	5	-3.03	-0.25	5.9	4	4.5 ± 0.3	3.2 ± 0.2	-	37.9	0
		2	1.43	9.03	4.56	5	-2.25	-0.44	6.19	4					
		3	2.49	8.19	4.26	5	-1.53	-0.54	6.42	4					
		4	0.93	9.95	5.22	5	-3.36	-1.09	6.2	4					
		5	1.8	9.36	5.09	5	-2.68	-1.5	6.56	4					
		6	2.81	8.47	4.72	5	-1.96	-1.6	6.79	4					
19	Gluteus Medius (inferior)	1	-3.88	11.87	2.51	5	-3.85	0.88	4.5	4	4.2 ± 0.3	2.5 ± 0.4	15.9 ± 3.1	60.8	1.92
		2	-6.02	10.15	-0.41	5	-4.01	0.86	3.97	4					
		3	-6.82	7.21	-2.31	5	-4.24	0.76	3.62	4					
		4	-4.81	13.46	2.07	5	-3.85	0.88	4.5	4					
		5	-7.34	12.41	-1.03	5	-4.51	0.39	4.66	4					
		6	-8.41	9.93	-3.06	5	-4.76	0.26	4.34	4					
20	Gluteus Minimus (lateral)	1	-0.08	7.89	3.31	5	-1.5	-2.27	6.16	4	3.5 ± 0.2	3.4 ± 0.3	-	10	0.1
21	Gluteus Minimus (medial)	1	-2.26	7.55	1.73	5	-1.5	-2.27	6.16	4	3.5 ± 0.2	2.8 ± 0.1	-	8.1	0.1
22	Gluteus Minimus (mid)	1	-4.03	6.51	0.07	5	-1.5	-2.27	6.16	4	3.5 ± 0.2	2.6 ± 0.2	-	7.4	0.1
23	Gracilis	1	1.65	-4.88	-7.39	5	7.7	-48.16	0.27	2	21.2 ± 4.7	3.2 ± 0.2	-	4.9	0.05
		2	3.67	-3.46	-7.98	5	7.7	-48.16	0.27	2					
24	Iliacus (lateral)	1	-2.95	13.23	2.75	5	-2.34	-5.12	0.37	4	13 ± 0.4	3.4 ± 0.2	26.5 ± 0	6.6	0.21
		2	-1.13	11.48	2.92	5	-2.34	-5.12	0.37	4					
		3	-0.34	10.01	2.78	5	-2.34	-5.12	0.37	4					
25	Iliacus (mid)	1	-5.58	13.54	0.03	5	-2.34	-5.12	0.37	4	6.6 ± 0.6	3.4 ± 0.2	-	13	0.07
		2	-4.32	11.03	-0.21	5	-2.34	-5.12	0.37	4					
		3	-3.08	8.61	-0.38	5	-2.34	-5.12	0.37	4					

26	Iliacus (medial)	1	-5.27	12.75	-3.9	5	-2.34	-5.12	0.37	4	10.3 ± 0.5	3.1 ± 0.2	-	7.6	0.48
		2	-4.67	10.77	-3.51	5	-2.34	-5.12	0.37	4					
		3	-3.68	8.13	-3.61	5	-2.34	-5.12	0.37	4					
27	Obturator Exturnus (inferior)	1	-0.04	-4.83	-6.75	5	-4.5	-5.54	2.77	4	7.1 ± 0.5	2.8 ± 0.3	-	5.5	0.1
		2	1.89	-3.95	-7.98	5	-4.5	-5.54	2.77	4					
28	Obturator Externus (superior)	1	3.88	-1.77	-8.02	5	-3.09	-1.18	2.56	4	2.8 ± 0.3	3.2 ± 0.3	-	24.6	
		2	2.11	-3.26	-7.72	5	-3.09	-1.18	2.56	4					
		3	-0.04	-4.33	-6.87	5	-3.09	-1.18	2.56	4					
29	Obturator Internus	1	-2.22	2.19	-4.19	5	-2.68	0.26	4	4	2 ± 0.2	2.6 ± 0.2	-	25.4	0.13
		2	-1.98	0.35	-4.92	5	-2.68	0.26	4	4					
		3	-0.93	-1.28	-5.9	5	-2.68	0.26	4	4					
30	Pectineus	1	3.47	1.38	-5.13	5	-1.82	-7.67	1.58	4	13.5 ± 0.3	3.2 ± 0.3	-	6.8	0
		2	3.97	1.03	-5.48	5	-1.66	-8.54	1.59	4					
		3	4.47	0.67	-5.83	5	-1.5	-9.41	1.6	4					
		4	4.97	0.32	-6.18	5	-1.82	-7.67	1.58	4					
31	Peroneus Brevis	1	2.59	-60.53	3.39	2	7.57	-89.43	3.62	1	3 ± 0.4	3 ± 0.2	23.1 ± 3.6	19	0.29
		2	3.16	-65.19	3.29	2	7.57	-89.43	3.62	1					
		3	3.78	-69.69	3.23	2	7.57	-89.43	3.62	1					
32	Peroneus Longus	1	1.67	-48.99	4.08	2	7.18	-87.15	3.54	1	3.6 ± 0.5	2.9 ± 0.2	15.8 ± 3.5	23.9	0.2
		2	1.9	-52.73	3.73	2	7.18	-87.15	3.54	1					
		3	2.16	-56.43	3.4	2	7.18	-87.15	3.54	1					
33	Peroneus Tertius	1	4.33	-68.61	3.55	2	11.08	-92.42	4.51	1	5.6 ± 0.3	3.6 ± 0.2	19.1 ± 3.8	6.2	0.05
		2	3.64	-63.48	3.51	2	11.08	-92.42	4.51	1					
		3	3.08	-58.34	3.49	2	11.08	-92.42	4.51	1					
34	Piriformis	1	-10.07	2.31	-7.42	5	-3.48	0.88	2.74	4	4 ± 0	2.8 ± 0.2	-	8.1	0.13
35	Plantaris	1	2.83	-38.59	3.73	4	4.51	-81.41	-2.33	1	5 ± 0.4	2.8 ± 0.1	-	2.4	0.13
36	Popliteus	1	2.74	-41.05	4.49	4	6.21	-51.18	0.37	2	2.8 ± 0.2	3.1 ± 0.2	-	10.7	0
		2	2.74	-41.05	4.49	4	4.91	-47.08	-0.08	2					
37	Psoas Minor	1	-5.06	25.28	-5.61	5	1.59	-1.79	-0.8	4	7.2 ± 0	3.3 ± 0.1	-	1.1	0
38	Psoas Major	1	-5.74	22.64	-5.56	5	-2.34	-5.12	0.37	4	11.9 ± 0.6	3.2 ± 0.2	13.4 ± 5.4	19.5	0.48
		2	-2.91	18.44	-5.96	5	-2.34	-5.12	0.37	4					
		3	-2.81	14.2	-5.88	5	-2.34	-5.12	0.37	4					
39	Quadratus Femoris	1	-0.9	-4.98	-6.3	5	-4.65	-2.43	2.81	4	2.9 ± 0.3	2.4 ± 0.3		14.6	0
		2	-1.54	-5.24	-5.5	5	-4.6	-3.22	2.87	4					
		3	-2.17	-5.5	-4.69	5	-4.54	-4.01	2.93	4					
		4	-2.8	-5.76	-3.89	5	-4.48	-4.8	2.99	4					
40	Rectus Femoris	1	3.02	4.27	2.03	5	9.46	-35.06	3.48	3	6.7 ± 0.3	2.3 ± 0.2	22 ± 3.3	28.9	2.79
		2	3.02	4.27	2.03	5	8.86	-35.03	4.48	3			-		
41	Sartorius (proximal)	1	3.2	7.49	3.5	5	7.94	-47.72	0.38	2	43.3 ± 0.6	3.4 ± 0.3	-	5.9	0.22
42	Satorius (distal)	1	3.2	7.49	3.5	5	7.94	-47.72	0.38	2	43.3 ± 0.6	3.4 ± 0.3	-	5.9	0.22
43	Semimembranosus	1	-2.8	-6.61	-2.03	5	4.12	-43.84	-2.97	2	7.1 ± 0.4	2.4 ± 0.3	25 ± 3.6	17.1	0.27
44	Semitendinosus	1	-4.03	-6.07	-2.78	5	7.22	-49.29	-0.24	2	15.7 ± 0.3	3 ± 0.1	-	14.7	0.13
45	Solius (medial)	1	1.85	-54.4	2.79	2	2.9	-81.98	-1.89	1	1.8 ± 0.2	2 ± 0.2	64.5 ± 10.1	94.3	10.6
		2	1.57	-51.72	2.92	2	2.9	-81.98	-1.89	1					
		3	0.97	-47.81	3.08	2	2.9	-81.98	-1.89	1					

46	Solius (lateral)	1	7.63	-58.1	0.81	2	4.18	-81.71	-2.71	1	1.9 ± 0.1	2 ± 0.2	58.7 ± 6.4	85.9	10.6
		2	7.21	-54.96	0.57	2	4.18	-81.71	-2.71	1					
		3	6.5	-52.52	0.27	2	4.18	-81.71	-2.71	1					
47	Tensor Faciae Latae	1	2.83	7.99	4.76	5	4.68	-38.51	5.4	2	11.5 ± 0.6	3.3 ± 0.3	-	8.8	0
		2	2.37	9.01	5.13	5	4.68	-38.51	5.4	2					
48	Tibialis Anterior	1	5.78	-46.65	4.26	2	14.55	-87.06	1.79	1	5.7 ± 0.3	3.4 ± 0.2	9.6 ± 1.8	26.6	3.1
		2	6.36	-49.36	3.89	2	14.55	-87.06	1.79	1					
		3	6.38	-54.64	2.94	2	14.55	-87.06	1.79	1					
49	Tibialis Posterior (medial)	1	5.04	-50.06	2.22	2	11.3	-83.54	1.54	1	1.9 ± 0.7	2.1 ± 0.2	25.2 ± 5.2	21.6	0
		2	5.51	-54.88	2.03	2	11.3	-83.54	1.54	1					
		3	6.12	-61.14	2.09	2	11.3	-83.54	1.54	1					
50	Tibialis Posterior (lateral)	1	2.91	-54.31	3.38	2	11.3	-83.54	1.54	1	1.9 ± 0.1	2 ± 0.2	58.7 ± 6.4	21.6	10.6
		2	3.74	-61.64	3.13	2	11.3	-83.54	1.54	1					
		3	4.64	-68.75	3.29	2	11.3	-83.54	1.54	1					
51	Vastus Intermedius	1	5.41	-22.86	2.55	4	9.46	-35.06	3.48	3	6.2 ± 0.5	2.2 ± 0.3	11.8 ± 0	38.1	2.79
		2	3.71	-17.44	2.95	4	9.46	-35.06	3.48	3					
		3	1.62	-11.67	3.74	4	9.46	-35.06	3.48	3					
		4	4.74	-23.17	3.53	4	8.86	-35.03	4.48	3					
		5	2.92	-17.81	4.11	4	8.86	-35.03	4.48	3					
		6	1.01	-11.97	4.64	4	8.86	-35.03	4.48	3					
52	Vastus Lateralis (inferior)	1	2.69	-29.27	2.17	4	8.86	-35.03	4.48	3	3.3 ± 0.4	2.1 ± 0.2	-	10.7	2.79
		2	2.09	-24.72	2.18	4	8.86	-35.03	4.48	3					
		3	1.19	-20.26	2.39	4	8.86	-35.03	4.48	3					
		4	-0.01	-15.88	2.81	4	8.86	-35.03	4.48	3					
		5	-1.51	-11.59	3.44	4	8.86	-35.03	4.48	3					
		6	-3.3	-7.38	4.28	4	8.86	-35.03	4.48	3					
53	Vastus Lateralis (superior)	1	-2.66	-3.32	6.1	4	8.86	-35.03	4.48	3	7.0 ± 0.5	2.1 ± 0.2		59	2.79
		2	-0.9	-1.61	5.16	4	8.86	-35.03	4.48	3					
54	Vastus Medialis (inferior)	1	4.17	-29.43	0.75	4	9.46	-35.06	3.48	3	6.2 ± 0.2	2.2 ± 0.2		9.8	2.79
		2	5.25	-29.22	0.78	4	9.46	-35.06	3.48	3					
55	Vastus Medialis (mid)	1	3.68	-24.91	1.22	4	9.46	-35.06	3.48	3	6.2 ± 0.1	2.2 ± 0.2	-	23.2	2.79
		2	4.73	-24.71	1.26	4	9.46	-35.06	3.48	3					
56	Vastus Medialis (superior)	1	2.59	-19.76	1.76	4	9.46	-35.06	3.48	3	6.8 ± 0.3	2.2 ± 0.2	-	26.9	2.79
		2	3.55	-19.58	1.79	4	9.46	-35.06	3.48	3					
		3	1.21	-14.6	2.29	4	9.46	-35.06	3.48	3					
		4	2.17	-14.42	2.32	4	9.46	-35.06	3.48	3					
		5	-0.08	-8.01	2.98	4	9.46	-35.06	3.48	3					
		6	0.42	-7.92	2.99	4	9.46	-35.06	3.48	3					

Note: O. Seg is the originating segment and I. Seg is the inserting segment. Segment numbers are as follows: 1-Foot, 2-Tibia, 3-Patella, 4-Femur, 5-Pelvis.

Muscle (part)	Via point	X (cm)	Y (cm)	Z (cm)	Segment
Extensor Digitorum Longus	1	7.4	-76.3	5.3	2
	2	7.6	-77.4	5.4	2
	3	7.7	-78.6	5.6	2
	4	7.8	-79.8	5.6	2
	5	9.3	-84.7	5.8	1
Extensor Hallucis Longus	1	8.3	-73.9	4.9	2
	2	8.7	-75.9	5	2
	3	9.1	-76.8	5	2
	4	9.5	-77.8	5	2
	5	9.7	-78.7	5	2
	6	9.9	-79.1	4.9	2
	7	13.2	-85.5	5.1	1
	8	14.2	-86.3	4.8	1
	9	15.3	-87.2	4.4	1
	10	16.5	-88.5	3.9	1
	11	17.2	-89.1	3.6	1
	12	18.1	-90.1	3.4	1
	13	18.6	-90.5	3.4	1
Flexor Digitorum Longus	1	7.5	-77.8	1	2
	2	8.2	-79	0.9	2
	3	8.4	-79.6	0.8	2
	4	8.7	-80.2	0.6	2
	5	9.1	-80.7	0.7	2
	6	9.4	-81.4	0.6	2
	7	10	-83.2	0.9	2
	8	10.1	-83.7	1.1	2
Flexor Hallucis Longus	1	6.7	-79.1	0.8	2
	2	7.2	-80	0.7	2
	3	7.5	-80.4	0.6	2
	4	7.7	-80.7	0.5	2
	5	7.8	-80.8	0.4	2
	6	8.2	-81.4	0.2	2
	7	8.8	-82.4	0.3	2
	8	9.3	-83.3	0.4	2
Gracilis	1	5.7	-44.1	-3.1	2
	2	6.2	-44.8	-2.6	2
	3	6.3	-44.8	-2.6	2
	4	6.8	-45	-2.3	2
	5	7.1	-45.6	-1.7	2
	6	7.2	-45.6	-1.7	2
	7	7.7	-46.1	-0.6	2
	8	8.1	-46.4	0.5	2
Iliacus (lateral)	1	2.34	3.15	-1.05	5
Iliacus (mid)	1	2.34	3.15	-1.05	5
Iliacus (medial)	1	2.34	3.15	-1.05	5
Obturator Exturns (superior)	1	-1.43	-3.28	0.57	4
Obterator Internus	1	-5.7	-2.5	-4.3	5
Peronius Brevis	1	4.7	-76.8	2.7	2
	2	4.8	-78.3	2.8	2
	3	5.1	-80.3	2.9	2
	4	5.5	-81.4	3.1	2
Peronius Longus	1	4.7	-76.8	2.7	2
	2	4.8	-78.3	2.8	2
	3	5.1	-80.3	2.9	2
	4	5.5	-81.4	3.1	2
Peronius Tertius	1	7.2	-77.1	5.3	2
	2	7.5	-78.7	5.5	2
	3	8.3	-80.8	5.6	2
Poplitius	1	2.6	-44.8	2.3	2

Psoas Major	1	2.34	3.15	-1.05	5
Sartorius (proximal)	1	5.3	-10.2	-1.1	4
	2	6.6	-18.7	0	4
	3	6.5	-19.7	-0.4	4
	4	6.5	-21.2	-0.9	4
	5	6.2	-22.3	-1.4	4
	6	5.8	-23.6	-1.9	4
	7	5.6	-24.8	-2.4	4
	8	5.4	-26.1	-2.6	4
	9	5.2	-27.5	-2.9	4
	10	5.2	-29	-3.1	4
	11	5.3	-30.5	-3.3	4
	12	5.3	-32	-3.6	4
	13	5.3	-32.3	-3.6	4
Sartorius (distal)	1	3	-37.3	-4.2	4
Semitendinosus	1	2.9	-43.5	-2.9	2
	2	3.1	-44.2	-2.9	2
	3	3.7	-44.9	-2.6	2
	4	4.4	-45.7	-2.2	2
	5	5	-46.2	-1.9	2
	6	5.4	-46.6	-1.7	2
	7	5.6	-47.2	-1.4	2
Tibialis Anterior	1	12	-78	2.8	2
	2	13.8	-85.2	2.6	1
Tibialis Posterior (medial)	1	7.5	-73.9	1.2	2
	2	7.9	-75.1	1.1	2
	3	8.2	-76	0.9	2
	4	8.4	-76.8	0.7	2
	5	8.5	-77.3	0.6	2
	6	8.7	-77.8	0.4	2
	7	9	-78.3	0.4	2
	8	9.2	-78.7	0.4	2
	9	9.6	-79.4	0.3	2
	10	10.3	-80	0.5	2
	11	11.2	-81.3	1.3	2
Tibialis Posterior (lateral)	1	7.9	-75.1	1.1	2
	2	8.2	-76	0.9	2
	3	8.4	-76.8	0.7	2
	4	8.5	-77.3	0.6	2
	5	8.7	-77.8	0.4	2
	6	9	-78.3	0.4	2
	7	9.2	-78.7	0.4	2
	8	9.6	-79.4	0.3	2
	9	10.3	-80	0.5	2
	10	11.2	-81.3	1.3	2

Appendix B – MVC Procedures for EMG Studies

Muscle(s)	SENIAM Guidelines	Study Protocol
Tibialis Anterior	• Support above the ankle joint • Ankle joint in dorsiflexion and the foot in inversion • Apply pressure against the medial dorsal surface of the foot in the direction of plantar flexion and eversion	• Participant seated on edge of a massage table with legs hanging over the side • Followed guideline
Gastrocnemii	• Plantar flexion of the foot with emphasis on pulling the heel upward more than pushing the forefoot • Apply pressure against the forefoot as well as against the calcaneus	• Participant seated in leg press machine with a leg straight, but not locked at the knee • Attempt plantar flexion of the foot against weighted resistance
Semitendinosus Biceps Femoris	• Press against the leg proximal to the ankle in the direction of knee extension	• Participant prone on a massage table • Flex knee joint to an angle of ~115º • Attempt knee flexion while manually resisting in the direction of knee extension
Vastus Lateralis Rectus Femoris Vastus Medialis	• Extend the knee without rotating the thigh while applying pressure against the leg above the ankle in the direction of flexion	• Participant seated in leg extension exercise machine • Extend knee joint to an angle of ~135º • Attempt extension of the knee against weighted resistance

Appendix C – Correlation of Outcome Variables with Regression Predictors

Table 7-1 Pearson correlation of the knee flexion angle at thigh-calf contact onset with predictor variables for each movement. Significant correlations are bolded with *, †, and ‡ indicating significant correlations at *p* = 0.05, < 0.01, and <0.001 levels respectively. Prx is proximal, Dst is distal, and Cir is circumference.

Predictor	Heels-up Squat	Flatfoot Squat	Dorsiflexed Kneel	Plantarflexed Kneel	Plantarflexed Unilateral Kneel	Dorsiflexed Unilateral Kneel
Height	-0.12	-0.21	**-0.28***	-0.18	-0.18	**-0.26***
Mass	**-0.27***	-0.36	**-0.42‡**	-0.24	**-0.39†**	**-0.46‡**
BMI	**-0.27***	-0.34	**-0.35†**	-0.19	**-0.38†**	**-0.42‡**
Thigh Length	0.09	-0.01	-0.17	-0.23	**-0.42‡**	0.03
Prx Thigh Cir	**-0.27***	-0.25	**-0.39†**	-0.21	**-0.37†**	**-0.51‡**
Mid-Thigh Cir	-0.22	-0.28	-0.26	-0.11	**-0.30***	**-0.40†**
Dst Thigh Cir	0.09	-0.01	-0.17	-0.23	**-0.42‡**	0.03
Thigh Skinfold	-0.06	0.15	-0.06	0.08	-0.07	-0.19
Shank Length	0.04	-0.23	-0.17	-0.09	-0.22	-0.13
Prx Shank Cir	-0.20	-0.41	**-0.31***	-0.13	**-0.33***	**-0.46‡**
Mid-Shank Cir	-0.17	-0.38	**-0.32***	-0.12	**-0.31***	**-0.44‡**
Dst Shank Cir	-0.03	-0.18	-0.26	-0.05	**-0.30***	**-0.35†**
Shank Skinfold	-0.12	0.14	-0.14	-0.05	-0.14	**-0.28***

Table 7-2 Pearson correlation of maximum knee flexion angle with predictor variables for each movement. Significant correlations are bolded with *, †, and ‡ indicating significant correlations at *p* = 0.05, < 0.01, and <0.001 levels respectively. Prx is proximal, Dst is distal, and Cir is circumference.

Predictor	Heels-up Squat	Flatfoot Squat	Dorsiflexed Kneel	Plantarflexed Kneel	Plantarflexed Unilateral Kneel	Dorsiflexed Unilateral Kneel
Height	**-0.32***	-0.41	**-0.29***	**-0.29†**	-0.19	**-0.33***
Mass	**-0.69‡**	**-0.68‡**	**-0.68‡**	**-0.61‡**	**-0.54‡**	**-0.70‡**
BMI	**-0.68‡**	**-0.61†**	**-0.69‡**	**-0.59‡**	**-0.55‡**	**-0.66‡**
Thigh Length	-0.05	-0.27	-0.01	-0.10	-0.08	-0.05
Prx Thigh Cir	**-0.61‡**	**-0.42***	**-0.63‡**	**-0.57‡**	**-0.54‡**	**-0.65‡**
Mid-Thigh Cir	**-0.40†**	**-0.47***	**-0.40†**	-0.36	**-0.31†**	**-0.42‡**
Dst Thigh Cir	-0.06	-0.27	-0.02	-0.10	-0.08	-0.05
Thigh Skinfold	-0.17	0.08	-0.17	-0.07	-0.15	-0.22
Shank Length	-0.15	-0.33	-0.10	-0.15	-0.04	-0.11
Prx Shank Cir	**-0.59‡**	**-0.54†**	**-0.61‡**	**-0.54‡**	**-0.52‡**	**-0.64‡**
Mid-Shank Cir	**-0.55‡**	**-0.53†**	**-0.58‡**	**-0.50‡**	**-0.47‡**	**-0.59‡**
Dst Shank Cir	**-0.38†**	-0.31	**-0.41‡**	**-0.36†**	**-0.32***	**-0.47‡**
Shank Skinfold	**-0.38†**	0.01	**-0.32†**	-0.21	-0.24	**-0.35†**

Table 7-3 Pearson correlation of total contact force with predictor variables for each movement. Significant correlations are bolded with *, †, and ‡ indicating significant correlations at *p* = 0.05, < 0.01, and <0.001 levels respectively. Prx is proximal, Dst is distal, and Cir is circumference.

Predictor	Heels-up Squat	Flatfoot Squat	Dorsiflexed Kneel	Plantarflexed Kneel	Plantarflexed Unilateral Kneel	Dorsiflexed Unilateral Kneel
Height	0.10	0.20	0.14	**0.28***	0.05	-0.08
Mass	0.20	0.24	0.08	**0.28***	0.03	-0.21
BMI	0.19	0.19	0.02	0.18	0.03	-0.20
Thigh Length	0.12	0.27	0.03	-0.04	-0.05	-0.02
Prx Thigh Cir	0.14	0.36	0.06	0.21	0.03	-0.18
Mid-Thigh Cir	0.14	0.36	0.08	0.18	0.07	-0.10
Dst Thigh Cir	0.11	0.27	0.02	-0.05	-0.05	-0.02
Thigh Skinfold	0.02	-0.25	-0.07	0.08	-0.09	-0.13
Shank Length	0.21	0.33	0.24	**0.26***	0.13	0.08
Prx Shank Cir	0.20	0.29	0.04	0.22	0.01	-0.21
Mid-Shank Cir	0.24	0.20	0.07	0.25	0.05	-0.18
Dst Shank Cir	0.17	0.34	0.05	0.22	0.03	-0.21
Shank Skinfold	-0.07	-0.23	-0.03	0.10	-0.04	-0.15
Max Angle	0.09	0.03	0.17	0.08	**0.32†**	**0.41‡**

Table 7-4 Pearson correlation of thigh-calf longitudinal center of force location with predictor variables for each movement. Significant correlations are bolded with *, †, and ‡ indicating significant correlations at *p* = 0.05, < 0.01, and <0.001 levels respectively. Prx is proximal, Dst is distal, and Cir is circumference.

Predictor	Heels-up Squat	Flatfoot Squat	Dorsiflexed Kneel	Plantarflexed Kneel	Plantarflexed Unilateral Kneel	Dorsiflexed Unilateral Kneel
Height	0.01	-0.19	-0.01	0.12	0.07	-0.12
Mass	-0.21	-0.36	**-0.35†**	-0.15	-0.25	**-0.45‡**
BMI	**-0.28***	-0.35	**-0.45‡**	**-0.27***	**-0.36†**	**-0.50‡**
Thigh Length	0.15	0.03	0.14	0.10	0.18	0.16
Prx Thigh Cir	-0.14	-0.12	**-0.31***	-0.16	**-0.27***	**-0.38†**
Mid-Thigh Cir	-0.19	-0.17	-0.22	-0.13	-0.13	**-0.27***
Dst Thigh Cir	0.15	0.03	0.14	0.10	0.17	0.16
Thigh Skinfold	-0.11	0.03	-0.17	-0.11	-0.25	-0.22
Shank Length	0.13	-0.08	0.14	0.13	0.19	0.10
Prx Shank Cir	-0.17	-0.34	**-0.38†**	-0.19	-0.25	**-0.39†**
Mid-Shank Cir	-0.02	-0.27	**-0.30***	-0.09	-0.18	**-0.33***
Dst Shank Cir	0.15	0.00	-0.06	0.10	0.04	-0.10
Shank Skinfold	-0.23	0.05	-0.23	-0.16	**-0.27***	**-0.32***
Max Angle	**0.46‡**	**0.63‡**	**0.68‡**	**0.50‡**	**0.70‡**	**0.69‡**

Table 7-5 Pearson correlation of thigh-calf contact area with predictor variables for each movement. Significant correlations are bolded with *, †, and ‡ indicating significant correlations at p = 0.05, < 0.01, and <0.001 levels respectively. Prx is proximal, Dst is distal, and Cir is circumference.

Predictor	Heels-up Squat	Flatfoot Squat	Dorsiflexed Kneel	Plantarflexed Kneel	Plantarflexed Unilateral Kneel	Dorsiflexed Unilateral Kneel
Height	0.10	0.05	0.18	**0.32***	0.16	-0.07
Mass	0.02	0.01	-0.08	0.14	-0.08	**-0.37‡**
BMI	-0.03	-0.01	-0.22	-0.03	-0.19	**-0.42‡**
Thigh Length	0.06	0.12	0.06	0.02	0.04	0.05
Prx Thigh Cir	0.03	0.16	-0.09	0.06	-0.13	**-0.33†**
Mid-Thigh Cir	0.03	0.14	-0.07	0.01	-0.08	**-0.21***
Dst Thigh Cir	0.06	0.12	0.05	0.02	0.04	0.05
Thigh Skinfold	0.02	-0.11	-0.08	0.03	-0.16	-0.19
Shank Length	0.18	0.15	**0.28***	**0.27***	0.23	0.15
Prx Shank Cir	0.02	0.04	-0.14	0.05	-0.11	**-0.32†**
Mid-Shank Cir	0.12	0.02	-0.05	0.14	-0.03	**-0.24***
Dst Shank Cir	0.14	0.20	0.05	0.22	0.08	-0.13
Shank Skinfold	-0.11	-0.08	-0.09	0.02	-0.15	**-0.27***
Max Angle	**0.32†**	0.30	**0.43‡**	**0.27***	**0.53‡**	**0.62‡**

Appendix D – Surface Electrode Sites

Muscle	Electrode Placement
Medial Gastrocnemius	1/3 of the distance along the line starting at the head of the fibula and ending at the heel
Lateral Gastrocnemius	1/3 of the distance along the line starting at the head of the fibula and ending at the medial malleolus
Tibialis Anterior	1/3 of the distance along the line starting at the tip of the fibula and ending at the medial malleolus
Vastus Medialis	80% of the line from the anterior superior iliac spine (ASIS) and ending at the joint space in front of the anterior border of the medial ligament
Rectus Femoris	1/2 the distance along the line from the ASIS to the superior part of the patella
Vastus Lateralis	2/3 of the distance along the line starting at the ASIS and ending at the lateral side of the patella
Biceps Femoris	1/2 of the distance along the line starting at the ischial tuberosity and ending at the lateral condyle of the tibia
Semitendinosus	1/2 of the distance along the line starting at the ischial tuberosity and ending at the medial condyle of the tibia
Gluteus Medius	50% of the line from the iliac crest to the trochanter
Gluteus Maximus	50% of the line between the sacral vertebrae and the greater trochanter. This corresponds with the largest prominence of the middle of the buttocks above the greater trochanter.

Appendix E – Deep Muscle EMG Waveforms

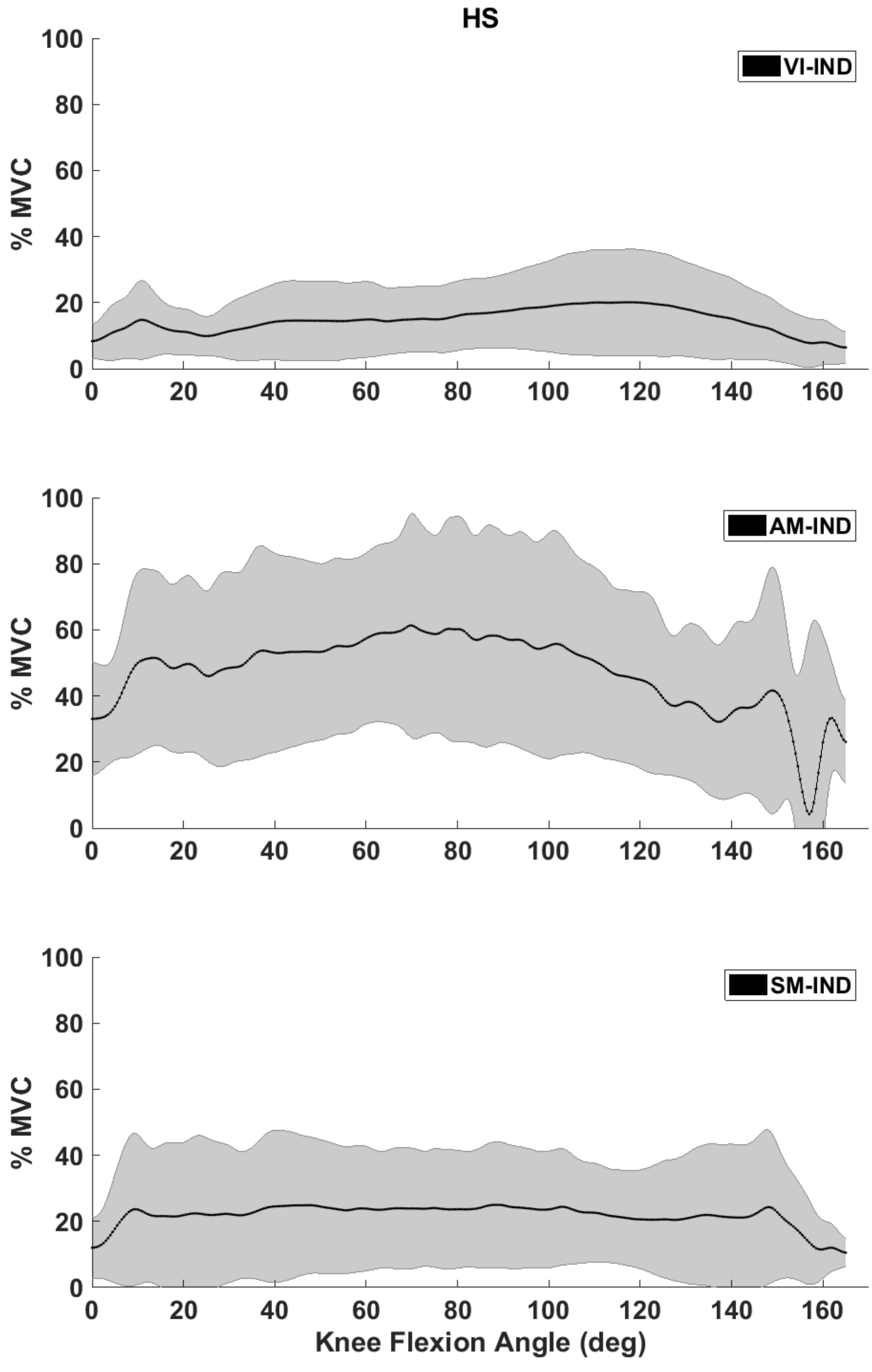

Figure 7.1 Mean fine-wire vastus intermedius (VI), adductor magnus (AM), and semimembranosus (SM) activation waveforms during a heels-up squat (HS). The shaded band represents ± 1 SD.

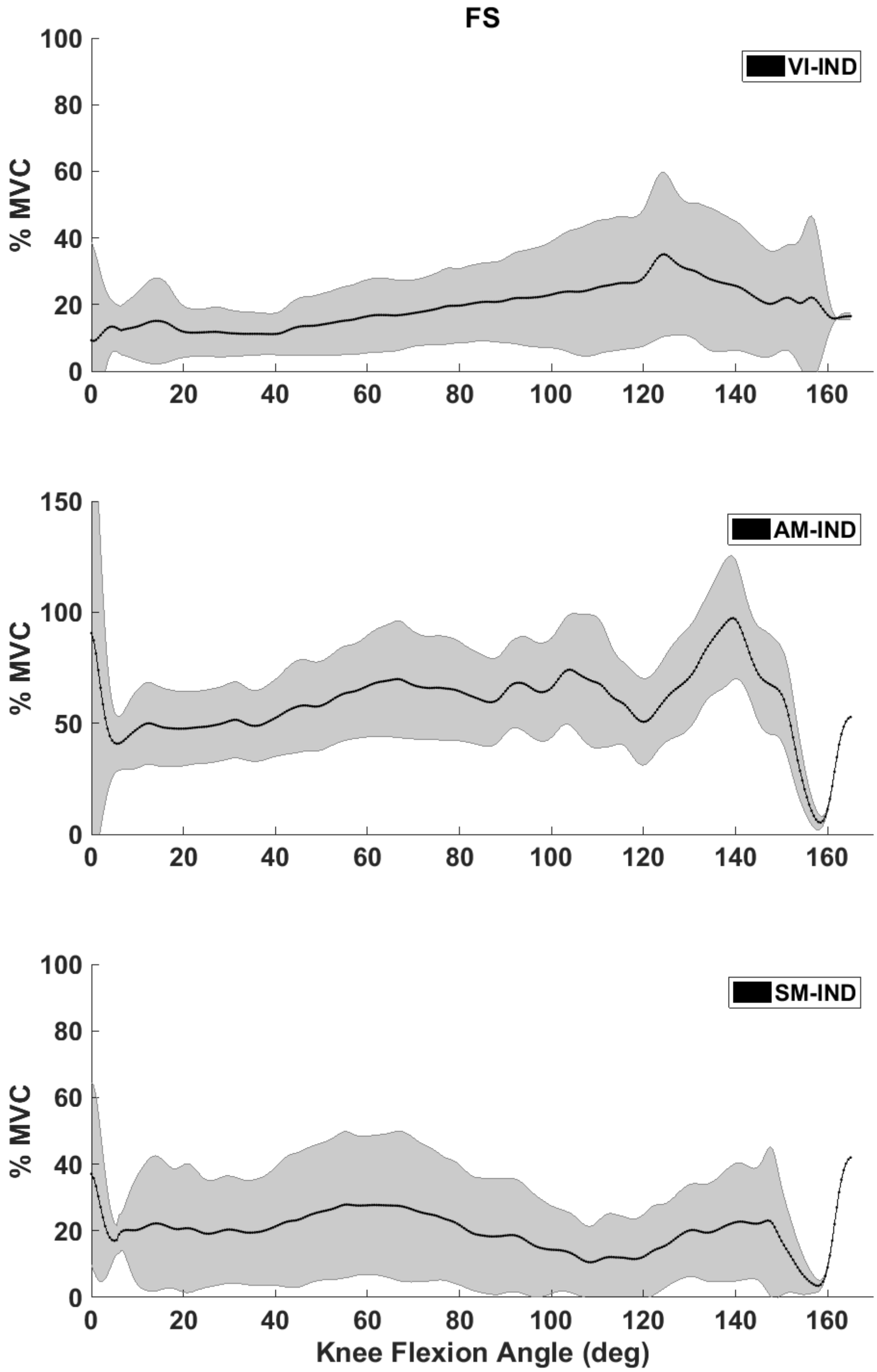

Figure 7.2 Mean fine-wire vastus intermedius (VI), adductor magnus (AM), and semimembranosus (SM) activation waveforms during a flatfoot squat (FS). The shaded band represents ± 1 SD.

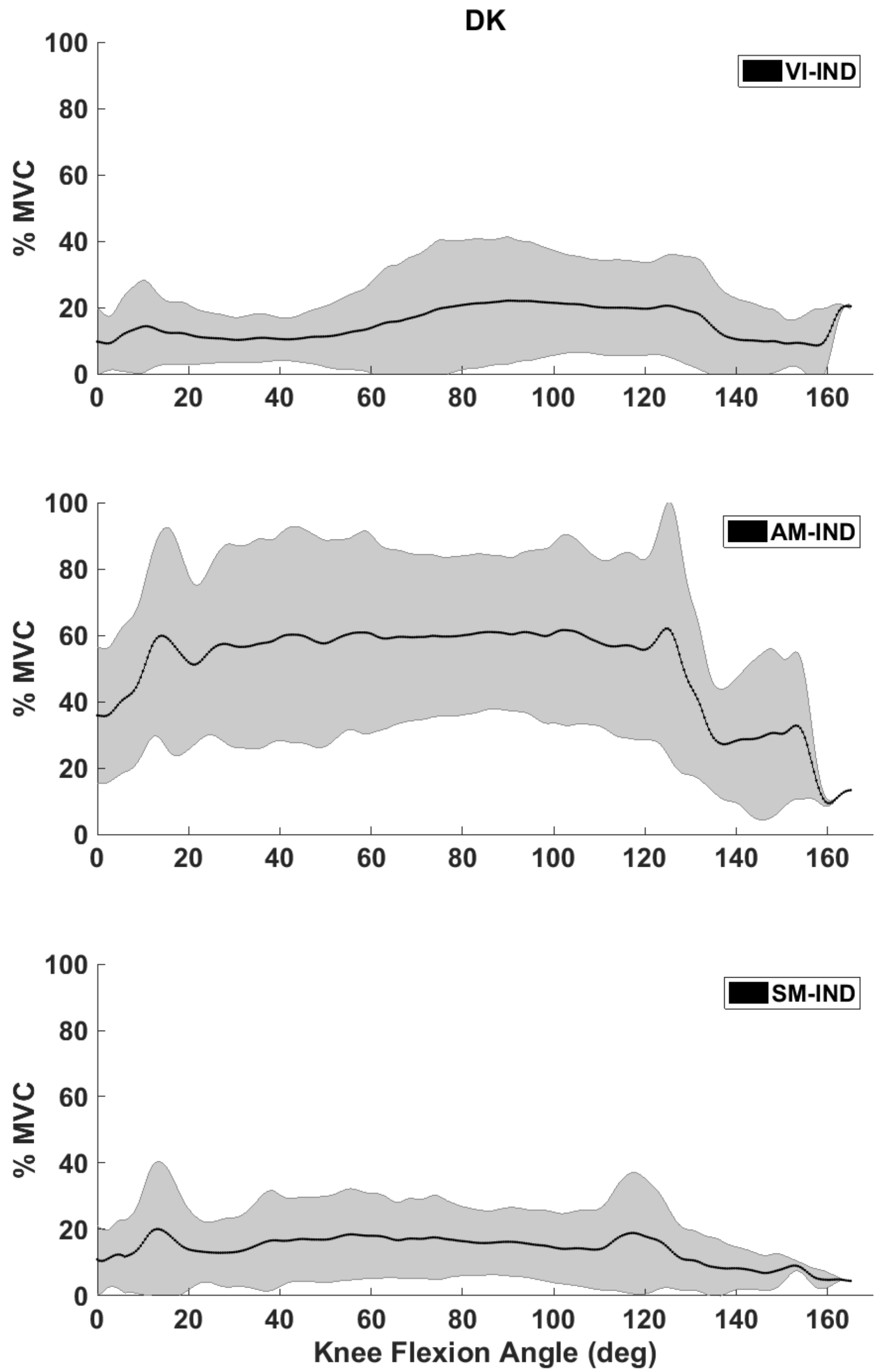

Figure 7.3 Mean fine-wire vastus intermedius (VI), adductor magnus (AM), and semimembranosus (SM) activation waveforms during a dorsiflexed kneel (DK). The shaded band represents ± 1 SD.

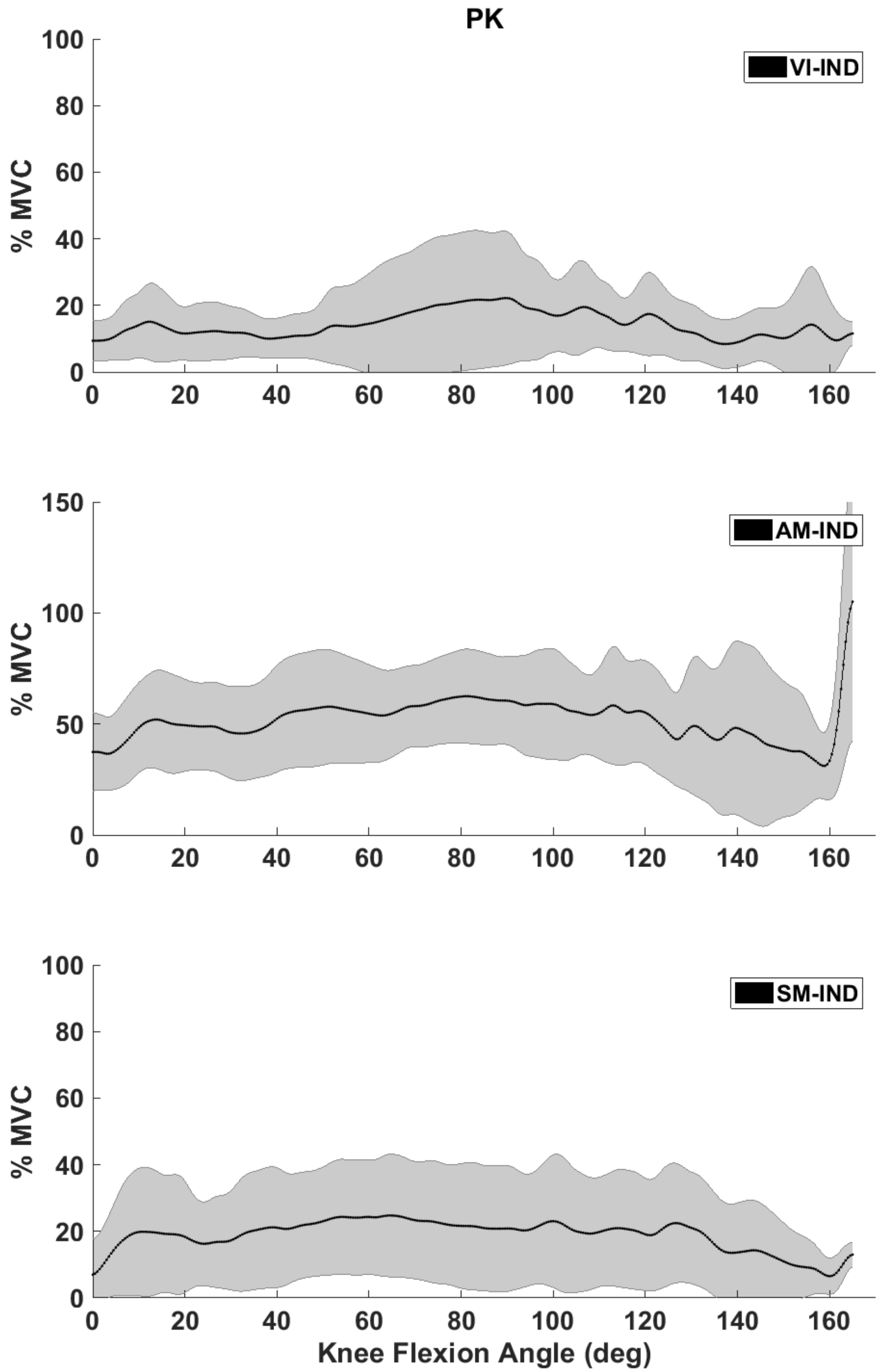

Figure 7.4 Mean fine-wire vastus intermedius (VI), adductor magnus (AM), and semimembranosus (SM) activation waveforms during a plantarflexed kneel (PK). The shaded band represents ± 1 SD.

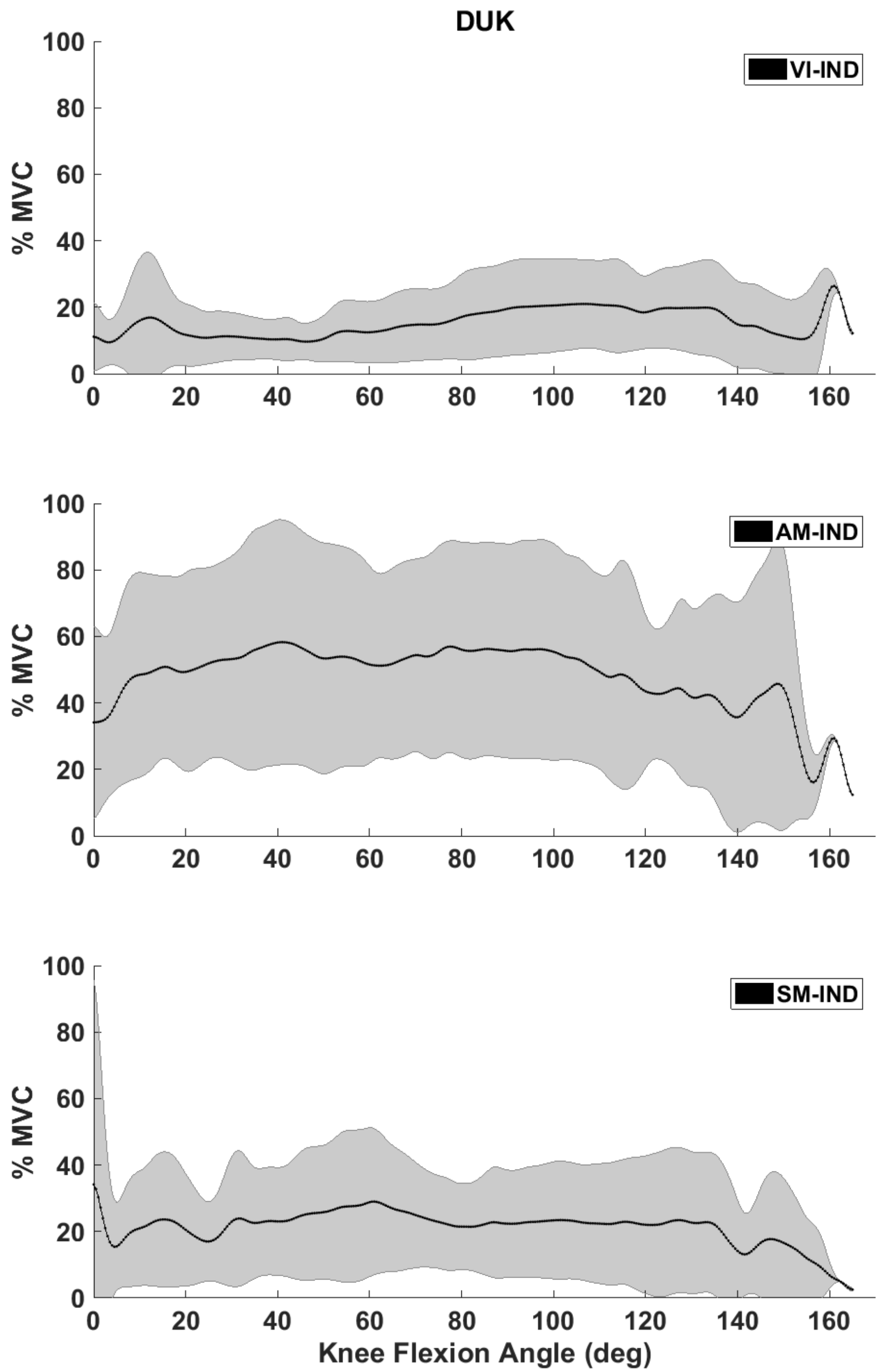

Figure 7.5 Mean fine-wire vastus intermedius (VI), adductor magnus (AM), and semimembranosus (SM) activation waveforms during a dorsiflexed unilateral kneel (DUK). The shaded band represents ± 1 SD.

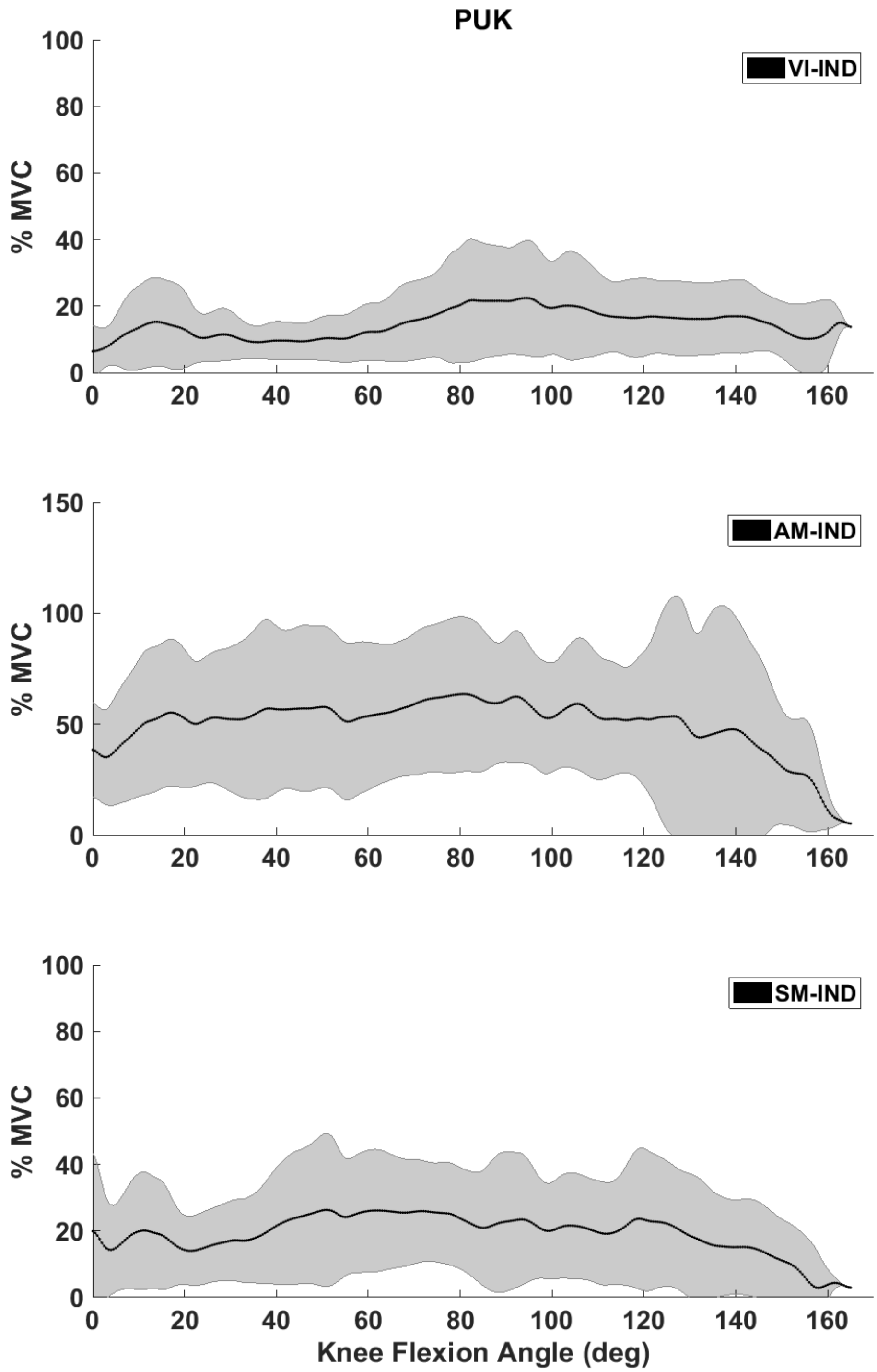

Figure 7.6 Mean fine-wire vastus intermedius (VI), adductor magnus (AM), and semimembranosus (SM) activation waveforms during a plantarflexed unilateral kneel (PUK). The shaded band represents ± 1 SD.

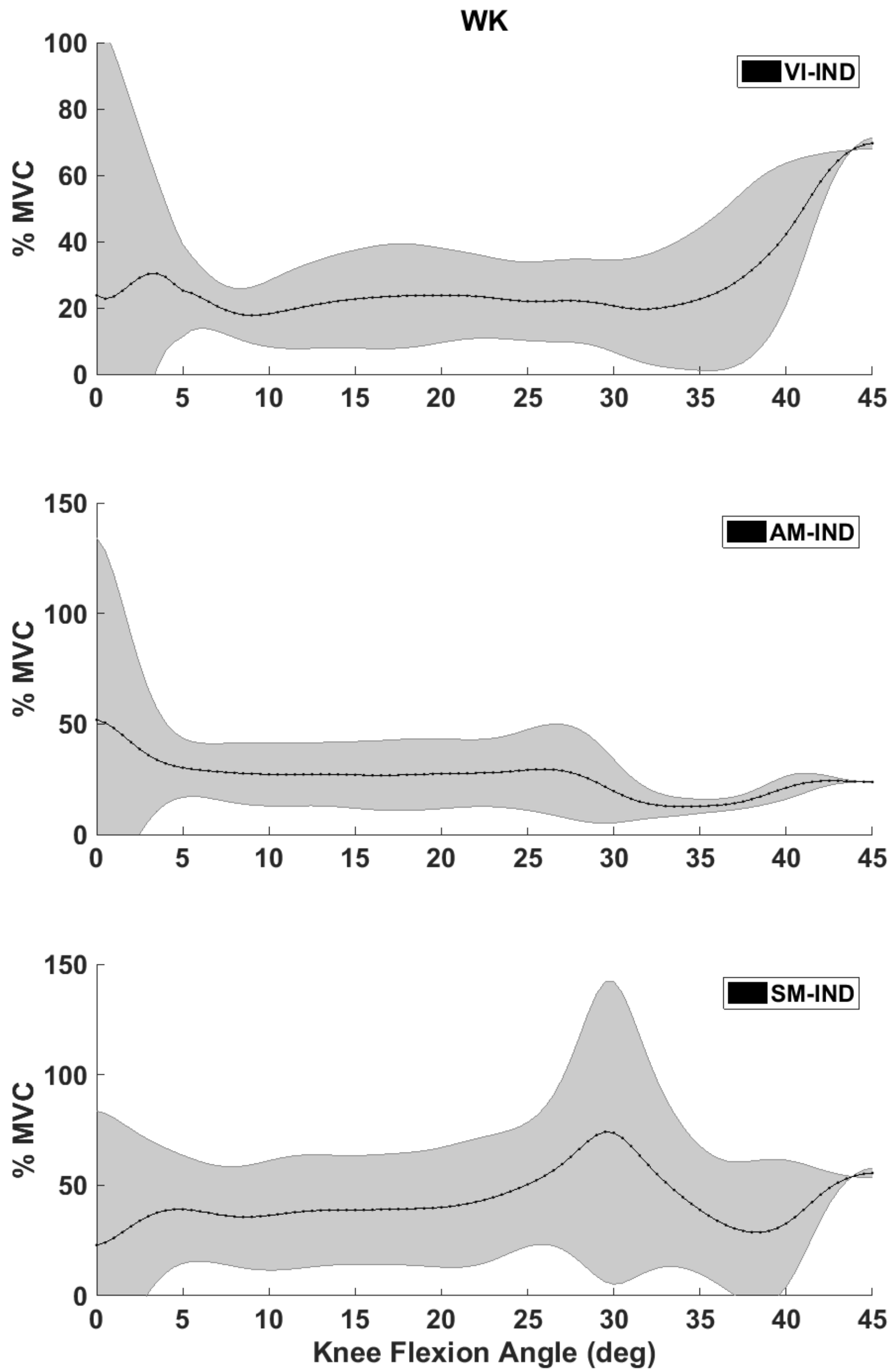

Figure 7.7 Mean fine-wire vastus intermedius (VI), adductor magnus (AM), and semimembranosus (SM) activation waveforms during a walking trial (WK). The shaded band represents ± 1 SD.

Appendix F – Lower limb segmental local coordinate system definitions

Pelvis	
Origin	Mid-point between the left and right anterior superior iliac spines
z-axis	Vector from the origin towards the right ASIS
y-axis	Cross product of temporary vector from the origin to the midpoint of left and right PSIS and z-axis
x-axis	Cross product of y and z-axes
Thigh	
Origin	Functional knee joint centre (Ehrig et al., 2007)
z-axis	Cross product of the x by y-axes
y-axis	Vector from origin to functional hip joint centre (Ehrig et al., 2006)
x-axis	Cross product of the y-axis and a temporary vector from the Origin to the lateral greater trochanter
Shank	
Origin	Midpoint of malleoli
z-axis	Cross product of x- by y-axes
y-axis	Vector from the mid-point between the malleoli to the functional knee joint centre
x-axis	Cross product of the y-axis and a temporary vector pointing from the origin to lateral malleoli
Foot	
Origin	Heel
z-axis	Cross product of x by y-axes
y-axis	Vector from the origin to the toe
x-axis	Cross product of the y-axis and temporary vector pointing from the origin to the midpoint of the malleoli

Appendix G – Grand Knee Challenge EMG compared to model estimates of muscle forces

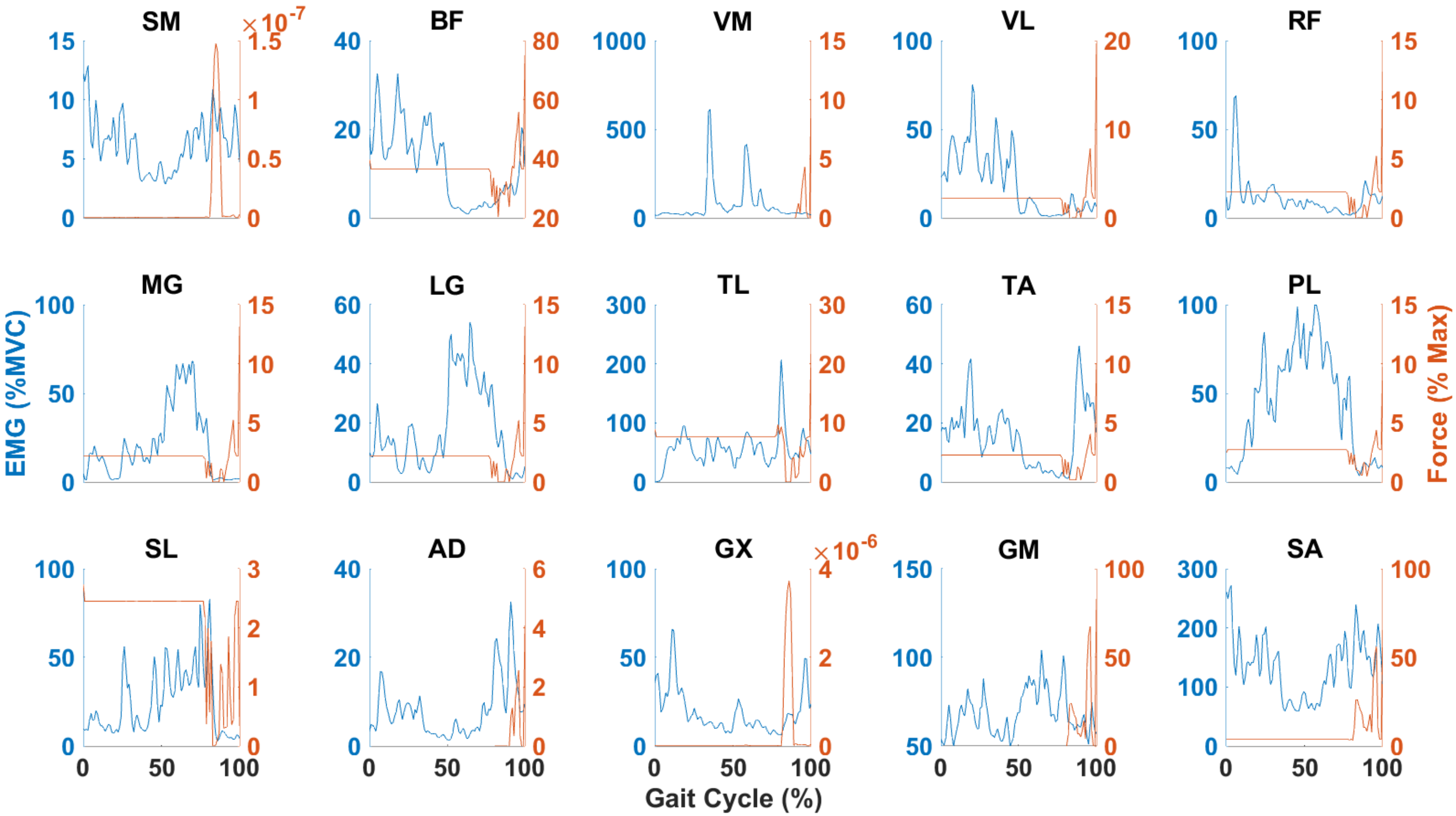

Figure 7.8 Muscle activations (blue) compared to mean muscle forces (orange) for a walking trial with a specific muscle tension of 61 N/cm^2. Muscles are: semimembranosus (SM), biceps femoris (BF), vastus medialis (VM), vastus lateralis (VL), rectus femoris (RF), medial gastrocnemius (MG), lateral gastrocnemius (LG), tensor fascia lata (TL), tibialis anterior (TA), peroneus longus (PL), soleus (SL), adductor magnus (AM), gluteus maximus (GX), gluteus medius (GM), and sartorius (SA).

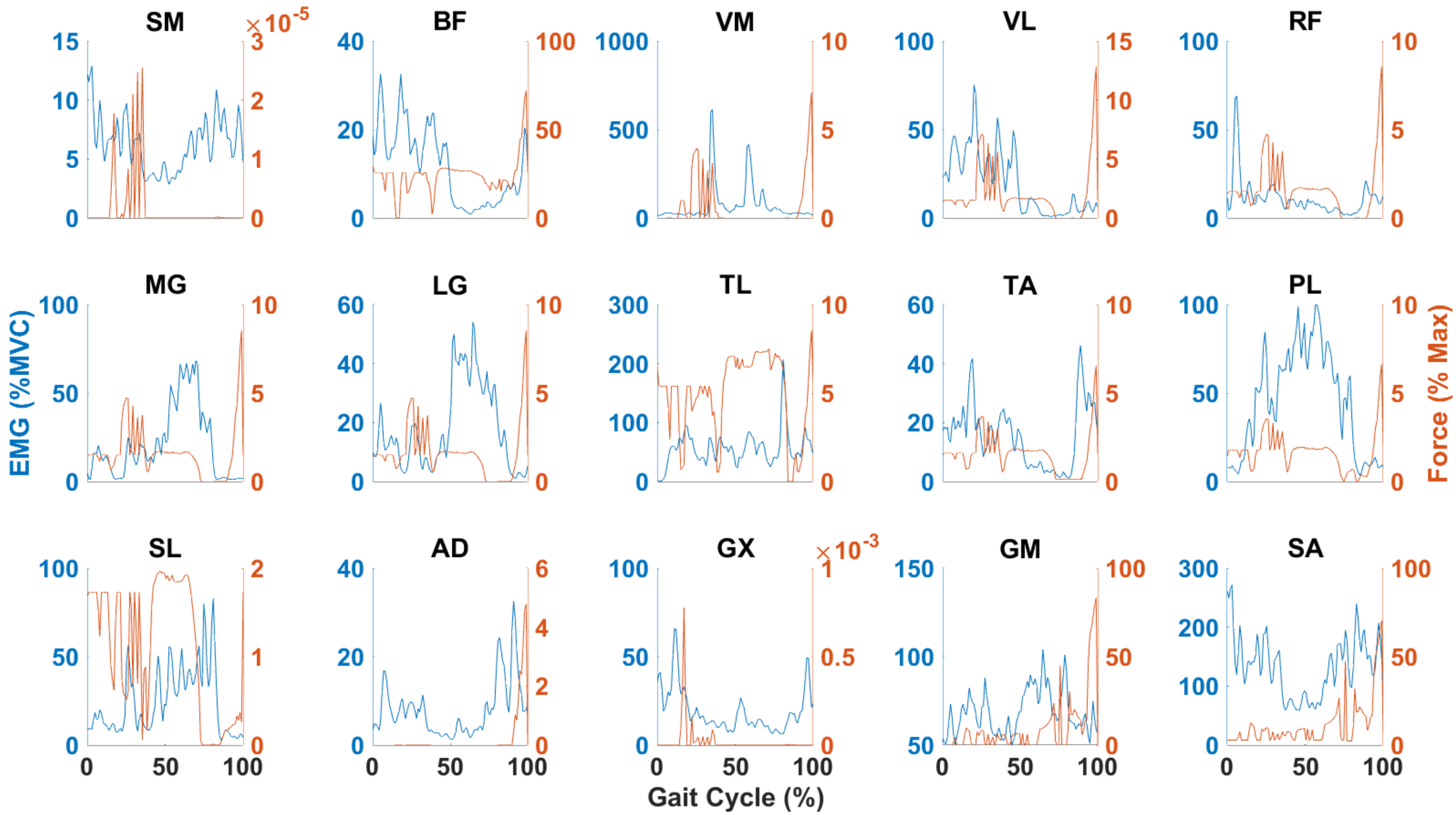

Figure 7.9 Muscle activations (blue) compared to mean muscle forces (orange) for a walking trial with a specific muscle tension of 88 N/cm^2. Muscles are the same as Figure 7.8.

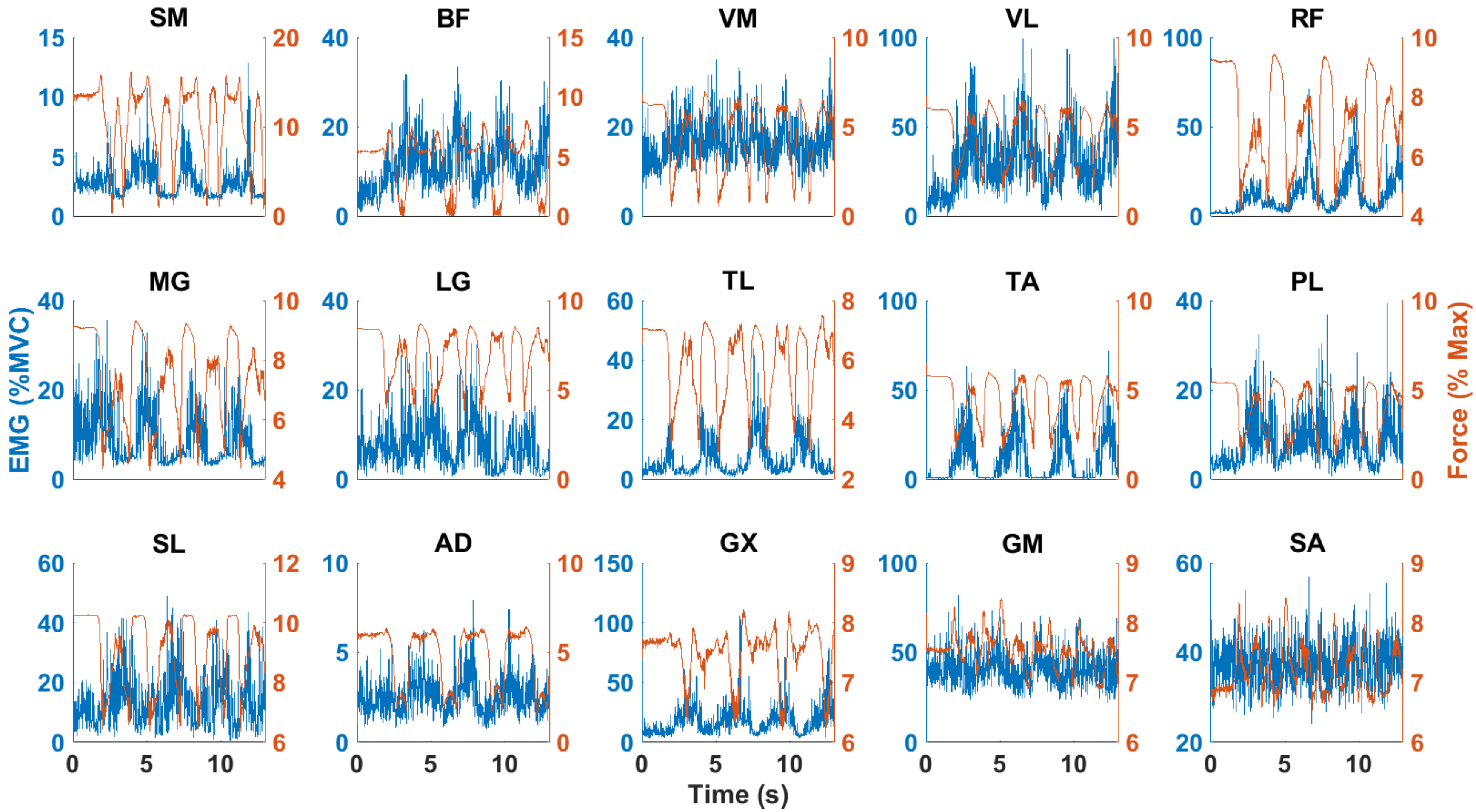

Figure 7.10 Muscle activations (blue) compared to mean muscle forces (orange) for a cyclic squatting trial with a specific muscle tension of 30 N/cm^2. Muscles are the same as Figure 7.8.

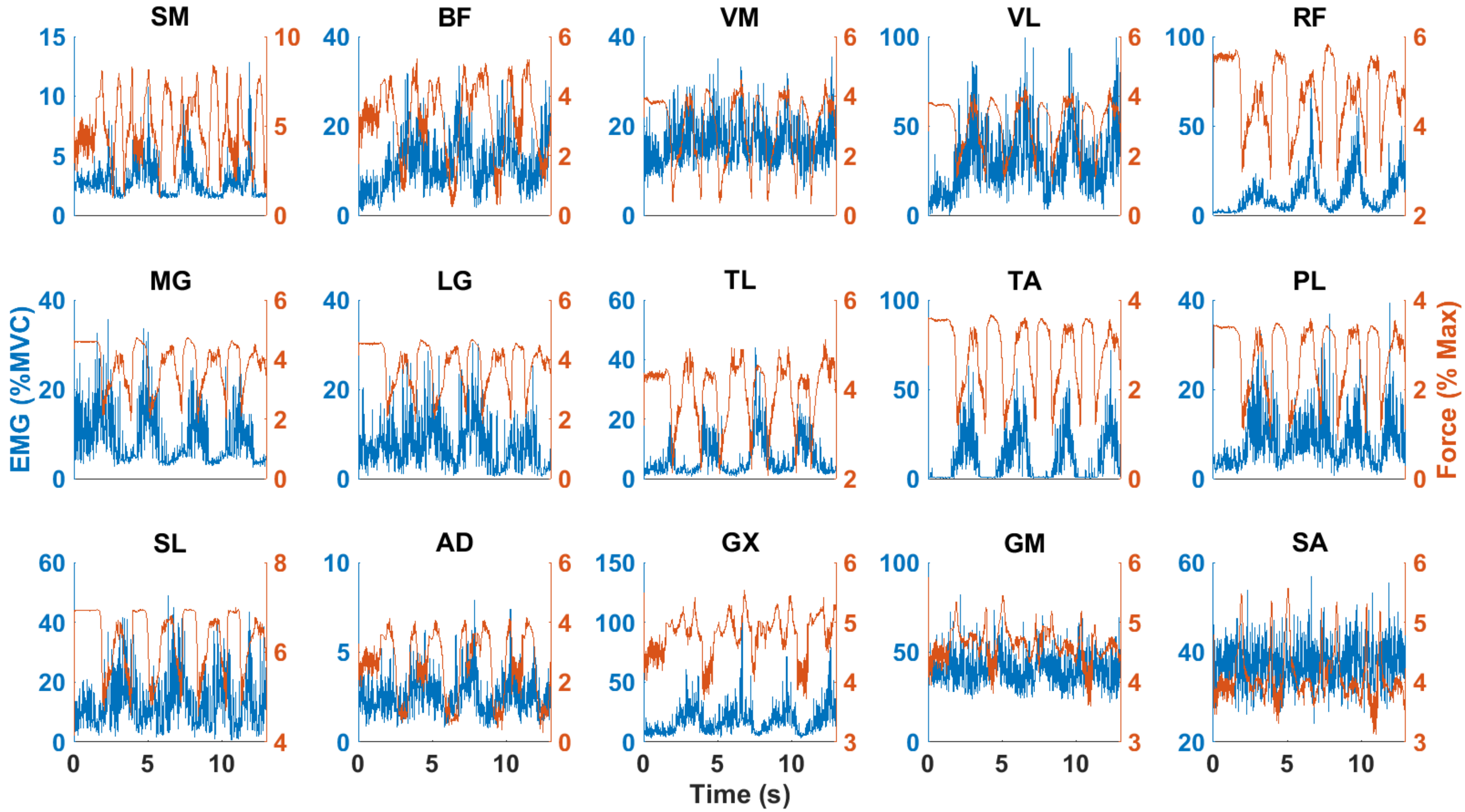

Figure 7.11 Muscle activations (blue) compared to mean muscle forces (orange) for a cyclic squatting trial with a specific muscle tension of 61 N/cm². Muscles are the same as Figure 7.8.

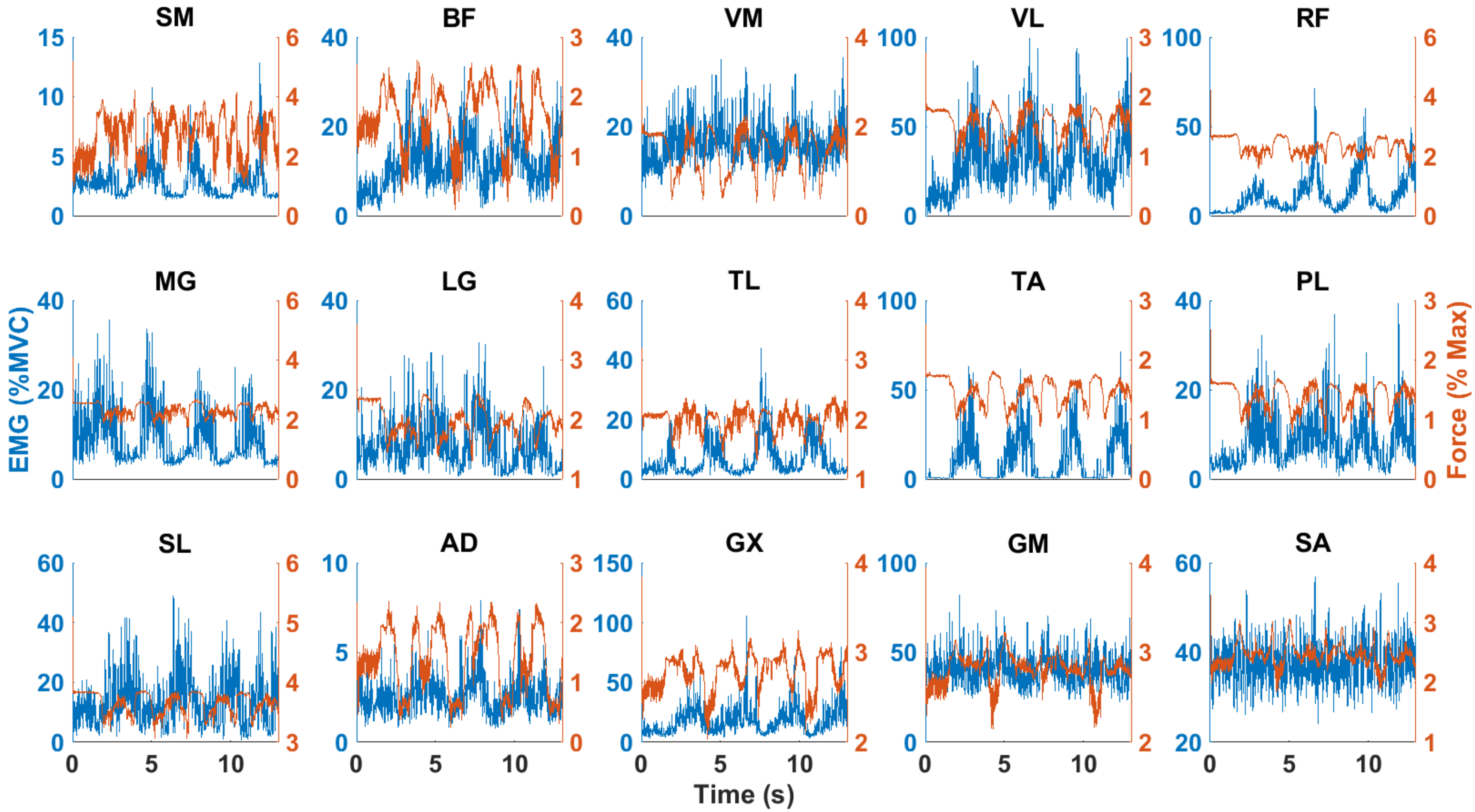

Figure 7.12 Muscle activations (blue) compared to mean muscle forces (orange) for a cyclic squatting trial with a specific muscle tension of 88 N/cm^2. Muscles are the same as Figure 7.8.

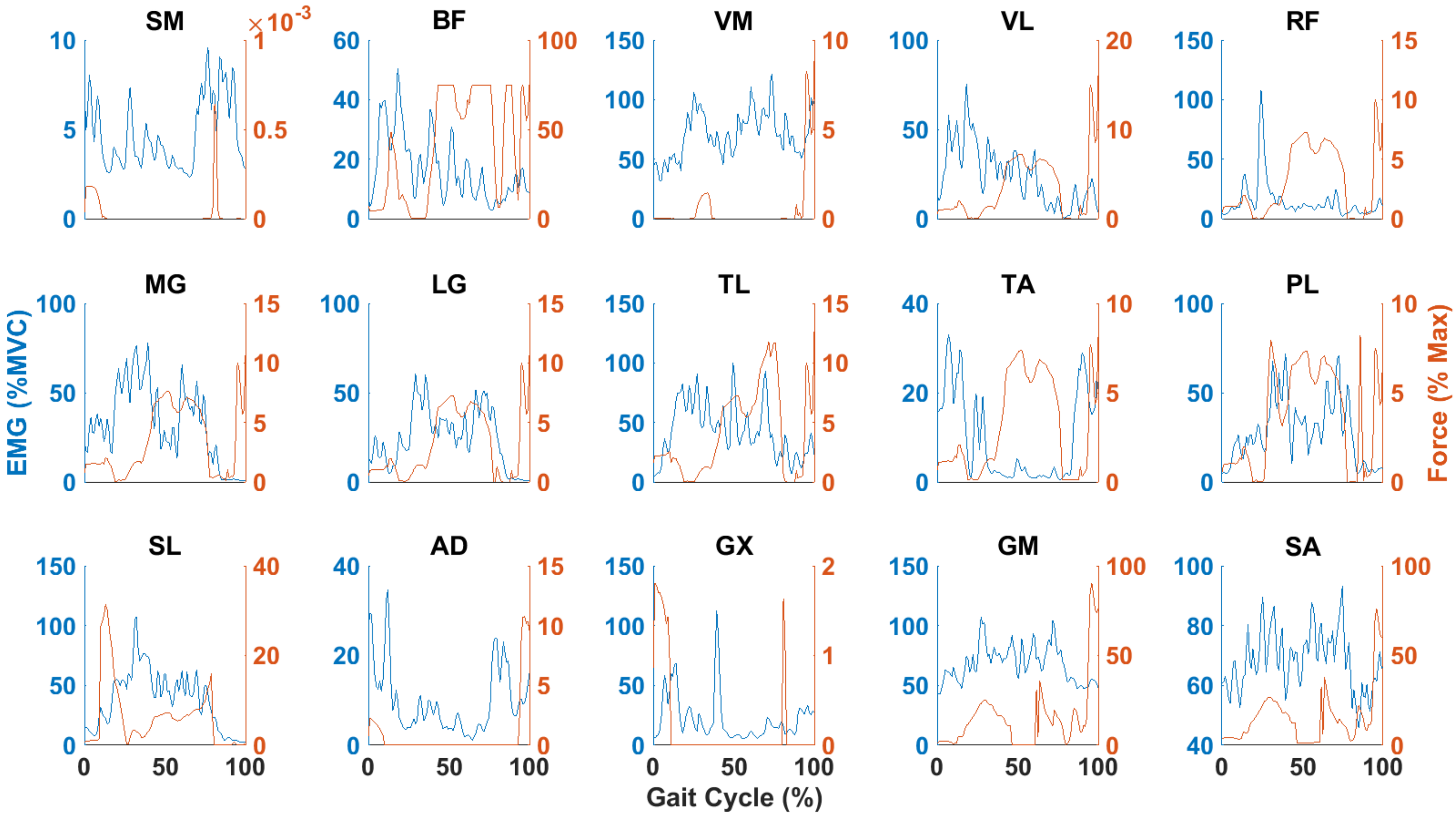

Figure 7.13 Muscle activations (blue) compared to mean muscle forces (orange) for a 'bouncy' walking trial with a specific muscle tension of 30 N/cm^2. Muscles are the same as Figure 7.8.

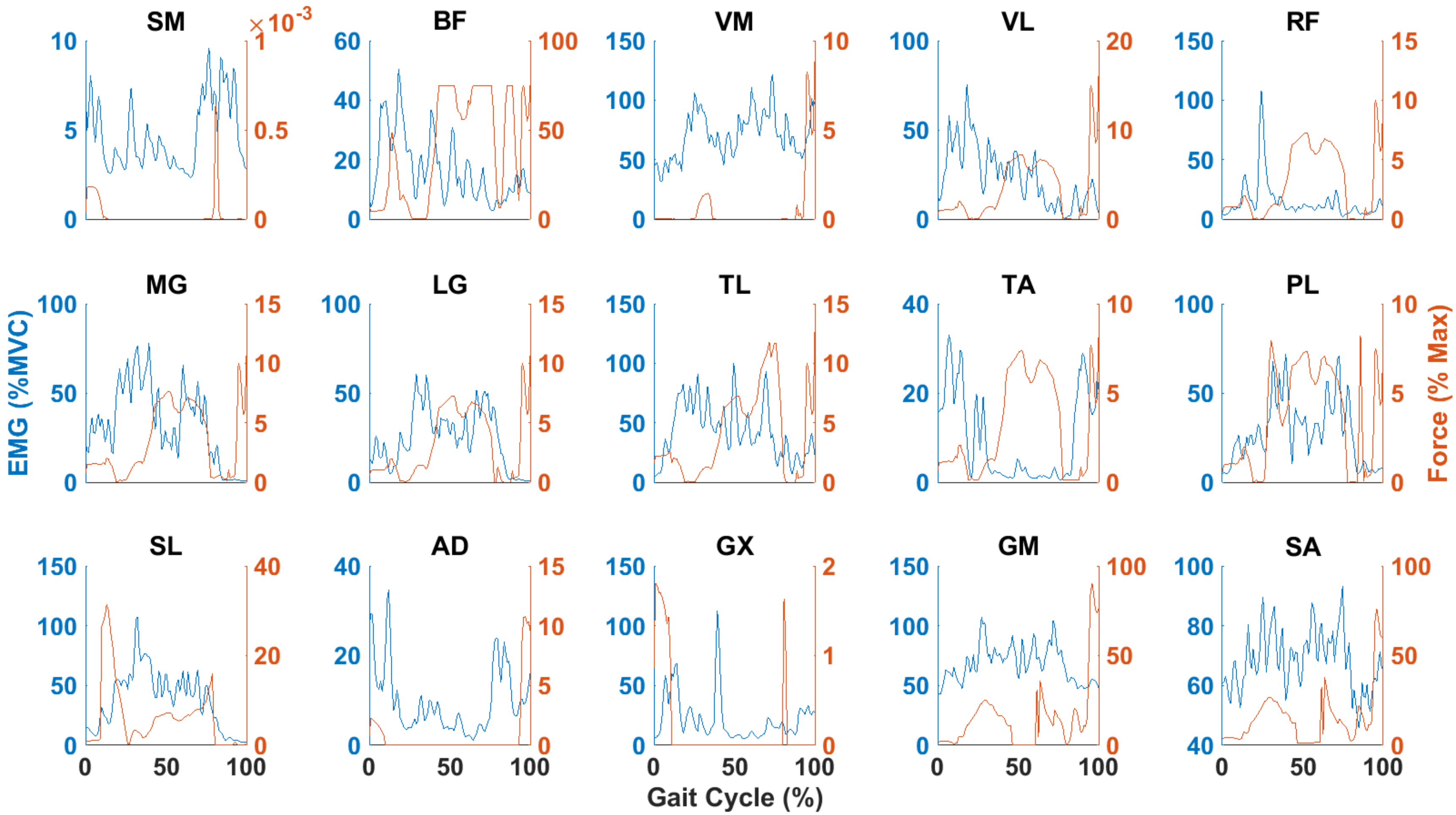

Figure 7.14 Muscle activations (blue) compared to mean muscle forces (orange) for a 'bouncy' walking trial with a specific muscle tension of 61 N/cm^2. Muscles are the same as Figure 7.8.

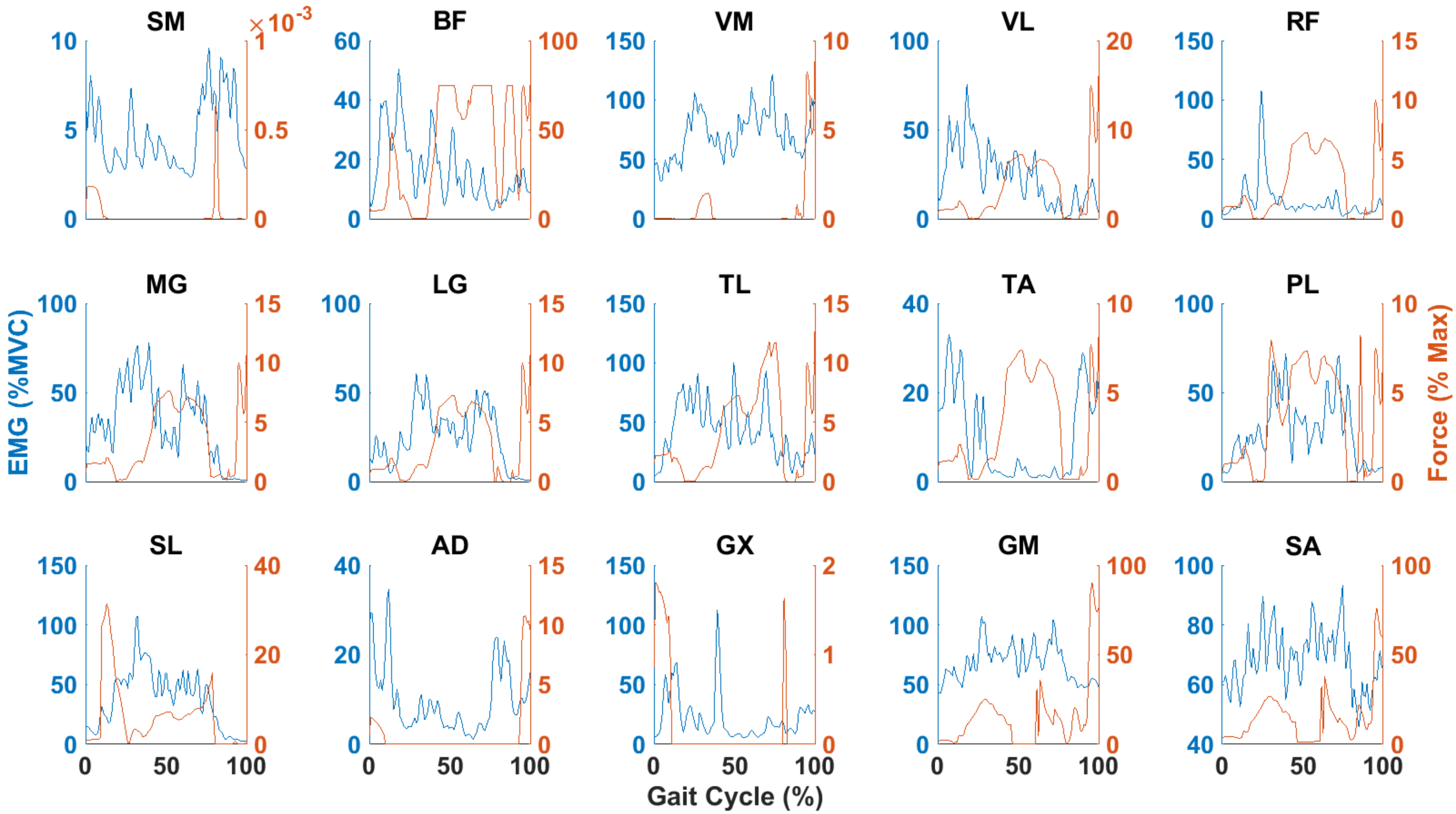

Figure 7.15 Muscle activations (blue) compared to mean muscle forces (orange) for a 'bouncy' walking trial with a specific muscle tension of 88 N/cm². Muscles are the same as Figure 7.8.

Appendix H – Muscle activation compared to force predictions during high knee flexion movements

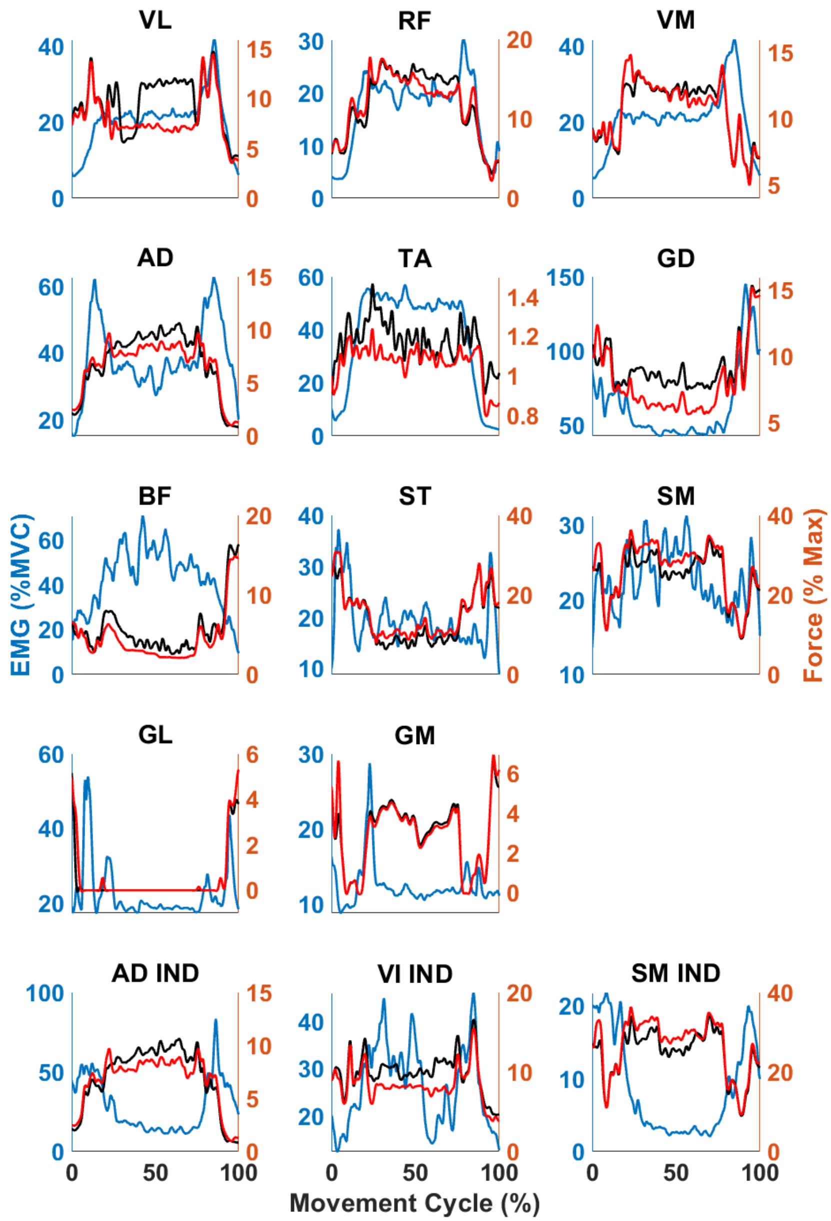

Figure 7.16 Mean muscle activations (blue) compared to mean muscle forces with (orange) and without intersegmental contact (black) for flatfoot squat (FS). Muscles are: vastus lateralis (VL), rectus femoris (RF), vastus medialis (VM), adductor magnus (AM), tibialis anterior (TA), gluteus medius (GD), biceps femoris (BF), semitendinosus (ST), semimembranosus (SM), lateral gastrocnemius (GL), medial gastrocnemius (GM), with indwelling recordings of adductor magnus (AD IND), vastus intermedius (VI IND), and semimembranosus (SM IND).

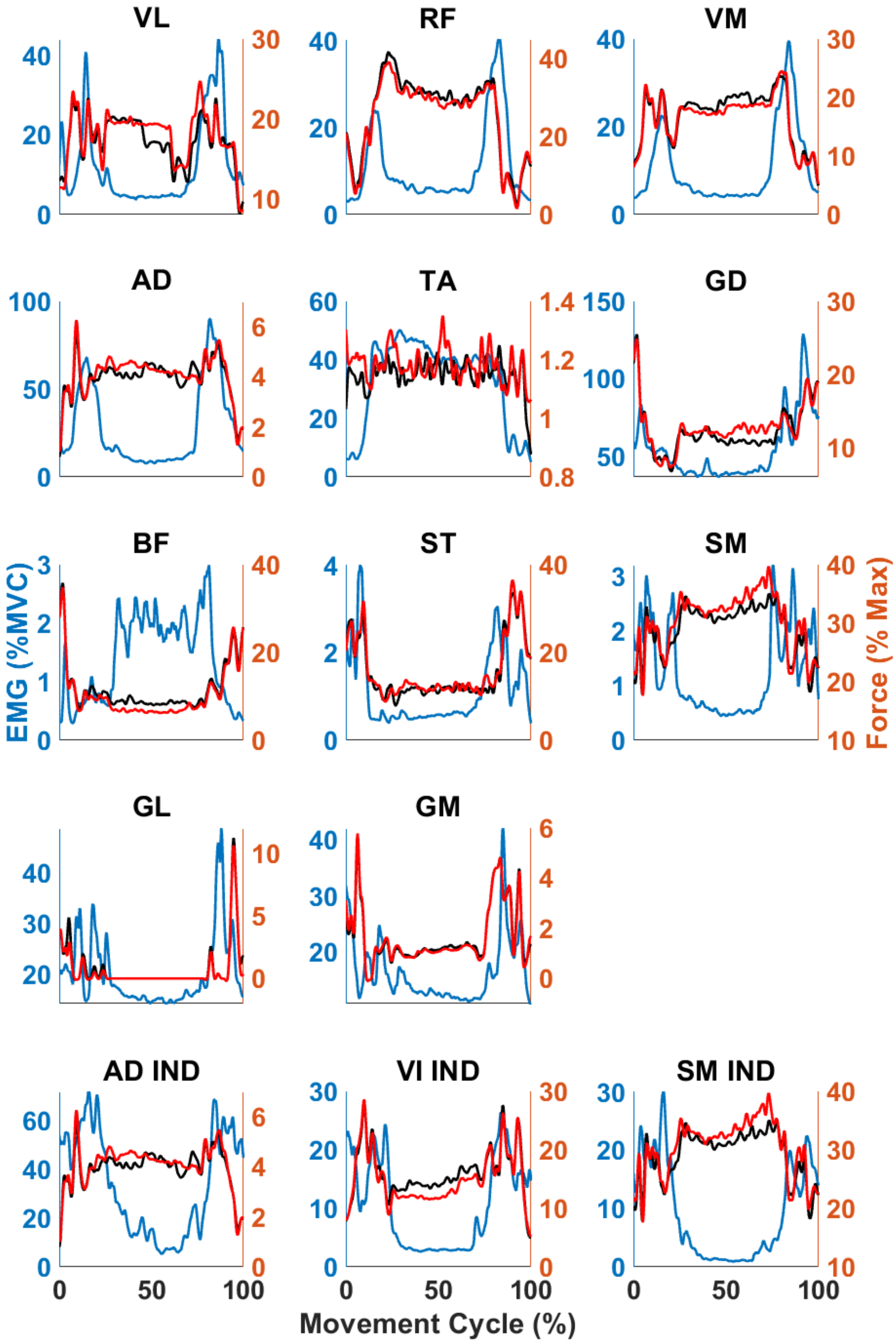

Figure 7.17 Mean muscle activations (blue) compared to mean muscle forces with (orange) and without intersegmental contact (black) for dorsiflexed kneel (DK). Muscles are the same as Figure 7.16.

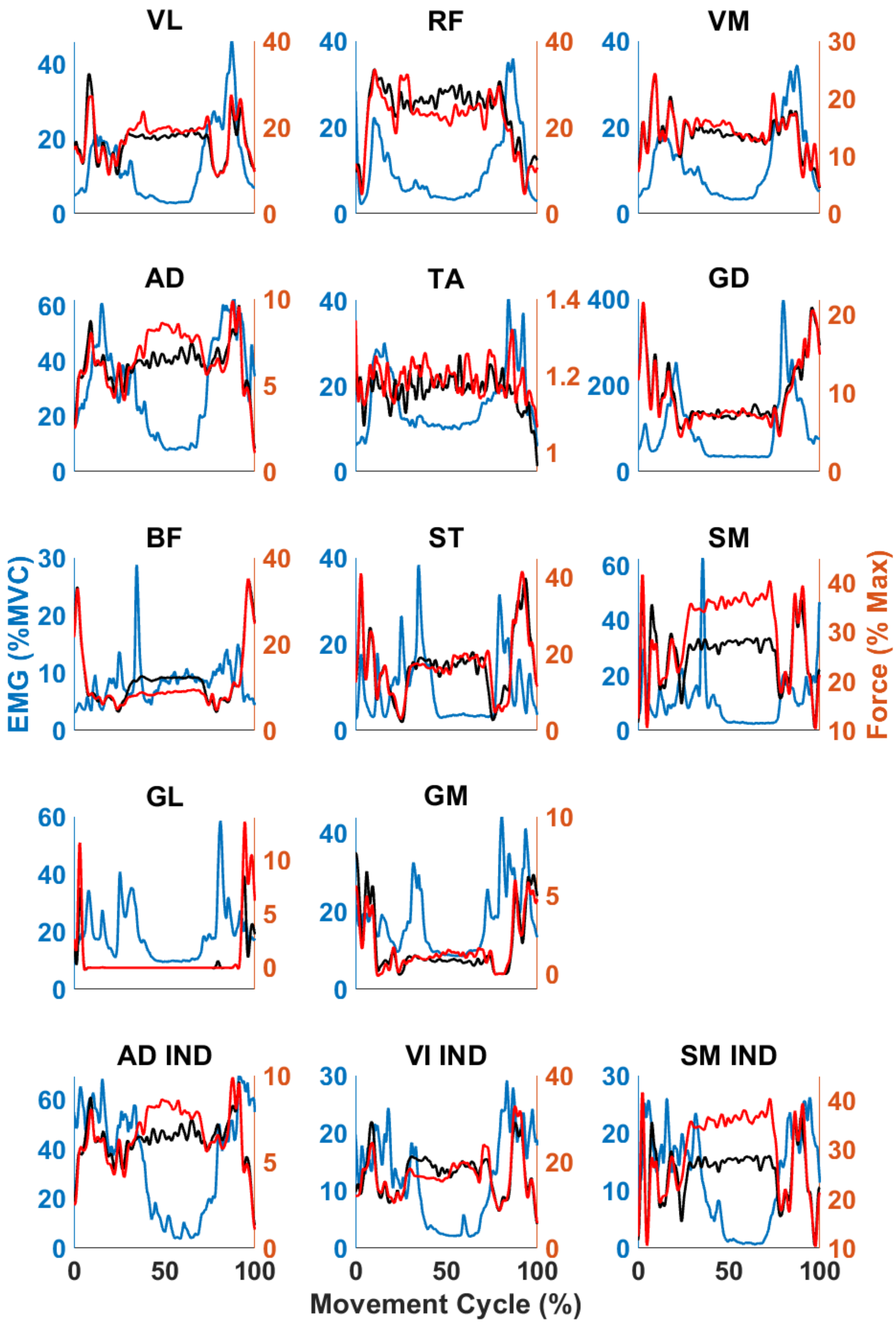

Figure 7.18 Mean muscle activations (blue) compared to mean muscle forces with (orange) and without intersegmental contact (black) for plantarflexed kneel (PK). Muscles are the same as Figure 7.16.

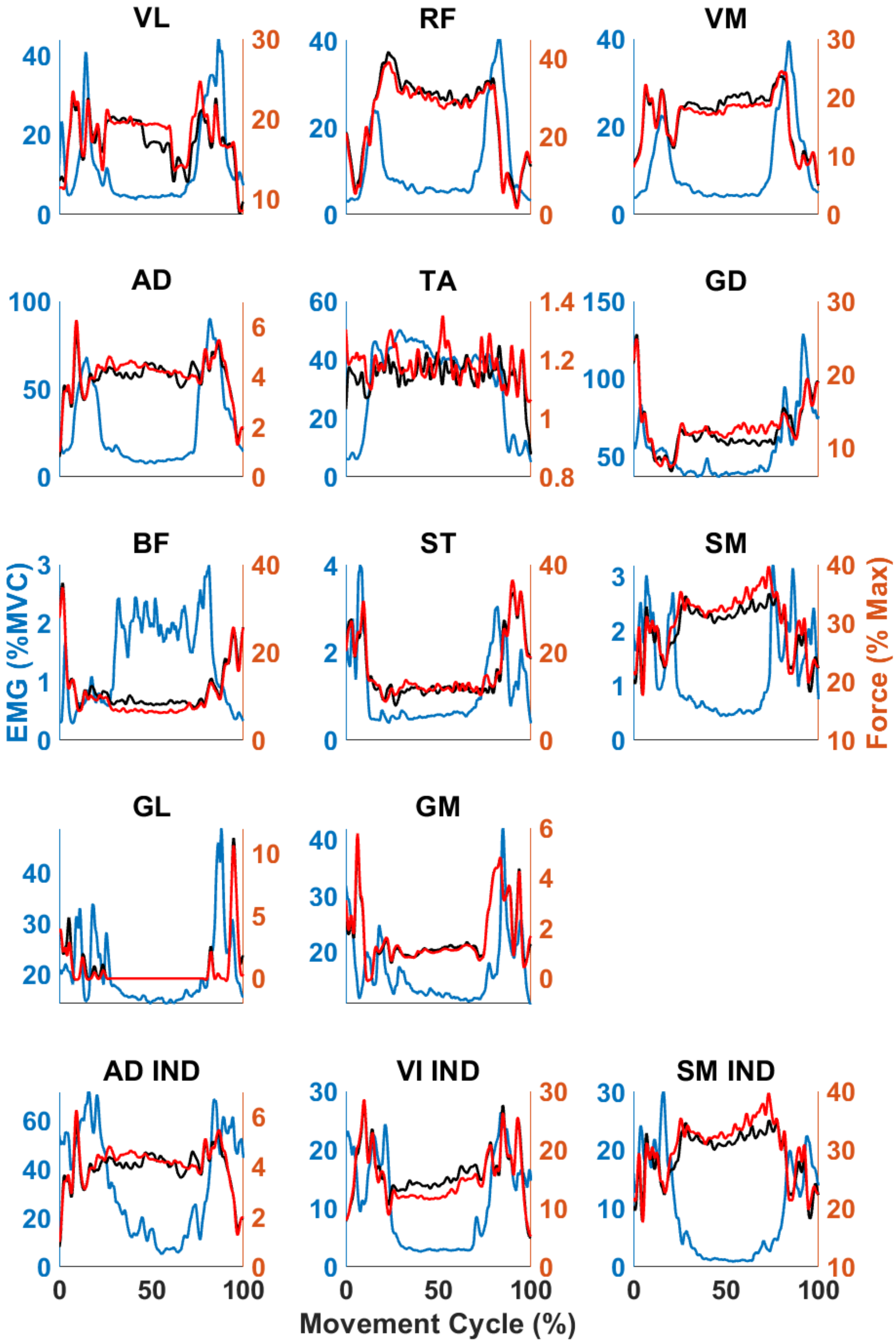

Figure 7.19 Mean muscle activations (blue) compared to mean muscle forces with (orange) and without intersegmental contact (black) for dorsiflexed unilateral kneel (DUK). Muscles are the same as Figure 7.16.

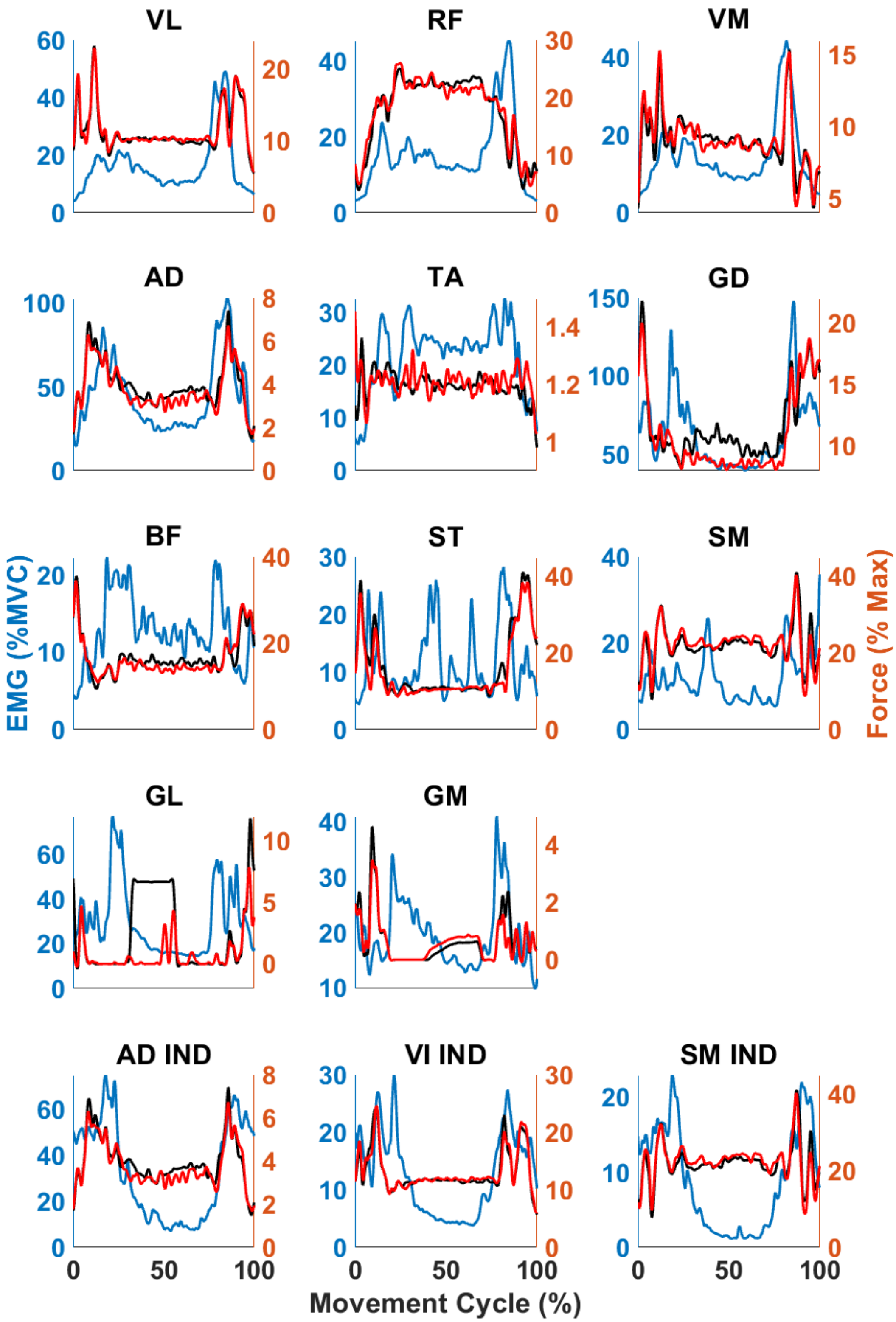

Figure 7.20 Mean muscle activations (blue) compared to mean muscle forces with (orange) and without intersegmental contact (black) for plantarflexed unilateral kneel (PUK). Muscles are the same as Figure 7.16.